UNIVERSITAT POLITÈCNICA DE CATALUNYA

DEPARTAMENT DE TEORIA DEL SENYAL I COMUNICACIONS

PH.D DISSERTATION

Synthesis and Design of Dissipative Filters with Improved Performance

---

Author: Alberto Padilla Díaz

Thesis Advisor:

Prof. Jordi Mateu Mateu

JULY 2015

ABSTRACT

Connect, upload, download, share and transfer anything at anytime and anywhere is not a futuristic vision and is indeed a real demand on current and future wireless and fixed communication systems. From the point of view of service providers efficient usage of the limited resource on the radio frequency (RF) spectrum is one of the biggest challenges. This technological challenge has to be faced from many different approaches and one is certainly the RF hardware equipment on the wireless devices, base stations and satellite equipment. Among the RF components into the RF chain, the filtering stage is without any doubt one of the most critical components, which usually have to be individual for any communication system or have to operate in a multistandard and multimode communication environment. Our devices are equipped with more and more radios and there are many scenarios where it is desirable from a user perspective to operate these simultaneously. Adding to the challenges, many of these bands are very close together and therefore require highly selective filters. When this happens it is essential that they can operate without detrimental mutual interference. These bands must be isolated to avoid interference.

The complexity of the filtering requirements and number of filters per device is steadily increasing. This demands for continuous research to filter a) *performance improvement* and b) *size reduction*. This is even more stringent in satellite equipment where the live of the device is longer and the size and weight of the equipment significantly contributes to the playload of the satellite and strongly affects the cost. The number of selective or channelizing filters in a satellite equipment are numerous and present into the input multiplexing, always present in any satellite transponder. Channel filters in input multiplexers take up a substantial portion of modern satellite payloads in terms of size and mass.

High selective filters can be achieved by the use of high quality factor resonators on the implementation of high order filter with usually a complex configuration - several transmission zeros to increase and tailored the selectivity and equalization zeros to obtain a linear group delay response of the filter.

Although several innovative technologies can achieve high performance filter with a considerable compact size, the required filter response flexibility and heritage demanded on the on-board satellite equipment, demands for using conventional technologies for the filter implementation. This results in bulky filter configurations, where a size reduction inherently involves a reduction on the quality factor, which in turn give rises into a degradation of the filter performance.

The goal of this work is the implementation of a new class of filters with the used of lossy resonators. Note that success of this goal will result in high performance filter with reduced sized and

suitable to be used in satellite equipment. As usually occurs in engineering, *"there are no free lunches"* and the size reduction, in this novel class of filters, comes along an increment of the overall filter insertion losses, although the filter shape factor it is still high-performed. Although this limits the application of such new class of filters, there are very promising in RF input front-end architectures where the filter (or input multiplexer filtering stage) connects after and amplifier structures, as in satellite equipment.

This demands for achieving three intermediate goals: 1) create a new mathematical formulation of the filter response which considers the limited losses of the resonators from the very beginning, 2) provide the suitable synthesized network of the new filter topologies. These new topologies usually results in conventional topologies with an additional coupled resistive network which provides a selective dissipation along the filter band, and 3) evaluate the technological issues for the implementation of this new class of filters. The later objective has been achieved by the implementation of three prototypes.

Adding to the achievement of the major goal and the three intermediate goals results of this work result also in a commercial software for synthesizing this type of novel filtering structures.

LIST OF FIGURES

Fig. 1 - Simplified Block diagram of a payload for illustration.

Fig. 2 - Typical scheme of an IMUX in a satellite.

Fig. 3 - Filter response with referred parameters

Fig. 4 - Equivalent circuit of a two port network

Fig. 5 - Ladder topology of a 3rd order Chebyshev low pass prototype filter.

Fig. 6 - Coupled resonators topology of a 3rd order Chebyshev low pass prototype filter.

Fig. 7 - Nodal notation of a inline three order filter

Fig. 8 - Equivalent circuit of a two port network a) represented as an *NxN* impedance matrix. b) represented as an *(N+2)x(N+2)* impedance matrix.

Fig. 9 - Outline of the N+2xN+2 coupling matrix. Note that the inner part correspond to the NxN coupling matrix.

Fig. 10 - a) Equivalent network of a transversal filter of order N. S and L represent the source and the load, $M_{S,L}$ the coupling between the source and the load, and the numbered boxes (from 1 to N) contain the resonator and coupling of the resonator to the source and load. b) Equivalent circuit of the resonator and its couplings to the source and load.

Fig. 11 - Equivalent circuit model of a 7th order folded network.

Fig. 12 - Outline of a folded coupling matrix, corresponding to the network of Fig. 12.

Fig. 13 - Indicates the order in which the elements of an 7x7 coupling matrix are turned to zero in order to obtain a *FCM*.

Fig. 14 - Outlined of conventional filter topologies

Fig. 15 - Displacement of the poles of the transfer function due to the dissipative effects.

Fig. 16 - Transfer and reflection coefficients of a band pass filter as a function of its Q.

Fig. 17 - a) Position of the poles before and after predistortion. b) position of the predistorted poles affected by the dissipation effects.

Fig. 18 - Left hand side: Transfer and reflection coefficient for a 6-order Quasi-elliptic filter form with resonators of Q=250 and synthesized using conventional techniques (black line), using classical predistortion (blue line) and using partial predistortion (red line). The solid and dashed lines correspond to the transfer and reflection coefficient respectively. Right hand side: Group delay.

Fig. 19 - Equivalent circuit of a predistorted circuit model with a cascaded circulator [18].

Fig. 20 - Equivalent circuit model of a 3-dB hybrid coupled cascaded with the impedances $Y_1(s)$ and Y2(s).

Fig. 21 - Two-port symmetric network

Fig. 22 - Six order filter with multipath loss distribution [21]

Fig. 23 - Transfer and reflection coefficient of the synthesizes filters with non-uniform Q techniques and predistortion techniques [21]

Fig. 24 a) Equivalent network of a transversal filter of order *N*. *S* and *L* represent the source and the load. b) Circuit representing the coupling between the source/load with the resonator, and the resonator itself.

Fig. 25 - Response of a 4th order lossy filter design (42),with k_{11}=0.9, k_{12}=*0.5*, k_{22}=*0.6*. Blue trace: $|S_{21}|$, red trace: $|S_{11}|$, black trace $|S_{22}|$.

Fig. 26 - Response of a 4th order lossy filter design (42), with k_{11}= k_{21}= k_{22}=0.75. Blue trace: $|S_{21}|$, red trace: $|S_{11}|$, $|S_{22}|$.

Fig. 27 - Equivalent network of a transversal filter of order *N*, corresponds to (47).

Fig. 28 - Frequency response of a 4th order Chebyshev lossy filter (47) with no stopband return loss, with *k*=0.75 and passband insertion loss of -20log_{10}(*k*)=2.5 dB. . Blue trace: $|S_{21}|$, red trace: $|S_{11}|$, $|S_{22}|$.

Fig. 29 - Equivalent network of a transversal filter of order *N*, corresponds to (49). The red node indicates the additional resonant node

Fig. 30 - Frequency response of the 4th pole Chebyshev lossy filter on Fig. 28 with an additional pole/zero (48) for k=0.75, δ=14. Blue trace: $|S_{21}|$, red trace: $|S_{11}|$, $|S_{22}|$.

Fig. 31 - Response of a lossy filter design, k_{11}= k_{12}= k_{22}=0.75 Q_{eff}=2000, FBW=1%. Blue trace: $|S_{21}|$, red trace: $|S_{11}|$, $|S_{22}|$.

Fig. 32 - Response of a lossy filter design, *k*=0.75 (48), δ=14, Q_{eff}=2000, FBW=1%.. Blue trace: $|S_{21}|$, red trace: $|S_{11}|$, $|S_{22}|$.

Fig. 33 - FCM for a lossy 6th order filter for a) Case A, b) case B, c) case B and d) case A+C responses. The black and grey circles represent lossy and lossless resonators, respectively.

Fig. 34 - Uniform loss distribution for a 4th order filter designed following cases A+C. Black circles correspond to the resonators with lowest *Q*; grey circles to resonators with *Q*= Q_{eff} (the *Q* for a prescribed rounding in the transmission response; circles labeled NS and NL correspond to non-resonant nodes and white circles correspond to the source/load. a) Transversal coupling topology

b) folded coupling topology (FCT), c) FCT with non-resonant nodes, d) topology after loss distribution

Fig. 35 - Dependence of the variable γ_{RL} as a function of the return losses.

Fig. 36 - Dependence of the variable ρ_a as function of the position of the transmission zero, normalized frequency, for *RL*=25 dB (green), 20 dB (red) and 15 dB (blue).

Fig. 37 a) Transversal network topology of a synthesized response of a 6th order filter. b) Folded coupled topology (FCT).

Fig. 38 - Dependence of the variable γ_{RL} as a function of the return losses.

Fig. 39 - Dependence of the variable ρ_a as function of the position of the transmission zero, normalized frequency, for *RL*=25 dB (green), 20 dB (red) and 15 dB (blue).

Fig. 40 - Transmission response of various synthesis alternatives: (thick-solid line) lossy synthesis equivalent to a infinite *Q* response requiring resonator *Qs* of 2780; (thin-solid line) lossless synthesis evaluated with *Qs* of 2780; (thick-dotted line) lossy synthesis equivalent to a finite *Q* response of 2000 requiring resonator *Qs* of 1160; (thin slashed line) lossless synthesis evaluated with *Qs* of 1160. Note the differences in insertion loss flatness and absolute insertion loss among the various design alternatives.

Fig. 41 - a) Folded coupling network (Case B (48)) before applying any hyperbolic rotation. b) Folded coupling network after applying hyperbolic rotation

Fig. 42 - Response of a lossy filter design, k=0.7 (48), δ=18, Blue trace: $|S_{21}|$, red trace: $|S_{11}|$, $|S_{22}|$.

Fig. 43 a) Transversal for the synthesis case B (8) b) Folded networks of a two resonators subnetwork c) Folded networks of a 4 resonator subnetwork after hyperbolic rotation. d) Parallel connected resulting sixth order network. a) Box section topology for a sixth order filter b), c) and d) Box section topology after annihilation of couplings 4-1 and 2-3.

Fig. 44 - Response of a lossy filter design, k=0.75 (8), δ=11, Blue trace: $|S_{21}|$, red trace: $|S_{11}|$, $|S_{22}|$.

Fig. 45 - Folded topology of a 10-4-4 filter with completely symmetric response.

Fig. 46 - a) Folded topology with resistive couplings in all Cascaded Quadruplets. b) Folded topology with resistive couplings only on the inner Cascaded Quadruplets.

Fig. 47 - Folded topology with resistive couplings on the inner Cascaded Quadruplets and additional resistive couplings between resonators 3-5 and 8-6.

Fig. 48 - Synthesized lossy responses in red, in comparison with a conventional response with Qs of 13000.

Fig. 49.- Transmission filter response for synthesizes response with Q ranging from 12000-2000. Group delay of synthesized responses: conventional synthesis (in black), lossy synthesis Q_0=2000 (blue), Q_0=5000 (green) y Q_0=7000 (red).

Fig. 50 - Network topology of an 4th order inline lossy filter with non-resonant nodes and uniform losses distribution

Fig. 51 - Frequency response of the synthesized lossy filter.

Fig. 52 - Transmission and reflection coefficient deviation when the conventional couplings are randomly changed within a +/-20%, for 15 trials.

Fig. 53 - Transmission and reflection coefficient deviation when resonant frequency of the resonators are randomly changes within a +/-0.2%, for 20 trials.

Fig. 54 - Transmission and reflection coefficient deviation when the resistive couplings are randomly changed within a +/-20%, for 30 trials. Inset: Zoom of the in-band transmission performance.

Fig.55 - Transmission and reflection coefficient deviation when the Q are randomly scaled, for 20 trials.

Fig. 56 - Transmission coefficient deviation when the Q are uniformly scaled within 500 to 100.

Fig. 57 - Details of the transmission and reflection coefficients deviation when the resistive couplings are uniformly changed.

Fig. 58 - The transmission and reflection coefficients when both Q and resistive coupling are uniformly scaled.

Fig. 59 - Outline and picture of the basic resonator for Filter 1.

Fig. 60 - FCM with uniform *Q* distribution of the filter to design

Fig. 61 - Network topology of the filter.

Fig. 62 - Frequency response of the filter to be developed. Corresponds to a screen shot from the software *lossyfilter.*

Fig. 63 - Filter configuration of Filter 1 without resistive couplings.

Fig. 64 - Frequency response of the synthesized and designed filter without resistive couplings.

Fig. 65 - (First) Lumped resistor, (Second) lumped resistor with two cascaded inverters at the input and output, (third) lumped resistor with a inverter cascaded to a transmission line at the input and output, (fourth) outlined layout.

Fig. 66 - Non-resonant node and resistive coupling, a) Circuit model b) layout

Fig. 67 - Outline of the filter topology with an electromagnetic domain and the circuit domain

Fig. 68 - Full-wave simulated (dotted line) response and synthesized response (solid line) of the filter defined by Fig. 60.

Fig. 69. Frequency response of the measured filter (solid-line), electromagnetic simulated response (dashed-line) and synthesized conventional response (dotted-line). Upper part: Details of the normalized to 0 dB in-band transmission responses. Inset: outlined of the implemented filter. Note that the measured frequency response has been shift up in frequency by 40 MHz, in order to be centered at 1 GHz.

Fig. 70. Picture of the fabricated filter

Fig. 71. Measured frequency response of the implemented filter, when the initial resistors are changed according to Table 30

Fig. 72 - Broadband frequency response of the transmission (in red) and reflection (in blue) coefficients. Dashed line corresponds to the simulated response of filter topology with resistive couplings, and solid line corresponds to the simulated response without the resistive couplings.

Fig. 73 - Measured response as a function of temperature

Fig. 74 - Detail of the temperature dependence of transmission and reflection responses in the passband

Fig. 75 - Detail In band filter response, showing the details of the insertion losses and rounding at the band-edges

Fig. 76 - a) frequency response of a single resonator as a function of temperature. b) Dependence of the Q factor as a function of temperature

Fig. 77 - Variation of the resistive value as a function of temperature

Fig. 78 - Measured and simulated insertion loss variation and flatness for Filter 1

Fig. 79 - Outline and picture of the basic resonator for Filter 2.

Fig. 80 - Outline of the filter network topology for the Filter 2.

Fig. 81 - Details on the coupling matrix corresponding to the synthesis filter of Fig. 80. The Q factors of the resonators are also indicated.

Fig. 82 - Frequency response of the filter to be developed.

Fig. 83 - Filter configuration of BB-2 without resistive couplings.

Fig. 84 - Frequency response of the synthesized and designed filter without resistive couplings.

Fig. 85 - Layout of the Filter 2.

Fig. 86 - Comparison between circuital simulations of the lossy filter and simulation ADS-Moementum of the planar filter of Fig. 85

Fig. 87 - Picture of the fabricated filter

Fig. 88 - Measured response (in red) shifted 27 MHz to higher frequencies, and simulated response (in blue).

Fig. 89 - Broadband frequency response of the transmission (in red) and reflection (in blue) coefficients. Dashed line corresponds to the simulated response of the filter topology with resistive couplings, and solid line corresponds to the simulated response without the resistive couplings.

Fig. 90 - Measured response of the filter as a function of temperature

Fig. 91 - In-band detailed of the measured response of the filter as a function of temperature

Fig. 92 - a) frequency response of a single resonator as a function of temperature. b) Dependence of the Q factor as a function of temperature.

Fig. 93 - Variation of the resistive value as a function of temperature.

Fig. 94 - Measured and simulated insertion loss variation and flatness for the filter response

Fig. 95 - Combline cavities fabricated for Q tests.

Fig. 96 - Outline of the basic combline resonator

Fig. 97 - Q of the combline resonator as a function of the ratio between the cavity and the aluminium rod.

Fig. 98 - Outlined of the basic combline resonator with rounded corners.

Fig. 99 - a) Folded coupling network indicating the hyperbolic rotations performed. b) Resulting network after applying the rotations.

Fig. 100 - Coupling matrix of the filter cavity to be designed

Fig. 101 - Network topology of the filter cavity to be designed

Fig. 102 - Transfer and return responses of the synthesis alternative LF_OPT

Fig. 103 - In-band normalized transmission response of LF_OPT (black trace), a lossless design with Q=3000 and 21dB return loss (red traces) and that of the original design using lossy filter synthesis LF (blue traces)). The straight black lines show the specs template for the transmission response

Fig. 104 - Top view of the filter structure

Fig. 105 - 3D outlined of the filter structure

Fig. 106 - Outline of two coupled cavities

Fig. 107 - Magnetic coupling between two resonators as a function of the aperture between the cavities

Fig. 108 - Deviation of the resonant frequency as a function of the aperture

Fig. 109 - Deviation of the resonant frequency as a function of the aperture

Fig. 110 - Structure used to design the external coupling

Fig. 111 - Frequency response of the first (last) resonator coupled to the source

Fig. 112 - Coaxial cable connected to a microstrip transmission line

Fig. 113 - Cavity with the coaxial cable to introduce the resistive couplings

Fig. 114 - Frequency response of the ideal filter after decoupling the input and output ports

Fig. 115 - Resonant frequencies of the modes of the structure of Fig. 114

Fig. 116 - Frequency response of the designed and synthesized filter without resistive coupling. The red and orange lines indicate the circuit evaluated response (synthesized response), whereas the blue and cyan lines indicate the full-wave designed response

Fig. 117 - In-band frequency response of the designed and synthesized filter without resistive coupling. The red and orange lines indicate the circuit evaluated response (synthesized response), whereas the blue and cyan lines indicate the full-wave designed response

Fig. 118 - 10-Ports HFSS- S matrix for the whole cavity simulation

Fig. 119 - Response of the coaxial to microstrip transition. Blue and red lines correspond to the reflexion coefficients to each port, and the purple line corresponds to the transmission coefficient

Fig. 120 - Resistive path including the HFSS simulations of the transitions. The length of the transmission lines and the values of the resistances are optimized to fit the theoretical response

Fig. 121 - Synthesized and designed response of the filter prototype

Fig. 122 - layout of the filter top showing the microstrip lines (pink) coupling probes (green), coupling screws (green), grounding screws (blue) and the outline of the combline cavities (yellow).

Fig. 123 - Manufactured Combline Lossy Filter

Fig. 124 - Cavity Filter (internal cavities)

Fig. 125 - Cavity filter lid (bottom view)

Fig. 126 - Custom RF feedthroughs (top and bottom views)

Fig. 127 - Measured and Simulated Filter Response without Resistive Coupling.

Fig. 128 - Measured (tuned response) and Simulated Filter Response with Resistive Coupling.

Fig. 129 - Insertion loss details of the measured (tuned response) vs simulated response of the filter with resistive coupling.

Fig. 130 - Test Bench for the Thermal Tests

Fig. 131 - Measured filter response at different temperatures. From -10 ºC to 85 ºC, with intervals of 10 ºC.

Fig. 132 - Measured filter response at different temperatures. From -10 ºC to 85 ºC, with intervals of 10 ºC.. Details on the reflection coefficient.

Fig. 133 - Measured filter response at different temperatures. From -10 ºC to 85 ºC, with intervals of 10 ºC. Details on the insertion loss.

Appendix Figures

Fig. A.1.1 - Example of a rotation matrix [R_r] of orden 7 with a [3,5] pivot.

Fig. A.2.1 - Equivalent network

Fig. A.4.1 - a) FCT before hyperbolic rotation b) FCT after hyperbolic rotation in a Quasi-Elliptic response c) FCT after hyperbolic rotation in a Chebyshev response. d) FCT after hyperbolic rotation in a Quasi-Elliptic response for a 6^{th} order filter.

Fig. A.7.1 - Roots of the F(s) extracted polynomials.

Fig. A.7.2 - Reflection response for each F(s) of Table A.7.3.

LIST OF TABLES

Table 1: Coupling matrix of the filter response of Fig. 25. Note that all terms are normalized by 0.1

Table 2: Coefficients of the characteristic polynomials low pass Chebyshev prototype of order 4.

Table 3: Roots of the characteristic polynomials of a 4^{th} order Chebyshev prototype

Table 4: Coupling matrix corresponding to Fig. 26 response. Note that all terms are normalized by 0.1

Table 5: Coefficients of the characteristic polynomials low pass Chebyshev prototype of order 4.

Table 6: Roots of the characteristic polynomials of a 4^{th} order Chebyshev prototype

Table 7: Coupling matrix corresponding to Fig. 28. Note that all terms are normalized by 0.1

Table 8: Coefficients of the characteristic polynomials low pass Chebyshev prototype of order 4, using case B.

Table 9: Roots of the characteristic polynomials of a 4^{th} order Chebyshev prototype, using case B.

Table 10: Coupling matrix corresponding to Fig. 30 response

Table 11: Coefficients of the characteristic polynomials low pass Chebyshev prototype of order 4, using case B.

Table 12: Roots of the characteristic polynomials of a 4^{th} order Chebyshev prototype, using case B.

Table 13: Coupling matrix corresponding to Fig. 31 response. Note that all terms are normalized by 0.1

Table 14: Coupling matrix corresponding to Fig. 32 response

Table 15: Summary of required Q vs IL

Table 16: Summary of required Q vs IL

Table 17: FCM with uniform Q distribution of the response of Fig. 26. Note that all terms are normalized by 0.1

Table 18: FCM with uniform Q distribution of the response of Fig. 31. Note that all terms are normalized by 0.1

Table 19: Comparison of various synthesis alternatives in terms of insertion loss (IL), insertion loss flatness (ΔIL) and its associated effective Q (Q_{eff}), and the required resonator Q (Q_0).

Table 20: FCM of the response of Fig.42. Note that all terms are normalized by 0.1

Table 21: FCM of the topology of Figure 43b

Table 22: FCM of the topology of Figure 43c (see example in main text).

Table 23: Coupling M of the topology of Figure 43d and response of Figure 44. Note that all terms are normalized by 0.1

Table 24: Coupling Matrix of the topology of Fig. 43e. Some resistive couplings have been neglected. There are no noticeable differences with respect to the frequency response in Fig. 44, except for a slight degradation in insertion loss flatness of 0.1 dB. Note that all terms are normalized by 0.1

Tabla 25: Q vs IL for the optimized responses

Tabla 26: Coupling matrix of the case under study in this section

Tabla 27: Summary of the filters implemented in the Chapter 3.

Table 28: Specification of the filter 1.

Table 29: Properties of the material used for implementing filter 1.

Table 30: Summary of the lumped resistors used in the topology of Fig. 70, whose measurements are outlined in Fig. 70.

Table31: Specification of the Filter 2.

Table 32: Properties of the material used in Filter 2

Table 33: Resulting dimensions and weight of the fabricated Filter 2.

Table 34: In-band filter specifications. See Table 35 for selectivity requirements.

Table 35: Summary of the comparison several synthesis alternatives made in [27] indicating the filter specifications (SPECS), a full pre-distortion synthesis (FPD2), a conventional synthesis (CONV2) and variations of a lossy filter synthesis (LF, LF_QR). Highlighted cells indicate that the specifications are not met.

Table 36: Measurements in various combline cavities tested. Quality factors agree within 10% with HFSS simulations.

Table 37: Properties of the material used for the fabrication of the cavity

Table 38: Nominal dimensions of the cavity to be used as a basic resonator

Table 39: BB3 filter: values of the SMD resistances

Appendix Tables

Table A.1.1: Resulting angles to eleminate the element of M_{mn} of the matris

Table A.7.1: Roots of the characteristic polynomial *E(s)* of a 4^{th} order Chebyshev filter with L_r = 20 dB

TableA.7.2: Selected roots for the polynomials S_{ed} and S_{od}, respectively

Table A.7.3: Coefficients of the resulting F(s) polynomials

Table of Contents

ABSTRACT **1**
LIST OF FIGURES **3**
LIST OF TABLES **11**
0 INTRODUCTION **16**
0.1 Objectives 17
0.2 Contents 21
1 CHATER I: THEORETICAL BACKGROUND ON FILTER SYNTHESIS **24**
1.1 Filter transfer function 25
1.2 Principles of Synthesis Techniques: Circuit and Matrix Approach 26
1.3 Synthesis of Network. Circuit Approach 27
1.4 Example of a synthesis network 28
1.5 Coupling Matrix Synthesis of Filter networks 31
1.6 Dissipation effects 38
1.7 Synthesis Techniques of Dissipative Filters 40
1.8 Predistortion synthesis Techniques 41
1.9 Synthesis techniques with Unequal Q distribution 48
1.10 Summary review on the dissipative synthesis techniques 53
1.11 Conclusions and summary 55
2 SYNTHESIS OF DISSIPATIVE FILTERS **56**
2.1 Introduction 56
2.2 Mathematical Formulation For the Synthesis of Lossy Filters 58
2.3 Strategies for resonator Q distribution in folded networks 71
2.4 Optimization approach 95
2.5 Sensitivity considerations in lossy filters: Case study of a 4th order Chebyshev filter 101
2.6 Conclusions 109
3 CHAPTER 3: IMPLEMENTATION OF DISSIPATIVE FILTERS **112**
3.1 4th order Chebyshev planar lossy filter. Direct Synthesis 113
3.2 6th order Chebyshev planar lossy filter. Optimization approach 130
3.3 Combline Channelizing lossy filter at C-Band 143
3.4 Conclusion 168
4 CHAPTER 4: CONCLUSION AND FUTURE RESEARCH WORK **170**
4.1 Conclusion 171
4.2 Future Research Work 174
PUBLICATIONS AND OUTCOMES **178**
APPENDIX 1: Matrix Rotation. From TCM to FCM **180**
APPENDIX 2: Output Scattering Reflection Parameter in Case A **184**
APPENDIX 3: Scattering Reflection Parameter in a Symmetric Network **186**
APPENDIX 4: Hyperbolic Rotation **188**

APPENDIX 5: Node Scaling 190
APPENDIX 6: Sixth order folded lossy coupling matrix 192
APPENDIX 7: Details on the transfer function obtained in Case B 194
APPENDIX 8: Matrices: Lossy filters on section 2.4 198
REFERENCES..... 200

0 INTRODUCTION

RF and microwave filters play a crucial role in almost any communication system. Its main function is to select the signal set into the desired frequency range and eliminate all other signals. The desired signal it would be ideally selected without any modification, this essentially means to maintain the amplitude of all frequency components of the signal. Although an ideal filter performance cannot even be synthesized as mathematical (polynomial) description, such a representation of the filter response assuming lossless components stays close to the desired *brick wall* filter behaviour.

A synthesized lossless filter would satisfy the main parameters defining the filter performance, these are insertion losses in the in-band of the filter, selectivity at the band edges of the passband, high attenuation out-of-the filter passband and very low reflection of the in-band input signal.

Even though a polynomial description of such a response it is possible, a real implementation of that is not due to the always existing losses of the implemented filter. So that in a real design and implementation, the filter designer should assume and trade off, when possible, between those filter parameters.

As communication systems, filters are used in many different applications and equipment which go from satellite communications to any wireless network or sensing system. In addition filters are used in different parts of the communication chain, this is in the transmit or receiver side, as a pre-select filter, intermediate frequency filter or as a channelizing filter in an IMUX or OMUX configuration, contributing therefore in the overall figure of merit of the communication system, such as the noise figure in the receiver stage.

Although an ideal filter response would be always desired the relevant filter performance parameters depend on the application and position of the filter in the communication chain. It is also true however that the filter performance may indeed affect the communication system architecture and all other components in the communication chain. For instance, with the existence of ideal filters (no insertion losses and very high frequency roll-off), amplifiers would be substantially reduced and the analogue digital conversion stage would be moved closer to the antenna. The intended application then also defines the technology used for the filter implementation.

Mostly all the filtering structures are based on resonant devices as a basic component. The losses of the resonator mostly define therefore the losses of the filter, which in turn affects the filter performance. It is well established the losses of a single resonator are defined by its quality factor (Q). The Q factor essentially relates the amount of energy stored into the resonant cavity with the dissipated power inside the cavity. So that, high Q factors required either of resonant structures which allow for storing large amount of energy or the used of very lossless materials where the dissipated power it is very small. Although the later approach would sound more convenient for compact devices, dissipated power is correlated with the field density which increases in miniaturized configurations, and this approach could be only used in superconductor resonators at expenses of using an additional cooling system. Being therefore the first approach the most commonly used to achieve high Q resonators, which goes to the conclusion that high filter performance requires of large filters usually with cavity (or dielectric) resonators. At this point it is worth to mention that acoustic filters (usually known as film bulk acoustic resonator, FBAR) can achieve substantially high Q in a very small size, nevertheless they still have some technological limitations, such as the operating frequency range and the achievable filter bandwidth which essentially limits its use on cellular applications.

The effects of using resonators with limited Q results in filters with degraded response. In a conventional design the filter is initially synthesized and design without considering such limitation and the losses are evaluated afterwards. The main effects of this procedure are filters with non-zero insertion losses, roundness in the band-edges of the filter, non-flat insertion losses in the filter in-band, loss of selectivity and less pronounced transmission zeros.

0.1 Objectives

The objective of this thesis is to development of a new class of synthesis approach to allow high filter performances with lossy structures. This is to consider the losses of the filter (and basically of a single resonator through its Q factor) from the very begining of the mathematical

description, in order of obtaining a close to ideal filter responses by the use of lossy materials and /or **very compact resonant structures**.

The results obtained in the thesis can be mostly extrapolated to any filter technology and application, nevertheless it is worth to mention here that the main focus has been put on the satellite application, where the mass and size reduction plays a significant role, and more importantly on the receiver side where the eventual high power issues are not a restriction. The main reason for that is also that the work developed during this thesis has been performed and partially supported in the framework of three research projects with the European Space Agency (ESA) and with industrial partners. These three projects are:

- Design and Synthesis of a New Class of Receiver Filter. ESA Contract. Industrial partner: MIER Communicaciones
- Study, development and verification of predistortion and lossy filter synthesis techniques. Industrial contract: THALES Alenia Space
- Compact Ku-band channel filters for input multiplexer. ESA Contract, ARTES 5.1 Programme. Industrial partner: THALES Alenia Space

As important objective it is not only the development of the mathematical tools for the synthesis of the new class of filter but also to prove its feasibility in real implementation. The viability of the novel mathematical filter formulation will be validated through the design, fabrication and testing of several filters.

0.1.1 Scope of the thesis

The use of filtering structures in a satellite system it is dominant and takes lot of the payload and volume of the communication equipment. Note that communication satellites are radio relay stations in space. They receive radio signals transmitted from the ground, amplify them, translate them in frequency, and retransmit them back to the ground. Since the satellites are at high altitude, they can see all the microwave transmitters and receivers on almost one-third of the earth. However, most earth stations are designed to stablish a communication link with only one satellite at a time, allowing satellites to use a huge bandwidth. Hence, most communication satellites cover C (4-8GHz), Ku (10.95-14.5GHz) or Ka (26.5-40GHz) bands. To select (filter in) the desired signal at a time it is crucial for ensuring the communication.

Satellite communication services are known to be one of the main drivers of the telecommunication research and innovation. They include fixed services (voice, data and video transmission) across all countries and continents between certain points on the Earth's surface. In addition, mobile satellite systems connect remote regions, vehicles, ships and aircrafts to other parts of the world and/or other mobile or stationary communitacion units. Scientific research satellites are also an important part of

the current satellite services. Commercial and noncommercial scientific research satellites are able to collect meteorogical information, land survey data (e.g., remote sensing), and other different research applications such as earth science, marine science, and atmospheric research.

Broadcast TV is one of the largest part of the satellite telecommunication market. The number of HDTV channels is growing since began to be on air on late 90's, and they will soon be the standard TV format. This directly implies an increase in capacity of broadcast satellite since HDTV requires up to 4 times more bandwidth than SDTV (DVB-S HDTV uses typically not less than 18MHz, while low quality SDTV channel needs at least 4MHz). This is only one example of the current satellite telecommunication needs of growth.

The influence of microwave filters in the capacity of a communication satellite is huge since large amount of them are present on both low and high power stages. A basic satellite payload scheme is shown in the next figure and the impact of microwave filters in satellite systems is discussed.

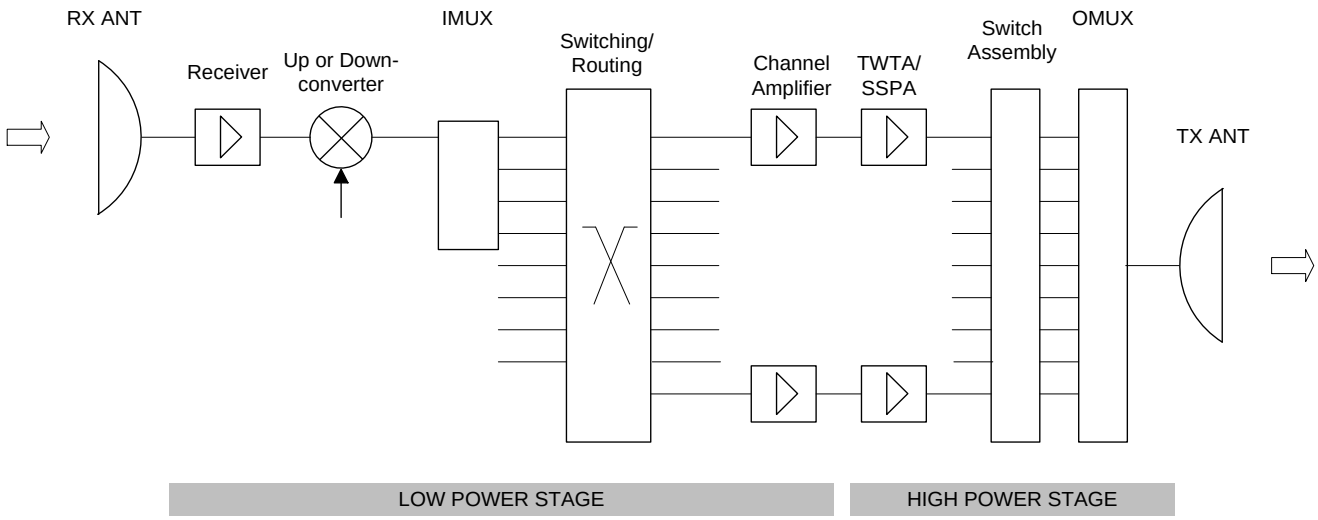

Fig. 1 - Simplified Block diagram of a payload for illustration.

Regardless of the satellite architectures, the block diagram of transponders is the same as of Fig. 1. A receive antenna is connected to a wideband filter, followed by a low-noise receiver. After that, the signal is channelized into its various transponders via an input multiplexing network (IMUX). The allocated frequency band in a satellite system is divided into a number of RF channels, often referred to as transponders. Then, each RF channel is amplified separately and recombined by an output multiplexer network (OMUX) into a composite wideband signal that feeds into the transmit antennas. Input and output switch matrices are there to provide onboard reconfiguration of traffic flow from one transponder to another or from one beam to another.

Both multiplexers are formed by a set of bandpass filters, and the electrical requirements of them are stringent and they vary as they are used in the low power (IMUX) or the high power (OMUX)

stage. Thus, as the number of RF channels increases in satellite communication system, more high performance microwave filters are needed and the impact of their mass and volume becomes extremely important.

Microwave filters used in IMUX usually requires high degree filter types (typically 10^{th} degree) to produce narrow channel bandwidth with very demanding flatness, phase linearity and close to in-band rejection. Current filters use waveguide/dielectric resonator technology to produce high Q_L filters. On the other hand, filters used in OMUX are usually medium degree filters with minimum dissipation losses and high power handling capabilities (100W per channel).

Multiplexing networks are formed by a large number of bandpass filters which are designed to divide the allocated frequency band into a number of RF channels. Next, a scheme of a 10 channel IMUX is presented.

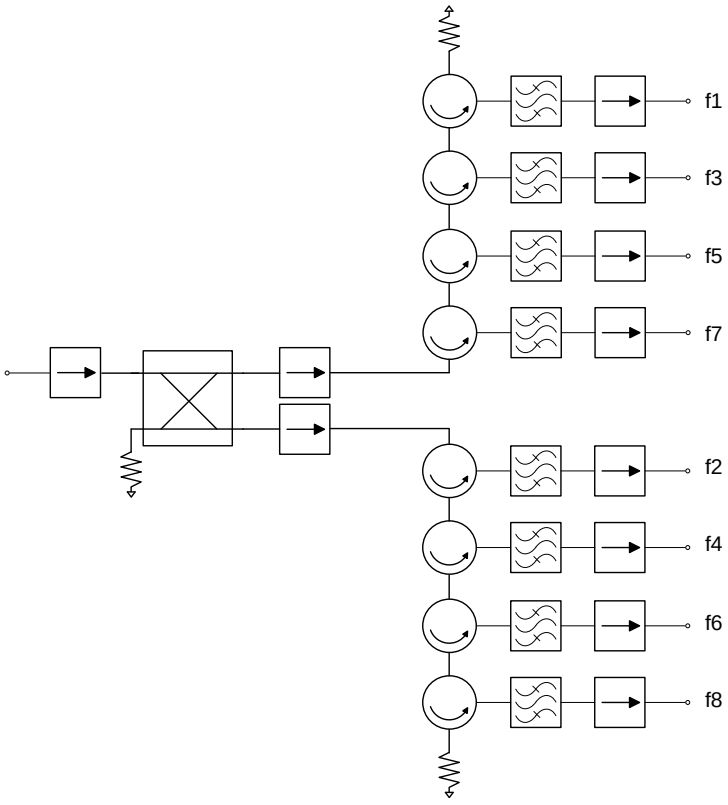

Fig. 2 - Typical scheme of an IMUX in a satellite.

Once the signal has been amplified by the LNA, the loss in the subsequent equipment is no longer critical. This is due to the fact that the receiver system noise temperature is reduced by the LNA, and the post-LNA losses have less impact. Instead, the design driver is the efficient channelization of the signal into its various RF channels or transponders with a minimum loss of bandwidth and, at the same time, providing enough isolation to control interference from other channels. Hence, channelizing filters largely determine the usable bandwidth of each RF channel, and the design of such channel filters must be close to that of an ideal filter.

Classical filter synthesis [1][2] techniques require the use of high quality factor (Q) resonators to achieve filters with high selectivity and flat passband response, like the ones needed in IMUX networks. This might be unfeasible or impractical in space systems having stringent weight and volume restrictions. However**, the development of synthesis techniques that take into account the limited Q of the filter resonators allows to optimize the filter selectivity and passband flatness, at the expense of other filter parameters (such as insertion loss) that might not be critical in channelizer filters, as said before. These techniques are usually known as *lossy filter synthesis*, and several works on these have been published in the recent years [3] [4] [5] [6]**.

0.2 Contents

Once the objective and scope of the thesis are presented, the following section outlines on the contents of this work and how they are presented to conduct to the final objective and conclusions. To support the following descripcion the diagram at the end of this section outlines also the contents of each chapter and the differents parts included.

The Thesis dissertation is divided into three main chapters, the chapter of conclusions plus additional details in the appendix sections. Although the appendices include important details of the mathematical development they have been remove from the main body of the document in order to keep a non-dispersive reading.

As depicted in the diagram, along with the three main chapter a commertial software tool has been developed to consider the new type of synthesis techniques. Most of the details of the software tool are given in www.tsc.upc.edu/lossyfilters. At this point it is worth to mention that the software developed also includes all the already conventional existing synthesis techniques, making it very useful for filter designers. Currently the software it is been used by ESA and all the industrial partners along these projects, this is MIER Comunicaciones and THALES Alenia Space.

The first chapter presents all the required mathematical tools for the development of the new approaches in chapter two. This is essentially the description of the conventional synthesis techniques, the effects of the losses on the filter synthesized response and also the outlined of the already existing advanced synthesis approaches, which are predistortion synthesis techniques and some of the initial steps on the lossy synthesis approaches (synthesis with dissipative networks). The conventional and predistortion techniques presented here result in a transversal network which will also be the based on the development of the novel synthesis methods.

Chapter two could be considered as the main chapter of the thesis since the results presented here are significantly the most innovative of this work. In fact this chapter could be considered as several subchapters. The firts part of the chapter defines the new mathematical description of the *ideal* filter

response of the filters considering the effects of losses. These new mathematical function essential consider the convential mathematical functions with additional flat losses over the passband of the transmit and reflected signal. Several combinations of these mathematical functions define the set of new filter responses. In addition, these mathematical responses can be tailored to adjust the actual flatness of the in-band filter. This last modification shown to be very useful to obtain a further reduction of the required Q of the resonator and therefore its size. All the proposed mathematical functions can be then expanded to result in a transversal network as in conventional filters (although the values defining the transversal network are now complex).

The following part of the chapter, entitled *Topologies* in the diagram below, uses the transversal network to define suitable filter solution space topologies. This is essentially topologies where the filters are coupled to each other in feasible way. The resulting topologies or procedures to go to such space filter solutions also substantially depends on the initial mathematical function proposed. This results in different approaches to obtain the final filter topology. The three techniques, referred as *direct synthesis, strategies for network transformation* and *optimization*. All these approaches are complementary and can be used together to finally obtain the desired topology. In fact the three approaches are used in the design of the three filter prototypes described in chapter three. These technique result also very useful for a better undertanding of the lossy filters and allow to obtain important desing rules, such as the minimum required Q for a certain filter response, or the best achievable filter performance for a given Q. Note that this would directly related with the required resonantor, these are size and/or technology to be used. It is also necessary to mention here that all the lossy filter topologies obtained from the developed techniques result in conventional filter networks like plus an additional resistive network coupled to it.

The third chapter present the desing of three different filters using the lossy synthesis approach, this is the mathematical description and definition of the final topologies of the filter following all the new developments of chapter two. This results in three filters, two filters with planar technologies and one filter based on cavity resonators. Although some parts of the filter design are substantially equal to a conventional filter design, the design of the resistive network and coupling to the conventional network it is a new issue that has been addressed and systematized. The implementation of this resistieve network would depend on the tecnology to be used, as will be reported along the document, and it is certainly a research line where further exploration can be done. The developed filters have been then fabricated and extensively measured. Measurements show the viability of this approach and stability over temperature.

The last chapter, chapter four, summarizes conclusions and outlines the future research lines opened along the findings of this work.

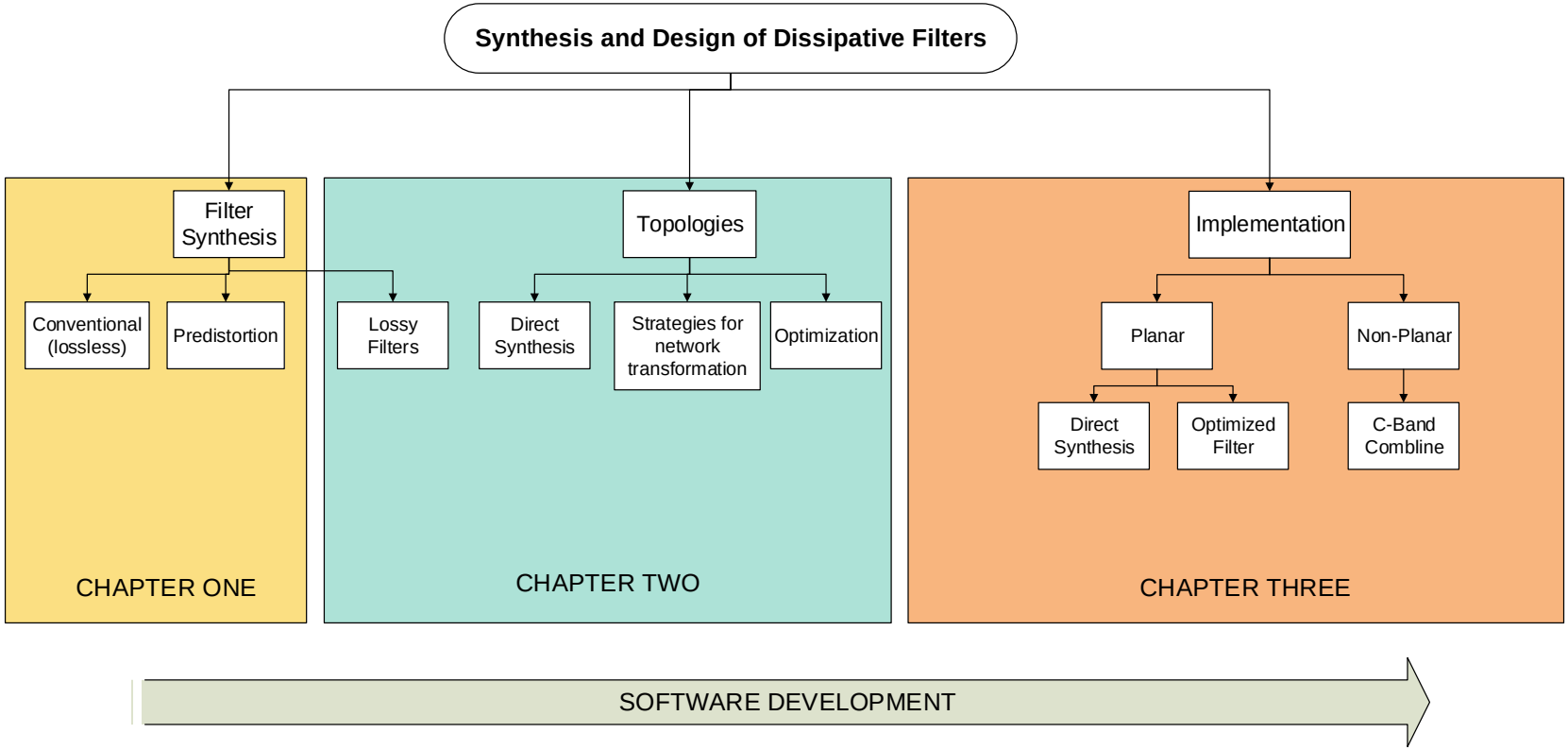

Diagram: outline of the Thesis contents

1 CHATER I: THEORETICAL BACKGROUND ON FILTER SYNTHESIS

This chapter gives a general overview of the theoretical background and tools used throughout the thesis for the development of novel synthesis techniques for dissipative filters. It starts by presenting the conventional parameters that defines the filter response, and their mathematical formulation by means of characteristic polynomials. The basic existing synthesis techniques based on a circuit approach and on a matrix approach are introduced. For the circuit approach only a brief introduction is outlined since this method will be barely used along the thesis. In contrast, the matrix approach is presented in details, since this approach will be the base of the developed procedure and main contribution of this thesis. In particular, the synthesis of (N+2)x(N+2) coupling matrix in its transversal initial topology. Transformation of the somehow impractical transversal topology in more adequate network topology is described and presented in Chapter 2 and in the Appendices 1-5.

Additionally, this first chapter presents a review of the existing synthesis techniques of dissipative filters. This is the synthesis techniques of predistorted responses, in all its variations: *conventional predistortion*, *partial predistortion* and *adaptive predistortion*, and the several approaches on the *so called* synthesis techniques of lossy filters.

This chapter finally presents a conclusion section which summarizes the advantages and disadvantages of the presented methodologies. These conclusions will be confirmed throughout the thesis and updated when necessary.

1.1 Filter transfer function

This section outlines the general specification parameters that are used to define the performance of any filter. These parameters will be widely used along the thesis and although those are very well-known, their definition may differ from the conventional one by considering the scope of dissipative filters. See also Fig. 3 as a reference.

- Passband (1) defines the region of frequencies where the filter allows the transmission of the signal.
- Insertion loss (2) defines the minimum value of the transmission parameter in the passband.
- Passband attenuation ripple (3) defines the insertion loss variation of the filter through the passband.
- Flatness in the passband or rounding in the passband (4) refers to the insertion losses in the passband versus frequency. Note that this only applies in filters with a finite Q response.
- Stopband (5) refers the portion of the frequency spectrum that is blocked by the filter, whether it is absorbed or reflected.
- Out of band attenuation (6) is defined as the amount of energy that is absorbed or reflected by the filter at a certain frequency in the stopband. It is also called rejection. Filters designed using classical synthesis techniques normally reflect the energy in the stopband, rather than absorb it.
- Return loss (7) defines the maximum value of the reflection parameter in the passband of the filter.
- Transmission zeros (8). They may exist or not and consists on the inclusion of zero transmission frequency points in order to increase the rejection in a certain frequency range.

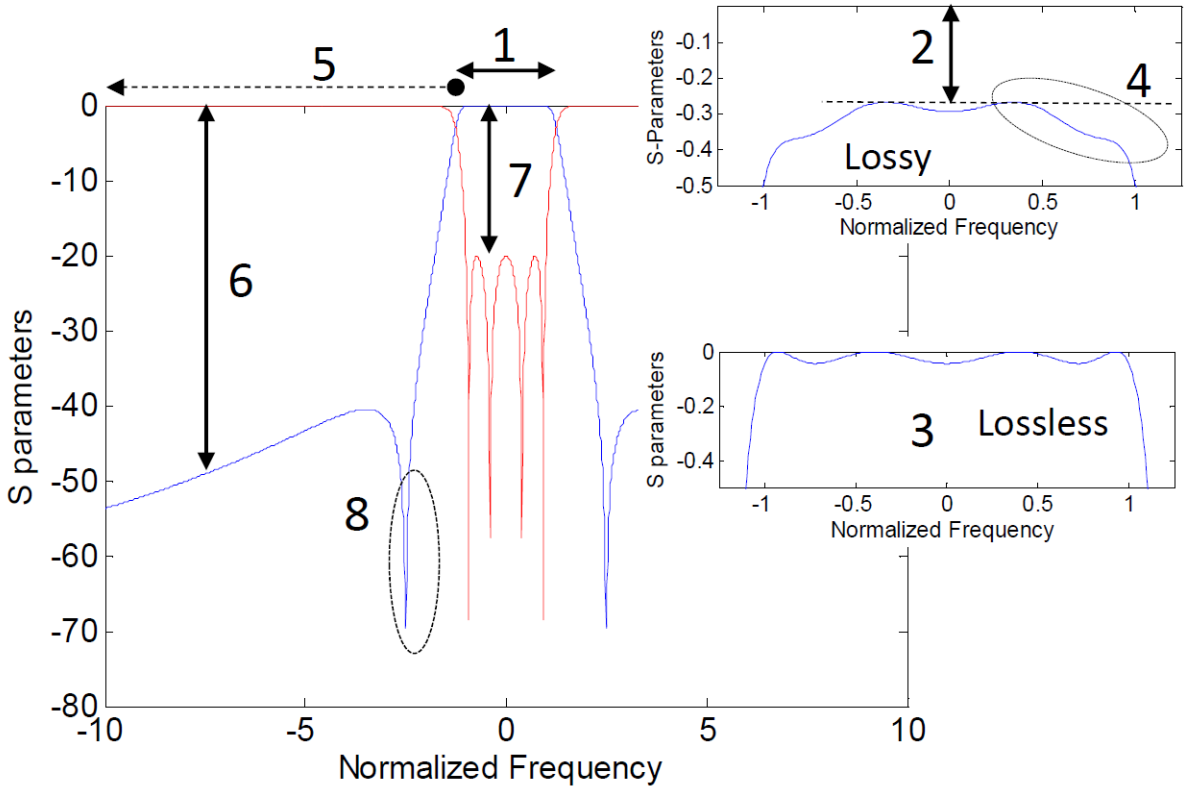

Fig. 3 - Filter response with referred parameters

1.2 Principles of Synthesis Techniques: Circuit and Matrix Approach

Most microwave filters can be represented by a two-port network as outlined in Fig. 4. For the majority of existing synthesis techniques, this network is assumed to be lossless, in other words, the filter would be composed by non-dissipative components.

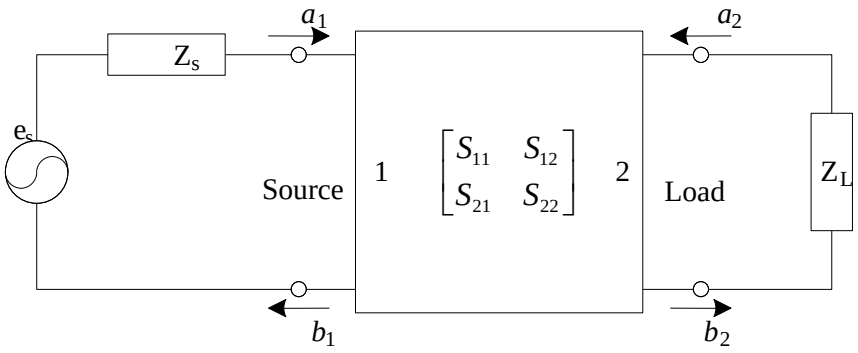

Fig. 4 - Equivalent circuit of a two port network

As usually done in microwave technology the two port network can be characterized by its scattering matrix. In the case of a lossless filter the scattering matrix of a filter of order *N* can be represented by the filter *characteristic polynomials*, *P(s)*, *F(s)* and *E(s)* [1]:

$$\begin{bmatrix} S_{11}(s) & S_{12}(s) \\ S_{21}(s) & S_{22}(s) \end{bmatrix} = \frac{1}{E(s)} \begin{bmatrix} \frac{F(s)}{\varepsilon_r} & \frac{P(s)}{\varepsilon} \\ \frac{P(s)}{\varepsilon} & \frac{(-1)^N F(s)^*}{\varepsilon_r} \end{bmatrix} \quad (1)$$

where ε and ε_r are constant values. The roots of *P(s)* and *F(s)* correspond to the transmission and reflection zeros respectively, and all their roots lie along the imaginary axis in conjugate pairs. The polynomial *E(s)* is the denominator of the reflection and transmission coefficients and it must be strictly Hurwitz, i.e., all its roots must lie in the left half side of the *s* plane.

At this point it is also worth to mention that the *characteristic polymonials* are defined in the low pass prototype [2], being therefore the variable *s* the Laplace parameter, which is related with the normalized frequency as $s=j\Omega$.

The synthesis will therefore consist in the process to define a two port network with a scattering matrix in the form of (1). Following in this section, the two of the most often used synthesis approaches for lossless filters is presented: *Circuit Approach* and *Coupling matrix synthesis of filter networks*.

1.3 Synthesis of Network. Circuit Approach

Using the notation above, the synthesis of a filter network by means of a circuit approach may be outlined as follows:

1. From the filter requirements the transfer function is defined as the scattering parameter S_{21}:

$$S_{21}(s) = \frac{P(s)/\varepsilon}{E(s)} \quad (2)$$

2. Using the unitary condition of a lossless network:

$$|S_{11}|^2 + |S_{21}|^2 = 1 \quad (3)$$

the reflection coefficient results in the fractional form

$$S_{11}(s) = \frac{F(s)/\varepsilon_r}{E(s)} \quad (4)$$

3. From the reflection coefficient, the input impedance *Z(s)* or admittance *Y(s)* of the filter network is obtained. The input impedance as a function of the *characteristic polynomials* results:

$$Z(s) = \frac{E(s) + F(s)/\varepsilon_R}{E(s) - F(s)/\varepsilon_R} \tag{5}$$

4. Once the input impedance or admittance is known, one can determine the type and value of the circuit elements using the well-known *element extraction* method [2][3][1].

Using this technique engineers have developed many direct synthesis methods, that is, obtaining specific network topologies for a given type of transfer functions. For example, cascaded quadruplet sections are used to obtain symmetric transmission zeros [4].

Circuit transformation techniques may then be applied to find alternative network topologies that give the same frequency response.

1.4 Example of a synthesis network

An illustrative example below it is shown the synthesis of a conventional ladder network by using the element extraction circuit approach. Although this is a widely reported procedure, here it is also used to introduce the following section on coupling matrix approach.

The procedure starts by selection of the characteristic polynomials. This case considers a 3rd order Chevyshev filter with 15 dB return losses:

$F(s) = s^3 + 0.75s$
$E(s) = s^3 + 1.787s^2 + 2.34s + 1.38$
$P(s) = 1$, Note that this value is 1 because there is not transmission zeros

Then equation (5) is used to write down the input impedance:

$$Z(s) = \frac{2s^3 + 1.787s^2 + 3.14s + 1.38}{1.787s^2 + 1.59s + 1.38}$$

The element extraction technique results in a ladder network as in figure below.

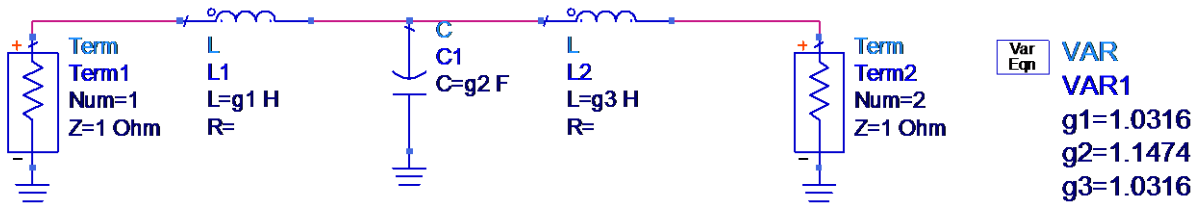

Fig. 5 - Ladder topology of a 3rd order Chebyshev low pass prototype filter.

As usually required in microwave application the equivalent circuit based on lumped components needs to be transformed for an implementation based on distributed elements [2]. This transformation may consist, as initial step, on the introduction of impedance/admittance inverters in order to transform the ladder topology in an eventually coupled resonator topology. This results in a filter topology as the one in Fig. 6.

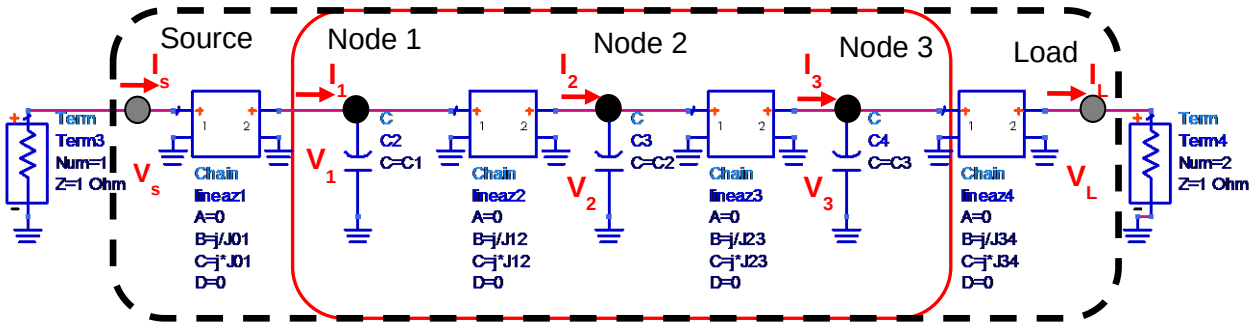

Fig. 6 - Coupled resonators topology of a 3rd order Chebyshev low pass prototype filter.

The general matrix of a 3x3 network relates the current getting into the node I_i (indicated as circle in the figure above) with the current dropped at the corresponding node V_i [5].

$$\begin{bmatrix} I_1 \\ I_2 \\ I_3 \end{bmatrix} = \begin{bmatrix} Y_{11} & Y_{12} & Y_{13} \\ Y_{21} & Y_{22} & Y_{23} \\ Y_{31} & Y_{32} & Y_{33} \end{bmatrix} \begin{bmatrix} V_1 \\ V_2 \\ V_3 \end{bmatrix}$$

For the circuit above, without including the source and load neither their couplings (admittance inverters) with the resonator, squared in red, the resulting admittance matrix is:

$$\begin{bmatrix} I_1 \\ I_2 \\ I_3 \end{bmatrix} = \begin{bmatrix} sC_1 & -jJ_{12} & 0 \\ -jJ_{12} & sC_2 & -jJ_{23} \\ 0 & -jJ_{23} & sC_3 \end{bmatrix} \begin{bmatrix} V_1 \\ V_2 \\ V_3 \end{bmatrix}$$

Which can be extended to include the source and the load as:

$$\begin{bmatrix} I_s \\ I_1 \\ I_2 \\ I_3 \\ I_L \end{bmatrix} = \begin{bmatrix} G_s & -jJ_{01} & 0 & 0 & 0 \\ -jJ_{01} & sC_1 & -jJ_{12} & 0 & 0 \\ 0 & -jJ_{12} & sC_2 & -jJ_{23} & 0 \\ 0 & 0 & -jJ_{23} & sC_3 & -jJ_{34} \\ 0 & 0 & 0 & -jJ_{34} & G_L \end{bmatrix} \begin{bmatrix} V_s \\ V_1 \\ V_2 \\ V_3 \\ V_L \end{bmatrix}$$

This admittance matrix it is also referred as the N+2xN+2 admittance matrix, where N is order of the filter, 3 in this case. The N+2xN+2 admittance matrix can then be written down as the summation of three matrices,

$$\begin{bmatrix} G_s & 0 & 0 & 0 & 0 \\ 0 & 0 & 0 & 0 & 0 \\ 0 & 0 & 0 & 0 & 0 \\ 0 & 0 & 0 & 0 & 0 \\ 0 & 0 & 0 & 0 & G_L \end{bmatrix} - j \begin{bmatrix} 0 & J_{01} & 0 & 0 & 0 \\ J_{01} & 0 & J_{12} & 0 & 0 \\ 0 & J_{12} & 0 & J_{23} & 0 \\ 0 & 0 & J_{23} & 0 & J_{34} \\ 0 & 0 & 0 & J_{34} & 0 \end{bmatrix} + s \begin{bmatrix} 0 & 0 & 0 & 0 & 0 \\ 0 & C_1 & 0 & 0 & 0 \\ 0 & 0 & C_2 & 0 & 0 \\ 0 & 0 & 0 & C_3 & 0 \\ 0 & 0 & 0 & 0 & 0 \end{bmatrix}$$

where the first matrix includes the source and the load, the second matrix include the coupling between resonators and the third matrix accounts for the frequency dependence.

The values of the matrix above can be scaled without affecting the relation between I_i and V_i [1] therefore without affecting the filter performance and obtaining the following matrices:

$$\begin{bmatrix} 1 & 0 & 0 & 0 & 0 \\ 0 & 0 & 0 & 0 & 0 \\ 0 & 0 & 0 & 0 & 0 \\ 0 & 0 & 0 & 0 & 0 \\ 0 & 0 & 0 & 0 & 1 \end{bmatrix} - j \begin{bmatrix} 0 & M_{01} & 0 & 0 & 0 \\ M_{01} & 0 & M_{12} & 0 & 0 \\ 0 & M_{12} & 0 & M_{23} & 0 \\ 0 & 0 & M_{23} & 0 & M_{34} \\ 0 & 0 & 0 & M_{34} & 0 \end{bmatrix} + s \begin{bmatrix} 0 & 0 & 0 & 0 & 0 \\ 0 & 1 & 0 & 0 & 0 \\ 0 & 0 & 1 & 0 & 0 \\ 0 & 0 & 0 & 1 & 0 \\ 0 & 0 & 0 & 0 & 0 \end{bmatrix}$$

It is now clear, from this notation, that all the information on the filter can be gathered into the coupling matrix, which values M_{ij} are the normalized coupling values.

The resulting coupling matrix for the characteristic polynomials above would result on:

$$\begin{bmatrix} 0 & 0.9453 & 0 & 0 & 0 \\ 0.9453 & 0 & 0.8779 & 0 & 0 \\ 0 & 0.8779 & 0 & 0.8779 & 0 \\ 0 & 0 & 0.8779 & 0 & 0.9453 \\ 0 & 0 & 0 & 0.9453 & 0 \end{bmatrix}$$

Although more details will be given in the following section, during the thesis the filter topology will be indicated as appears in the following figure, Fig. 7, where the black circles corresponds to the resonators forming the filter, the grey circles represent the load and the source, respectively and the connecting lines indicate the coupling resonators. Note that in this topology there is no cross-coupling, this is coupling between non-adjacent resonators, and therefore results in a inline topology [1][2][3].

Fig. 7 - Nodal notation of an inline three order filter

This section concludes that although the synthesis technique based on a circuit approach is suitable for microwave filters it is more convenient to obtain directly the coupling matrix of the filter topology, since this directly relates with the space solution of the final configuration.

1.5 Coupling Matrix Synthesis of Filter networks

In contrast with the circuit synthesis approach above where the *characteristic polynomials* of (1) are used to obtain the input impedance and its circuit network afterwards, the matrix approach uses these polynomials to obtain the coupling matrix of the filter. As in example of section 1.4 we will use the coupling matrix in its N+2xN+2 format [6], instead of the also classical NxN format. Note that the later does not consider possible couplings between the source and the load. Moreover as will be seen in the following chapter the existence of the source and load nodes in the coupling matrix is convenient on the synthesis of dissipative filters.

This essentially consists on transforming the equivalent circuit of Fig. 8a to the equivalent circuit of Fig. 8b, which is now defined by and *(N+2)x(N+2)* impedance matrix. The general resulting coupling matrix is now also an N+2 matrix. Fig. 9 outlines the coupling matrix of a filter composed by four resonators. The external elements of the matrix $M_{S,i}$, $M_{i,S}$, $M_{L,i}$ and $M_{i,L}$ correspond to the coupling between the source and load to the resonators. The internal elements of the matrix form the coupling matrix and account for the coupling between resonators. The values on the main diagonal M_{ii} referred to the mutual couplings [1].

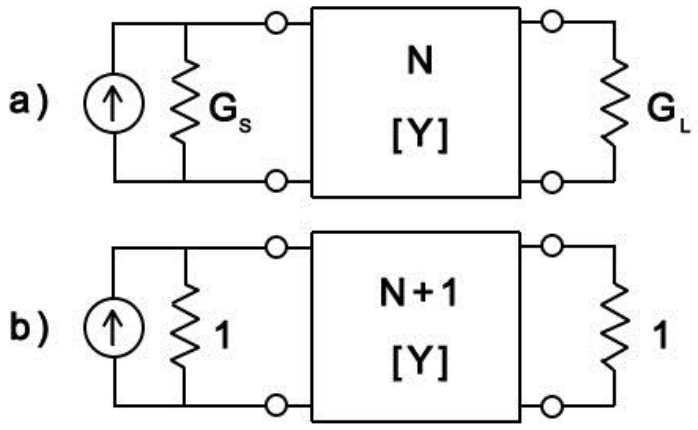

Fig. 8 - Equivalent circuit of a two port network a) represented as an *NxN* impedance matrix. b) represented as an *(N+2)x(N+2)* impedance matrix.

	S	1	2	3	4	L
S	$M_{S,S}$	$M_{S,1}$	$M_{S,2}$	$M_{S,3}$	$M_{S,4}$	$M_{S,L}$
1	$M_{S,1}$	$M_{1,1}$	$M_{1,2}$	$M_{1,3}$	$M_{1,4}$	$M_{1,L}$
2	$M_{S,2}$	$M_{1,2}$	$M_{2,2}$	$M_{2,3}$	$M_{2,4}$	$M_{2,L}$
3	$M_{S,3}$	$M_{1,3}$	$M_{2,3}$	$M_{3,3}$	$M_{3,4}$	$M_{3,L}$
4	$M_{S,4}$	$M_{1,4}$	$M_{2,4}$	$M_{3,4}$	$M_{4,4}$	$M_{4,L}$
L	$M_{S,L}$	$M_{1,L}$	$M_{2,L}$	$M_{3,L}$	$M_{4,L}$	$M_{L,L}$

Fig. 9 - Outline of the N+2xN+2 coupling matrix. Note that the inner part corresponds to the NxN coupling matrix.

The synthesis procedure starts by recalling the scattering parameters of the network as a function of the characteristic polynomials (1). The scattering matrix can then be transform to the Y matrix of Fig. 9b, by following matrix conversion from S to Y [5]. Doing so, the admittance matrix of the two port network of Fig. 9b might be written as:

$$\begin{bmatrix} Y_{11}(s) & Y_{12}(s) \\ Y_{21}(s) & Y_{22}(s) \end{bmatrix} = \frac{1}{Y_d(s)} \begin{bmatrix} Y_{11n}(s) & Y_{12n}(s) \\ Y_{21n}(s) & Y_{22n}(s) \end{bmatrix} \tag{6}$$

where the numerators and denominator of the admittance matrix may be written as a function of the characteristic polynomials as detailed in the following set of equation:

$$Y_d(s) = \frac{(E(s) + F(s)/\varepsilon_r)(E(s) + (-1)^N F^*(s)/\varepsilon_r) - (P(s)/\varepsilon)^2}{2E(s)}$$

$$Y_{21n}(s) = Y_{12n}(s) = P(s)/\varepsilon \tag{7}$$

$$Y_{d11n}(s) = \frac{(E(s) - F(s)/\varepsilon_r)(E(s) + (-1)^N F^*(s)/\varepsilon_r) + (P(s)/\varepsilon)^2}{2E(s)}$$

$$Y_{d22n}(s) = \frac{(E(s) + F(s)/\varepsilon_r)(E(s) - (-1)^N F^*(s)/\varepsilon_r) + (P(s)/\varepsilon)^2}{2E(s)}$$

* Note that N accounts for the order of the filter.

** Also note that we used a normalized source and load impedance to 1.

As outlined in (7) it results in a set of rational fractions where both the numerator and the denominator are polynomials. In such a case we may perform *partial fraction expansion* (also known as *partial fraction decomposition*) [8]. This operation consists in expressing the fraction as a sum of polynomials with a simpler denominator. From the nature of the characteristic polynomials, the

resulting rational fraction above can be decomposed in a sum of polynomials where the numerators are residuals and the denominators are first order polynomials of first order. This is illustrated in the expression below, where r_i are the residuals and p_i are the poles of the rational function.

$$\frac{B(s)}{A(s)} = \frac{r_1}{s-p_1} + \frac{r_2}{s-p_2} + \frac{r_3}{s-p_3} + \cdots + \frac{r_4}{s-p_4} \tag{8}$$

By applying this to the rational functions of the two port admittance matrix, as in (7), the decomposition results on [1] [6]:

$$\begin{bmatrix} Y_{11}(s) & Y_{12}(s) \\ Y_{21}(s) & Y_{22}(s) \end{bmatrix} = \frac{1}{Y_d(s)} \begin{bmatrix} Y_{11n}(s) & Y_{12n}(s) \\ Y_{21n}(s) & Y_{22n}(s) \end{bmatrix} = \sum_{k=1}^{N} \frac{1}{(s-j\lambda_k)} \begin{bmatrix} r_{11k} & r_{12k} \\ r_{21k} & r_{22k} \end{bmatrix} \tag{9}$$

where r_{ijk} are the residues and λ_k are the eigenvalues. The eigenvalues are obtained from the roots of $Y_d(s)$, $j\lambda_k$, and in case of characteristic polynomials corresponding to an ideal lossless response result in purely imaginary roots, therefore purely real eigenvalues. Note that this will not be the case in dissipative filters, detailed in the following chapter, where the eigenvalues will became complex.

The residues can be obtained from

$$r_{ijk} = \left. \frac{Y_{ijn}(s)}{Y'_d(s)} \right|_{s=j\lambda_k} \tag{10}$$

where $Y'_d(s)$ is the first derivative $Y_d(s)$.

Note that the conclusions above are very significant [6] and state that any response following the performance of the characteristic polynomials in (1) can be synthesized by a network consisting on shunt connection of first order filters, i.e., resonators. This type of topology is known as *transversal topology*.

To go further on this statement and Fig. 10.a outlines an equivalent circuit network of a canonical transversal filter. Considering the topology of a four order filter the resulting coupling matrix is:

$$\begin{bmatrix} 0 & M_{S1} & M_{S2} & M_{S3} & M_{S4} & M_{SL} \\ M_{1S} & M_{11} & 0 & 0 & 0 & M_{1L} \\ M_{2S} & 0 & M_{22} & 0 & 0 & M_{2L} \\ M_{3S} & 0 & 0 & M_{33} & 0 & M_{3L} \\ M_{4S} & 0 & 0 & 0 & M_{44} & M_{4L} \\ M_{LS} & M_{L1} & M_{L2} & M_{L3} & M_{L4} & 0 \end{bmatrix}, \tag{11}$$

indicating that each resonator is only coupled to the source and load and there are no couplings between resonators.

Considering the equivalent circuit model of each resonator coupled to the source and load of Fig. 10.b, we can obtain the two port admittance matrix of the network as [1]:

$$[Y] = \begin{bmatrix} Y_{11}(s) & Y(s) \\ Y_{21}(s) & Y_{22}(s) \end{bmatrix} = j \begin{bmatrix} 0 & M_{LS} \\ M_{SL} & 0 \end{bmatrix} + \sum_{k=1}^{N} \frac{1}{sC_k + jB_k} \begin{bmatrix} M_{Sk}^2 & M_{Sk}M_{Lk} \\ M_{Sk}M_{Lk} & M_{Lk}^2 \end{bmatrix} \tag{12}$$

Note that the elements of the admittance matrix Y_{ij} *(s)* can be obtained as a function of the *characteristic polynomials* [1].

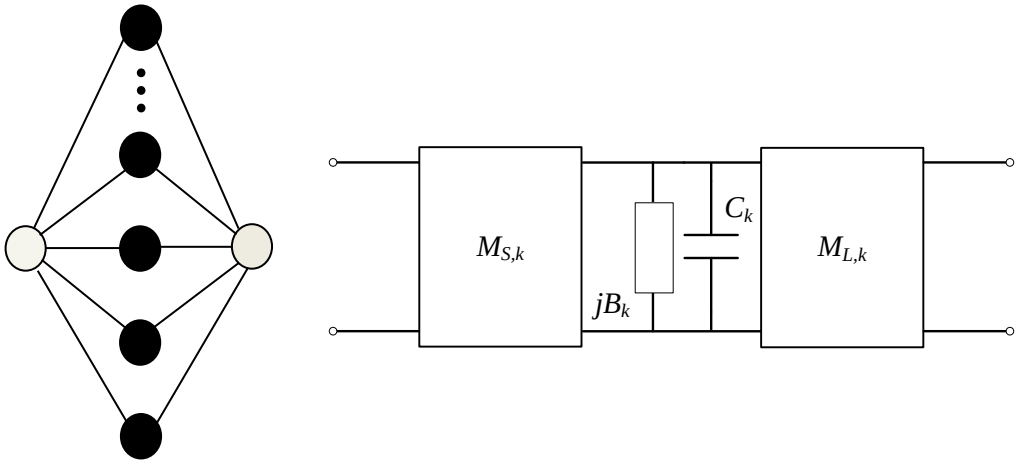

Fig. 10 - a) Equivalent network of a transversal filter of order N. S and L represent the source and the load, $M_{S,L}$ the coupling between the source and the load, and the numbered boxes (from 1 to N) contain the resonator and coupling of the resonator to the source and load. b) Equivalent circuit of the resonator and its couplings to the source and load.

Now the outer terms of the coupling matrix M_{kS}, M_{Sk}, M_{kL} and M_{Lk} can be found from the residues of the admittance matrix terms, as outlined in (10).

The other elements in matrix M, that is its diagonal elements M_{kk} can be found by equating the real and imaginary part of the elements of left hand side with the elements of the right hand side of (9) and (12). Doing so results in:

$$C_k = 1, \qquad B_k(\equiv M_{kk}) = -\lambda_k \tag{13}$$

Therefore, the diagonal of the coupling matrix is formed by the eigenvalues of the coupling matrix.

As previously mentioned the conclusion resulting from this section are very significant and will be also valid for dissipative filters. This means than any filter response either lossless or lossy can be synthesizes as a transversal network.

Nevertheless in real implementation this topology results impractical and more suitable topologies need to be obtained. In a coupling matrix representation of the filter topologies this can be done by means of *matrix transformation,* also referred in the following section as Coupling matrix reduction.

1.5.1 Coupling matrix reduction

By applying coupling matrix reduction technique one can obtain different network topologies for a given transfer function, i.e., for a given set of *characteristic polynomials*. The synthesized transversal network of Fig. 10a can be transformed into different topology as the ones outlined in the current section.

There are different sets of matrix reduction techniques. All those techniques or operations have in common that operation on the coupling matrix and whichever is the transformation the resulting eigenvalues of the new matrix remain constant. Otherwise we will be obtaining a different filter response, i.e., the transfer and reflection characteristics remain unchanged.

One of the most common filter topologies for real implementation is the so called *Folded Topology*. The following figure, Fig. 11, outlines the folded topology for a seventh order filter and its corresponding coupling matrix, in Figure 12. In this figure the couplings between adjacent resonators are indicated in solid lines whereas the couplings between nonadjacent resonators, also known as *cross-couplings* are indicated in dashed line. The former correspond to the values in the upper and lower diagonal, whereas the later are off the diagonal.

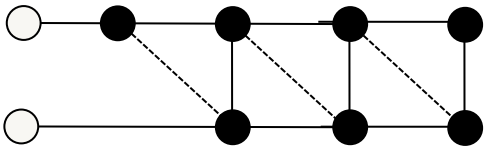

Fig. 11 Equivalent circuit model of a 7th order folded network.

	1	2	3	4	5	6	7
1	s	m					xa
2	m	s	m			xa	xs
3		m	s	m	xa	xs	
4			m	s	m		
5			xa	m	s	m	
6		xa	xs		m	s	m
7	xa	xs				m	s

Non-zero elements

s – Self coupling
m – Main coupling
xa and xs - cross-coupling

Fig. 12 - Outline of a folded coupling matrix, corresponding to the network of Fig. 12.

1.5.2 From Transversal coupling matrix to Folded coupling matrix

Although the recipe for the transformation above it is well reported elsewhere [1], matrix transformation will be widely used on the way to find the more suitable topologies in dissipative filters and it is also the key to obtain the desired loss distribution along the network.

This section shows the procedure to obtain a folded coupling network from the resulting transversal network. Although, depending on the technology, other topologies might be more convenient to the filter implementation, the transformation from the transversal coupling matrix to the folded coupling matrix (TCM to FCM) shows the basic for the circuit transformation.

To do that, we use the concepts of matrix rotations, describe in Appendix 1. This technique essentially consists in moving the elements of the matrix in such a way that eigenvalues of the matrix are maintained and the transfer and reflection characteristics remain unchanged.

To obtain the equivalent FCM from a general *N+2*x*N+2* coupling matrix M it is necessary to turn zero the elements of the matrix which do not correspond to couplings existing in a folded topology. Next figure, Fig. 13, considers a 7x7 coupling matrix (corresponding to an N=5). The numbers in circles indicate the order in which the elements of the matrix are turn to zero. Note that the elements of the matrix that are not in circles (M_{ij}) correspond to the final elements defining the coupling matrix.

	1	2	3	4	5	6	7
1	M_{11}	M_{12}	4	3	2	1	M_{17}
2	M_{12}	M_{22}	M_{23}	9	8	M_{26}	M_{27}
3	4	M_{23}	M_{33}	M_{34}	M_{35}	M_{36}	5
4	3	9	M_{34}	M_{44}	M_{45}	10	6
5	2	8	M_{35}	M_{45}	M_{55}	M_{56}	7
6	1	M_{26}	M_{63}	10	M_{56}	M_{66}	M_{67}
7	M_{17}	M_{27}	5	6	7	M_{67}	M_{77}

Fig. 13 - Indicates the order in which the elements of an 7x7 coupling matrix are turned to zero in order to obtain a *FCM*.

In order to give more details on the procedure to obtain the FCM, the following table outlines each step of the Fig.13, indicating the pivot and element turn to zero in each step. The procedure to obtain the rotation angles to achieve zero at the given positions is described in Appendix 1.

St	***m***	***n***	***i***	***j***
1	1	6	5	*6*
2	1	5	4	*5*
3	1	4	3	*4*
4	1	3	2	*3*
5	3	7	3	*4*
6	4	7	4	*5*
7	5	7	5	*6*
8	2	5	4	*5*
9	2	4	3	*4*
10	*4*	*6*	*2*	*3*

Note that:

1. Only the elements of the i row and j column are affected by the matrix rotation
2. If the elements [k,i] and [k,j] or [I,k] and [j,k] are zero then these element remain zero after the rotation.

1.5.3 Additional topologies

Other topologies may be found using analogous procedures as the one described above and by applying matrix rotation techniques [1]. The selection of the topology may depend on the technology to be used, on space restrictions and also on temperature requirements for instance. Although in the document is not reported the way to obtain such topologies, the following figure outlines some of the more conventional ones which will be referred along the thesis.

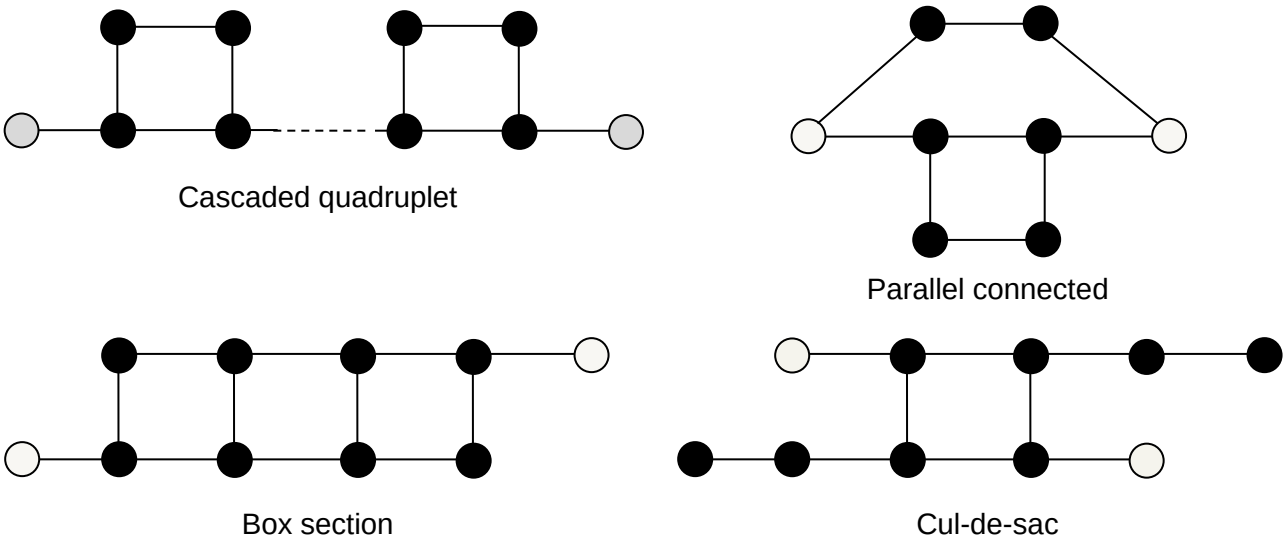

Fig. 14 - Outlined of conventional filter topologies

At this point it is also worth to mention that, the commercial software (www.tsc.upc.edu/lossyfilters) developed, in the framework of the ESA project listed in the introduction, all the conventional synthesis techniques based on coupling matrix described above and also all the matrix transformation depicted in Fig.14..

1.6 Dissipation effects

Although the procedures outlined above assume lossless components, they are widely used for synthesis and design of filters with limited Q, and usually the consequences of existing losses are evaluated afterwards. To do that one could simply add a positive real factor σ to the purely imaginary variable $s = j\omega$, on the transfer function expression $S_{21}(s)$. This is equivalent to move all the poles of the transfer function to the left. The value of σ for a band pass filter can be expressed as:

$$\sigma = \frac{1}{Q \cdot FBW} \tag{14}$$

where *FBW* is the fractional bandwidth of the filter. Fig. 15 illustrates, for a six order filter, the dissipation effects by shifting the poles in the *s* plane:

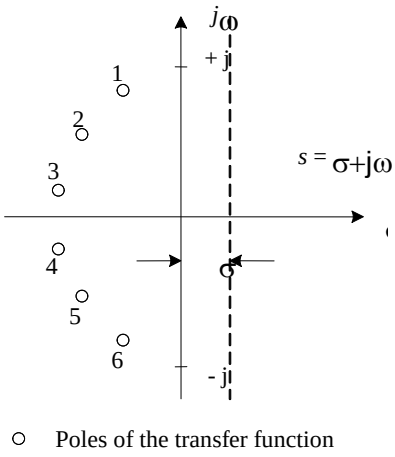

Fig. 15 - Displacement of the poles of the transfer function due to the dissipative effects.

Alternatively one could include dissipative elements *R* and *G* on the purely reactive elements of the synthesized resulting network. In any case, the effects of dissipation in a bandpass filters are:

- The insertion loss increases
- A rounding off of the insertion loss curve at the band edges occurs. This diminishes the width of the passband and reduces the selectivity of the filter.
- Transmission and reflection zeros are less distinct.

These three features are more prominent when the losses increase or when the fractional bandwidth of the filters decrease.

Figure 16 depicts the effects of losses in the transfer function and reflection coefficient for a six order Quasi-Elliptic filter of 14 % fractional bandwidth, with a single pair of transmission zeros. The black curve corresponds to the ideal response of the filter, this is *Q*=*Inf*, whereas the blue, green and red curves represent the filter response for finites Qs of 1000, 300 and 100, respectively.

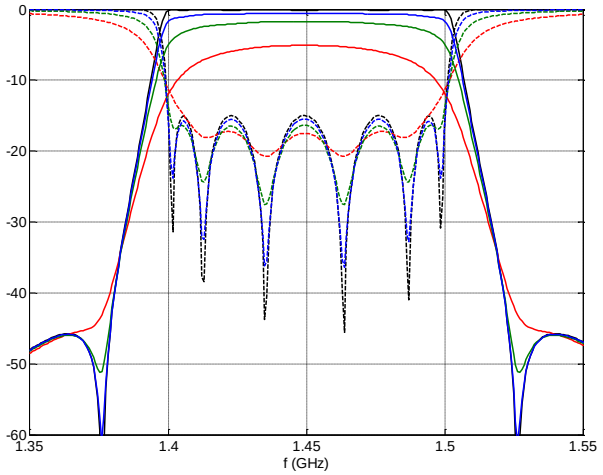

Fig. 16 - Transfer and reflection coefficients of a band pass filter as a function of its Q.

These effects affect in the overall system performance. In some situations is the effects are such that is necessary to use advanced synthesis techniques that do not ignore the resonator losses.

1.7 Synthesis Techniques of Dissipative Filters

The different approaches for the synthesis of lossy filters seek to design filters in such a way that losses are taken into account in the synthesis process. By doing this, one can avoid most of the unwanted effects that come up in filters implemented from a synthesized transfer function that assumes lossless components (see Fig. 16).

Filter design is usually a tradeoff between the insertion loss, loss and group delay variation in the passband, isolation, physical dimensions and mass. This is also true in the case of using synthesis techniques of lossy filters. In this case one usually tolerates an additional offset in the insertion loss, in order to obtain a close to ideal frequency response (high selectivity, isolation and flat amplitude response in the passband) of the filter. This is valid in applications where the in-band insertion loss is not a critical parameter, such as in the channelizer, where -as long as the IL is not excessive- it can be recovered by the gain of the LNA without having impact on the system performance.

Moreover these approaches not only improve the filter performance but may also significantly reduce the size and mass of the physical filter, which in satellite applications are very critical considerations.

The following sections introduce the existing techniques reported for synthesis of lossy filters. They can be classified in: *Predistortion Techniques*, *Reflection Mode Predistortion Techniques* and *Synthesis Techniques with Unequal Q distribution*. The basic idea of these techniques is briefly

described, and the scientific papers where they are detailed are referenced. An outline of the merits and drawbacks of each technique is also pointed out.

1.8 Predistortion synthesis Techniques

The basic idea of predistortion consists of using the *a priori* information of the finite Q of the resonators to alter the lossless transfer function in such a way that the ideal response is recovered when dissipation is included [9][10][11]. As stated above, the dissipation effects can be modeled by a shift of the imaginary axis of the complex plane, $j\omega$, to the right by an amount of σ. Note that this can also be seen as a shifting of the poles and zeros to the left of σ of the complex plane. Figure 17.a shows how the poles of the transfer function are shifted in order to predistort and Fig. 17.b shows how after introducing the dissipation effects the pole position is completely recovered [1].

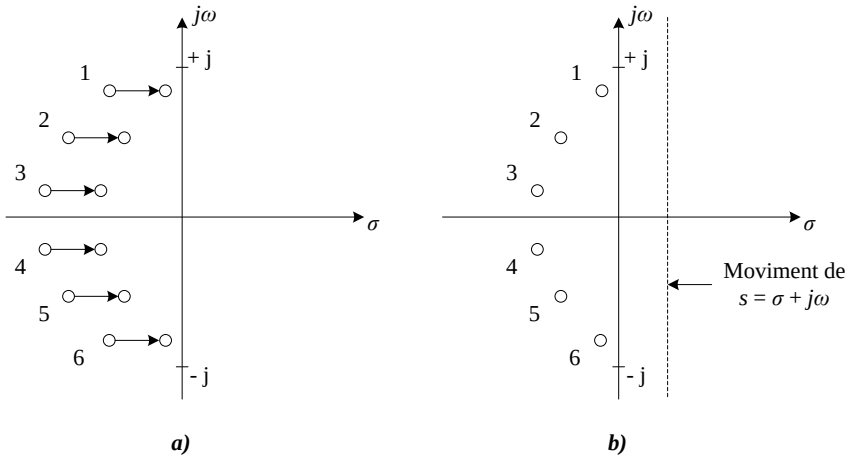

Fig. 17 - a) Position of the poles before and after predistortion. b) position of the predistorted poles affected by the dissipation effects.

The new predistorted transfer function $S_{21}^{p}(s)$ is then synthesized as a lossless network by applying any of the procedures outlined in section 1.5.

Therefore the steps describing the predistortion synthesis can be outlined as:

1. Define the transfer function as the scattering parameter S_{21}, using the *characteristic polynomials*.
2. Determine the loss factor σ from the finite Q of the resonator as in (14)
3. Define the predistorted transfer function S_{21}^{p} by moving all the poles to the right, this is

$$E(s) = c\big(s - (r_1 - \sigma)\big)\big(s - (r_2 - \sigma)\big) \dots (s - (r_n - \sigma)) \quad (15)$$

where r_i are the poles of the non-predistorted transfer function.

4. Obtain the (predistorted) reflection function of the filter (S_{11}^p) using the unitary condition of a lossless network, (3).
5. From the new (predistorted) *characteristic polynomials* we can use any of the synthesis procedures above to obtain the network and coupling matrix of the synthesized filter.

Since transmission zeros have to show symmetry relative to the imaginary, they cannot be shifted to the same direction on both sides of the imaginary axis, therefore they do not recover their ideal position.

The disadvantage of predistortion techniques is that the flat passband and high selectivity is achieved by increasing the reflected power in the passband. This decreases the passband return losses and in practice predistorted filter may require to be cascaded with isolators. Moreover this technique tends to give an undesirable group delay. This penalty on insertion loss, decreased return losses, and undesirable group delay limits this technique for some practical applications [9].

In order to smooth the high insertion loss and reduced return loss variations on the conventional predistortion technique have been reported.

The first one could consist in predistoring the transfer function of the lossy filter to only partially recover its ideal. That is, instead of moving the pole positions to restore a lossless case (infinity Q) move them a fixed amount σ' to emulate the transfer function corresponding to a higher Q_{eff}, higher than the actual Q. In this case the shift to be applied to the poles of the transfers function would be:

$$\sigma' = \frac{1}{FBW}\left(\frac{1}{Q} - \frac{1}{Q_{eff}}\right) \quad (16)$$

Then the resulting *E(s)* polynomial can be read as:

$$E(s) = c\big(s - (r_1 - \sigma')\big)\big(s - (r_2 - \sigma')\big) \dots (s - (r_n - \sigma')) \quad (17)$$

At this point is worth to mention that the shift of the poles (σ or σ') is constrained to *real[s- σ]<0*, otherwise the filter would not be realizable [2].

As an illustrative example Fig. 18 depicts the frequency response of three synthesized transfer functions. Solid and dashed lines represent transmission and reflection frequency response of the filter. Black lines correspond to the lossless synthesized response with a practical Q of 250. In blue and red lines it is shown the full predistorted filter this is using (14) and the partially predistorted filter, using (16), to emulate a filter of Q_{eff}*=1000*.

From Fig.18 we see that predistortion techniques can be used to recover the flatness at the passband of the filter at the expense of increasing the insertion and return losses. Partial predistortion (in red) shows how the flatness of passband is improved in comparison with conventional synthesis (in black), and the return losses are improved in comparison with classical predistortion.

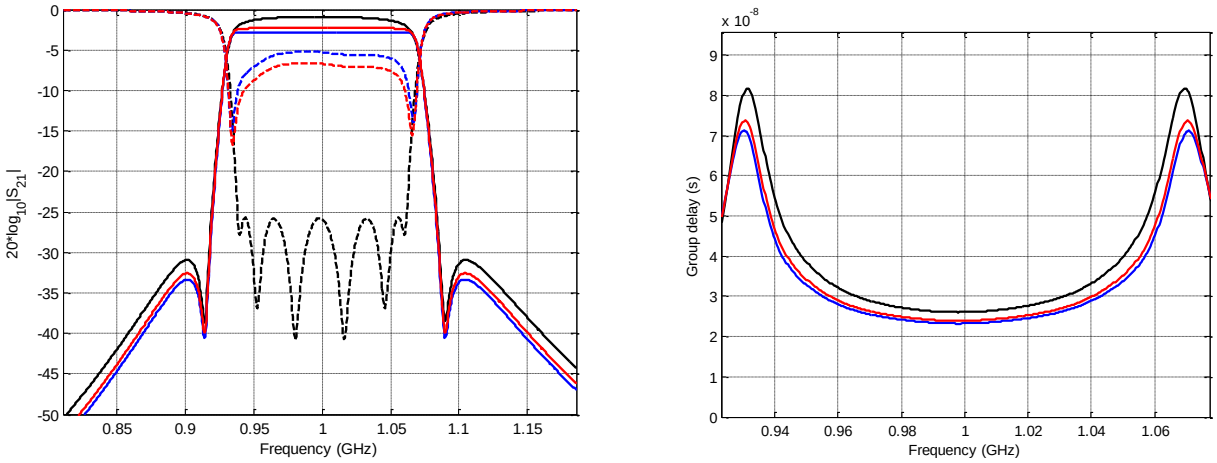

Fig. 18 - Left hand side: Transfer and reflection coefficient for a 6-order Quasi-elliptic filter form with resonators of Q=250 and synthesized using conventional techniques (black line), using classical predistortion (blue line) and using partial predistortion (red line). The solid and dashed lines correspond to the transfer and reflection coefficient respectively. Right hand side: Group delay.

Disadvantages

Although some have already mentioned throughout the text, the main disadvantage concerning predistortion techniques are outlined in the following points:

- Selectivity improvement is achieved by reflecting power in the passband, as a result severely degrading the return loss, and thus the use of isolators is often required.
- The zeros are not predistorted, thus classical predistortion is only applicable to bandpass filters.
    - Predistortion technique is only applicable to transfer functions with all zeros at infinity (i.e., ladder network realizations). Furthermore, it is not directly applicable to highpass prototypes nor does it yield a good input or output match.
- For higher degree solution the input and output return loss result in asymmetric networks with different values for S_{11} and S_{22}.
- For higher degree solutions a significant price is paid in terms of extra insertion loss above the band-edge loss of the original non-predistorted network.
- Difficult to tune in production environment.

- This is complicated by the fact that return loss is different at the input and output ports.
- Although in today advances in computer-aided tuning techniques, the tuning problem is of lesser concern.

- The (classical) predistortion technique inherently leads to undesirable increase in the group delay.
- Needs the use of two isolators at both ports due to the poor return loss characteristics.

1.8.1 Adaptive predistortion technique

An alternative approach to the predistortion techniques mentioned above consists of performing an *adaptive* predistortion to the poles of the transfer function [2]. That is, displacing each pole of the transfer function by a different amount σ_i. The resulting *characteristic polynomial* containing the poles of the transfer function is:

$$E(s) = c\big(s - (r_1 - \sigma_1)\big)\big(s - (r_2 - \sigma_2)\big) \dots (s - (r_n - \sigma_n)) \tag{18}$$

We can then use an optimization technique to obtain the values of σ_i, in order to adapt into different filter functions. Note that, as occurred in the conventional case, the transmission zeros (roots of *P(s)*) do not change.

This adaptive predistortion technique can be used to obtain predistorted filters with:

- Improved insertion loss
- Equalized group delay

As a consequence this technique can be used to obtain high performance filters with low Q, which could significantly reduce the physical dimensions and mass of the filter. This also enables the possibility of using technologies for the filter implementation not yet considered for space applications.

Since the final predistorted filter is performed by optimization technique, it can be optimized to improve the overall system response, this is considering all the transponder components (not only the channelizer receive filter) on the optimization routine. This is definitely an added value of using the adaptive predistortion technique instead of using the conventional predistortion technique.

1.8.2 Reflection-Mode predistortion techniques

This technique appeared as an alternative to the predistorted transmission filter. In contrast with the predistortion techniques described above, the reflection-mode predistortion technique consists in predistorting the reflection coefficient S_{11}, instead of transmission coefficient S_{21}. Then the

predistorted reflection coefficient is synthesized as a one-port network and converted to a transmission filter using a three-port circulator. Figure 19 shows the network to synthesize coupled to port 2 of a circulator. Note that the reflection coefficient $S_{11}(s)$ of the network results to be the transmission coefficient from port 1 to 3 of the circulator [17].

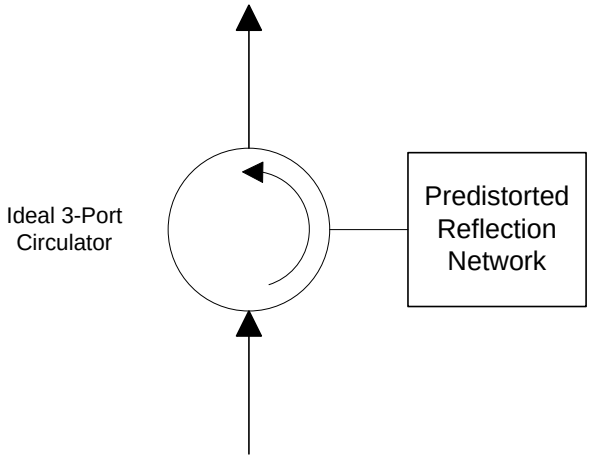

Fig. 19 - Equivalent circuit of a predistorted circuit model with a cascaded circulator [18].

In order to compensate the effects of dissipation, the poles and zeros of S_{11} are shifted to the right by a constant amount σ. The reflection coefficient is also multiplied by a constant $k<1$ to include the resonator losses, and its value must be chosen to result in passive network. Doing so, the predistorted reflection coefficient may be written as:

$$S_{11}(s) \rightarrow kS_{11}(s-\sigma) \tag{19}$$

The value of σ has to be chosen so that at some frequency ω_0 satisfies the following conditions:

$$k^2|S_{11}(j\omega_0-\sigma)|^2 = 1 \tag{20}$$

and

$$\frac{d}{d\omega}|S_{11}(j\omega_0-\sigma)|^2 = 0 \tag{21}$$

Note that the conditions above force the reflection coefficient to be completely reflective at $\sigma=j\omega_0$.

Once we know the values of k, σ and ω_0 the input impedance of the network is formed as:

$$Z_{in}(s) = \frac{1 \pm kS_{11}(s-\sigma)}{1 \mp kS_{11}(s-\sigma)} \tag{22}$$

The resulting fractional polynomial can be then synthesized using conventional element extraction techniques.

Alternatively, for the case of having a symmetric reflection coefficient the input impedance must have a transmission zero pair at $\sigma = \pm j\omega_0$, which can be synthesized through a Brune section [17]. Whereas for the case of asymmetrical reflection coefficient with only a transmission zero at a single frequency, $\sigma = -j\omega_0$ or $\sigma = j\omega_0$, which can be synthesized with a Triplet section [17]. After the extraction of the pair of transmission zeros or single zeros from the input impedance, the remaining impedance, $Z_1(s)$, can be synthesized by means of a ladder network.

However, from a realization point of view it could be useful to replace the ladder network by further cascaded Brune or Triplet sections. To do that, [18] presents an extension of the classical reflection predistortion, that allows to introduce a Brune or Triplet section at any stage of the network. This method is known as a *stage-predistortion*, and consists in predistorting the remaining impedance $Z_1(s)$, [$Z_i(s)$ for the i^{th} step]. The resulting reflection coefficient at i^{th} step is:

$$S_{11}(s-\beta_i)|_i = \frac{1 \pm Z_i(s-\beta_i)}{1 \mp Z_i(s-\beta_i)} \tag{23}$$

As done for the original reflection coefficient (19), the reflection coefficient at ith stage should satisfy:

$$|S_{11}(j\omega_{0i}-\beta_i)|^2| = 1 \quad \text{and} \quad \frac{d}{d\omega}|S_{11}(j\omega_{0i}-\beta_i)|^2 = 0 \tag{24}$$

where β_i is the stage loss and has to be defined in such a way that the passband loss is not altered [17]. ω_{0i} is a frequency close to the passband edge.

By doing so, the series resistances are transformed to be contained in the resonator losses, thus leading to unequal uniform Q distribution along the network. Moreover these networks can then be implemented by means of cascading Brune or Triplet sections.

Disadvantages

- The main disadvantage of this technique is that the synthesis procedure is not yet developed to directly obtain a realizable network. It needs circuit extraction.
    - With the transformation of stage-predistortion the synthesis of lossy filters gives specific topologies, which is very useful.
- Requires a circulator to convert the predistorted reflection coefficient into transmission.

1.8.3 Reflection-Mode hybrid predistortion technique

In contrast with the two previous techniques, classical predistortion and reflection-mode predistortion, this technique applies predistortion either at the transmission and reflection coefficients, $S_{21}(s)$ and $S_{11}(s)$ respectively. Moreover this technique allows to do that without the need of using

isolator, as in the classical predistortion neither circulators as in the reflection-mode predistortion. Instead it is using a 3-dB hybrid coupler and synthesizes two admittances networks $Y_1(s)$ and $Y_2(s)$, as outlined in Fig. 20.

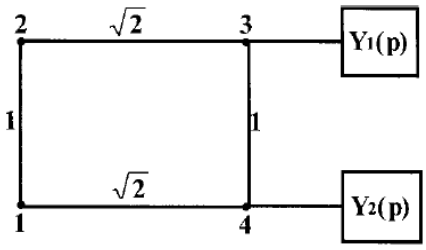

Fig. 20 - Equivalent circuit model of a 3-dB hybrid coupled cascaded with the impedances $Y_1(s)$ and Y2(s).

Using the equivalent circuit above the scattering parameters between port 1 and 2 of the 3dB-hybrid, $S_{21}(s)$ and $S_{11}(s)$ can be written as a function of the two admittance networks $Y_1(s)$ and $Y_2(s)$ as:

$$S_{21}(s) = \frac{j(Y_1(s)Y_2(s) - 1)}{(1 + Y_1(s))(1 + Y_2(s))}$$
$$S_{11}(s) = \frac{Y_1(s) - Y_2(s)}{(1 + Y_1(s))(1 + Y_2(s))} \quad (25)$$

And $S_{11}(s)=-S_{22}(s)$. The equation above can be rewritten to obtain the admittances $Y_1(s)$ and $Y_2(s)$ as a function of the scattering parameters of the filter:

$$Y_1(s) = \frac{1 - jKS_{21}(s) + KS_{11}(s)}{1 + jKS_{21}(s) - KS_{11}(s)}$$
$$Y_2(s) = \frac{1 - jKS_{21}(s) - KS_{11}(s)}{1 + jKS_{21}(s) + KS_{11}(s)} \quad (26)$$

The resulting networks $Y_1(s)$ and $Y_2(s)$ are therefore defined by the scattering matrix which in turn are obtained from the *characteristic polynomials*.

Now the resulting admittances can be separately predistorted, $Y_1(s\text{-}\alpha_e)$ and $Y_2(s\text{-}\alpha_o)$, and must satisfy:

$$Re\left[Y_1(j\omega_p - \alpha_e)\right] = 0 \text{ or } Re\left[Y_2(j\omega_p - \alpha_o)\right] = 0 \quad (27)$$

and

$$\frac{d}{d\omega}\left[Re\left[Y_1(j\omega_p - \alpha_e)\right]\right] = 0 \text{ or } \frac{d}{d\omega}\left[Re\left[Y_2(j\omega_p - \alpha_o)\right]\right] = 0 \quad (28)$$

Once all unknowns are found, the admittances may be synthesized. The first section of the two networks can be synthesized through a Brune or a Triplet depending on whether the transfer function is symmetric or asymmetric. The remaining network can be a combination of different sections. As

seen in previous section, stage predistortion can be applied to the remaining sections and synthesized with a cascaded Brune or Triplet sections.

Reference [18] applies this technique to implement a filter with symmetric response and a filter with asymmetric response. For the asymmetric case, the synthesized network results in an unequal Q for the odd and even network. In spite of that, the average Q is equal to the resulting from reflection-mode predistortion technique, which means that the overall size of the filter would be almost same. For the symmetric case, the synthesized network results in a $\alpha_e=\alpha_o$, so the Q of both networks $Y_1(s)$ and $Y_2(s)$ is the same.

1.9 Synthesis techniques with Unequal Q distribution

The approaches presented in this section are conceptually different to predistortion techniques presented above and they essentially consist in shaping the transfer function response by both absorption and reflection rather than only by reflection. To do that, they either use existing losses or add new losses to improve the filter performance, which in terms of circuit synthesis give rise to networks with resistive elements among purely reactive components and result in nonuniform dissipation distribution along the network. Note that, with exception of reflection mode realizations, predistorted filters have uniform dissipation. The resulting filter performance exhibits improved return losses in comparison with the ones achieved with classical predistortion techniques. Another advantage of this technique over the predistortion is the ease to tune synthesized networks.

We present below two alternative published techniques for the synthesis of filter with Unequal Q distribution: *Synthesis technique of filter with non-Uniform Q* [20][21], and *Exact synthesis of microwave filters with non-Uniform dissipation* [22].

1.9.1 Synthesis technique of filters with non-uniform Q

This method essentially consists in taking into account the dissipation effect of the filter from the very beginning. This is by assuming a transfer function:

$$S_{21}(s) \rightarrow kS_{21}(s) \tag{29}$$

where $k<1$, thus $|S_{11}(s)|^2+|S_{21}(s)|^2<1$. Because of that one cannot use the unitary condition of (3), to obtain the reflection coefficient $S_{11}(s)$.

This method proposes another way to find $S_{11}(s)$ and then applies the *Circuit approach* synthesis technique of section 1.5 to obtain the network of the filter.

For a symmetric network as the one in Fig. 21, the reflection S_{11} and transmission S_{21} scattering parameters can be expressed as a function of the even- and odd admittances Y_e and Y_o [20]:

$$S_{21} = \frac{Y_o - Y_e}{(1 + Y_o)(1 + Y_e)}$$

$$S_{11} = \frac{1 - Y_o Y_e}{(1 + Y_o)(1 + Y_e)} \tag{30}$$

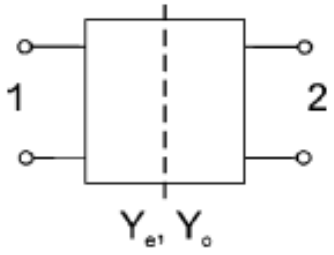

Fig. 21 - Two-port symmetric network.

And the even- and odd reflection coefficients S_e and S_o result as:

$$S_{11} + S_{21} = \frac{1 - Y_e}{1 + Y_e} = S_e$$

$$S_{11} - S_{21} = \frac{1 - Y_o}{1 + Y_o} = S_o \tag{31}$$

Doing so for an all-pole lossy transfer function it is obtained:

$$S_{21}(s) = \frac{k}{(s + r_1)(s + r_2) \dots (s + r_n)} \tag{32}$$

and this gives a reflection coefficient:

$$S_{11}(s) = \frac{s^n + a_{n-1}s^{n-1} + \cdots + a_1 s + a_0}{(s + r_1)(s + r_2) \dots (s + r_n)} \tag{33}$$

where the r_i are the poles of the transmission and reflection coefficient. Since the even and odd reflection coefficient should be reflective at the poles of the transfer function, the coefficients of numerator of $S_{11}(s)$, a_{n-1}, a_{n-2} … a_0, may be found making zero the numerator of the even and odd reflection coefficients at the poles of the transfer function:

$$num(S_e)|_{s=r_1 \dots r_{n/2}} = 0$$

$$num(S_o)|_{s=r_{(n+1)/2} \dots r_n} = 0 \tag{34}$$

Now from the reflection coefficient we obtain the input impedance of the network and may use *circuit approach* synthesis technique to obtain the network of the filter.

This method allows create lossy elements in the original synthesized network and may therefore originate networks with nonuniform dissipation. The final performances of these filters with finite Q are an identical flat attenuation in the passband and slope of the cut-off band edges that of a lossless prototype, at expense of tolerating an offset in the insertion loss.

This process essentially results to a filter network with finite Q for the input and output resonators and an infinite Q for the central resonators, which actually corresponds to a lossless bandpass filter with attenuation at the input and output. Note however that this would not correspond to a real case, where all resonators (and other component) present dissipative effects.

In order to place dissipative components on the central elements of the network, [21] uses two different techniques: *Resistive cross coupling* [21] and *multiple-path loss distribution* [21]. These techniques are presented below:

- *Resistive cross coupling*

This technique consists of adding a new pole-zero pair into the transfer function, as [21] [21]:

$$S_{21}(s) \rightarrow kS_{21}(s)\frac{s-p}{s+p} \tag{35}$$

which introduces a new transmission path through a low Q cross coupled resonator, which does not affect the amplitude response and moreover improve the return losses. However it may result in a very complex synthesis procedure for high order filters.

Alternatively, one could only introduce a new transmission zero,

$$S_{21}(s) \rightarrow kS_{21}(s)(s-p) \tag{36}$$

which usually results in a less complex mathematically formulation. Moreover, the difference between the transfer function resulting from (35) and (36) can be only appreciated in a small reduction on the selectivity [21].

The technique described so far can be supported by *matrix rotations* afterwards. This can be used to change the physical topology of a network without affecting the electrical response, such as to move loss from the outside resonators to the central resonators.

In contrast with the uniform distribution of losses along the filter network, a proper nonuniform distribution of the losses may increase selectivity and reduce insertion losses, and still keeping a good group delay response.

- *Multiple-Path Loss Distribution*

Another technique to distribute the losses along the network is the concept of *Multiple-Path Loss Distribution* technique which defines two signals paths on the transfer function, a high Q resonator path and a low Q resonator path [21]. The function of the high –Q path is to perform the transfer response at the edge band (provides peaks in the band edges) of the filter response, while the low-Q resonators performs the response in the center of the passband. To illustrate this technique Fig. 22 outlines a six order filter configuration, where the 5^{th} and 6^{th} resonators perform the high-Q path. The order of the filter can be increased by adding resonators on the low Q path.

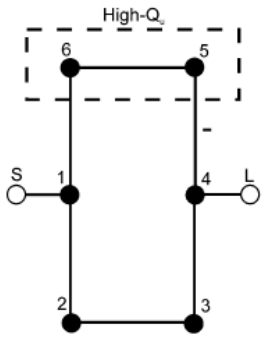

Fig. 22 - Six order filter with multipath loss distribution [21]

The techniques for loss distribution introduced above (resistive cross-coupling and multiple-path) are effectively combined together, and may also be used with matrix rotation techniques and computer optimization routines. Their combination may give rise to an improved filter response, eventually superior to the ones obtained from predistortion techniques [21].

Next figure, Fig. 23, outlines the transmission and reflection coefficients of a six order filter, synthesized with technique described in this section and the classical predistortion technique of section 1.6 [21]. The results show how the present technique can achieve equal flat amplitude response in the pass band, improved selectivity and improved return losses in comparison with the predistorted filter. Also note the asymmetry, mentioned above, on the reflection coefficients, S_{11} and S_{22}, is observed in the predistorted filter.

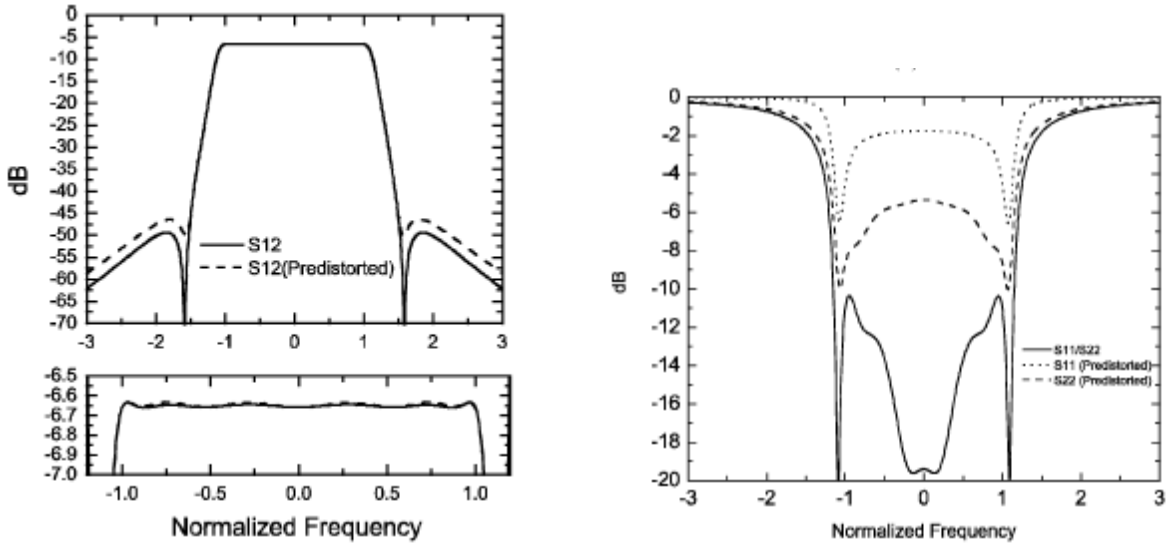

Fig. 23 - Transfer and reflection coefficient of the synthesizes filters with non-uniform Q techniques and predistortion techniques [21]

1.9.2 Exact synthesis of microwave filters with nonuniform dissipation

This method has been recently published [22]. It is essentially an alternative or extension technique to the procedure outlined in previous section.

As done in the reflection-mode hybrid technique [18], this method starts by defining the even and odd reflection coefficients of a symmetrical lossless filter $S_e(s)$ and $S_o(s)$, respectively. These are then multiplied by k (k<1) to take the losses into account:

$$S_e(s) = K(S_{11}(s) + S_{21}(s)) \tag{37}$$

$$S_o(s) = K(S_{11}(s) - S_{21}(s))$$

Applying predistortion to (37), the even and odd reflection coefficient can be read as:

$$S_e(s - \sigma_e) \tag{38}$$

$$S_o(s - \sigma_o)$$

where σ_e and σ_o are the dissipation factor and must be obtained to satisfy:

$$|S_e(j\omega_0 - \sigma_e)|^2 = 1 \tag{39}$$

$$|S_{eo}(j\omega_0 - \sigma_o)|^2 = 1$$

and

$$\frac{d}{d\omega}|S_e(j\omega_0 - \sigma_e)|^2 = 0$$

$$\frac{d}{d\omega}|S_o(j\omega_0 - \sigma_o)|^2 = 0 \tag{40}$$

being ω_o a frequency close to the passband of the filter.

Now the resulting even and odd reflection coefficients can be synthesized as separate sub networks. As outlined in section 0 these networks can be synthesized by cascading Brune and Triplet sections. Then the symmetrical network is constructed. Note moreover that this eliminates the need for a 3dB-hybrid coupler, as in reflection-mode hybrid technique, and thus significantly increases the useable bandwidth of the filter.

The presented approach to perform symmetrical networks from the predistorted even and odd reflection coefficient sub networks is applicable to filters of any order.

1.10 Summary review on the dissipative synthesis techniques

The following table summarizes the synthesis techniques for lossy filters presented above, outlining the basic idea of each technique and listing their merits and drawbacks. Note that more details are given throughout previous sections and the cited references.

SYNTHESIS TECHNIQUES FOR LOSSY FILTERS		
CONCEPT	**MERITS**	**DRAWBACKS**
PREDISTORTION TECHNIQUES (PD)		
-Uses the apriori information of the losses to predistort the poles of the transfer function by a fix amount. -Selectivity and flatness in the passband is achieved by reflecting power in the passband	-Flat attenuation response -High selectivity. -Synthesis applying lossless synthesis techniques. -Synthesizable with coupling matrix approach and circuit approach.	- Severely degraded RL - The zeros are not predistorted - Only applicable to bandpass filters. - For higher degree solution the input and output return loss result in asymmetric networks. -For higher degree solutions a significant price is paid in terms of extra IL. -Difficult to tune in production environment. (In today advances in computer-aided tuning techniques, the tuning problem is of lesser concern.) -Increase of the GD. -Use is limited to high-Q filters for emulate an even higher-Q -Needs the use of two isolators at both ports.

ADAPTIVE PREDISTORTION TECHNIQUE[1] (APD)		
- Adaptively predistort each pole of the transfer function	- Improved IL over PD - Improved RL over PD - Equalized GD over PD -Can be used to improve the overall performance of the communication change. -Applicable for lower-Q filters than PD.	- It requires numerical optimization
REFLECTION MODE PREDISTORTION TECHNIQUES (RPD)		
-Consists of predistorting the reflection coefficient S_{11}. -Then the predistorted reflection coefficient is synthesized as a one-port network and converted to a transmission filter using a three-port circulator.	-High selectivity - Flat attenuation response -Improved RL over PD and ADP -Applicable to notch and highpass filters. -With the transformation of stage-predistortion the synthesis of lossy filters gives specific topologies, based on Brune and Triplet sections.	- The synthesis procedure is not yet developed to directly obtain a realizable network. (Need circuit extraction.) - Requires a circulator to convert the predistorted reflection coefficient into transmission.
REFLECTION MODE HYBRID PREDISTORTION TECHNIQUE[2] (RHPD)		
- Applies predistortion either at the transmission and reflection coefficients.	- more suitable for asymmetric filters	- uses a 3-dB hybrid coupler
SYNTHESIS TECHNIQUES WITH UNEQUAL Q DISTRIBUTION		
SYNTHESIS TECHNIQUES OF FILTERS WITH NON-UNIFORM Q (NU-Q)		
-Selectivity and flatness in the passband is achieved by absorbing power in the passband	- High selectivity - Flat attenuation response - Improved RL over PD and APD -Easier to tune than PD filters -Achieves higher performance with low-Q resonators than PD and APD	-Complex to synthesize. -Requires resistive components for the filter realization.
EXACT SYNTHESIS WITH NON-UNIFORM DISSIPATION [3] (ENU-Q)		
-Applies absorptions to the even and odd reflection mode.	- Synthesized to even and odd reflection networks, separately. - Can be applied to filters of any order	

[1] Merits and drawbacks of PD and ADP are shared expect for the ones detailed in the table.

[2] Merits and drawbacks of RPD and RHPD are shared except for the ones outlined in the table.

[3] Merits and drawbacks of synthesis technique with NU-Q and ENU-Q are shared except for the ones outlined in the table.

1.11 Conclusions and summary

The first chapter introduced the main existing synthesis techniques and tools that will be used along the thesis for the development of novel synthesis approaches of dissipative filters. This is with special emphasis on the extraction of the transversal coupling matrix and all the necessary matrix reduction techniques to transform the impractical coupling matrix into more suitable structures for a final implementation. Although the main topic of the thesis is on dissipative filters the tools on standard synthesis will be the base of the new developed procedures.

At this point it also worth recalling that the result obtained through the thesis have been used for the realization of commercial software in the scope of an ESA project, listed in the introduction Chapter. This is also valid for the conventional synthesis approach reported in section 1.5. So the procedure above has been included also in the software. Additionally the software also includes all the matrix transformation outlined in section 1.5.1 and other that might be performed by matrix rotation by the user. We are emphasizing this because the software has been also used along the thesis for the synthesis of the prototypes in Chapter 3.

Once the conventional techniques were introduced a review of the existing synthesis on dissipative filters are also reported, basically predistortion techniques and non-uniform Q synthesis techniques. Although a different approach will be developed in the thesis, some of the existing ones are also included in the software and will be used along the thesis as a comparison benchmark, mainly those based on predistortion techniques and widely used in space applications.

2 SYNTHESIS OF DISSIPATIVE FILTERS

This chapter describes the synthesis of lossy filters by taking into account the limited Q of the filter resonators. The insertion loss flatness in the transfer response can be made equal to that of a filter having either a prescribed finite Q or an infinite Q. The filter selectivity is optimized at the expense of other filter parameters such as the insertion losses and the out-of-band return losses at each port, which can also be prescribed in the design process. The (N+2)x(N+2) transversal lossy coupling network is the initial topology obtained in the design process and can be later transformed into a number of alternative topologies of practical interest. Several examples are discussed to illustrate the various alternatives on how to prescribe insertion loss, insertion loss flatness and stopband return loss and how to implement these in various network topologies. In particular a direct synthesis of 4^{th} and 6^{th} order lossy filter with uniform Q distribution for infinite and finite Q responses is reported.

2.1 Introduction

Previous chapter concludes on the limitation of conventional synthesis techniques when lossy components are used on the final implementation of the filter. This is due to the fact that conventional filter synthesis techniques [1] [3] do not take loss directly into account from the very beginning of the synthesis procedure. Instead, to evaluate the effects of loss, a finite *Q* has to be introduced in the resonators of the lossless networks resulting from the synthesis (see section 1.6). Among other effects, this approach leads to filters with minimum insertion loss in the passband at one frequency at the expense of additional passband rounding towards the band-edges. Thus, stringent flatness requirements in the transmission response may only be achieved with very high *Q* resonators. This might be undesirable due to impact in size, mass and cost, in particular in space systems with severe

weight and volume restrictions, or in wireless and handset components with strong demand for low-cost and small size.

Driven by the requirements to achieve flat passbands, much effort has been spent over the years to develop novel synthesis procedures, namely (adaptive) pre-distorted filters [11] as maybe one of the major achievements (in particular for satellite applications). This procedure still synthesizes a lossless network which, after introducing the losses, produces the desired (improved) in-band flatness; however, this is at the expense of increased in-band signal reflections. This synthesis approach has been described in section 1.7 and will be used along the thesis as a benchmark filter performance.

An alternative to pre-distortion is to consider the limited Q of the available resonator technology from the very beginning of the synthesis [13]-[23] which, among other advantages, improves the mismatch limitations of pre-distorted synthesis. Two different methods to perform this type of synthesis are described in [15][21], both of which start by obtaining a set of equivalent lossless S parameters of the filter. In [15], the lossy S parameters to be realized are obtained by scaling down their lossless counterparts, whereas in [21] only S_{21} (and S_{12}) is scaled and S_{11}, S_{22} are obtained assuming symmetry in the network to be realized. Both approaches have their relative merits. The first one [15] yields responses with very good passband return loss, but cannot obtain a reflective stopband behaviour at both ports. The second approach yields reflective stopband behaviour at both ports, but passband return loss cannot be controlled and sometimes an extra pole/zero pair has to be included in the response. In addition, there is no reported general method to obtain the transversal network for the second approach [21].

This thesis goes one step further by providing a unified synthesis approach which may moreover consider all different types of lossy filter responses. In particular this thesis extends previous works on:

i) Providing an alternative formulation to [15] that does not impose restrictions on the scaling constants for S_{11} and S_{22}, thus allowing to independently set the out-of band return loss at each filter port;
ii) Generalizing the work in [21] to show how the transversal network can be systematically obtained for any filter order;
iii) Introducing lossy filters with prescribed insertion loss and prescribed insertion loss flatness (i.e. rounding of the band edges due to finite Q) in the transmission response;
iv) Extending previous work on loss distribution in lossy filters [13]-[23] having topologies of practical interest (folded and others). For example, we establish closed-form equations for obtaining uniform Q requirements in 4^{th} and 6^{th} order folded-coupling filters.

The synthesis of lossy filters referred to in i) and ii) takes into account the limited Q of the resonators to achieve the best possible insertion loss flatness, equivalent to that of a filter with infinite

Q. In many occasions this exceeds by far the specifications and thus, the resonator *Q*s required are higher than strictly needed. These requirements can be lowered with the design techniques referred to in point iii) above, which can be superposed to those in points i) and ii).

2.2 Mathematical Formulation For the Synthesis of Lossy Filters

We start by defining the two port *S*-parameters S_{ij} of a filter as:

$$\begin{matrix} S_{11}(s) = k_{11}S'_{11}(s) \\ S_{22}(s) = k_{22}S'_{22}(s) \end{matrix} \quad S_{21}(s) = S_{12}(s) = k_{21}S'_{21}(s) \tag{41}$$

where the scaling constants k_{11}, k_{22} and k_{21} ($\in$]0,1]) set prescribed insertion and return losses and S'_{ij} sets the shape of the filter response. From the set of *S*-parameters S_{ij} (1) we obtain the two port admittance matrix polynomials, as in section 1.5 , where the numerators are labeled as $Y_{ijn}(s)$ and their common denominator is $Y_d(s)$, see (7).

The value of the constants k_{ij} and the choice of S'_{ij}, in (41), prescribe the insertion and return loss and define *cases A* and *B* out of the three different cases of filter transfer function to be considered in the thesis:

- **Case A**: Prescribed insertion loss and prescribed stopband return loss at port 1 and port 2. Insertion loss flatness is equivalent to that of a lossless filter (infinite *Q* response).
- **Case B**: Prescribed insertion loss. Return loss in the passband cannot be prescribed but the filter is fully reflective in the stopband. Insertion loss flatness is equivalent to that of a lossless filter (infinite *Q* response).
- **Case C**: Filter designed following cases A or B whose response is further modified to allow a prescribed tolerance in insertion loss flatness.

2.2.1 Case A: Prescribed insertion loss and stopband return loss with insertion loss flatness equivalent to an infinite Q response

In this case, out-of band return loss can be symmetrically or asymmetrically prescribed at both filter ports. Additionally, this case also includes the symmetrical situation where the out-of band return loss is identical to the passband insertion loss (k_{11}=k_{22}=k_{21}).

An asymmetrical out-of band return loss might be of interest in some architectures like channel-drop multiplexers where channel filters with a reflective out-of band input are required, being their output return-loss of little relevance [24].

The frequency response synthesized in this case can be defined by

$$S_{11}(s) = k_{11}S_{11\_lossless}(s);\ S_{22}(s) = k_{22}S'_{22}(s)$$
$$S_{21}(s) = S_{12}(s) = k_{21}S_{21\_lossless}(s) \quad (42)$$

where the scaling constants k_{11}, k_{22} and k_{21} may be different and selected independently. The term $S_{ij\_lossless}$ corresponds to the response from a lossless synthesis [1][2][3]. Whereas S'_{22} can be obtained from

$$S'_{22}(s) = \left(1 - \left(\frac{k_{21}}{k_{11}}\right)^2 + \frac{k_{21}^2}{k_{22}k_{11}}S_{11\_lossless}(s)\right) \quad (43)$$

Details on the derivation of S'_{22} (43) may be found in the Appendix 2.

To derive the transversal network, we follow a similar procedure to that of the synthesis of lossless filters described in section 1.5. The partial polynomial expansion of the two-port admittance matrix can now be written as

$$[Y] = j\begin{bmatrix} 0 & K_0 \\ K_0 & 0 \end{bmatrix} + \sum_{k=1}^{N} \frac{\begin{bmatrix} r_{11k} & r_{12k} \\ r_{21k} & r_{22k} \end{bmatrix}}{s - j(\lambda_{kr} + j\lambda_{ki})} + \begin{bmatrix} KK_{11} & 0 \\ 0 & KK_{22} \end{bmatrix} \quad (44)$$

where K_0 sets the direct coupling between source and load, N is the order of the filter, the roots of the polynomial expansion are $\lambda_k = \lambda_{kr} + j\lambda_{ki}$ and, unlike in the lossless case in section 1.5, the residues r_{ij} are complex. For the circuit network point of view this corresponds to resistive and reactive elements. Moreover, the partial polynomial expansion (44) results in an additional diagonal matrix whose terms are KK_{11} and KK_{22}. The equivalent network resulting from (44) has N+2 nodes, as outlined in Fig.24a, where now each of the N solid black circle represents a lossy resonator coupled to the source and load by means of a coupling admittance having a resistive and a reactive part. The box labeled by M_{SL} indicates the direct coupling between the source and load. Additionally, shunt resistors ($1/G_S$ and $1/G_L$) at the source and load are required to account for the residual element KK_{11} and KK_{22}, respectively.

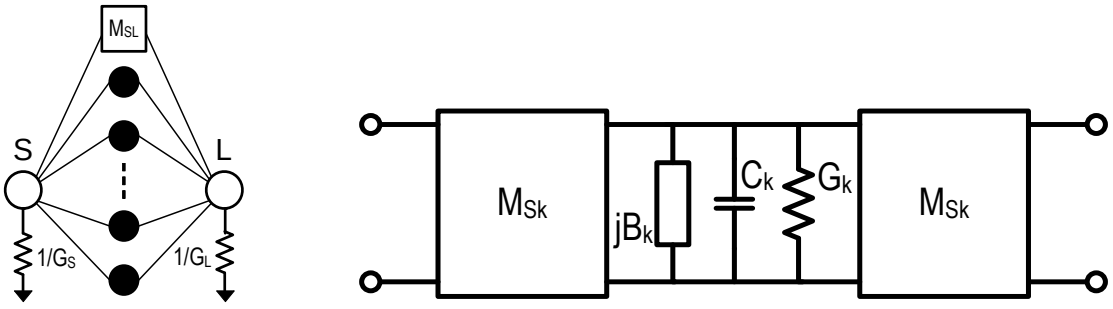

Fig. 24 a) Equivalent network of a transversal filter of order N. S and L represent the source and the load. b) Circuit representing the coupling between the source/load with the resonator, and the resonator itself.

In Fig. 24b the coupling between the source (load) and the k^{th} lossy resonator is defined by M_{Sk} (M_{Lk}) and the lossy resonator is characterized by the frequency independent reactive element B_k, by the capacitance C_k and by the conductance G_k. By identifying these circuit elements with the mathematical expression (44), the following identities can be established: $G_S=KK_{11}$, $G_L=KK_{22}$, $G_k=\lambda_{ki}$, $B_k=-\lambda_{kr}$, $C_k=1$, $M_{LK}=\sqrt{r_{22k}}$ and $M_{LK}=r_{21k}/\sqrt{r_{22k}}$. Note as well that G_S and G_L are related with the stopband return loss, since:

$$G_S=(1-k_{11})/(1+k_{11})$$
$$G_L=\left(1-k_{eq}\right)/\left(1+k_{eq}\right) \qquad (45)$$
$$k_{eq}=k_{22}\left(1-(k_{21}/k_{11})^2+k_{21}^2/(k_{22}k_{11})\right)$$

and stopband return loss at the input and output is given by k_{11} and k_{eq} respectively.

The network topology in Fig. 24a is general for any filter response given by (42), this is for symmetric or asymmetric filter responses and even for self-equalized linear responses.

The ability to independently select the various k_{ij} values might prove useful in the allocation of loss within the network for some particular filter topologies. For example (section 2.2.2), in the folded coupling topology, choosing $k_{11}=1$ (no stopband return loss at the input) forces the first resonator to be lossless. Conversely, if the stopband return loss at both ports is irrelevant, the choice $k_{11}=k_{22}<1$ may be of interest. Another interesting choice is to select $k_{11}\approx 1$ (i.e., first resonator having high Q to provide low stopband return loss) while having k_{22} (and k_{21}) significantly less than 1 to reflect the loss in the other filter resonators.

Below we list a couple of simple examples to illustrate symmetric ($k_{11}=k_{22}$) or asymmetric responses ($k_{11}\neq k_{22}$).

- **Example: Asymmetric Response ($k_{11}\neq k_{22}$)**

As an illustrative example Fig. 25 and Table 1 shows the frequency response and the transversal coupling matrix (TCM) of a 4th order Chebyshev response, whose ripple in S_{21} is that of a lossless filter with 20 dB passband return losses and $k_{11}=0.9$, $k_{12}=0.5$, $k_{22}=0.6$. Note that, once synthesized, passband return losses at the input port in dB are $20\text{-}20log_{10}(k_{11})=20.9$ dB and stopband return losses are $-20log_{10}(k_{11})=0.9$ dB.

Note that in asymmetric responses like this one, as a result of (42), the output reflection coefficient is degraded with respect to that at the input. Thus, these types of designs should only be used in application where passband output return loss is irrelevant.

Further details on the mathematical process, corresponding to Fig. 25 response, are shown in the following tables (Table 2 and 3). Table 2 shows the coefficients of the characteristic polynomials, whereas Table 3 shows their roots. Note that, in this case, the characteristic polynomials P(s), F(s) and E(s), are equal to the ones obtained from a standard synthesis, detailed in section 1.5, whereas the characteristic polynomial $F_{22}(s)$, resulting from S_{22} (22) has different coefficients.

-0.5j	-4.6-0.7j	4.6-0.7j	-5.7-0.11j	5.7+0.11j	0
-4.6-0.4j	12.7-1.0j	0	0	0	2.1-1.1j
4.6-0.4j	0	-12.7-1.0j	0	0	2.1+1.1j
-5.7-0.11j	0	0	-5.9-2.8j	0	4.2+0.6j
5.7+0.11j	0	0	0	5.9-2.8j	4.2-0.6j
0	2.1-1.2j	2.1+1.2j	4.2+0.6j	4.2-0.6j	- 1.8j

Table 1: Coupling matrix of the filter response of Fig. 25. Note that all terms are normalized by 0.1

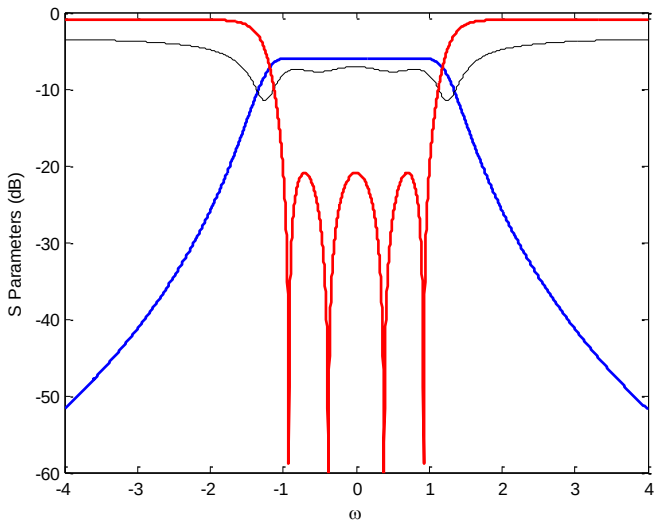

Fig. 25 Response of a 4th order lossy filter design (42),with k_{11}=0.9, k_{12}=*0.5*, k_{22}=*0.6*. Blue trace: $|S_{21}|$, red trace: $|S_{11}|$, black trace $|S_{22}|$.

i =	***P(s)***	***F(s)***	***F_{22}(s)***	***E(s)***
4	0	*8.000*	*1.0000*	*1.0000*
3	0	*0*	*1.6073*	*2.143*
2	0	*8.000*	*2.7223*	*3.296*
1	0	*0*	*2.1201*	*2.826*
0	*1.000*	*1.000*	*0.9687*	*1.25*
ε			*0.1005*	
$ε_R$			*8.000*	

Table 2: Coefficients of the characteristic polynomials low pass Chebyshev prototype of order 4.

Roots of P(s)	*Roots of F(s)*	*Roots of $F_{22}(s)$*	*Roots of E(s)*
-	*-j·0·923*	*-0.2245 – j·1.2428*	*–0.313+j·1.194*
-	*j·0.923*	*-0.2245 + j· 1.2428*	*–0.313–j·1.194*
-	*-j·0.382*	*-0.5792 - j· 0.5215*	*–0.757+j·0.494*
-	*j·0.382*	*-0.5792 + j· 0.5215*	*–0.757+j·0.494*

Table 3: Roots of the characteristic polynomials of a 4th order Chebyshev prototype

From the previous table we can see that the roots of $F_{22}(s)$ appear in conjugated pairs.

- **Example: Symmetric Response ($k_{11}=k_{22}=k_{21}$)**

If all the scaling factors k_{ij} in (42) are chosen to be equal to k the output reflection coefficient will be $S_{22}(s)=k\cdot S_{22\_lossless}(s)$ and therefore $KK_{11}=KK_{22}$ in the right-hand side of (44). This case is equivalent to the responses presented in [14]. Figure 26 and Table 4 show the frequency response and the transversal coupling matrix of 4th order Chebyshev response, whose ripple in S_{21} is that of a lossless filter with 20 dB passband return losses and k=0.75. Note that, once synthesized, passband return losses at the input port in dB are $20\text{-}20log_{10}(k)$ =22.5 dB and stopband return losses are $-20log_{10}(k)$ =2.5 dB.

Unlike the previous example, the applications where this type of design are of interest are those where both input and output return loss in the passband are of interest and there is no objection in having a significant stopband return loss at both ports.

The following tables show the coefficients and roots of the characteristic polynomials corresponding to the synthesized response of Fig.26. Note that, in this case, the characteristic polynomials P(s), F(s) and E(s), defining the frequency response are also equal to the ones obtained from a standard synthesis, detailed in section 1.5.

-1.4j	-4.1+0.2j	5.9-0.15j	-5.9-0.15j	4.1+0.2j	0
-4.1+0.2j	13.2-0.5j	0	0	0	4.1-0.2j
5.9-0.15j	0	6.2-1.0j	0	0	5.9-0.15j
-5.9-0.15j	0	0	-6.2-1.0j	0	5.9+0.15j
4.1+0.2j	0	0	0	-13.2-0.5j	4.1+0.2j
0	4.1-0.2j	5.9-0.15j	5.9+0.15j	4.1+0.2j	- 1.4j

Table 4: Coupling matrix corresponding to Fig. 26 response. Note that all terms are normalized by 0.1

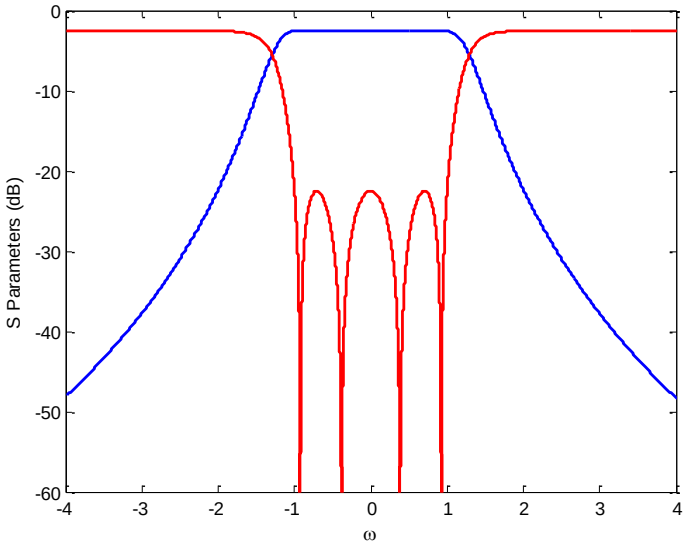

Fig. 26 Response of a 4th order lossy filter design (42), with $k_{11}= k_{21}= k_{22}=0.75$. Blue trace: $|S_{21}|$, red trace: $|S_{11}|$, $|S_{22}|$.

i =	*P(s)*	*F(s)*	*E(s)*
4	0	*8.000*	*1.0000*
3	0	*0*	*2.143*
2	0	*8.000*	*3.296*
1	0	*0*	*2.826*
0	*1.000*	*1.000*	*1.25*
ε		*0.1005*	
ε_R		*8.000*	

Table 5: Coefficients of the characteristic polynomials low pass Chebyshev prototype of order 4.

Roots of P(s)	*Roots of F(s)*	*Roots of E(s)*
-	*-j·0·923*	*–0.313+j·1.194*
-	*j·0.923*	*–0.313–j·1.194*
-	*-j·0.382*	*–0.757+j·0.494*
-	*j·0.382*	*–0.757+j·0.494*

Table 6: Roots of the characteristic polynomials of a 4th order Chebyshev prototype

2.2.2 Case B: Prescribed insertion loss with no stopband return loss and insertion loss flatness equivalent to an infinite Q response

This corresponds to a frequency response that allows a scaling of the transmission coefficient [21]

$$S_{21}(s) = k\, S_{21\_Lossless}(s) \tag{46}$$

and having both ports purely reflective at the stopband. As mentioned previously, this could be useful for channel filters to be used in input multiplexers [24]. Unlike case A, $S_{11}(s)$ and $S_{22}(s)$ are obtained under the condition of a symmetric filter network ($S_{11}(s)=S_{22}(s)$) [21] (See Appendix 3). Here, we extend the work in [21] by establishing a systematic procedure for the synthesis of the transversal network for this type of response, as described in the following paragraphs.

Once the S parameters are known from (46) and (A.3.1)-(A.3.4), we perform the additional steps to determine the transversal network: we obtain the admittance matrix from (7) and the additional restrictions imposed by the symmetry of the matrix (see (A.3.5) in the Appendix 3). We then perform the partial polynomial expansion of the resulting admittance matrix

$$[Y] = j\begin{bmatrix} 0 & K_0 \\ K_0 & 0 \end{bmatrix} + \sum_{k=1}^{N} \frac{\begin{bmatrix} r_{11k} & r_{12k} \\ r_{21k} & r_{22k} \end{bmatrix}}{s - j(\lambda_{kr} + j\lambda_{ki})} \tag{47}$$

where the terms in (47) are defined as those in (44).

The resulting transversal network (Fig.27) does not require the shunt resistors in the source and load shown in Fig. 24a. The resonators are lossy and the coupling between the source/load and each resonator is complex.

Note that the procedure described is general and not limited to a given filter order *N*.

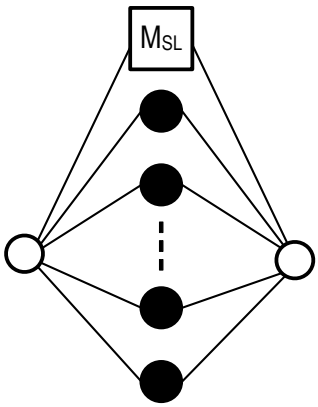

Fig. 27 Equivalent network of a transversal filter of order *N*, corresponds to (47).

- **Example: No additional pole-zero**

Figure 28 and Table 7 show the coupling matrix and frequency response using k=0.75 and a 4th order Chebyshev transfer function whose ripple in S_{21} is that of a lossless filter with 25 dB passband return losses.

It is interesting to observe that, although the transfer function corresponds to an ideal response (infinite Q) with prescribed insertion loss as in case A, here the filter is not absorptive in the stopband, but fully reflective. However, the passband reflection coefficient cannot be chosen and a poor in-band return loss is obtained which might not be useful for some applications.

0	-4.0+0.4j	4.0+0.4j	5.8-0.3j	-5.8-0.3j	0
-4.0+0.4j	14.8-1.0j	0	0	0	4.0-0.4j
4.0+0.4j	0	-14.8-1.0j	0	0	4.0+0.4j
5.8-0.3j	0	0	7.1-2.2j	0	5.8-0.3j
-5.8-0.3j	0	0	0	-7.1-2.2j	5.8+0.3j
0	4.2-0.4j	4.0+0.4j	5.8-0.3j	5.8+0.3j	0

Table 7: Coupling matrix corresponding to Fig. 28. Note that all terms are normalized by 0.1

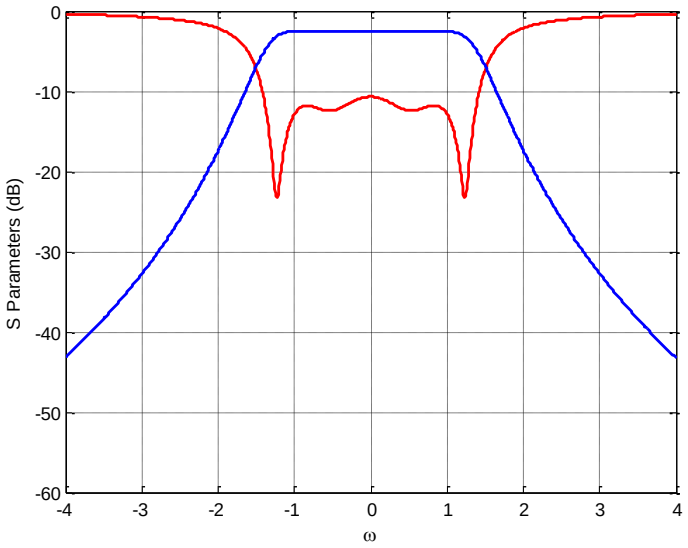

Fig. 28 Frequency response of a 4th order Chebyshev lossy filter (47) with no stopband return loss, with k=0.75 and passband insertion loss of $-20log_{10}(k)$=2.5 dB. . Blue trace: $|S_{21}|$, red trace: $|S_{11}|$, $|S_{22}|$.

The following tables (Tables 8 and 9) show the coefficients and roots of the characteristic polynomials corresponding to the synthesized response of Fig. 28. Note that P(s) and E(s) are equal than in standard synthesis, whereas F(s) is recalculated using (A.2.1)-(A.2.3)

i =	*P(s)*	*F(s)*	*E(s)*
4	0	*1.000*	*1.0000*
3	0	*0.5358*	*2.143*
2	0	*1.5741*	*3.296*
1	0	*0.7067*	*2.826*
0	*1.000*	*0.4063*	*1.25*
ε		*0.1005*	
ε_R		*8.000*	

Table 8: Coefficients of the characteristic polynomials low pass Chebyshev prototype of order 4, using case B.

Roots of P(s)	*Roots of F(s)*	*Roots of E(s)*
-	*0.0139 – j·1.1268*	*–0.313+j·1.194*
-	*0.0139 + j· 1.1268*	*–0.313–j·1.194*
-	*-0.2818 - j· 0.4904*	*–0.757+j·0.494*
-	*-0.2818 + j·0.4904*	*–0.757+j·0.494*

Table 9: Roots of the characteristic polynomials of a 4th order Chebyshev prototype, using case B.

From the previous table we can see that the roots of *F(s)* appear in conjugated pairs.

Additional pole-zero

A variation of such frequency response may be obtained by the inclusion of additional pole/zero placed at δ into the transfer function response [21], as

$$S_{21}(s) = k\, S_{21\_Lossless}(s)\frac{s-\delta}{s+\delta} \tag{48}$$

The corresponding reflection coefficient is found as for (47) and the resulting partial polynomial expansion is

$$[Y] = j\begin{bmatrix} 0 & K_0 \\ K_0 & 0 \end{bmatrix} + \sum_{k=1}^{N} \frac{\begin{bmatrix} r_{11k} & r_{12k} \\ r_{21k} & r_{22k} \end{bmatrix}}{s - j(\lambda_{kr} + j\lambda_{ki})} + \frac{\begin{bmatrix} r_{11\delta} & r_{12\delta} \\ r_{21\delta} & r_{22\delta} \end{bmatrix}}{s - j(\lambda_{\delta r} + j\lambda_{\delta i})} \tag{49}$$

Note that this results in an *N*+2+1 transversal coupling network, where *N* of the nodes correspond to resonators, 2 of the nodes correspond to the input and output, and the additional resonant node accounts for the inclusion of the pole/zero in (48). Its corresponding topology is depicted in Fig .29, where the red circle indicates the additional pole/zero. The residues $r_{ij\delta}$ define the coupling between source/load and the added pole/zero. Since resonant frequency of this node (defined by $\lambda_{\delta r}$) is far from the passband, it could also be viewed as a non-resonant node without an appreciable impact in the response [21].

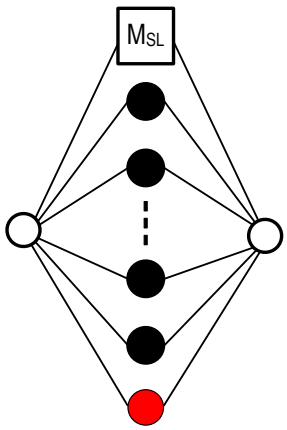

Fig. 29 Equivalent network of a transversal filter of order *N*, corresponds to (49). The red node indicates the additional resonant node

- **Example: Additional pole/zero**

This approach (48) is used to improve the in-band return losses of the filter response in Fig. 28. To do that we include an additional pole/zero at δ=14 (normalized frequency). The resulting frequency response and transversal coupling matrix are shown in Fig.30 and Table 10, respectively. We use bold characters to indicate the additional row and column due to the inserted pole/zero in the transversal coupling matrix.

0	**0.017+0.017j**	0.43+ 0.03j	-0.43+0.03j	0.64- 0.02j	-0.64-0.02j	0
0.017+0.017j	**-1.3e-3-14j**	**0**	**0**	**0**	**0**	**0.017+0.017j**
-0.43+0.03j	**0**	-1.41- 0.04j	0	0	0	0.43-0.03j
0.43+0.03j	**0**	0	1.41-0.04j	0	0	0.43+0.03j
0.64-0.02j	**0**	0	0	-0.64-0.09j	0	0.64-0.02j
-0.64-0.02j	**0**	0	0	0	0.64-0.09j	0.640.02j
0	**0.017+0.017j**	0.43-0.03j	0.43+ 0.03j	0.64-0.02j	0.64+0.02j	0

Table 10: Coupling matrix corresponding to Fig. 30 response

Note that the frequency dependence of the additional resonant mode has a negligible impact on the frequency response of the filter (Fig. 30) and thus, it could be treated as a non-resonant node with no appreciable error.

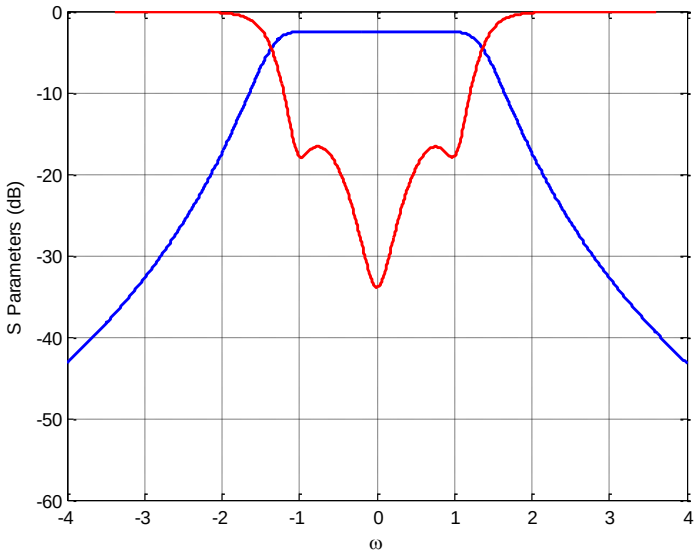

Fig. 30 Frequency response of the 4th pole Chebyshev lossy filter on Fig. 28 with an additional pole/zero (48) for k=0.75, δ=14. Blue trace: $|S_{21}|$, red trace: $|S_{11}|$, $|S_{22}|$.

Although no reported here, it is good to notice that the group delay barely changes in comparison with the one obtained in a standard synthesis.

The following tables (Tables 11 and 12) show the coefficients and roots of the characteristic polynomials corresponding to the synthesized response of Fig.30. From the previous table we confirm again that the roots of *F(s)* appear in conjugated pairs.

i =	***P(s)***	***F(s)***	***E(s)***
5	0	*1.000*	*1.000*
4	0	*12.75-j·0.0011*	*14.64*
3	0	*4.22-j·0.0024*	*30.08*
2	0	*13.09-j·0037*	*44.032*
1	1	*1.0455-j·0.0032*	*36.58*
0	*-12.5*	*0.70-j·0.0014*	*15.62*
ε		*0.1005*	
ε_R		*8.000*	

Table 11: Coefficients of the characteristic polynomials low pass Chebyshev prototype of order 4, using case B.

Roots of P(s)	***Roots of F(s)***	***Roots of E(s)***
-	*-1.2500e1 +j·9.6849e-4*	*-12.5*
-	*-9.2042e-2 + j·9.8067e-1*	*-3.1385e-1 + j·1.1948*
-	*-9.2102e-2 - j·9.8074e-1*	*-3.1385e-1 - j·1.1948*
12.5	*-3.5014e-2 + j·2.3921e-1*	*-7.5770e-1 + j·4.9492e-1*
	-3.5434e-2 - j·2.3898e-1	*-7.5770e-1 - j·4.9492e-1*

Table 12: Roots of the characteristic polynomials of a 4th order Chebyshev prototype, using case B.

At this point it is worth to mention that further details on the transfer function corresponding to case B, this is the extraction of the characteristic polynomials can be found on Appendix 7.

2.2.3 Case C: Insertion loss flatness equivalent to a prescribed finite Q

The aim of this case is to synthesize filters whose insertion loss flatness can be prescribed and made equivalent to that of finite *Q* response. This might result in lowering the requirements in resonator *Q* beyond those attainable by just using the techniques described in cases A and B above.

This case also requires tolerating additional insertion or return losses k_{ij}, as in (41) (42) (46) and (48), however for a given *Q*, now we could use a higher k_{ij}, or analogously for a given k_{ij}, we could use a lower *Q*.

To formulate this approach we use the lossy responses in (42) (46) and (48), (case A and B in previous sections), then the elements of the two port [Y] are modified to emulate an in-band response with finite *Q*. This can be done by shifting the roots of the Y polynomials ($Y_d(s)$, and $Y_{ijn}(s)$) to the left of the s-plane by σ, where σ is obtained from the prescribed finite *Q* value of the response to be emulated (referred to as Q_{eff}) and the fractional bandwidth of the filter (FBW) as, $\sigma = 1/(FBW \cdot Q_{eff})$, being σ the shift in root placement that would occur in a filter designed with classical (lossless) techniques when implemented with resonators having Q=Q_{eff}, as in section 1.6.

We then apply partial polynomial expansion into the new two-port admittance matrix. The resulting polynomial expansion can be expressed as in (44), (47) or (49) depending on whether the S-parameters have been defined using (42), (46) or (48). This, in turn, sets the topology to be either that in Fig. 25a, Fig. 28, or Fig. 30 respectively. In (44), (47) or (49) the real part of the eigenvalues (λ'_{ki}) will be

$$\lambda'_{ki} = \lambda_{ki} + \sigma \tag{50}$$

being λ_{ki} the eigenvalues in the lossless case. **This change in the eigenvalues implies added losses in the filter resonators. On the other hand, since the residues r_{ijk} do not change, there is no change in the coupling among resonators.**

- **Example: Prescribed insertion loss, insertion loss flatness and stopband return loss**

Figure 31 and Table 13 illustrate the frequency response and the coupling matrix of a synthesized response as the one in Fig. 26 but emulating a finite *Q* response of 2000, for a 1% fractional bandwidth filter.

-1.4j	-4.1+0.2j	5.9-0.15j	-5.9-0.15j	4.1+0.2j	0
-4.1+0.2j	13.2-1.0j	0	0	0	4.1-0.2j
5.9-0.15j	0	6.2-1.6j	0	0	5.9-0.15j
-5.9-0.15j	0	0	-6.2-1.6j	0	5.9+0.15j
4.1+0.2j	0	0	0	-13.2-1.0j	4.1+0.2j
0	4.1-0.2j	5.9-0.15j	5.9+0.15j	4.1+0.2j	- 1.4j

Table 13: Coupling matrix corresponding to Fig. 31 response. Note that all terms are normalized by 0.1

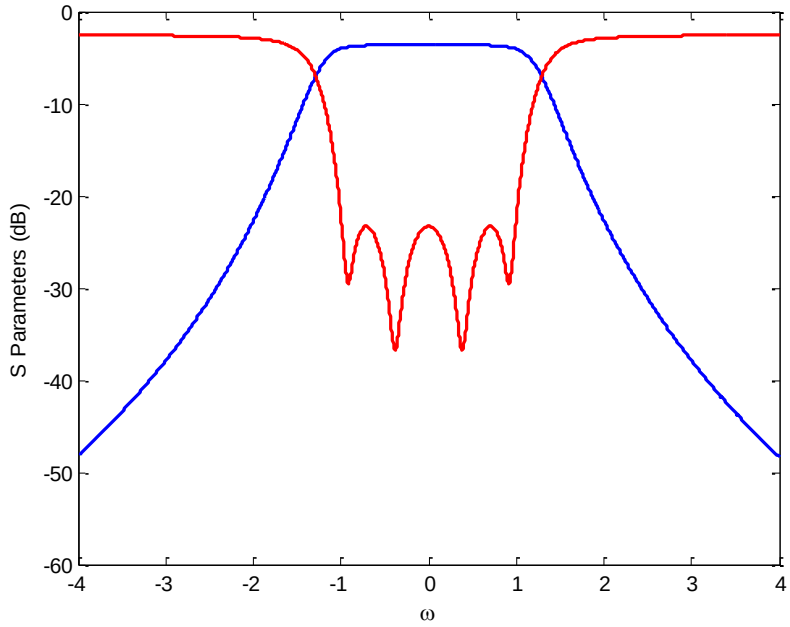

Fig. 31 Response of a lossy filter design, $k_{11}= k_{12}= k_{22}=0.75$ $Q_{eff}=2000$, FBW=1%. Blue trace: $|S_{21}|$, red trace: $|S_{11}|$, $|S_{22}|$.

- **Example: Prescribed insertion loss and insertion loss flatness with no stopband return loss**

The following example shows the synthesis of the frequency response of Fig. 30 for a prescribed finite *Q* response of 2000 and a fractional bandwidth on 1%. The coupling matrix and frequency response are depicted in Fig. 32 and Table 14, respectively.

As expected, the matrices in Table 13 and 14 are equal to the matrices in Table 4 and 10 respectively, except for the imaginary part of the diagonal entries.

0	**0.017+0.017j**	0.43+ 0.03j	-0.43+0.03j	0.64-0.02j	-0.64-0.02j	0
0.017+0.017j	**-1.3e-3-14.05j**	**0**	**0**	**0**	**0**	**0.017+0.017j**
-0.43+0.03j	**0**	-1.41- 0.1j	0	0	0	0.43-0.03j
0.43+0.03j	**0**	0	1.41-0.1j	0	0	0.43+0.03j
0.64-0.02j	**0**	0	0	-0.64-0.14j	0	0.64-0.02j
-0.64-0.02j	**0**	0	0	0	0.64-0.14j	0.64+0.02j
0	**0.017+0.017j**	0.43-0.03j	0.43+ 0.03j	0.64-0.02j	0.64+0.02j	0

Table 14: Coupling matrix corresponding to Fig. 32 response

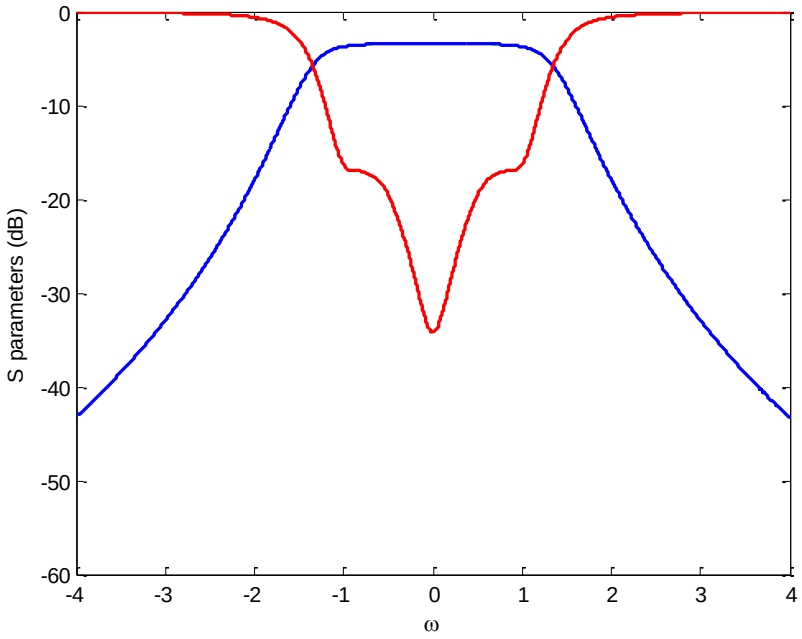

Fig. 32 - Response of a lossy filter design, k=0.75 (48), δ=14, Q_{eff}=2000, FBW=1%.. Blue trace: $|S_{21}|$, red trace: $|S_{11}|$, $|S_{22}|$.

2.3 Strategies for resonator Q distribution in folded networks

All the networks synthesized so far result in transversal coupling networks which may be transformed into other topologies which are easier to implement. Besides topological considerations, a close to uniform distribution of losses among the filter resonators is desired to avoid uneven requirements of Q in the resonators. Furthermore, care has to be taken in how to implement circuit transformations since they may result in complicated structures including resistive and complex coupling between resonators, which might be unfeasible or hard to implement. Hence, in the following sections some useful strategies for uniform Q distribution are given. Moreover, for a 4^{th} and 6^{th} degree network a rigorous derivation between the relation of insertion loss, fractional bandwidth and required resonator Q is given for Butterworth, Chebyshev and Chebyshev responses with a single pair of symmetrical transmission zeros, which, apart from being extremely useful for the

practicing engineer, provides significant insight in the limitations of lossy filters with uniform *Q* distribution.

2.3.1 TCM to Folded Coupling Matrix (FCM)

The transversal coupling networks in Figs. 24a, 27 and 29 can be transformed into folded coupling topologies by following the same procedure than in a lossless case [1], which is detailed in section 1.5.2 and Appendix 1. This results in the folded coupled networks summarized in Fig. 33 which, for simplicity, have been drawn for the specific case of a 6^{th} order filter network.

For the synthesized responses of case A, the transformation results in a FCM (Fig. 33a) where the losses are concentrated in the first and last resonators and in the shunt resistors at the source and load, also present in the transversal topology (Fig. 24a). The other resonators are lossless. The resulting matrix is identical to the one obtained in a lossless case for the inner resonators and all coupling elements in the resulting network are reactive. Since the losses are not distributed throughout the network, additional transformation will be required.

Figure 33b shows the folded coupling matrix for a filter designed using case B. In this case the losses are also concentrated in the first and last resonator and the coupling between resonators is reactive. As above, additional circuit transformation will be required for a better loss distribution.

When an additional pole/zero is inserted in the transmission response, the transformation from the TCM to the FCM results in a network like the one in Fig. 33c, in which the losses are now distributed along the network and coupling resistors appear after this first transformation. Although for this case the losses are already distributed, their allocation is usually too uneven for a practical implementation, to the point where it sometimes results in requirements of negative *Qs* for some of the resonators. Therefore further transformations are required for the final design.

Note that the matrix rotation steps to go from the TCM to the FCM do not consider the additional transversal node due to the inserted pole/zero. Formally, this node should appear coupled from the source to the load in Fig. 33c and the other topologies resulting from this one. Note however that this node barely affects the transmission filter performance and it is used to improve the return losses and facilitate the loss distribution [21], so it will be omitted in the figures.

The transformation to obtain the folded network can also be performed in the transversal networks synthesized from case C. In this case the folded network would be as the ones Figs. 33a, 33b and 33c, depending on the type of synthesized response (42), (46) and (48), respectively. However the network would present uniform additional losses at each resonator. Note that when such additional losses go into a lossless resonator (as the inner resonators of Figs. 33a and 33b) the resulting Q is that given by the rounding in the transmission response (Q_{eff}, see section 2.2.3). Therefore, for a topology as Fig. 33a its counterpart with additional losses would be Fig. 33d. Even though now all resonators in Fig. 33d are lossy, without any further loss distribution, the minimum required Q would never be lower than the one required with standard synthesis techniques, so that additional loss is needed lower Q by transferring loss from the outer resonators (1 and 6 in Fig. 33d) to the inner ones (2 to 5 in Fig. 33d).

The following sub-sections describe how to distribute losses by means of hyperbolic rotations in the various folded network topologies of Fig. 33. Details on how the hyperbolic rotation proceeds are documented in Appendix 4.

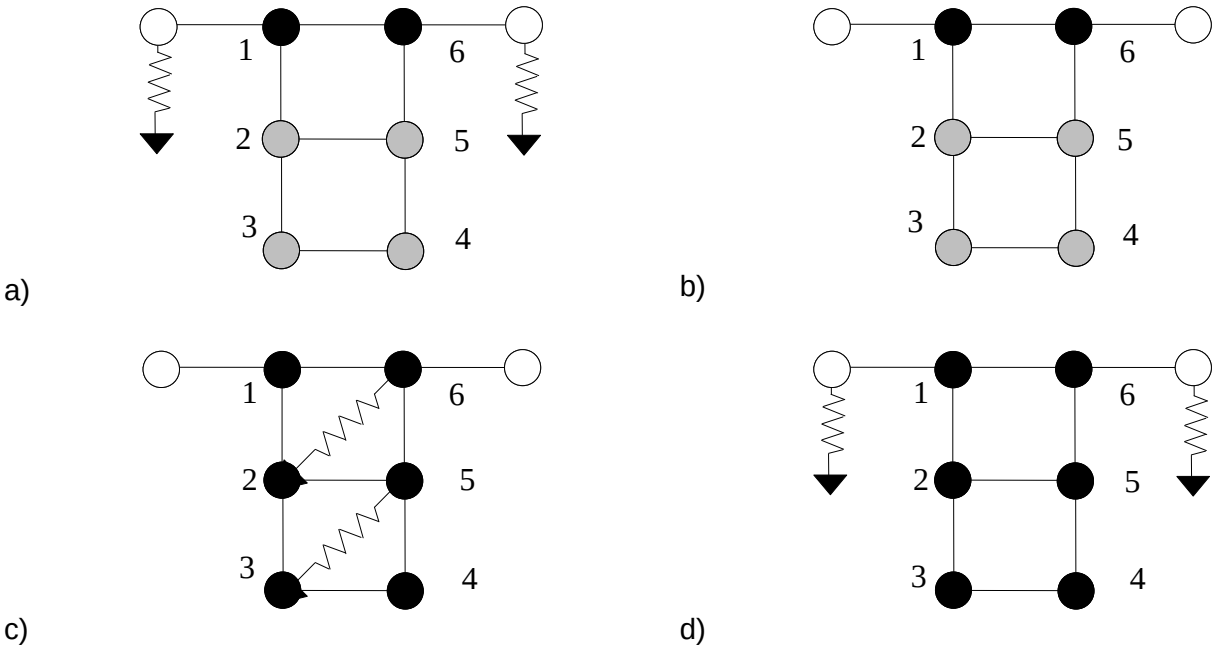

Fig. 33 - FCM for a lossy 6th order filter for a) Case A, b) case B, c) case B and d) case A+C responses. The black and grey circles represent lossy and lossless resonators, respectively.

2.3.2 Uniform Loss Distribution in cases A and A+C

This procedure applies to 4th and 6th order Chebyshev filters with a single pair of symmetric transmission zeros having topologies as the ones in Figs. 33a and 33d. As stated above, in these topologies losses are mostly allocated at the shunt resistors and at the input and output resonators. We will consider the case where $k_{12}=k_{11}=k_{22}=k$ in (42) for 4^{th} and 6^{th} order filters. Extension to higher order filters and different k values could be eventually performed by using the same procedure.

- **4th degree network- Direct Synthesis**

We start from a general folded 4^{th} order symmetric network (Figs. 34a - 34b) with lossless in the inner resonators 2 and 3. For convenience in the subsequent distribution of losses, additional non-resonant nodes are introduced at the input and output of the filter, as outlined in Fig. 34c. The input and output non-resonant nodes are indicated as *NS* and *NL*, respectively.

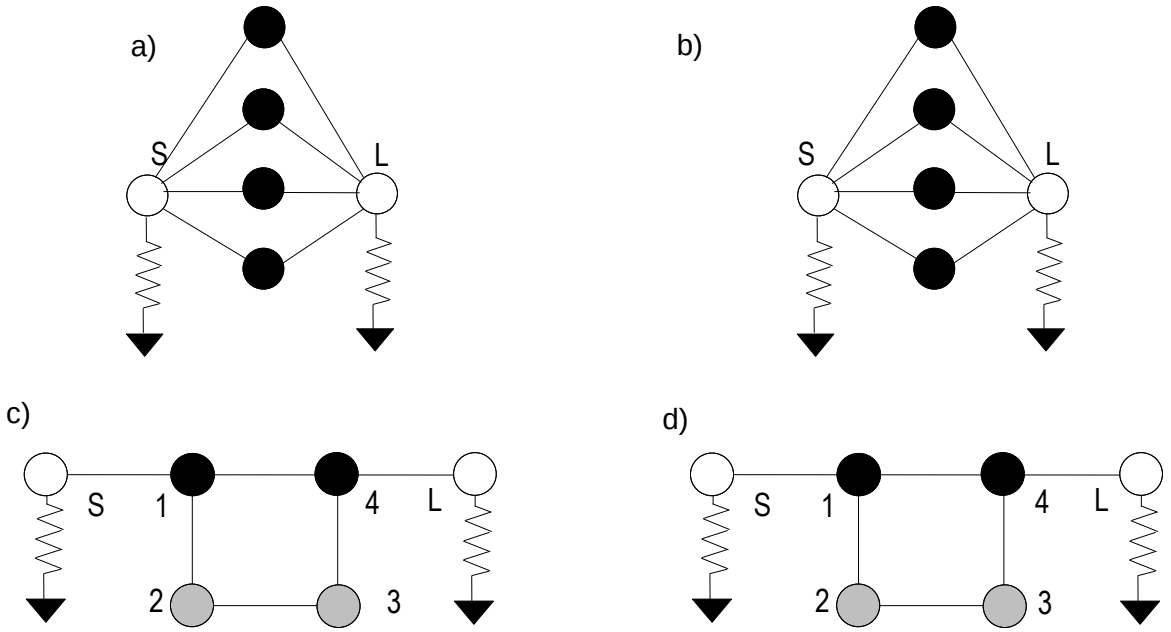

Fig. 34 - Uniform loss distribution for a 4^{th} order filter designed following cases A+C. Black circles correspond to the resonators with lowest Q; grey circles to resonators with $Q= Q_{eff}$ (the Q for a prescribed rounding in the transmission response; circles labeled NS and NL correspond to non-resonant nodes and white circles correspond to the source/load. a) Transversal coupling topology b) folded coupling topology (FCT), c) FCT with non-resonant nodes, d) topology after loss distribution.

The resulting network can then be outlined as in Fig. 34c, and its corresponding *(N+4)x(N+4)* coupling matrix is as follows:

	S	*NS*	*1*	*2*	*3*	*4*	*NL*	*L*
S	*0*	*1*	*0*	*0*	*0*	*0*	*0*	*0*
NS	*1*	*-jG*	M_{01}	*0*	*0*	*0*	*0*	*0*
1	*0*	M_{01}	*-jG*$_1$	M_{12}	*0*	M_{14}	*0*	*0*
2	*0*	*0*	M_{12}	*0*	M_{23}	*0*	*0*	*0*
3	*0*	*0*	*0*	M_{23}	*0*	M_{12}	*0*	*0*
4	*0*	*0*	M_{14}	*0*	M_{12}	*-jG*$_1$	M_{01}	*0*
NL	*0*	*0*	*0*	*0*	*0*	M_{01}	*-jG*	*1*
L	*0*	*0*	*0*	*0*	*0*	*0*	*1*	*0*

The matrix above reveals that losses are not distributed throughout the network, and the central resonators *2* and *3* result to be lossless. Note moreover that the central part of the matrix (i.e., the matrix elements indicated in grey), is identical to the one obtained in a lossless case. The shunt conductances appearing in the nonresonant nodes can be directly obtained from the initially set insertion losses *k* as:

$$G = \frac{1-k}{1+k} \tag{51}$$

Being k the pre-inscribed insertion loss into the transmission and reflection S parameters. And the losses in the first and last resonator G_1, can be obtained as

$$G_1 = GM_{01\_Lossless} \tag{52}$$

where $M_{01\_Lossless}$ corresponds to the coupling between the source and first resonator in a lossless case.

The next step is to shift losses to the centre resonators 2 and 3 from the lossy resonators 1 and 4. To do that, we may use hyperbolic matrix rotation (Appendix 4) on the matrix above. By doing so, we are also introducing some additional resistive couplings from the non-resonant nodes to the centre resonators and resistive couplings from resonator 1 to resonator 3 and from resonator 2 to resonator 4. Details of the resistive coupling distribution are outlined in Fig. 34d, through resistive elements.

The hyperbolic rotation is set by

$$c_r = \cosh\alpha \quad \text{and} \quad j \cdot s_r = j \cdot \sinh\alpha \tag{53}$$

where α is the rotation angle.

Since the initial folded coupling matrix (matrix above) is symmetric, we may keep the symmetry of the matrix by just applying the same hyperbolic rotation to transfer losses from 1 to 2 than that used in the transfer of loss from 4 to 3. The following matrix shows the elements of the coupling matrix

used to obtain the uniform Q distribution condition. Note that, because of its symmetry, only some of the matrix elements are shown below.

	S	*NS*	*1*	*2*
S	*0*	*1*	*0*	*0*
NS	*1*	*-jG*	$c_r M_{01}$	$js_r M_{01}$
1	*0*	$c_r M_{01}$	$-j(c_r^2 G_1 + 2s_r c_r M_{12})$	$M_{12}(c_r^2 + s_r^2)+G_1 c_r s_r$
2	*0*	$js_r M_{01}$	$M_{12}(c_r^2 + s_r^2)+G_1 c_r s_r$	$js_r (s_r G_1 + 2c_r M_{12})$
3	*0*	*0*	$jc_r s_r(M_{14}-M_{23})$	$c_r^2 M_{23} - s_r^2 M_{14}$
4	*0*	*0*	$c_r^2 M_{14} - s_r^2 M_{23}$	$jc_r s_r(M_{14}-M_{23})$
NL	*0*	*0*	*0*	*0*
L	*0*	*0*	*0*	*0*

The lossy terms in the diagonal of the matrix (in grey) account for both the losses in the resonator (quality factor) and the resistive coupling between the resonators, whereas the lossy off-diagonal terms (in grey also) account for the resistive coupling between two nodes. Therefore the Q of each resonator can be obtained from the imaginary terms in each row.

Therefore to achieve a uniform Q distribution in the network one only needs to find the angle α (c_r and s_r) that satisfies that the losses corresponding to the Q of the imaginary terms of third row (corresponding to 1st resonator) is equal to losses corresponding to the Q of the imaginary terms of the fourth row (corresponding to the 2nd resonator), as long as the resulting Q>0.

However this does not give the minimum required Q for the synthesized response. To obtain the minimum Q we need to move all the losses in the non-resonant nodes to the rest of the filter network. This occurs when no shunt resistance exists at the non-resonant nodes and thus, the addition of all imaginary elements in the *NS* (or *NL*) row should be zero. To this end, the non-resonant node is scaled by a constant value *h*, as indicated in the matrix above. Node scaling is a well-known procedure on matrix transformations. Details on this process are outlined in Appendix 5. For a minimum required Q, *h* should be:

$$h = \frac{s_r M_{01}}{G} \tag{54}$$

Note that this value (54) allows to remove the shunt resistor from the nonresonant node and transfer the losses into the inner resonators.

	S	NS	1	2
S	0	$\boldsymbol{h}$	0	0
NS	$\boldsymbol{h}$	$-j\boldsymbol{h}^2G$	$\boldsymbol{h}c_rM_{01}$	$j\boldsymbol{h}s_rM_{01}$
1	0	$\boldsymbol{h}c_rM_{01}$	$-j(c_r^2G_1+2s_rc_rM_{12})$	$M_{12}(c_r^2+s_r^2)+G_1c_rs_r$
2	0	$j\boldsymbol{h}s_rM_{01}$	$M_{12}(c_r^2+s_r^2)+G_1c_rs_r$	$js_r(s_rG_1+2c_rM_{12})$
3	0	0	$jc_rs_r(M_{14}-M_{23})$	$c_r^2M_{23}-s_r^2M_{14}$
4	0	0	$c_r^2M_{14}-s_r^2M_{23}$	$jc_rs_r(M_{14}-M_{23})$
NL	0	0	0	0
L	0	0	0	0

The quality factor of the first and second resonator result:

$$Q_1 = M_{12}s_rc_r + c_r^2G_1 + c_rs_r(M_{14}-M_{23})$$

$$Q_2 = s_r^2G_1 + 2c_rM_{12} - c_rs_r(M_{14}-M_{23}) - \frac{s_r^2M_{01}^2}{G} \tag{55}$$

Now by equating the resulting Qs in resonator 1 and 2, we obtain:

$$c_r^2G_1 + 2c_rs_rM_{12} - c_rs_r(M_{14}-M_{23}) = -s_r^2G_1 - 2c_rs_rM_{12} - c_rs_r(M_{14}-M_{23}) - s_rhM \tag{56}$$

Which results in the following equation:

$$(c_r^2+s_r^2)G_1 + 4c_rs_rM_{12} = -s_r^2\frac{M_{01}^2}{G} \tag{57}$$

Substituting (53) into (57),

$$\left(2G_1 + \frac{M_{01}^2}{G}\right)\cosh 2\alpha + 4M_{12}\sinh 2\alpha - \frac{M_{01}^2}{G} = 0 \tag{58}$$

Solving (58) we obtain the angle which give uniform Q distribution in all resonators:

$$\alpha = \frac{1}{2}\ln\left[\frac{\frac{M_{01}^2}{G} \pm \sqrt{4G_1\frac{M_{01}^2}{G} - 4G_1^2 + 16M_{12}^2}}{2G_1 + \frac{M_{01}^2}{G} + 4M_{12}}\right] \tag{59}$$

The equation above has two possible solutions, only one of them potentially fulfilling the Q>0 requirement. There are even cases where none of the two angles obtained from (59) satisfies the Q>0 requirement. These are cases where a high selectivity is required, e.g. frequency responses with transmission zeros very close to the passband, so they would require high Q, but at the same

time the imposed insertion losses, *k*, are high, so the value of *G* and G_1 set a given amount of losses to be distributed. In those cases uniform Q distribution would not be possible.

- **Insertion Loss requirements**

In this section a relation between the rotation angle α (59), insertion loss and minimum required Q is derived for:

- Butterworth Filters
- Chebychev Filters (15, 20, 25 dB return loss)
- Generalised Chebychev Filtres with a single transmission zero at the normalized position *a*.

Table 15 summarizes the required Q for a given insertion loss. In a 4-order Butterworth filter defines a general formulation for the required Q. For a Chebyshev filter, the required Q depends on the return losses by a factor γ_{RL} as indicated in the table. Table 15 lists the value of γ_{RL} for several values of return loss (RL). The dependence of γ_{RL} on RL is depicted in Fig. 35. In this case the required Q increases when the RL decreases, which is consistent with the fact that, for a given filter order, the selectivity of the filter (slope of $|S_{21}|$ at the edge of the stop-band) increases when the RL is reduced and therefore the Q to achieve such performance should be higher.

When transmission zeros are introduced, the required Q required is scaled by a factor ρ_a, whose dependence on the position of the transmission zero is outlined in Fig. 36. The ρ_a values for several positions of the transmission zeros and for a RL=20 dB are also listed in Table 15. As expected the required Q sharply increases when the zeros are set very close to the passband, due again to the high selectivity introduced by the transmission zeros. Note that the value of γ_{RL} for Chebyshev with transmission zeroes is the same as that of the previous case.

Also note that ρ_a dependence on the transmission zero is different for each value of return losses. When the return losses increases the required Q as a function of the transmission zero increases. Note that this is consistent with the fact that for higher return losses roll-off selectivity close to the bandpass edges is smoother than for lower values of return losses, then to achieve the desired selectivity introduced by the transmission zero a higher Q is required.

BUTTERWORTH

$$Q_0 \approx \frac{71}{IL(dB)FBW}$$

CHEBYSHEV

$$Q_0 \approx \frac{\gamma_{RL}}{IL(dB)FBW}$$

RL (dB)	25	20	15
γ_{RL}	60	72	88

CHEBYSHEV WITH TRANSMISSIONZEROS

$$Q_0 \approx \frac{\rho_a \cdot \gamma_{RL}}{IL(dB)FBW}$$

a	5	2	1.7	1.6	1.5
ρ_a	1	1.6	2.5	3.6	10.7

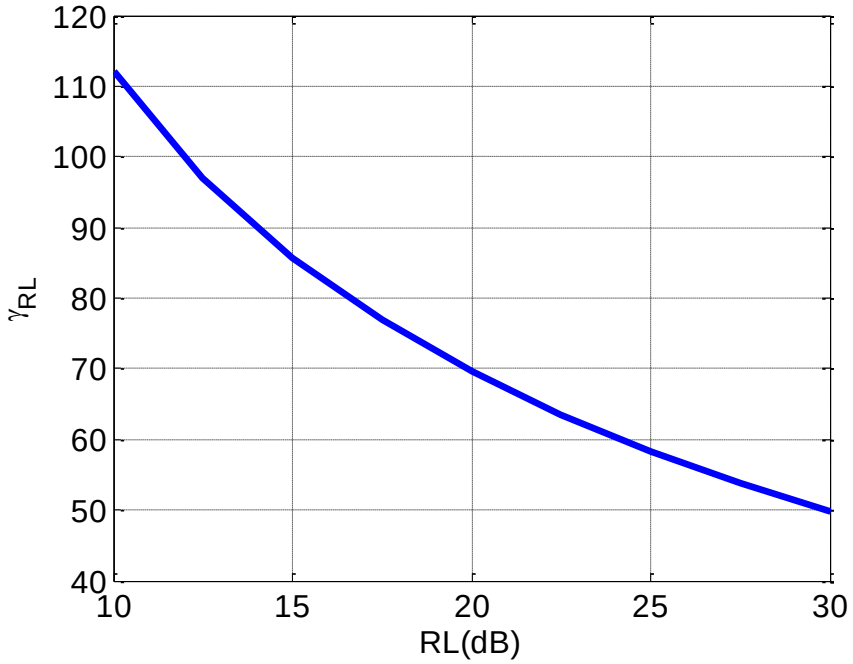

Fig. 35 - Dependence of the variable γ_{RL} as a function of the return losses.

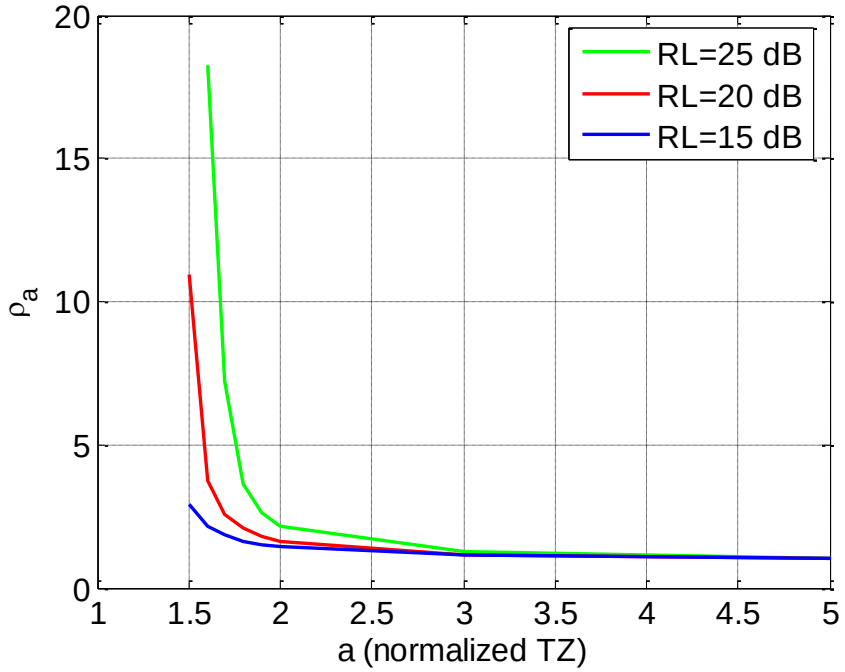

Fig. 36 - Dependence of the variable ρ_a as function of the position of the transmission zero, normalized frequency, for *RL*=25 dB (green), 20 dB (red) and 15 dB (blue).

- **6th degree network**

This follows analogous procedure than in previous section for a 4th order filter. In this case the starting topology is shown in Figure 37 a.

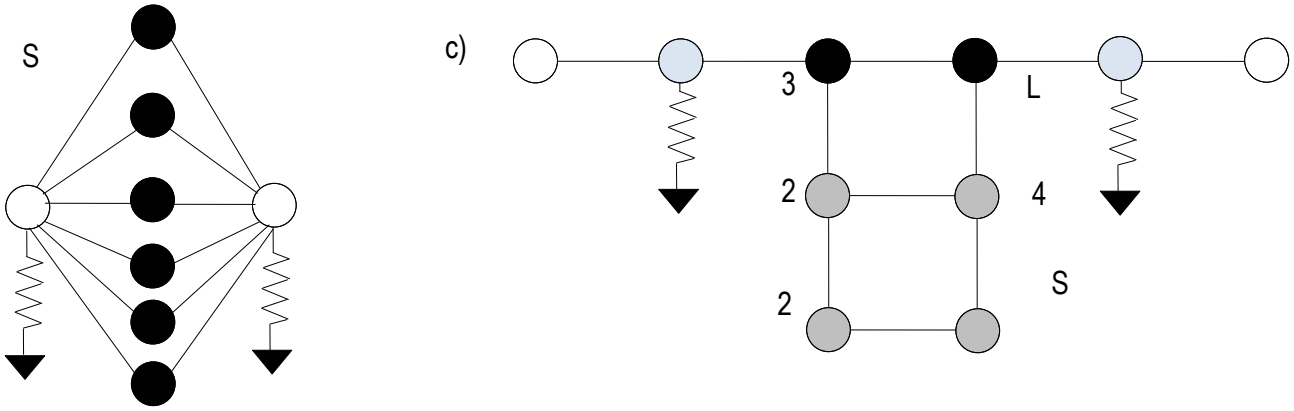

Fig. 37 a) Transversal network topology of a synthesized response of a 6th order filter. b) Folded coupled topology (FCT).

The transversal coupling matrix is then transformed to the folded coupling matrix, resulting in a topology as the one shown in Figure 37b, which coupling matrix reads as:

	S	NS	1	2	3	4	5	6	NL	L
S	0	1	0	0	0	0	0	0	0	0
NS	1	-jG	M_{01}	0	0	0	0	0	0	0
1	0	M_{01}	$-jG_1$	M_{12}	0	0	0	0	0	0
2	0	0	M_{12}	0	M_{23}	0	0	0	0	0
3	0	0	0	M_{23}	0	M_{34}	0	0	0	0
4	0	0	0	0	M_{34}	0	M_{23}	0	0	0
5	0	0	0	0	0	M_{23}	0	M_{12}	0	0
6	0	0	0	0	0	0	M_{12}	$-jG_1$	M_{01}	0
NL	0	0	0	0	0	0	0	M_{01}	-jG	1
L	0	0	0	0	0	0	0	0	1	0

Note again that this corresponds to a folded coupling matrix where the losses are not properly distributed and appear gathered in the nonresonant nodes, by *G*, and in the first and last resonators by G_1. In this case the values of G and G_1 can be directly calculated by using (51) and (52).

To distribute the losses we need to apply hyperbolic rotation in the folded coupling matrix above. The hyperbolic rotation now will consist on moving symmetrically losses from resonator 1 to 2 and from resonator 6 to 5 using the same rotation angle α. This would result in a folded coupling matrix where only the inner resonators 3 and 4 are lossless. We will then distribute losses (symmetrically) from resonator 2 to 3 and from resonator 5 to 4, using a rotation angle α_1. The resulting coupling matrix is detailed in the Appendix 6.

Now, therefore the hyperbolic rotation is set by:

$$c_r = \cosh\alpha \quad \text{and} \quad j \cdot s_r = j \cdot \sinh\alpha,$$
$$c_{r1} = \cosh\alpha_1 \quad \text{and} \quad j \cdot s_{r1} = j \cdot \sinh\alpha_1, \tag{60}$$

Again in this case we will impose the condition of moving all the losses into the nonresonant nodes into the resonators by applying node scaling into the nonresonant node. The node scaling term *h* would result:

$$h = \frac{-s_r c_{r1} M_{01}}{G} \tag{61}$$

The resulting folded coupled matrix after performing node scaling is also detailed in the Appendix 6. Now from this resulting coupling matrix we may obtain the resulting Q at each resonator as a function of the couplings of the initial synthesis and the rotation angles α and α_1, as:

$$
\begin{aligned}
Q_1 &= c_r^2 M_{12} s_{r1} - c_r^2 G_1 + s_r^2 M_{12} s_{r1} + 2c_r s_r M_{12} - s_r c_{r1} M_{23} - c_r s_r G_1 s_{r1} \\
Q_2 &= c_{r1}\left(s_r^2 G_1 c_{r1} - M_{34} s_{r1} + \frac{-s_r^2 c_{r1} M_{01}^2}{G} + 2c_r M_{23} s_{r1} - 2c_r s_r c_{r1} M_{12} \right) \\
Q_3 &= c_r^2 M_{12} s_{r1} + 2M_{12} c_r s_r s_{r1}{}^2 - G_1 c_r s_r s_{r1} - 2c_{r1} M_{23} c_r s_{r1} - G_1 s_r{}^2 s_{r1} - c_{r1} M_{23} s_r - c_{r1} M_{34} s_{r1}
\end{aligned}
\tag{62}
$$

Equating the values of the Qs (62) we obtain the following two equation, which will be used to extract the unknown rotation angles α and $\alpha 1$.

$$
\begin{aligned}
s_r^2 c_{r1}^2 M_{01}^2 - G_1 G(c_r^2 + c_r s_r s_{r1} + s_r^2 c_{r1}^2) + M_{12} G(c_r^2 s_{r1} + s_r^2 s_{r1} + 2c_r s_r + 2c_r s_r c_{r1}^2) \\
- M_{23} G(s_r c_{r1} + 2c_r c_{r1} s_{r1}) + G c_{r1} M_{34} s_{r1} = 0
\end{aligned}
\tag{63}
$$

$$
-G_1 c_r^2 - 2M_{12} c_r s_r (s_{r1}^2 - 1) + 2M_{23} c_{r1} s_{r1} c_r + G_1 s_r{}^2 s_{r1}^2 + c_{r1} M_{34} s_{r1} = 0 \tag{64}
$$

The equation above (63) and (64) cannot be solved analytically and optimization routines are used to extract the rotation angles.

- **Insertion loss requirements**

As performed for a 4th order filter a closed form expressions to relate the required Q with the initially set insertion losses (IL) for a 6th order filter it is possible. To do that, we used the obtained angles from the expressions above (63) and (64).

TABLE 16: SUMMARY OF REQUIRED Q VS IL

BUTTERWORTH

$$Q_0 \approx \frac{127}{IL(dB)FBW}$$

CHEBYSHEV

$$Q_0 \approx \frac{\gamma_{RL}}{IL(dB)FBW}$$

RL (dB)	25	20	15
γ_{RL}	152	176	211

CHEBYSHEV WITH TRANSMISSIONZEROS

$$Q_0 \approx \frac{\rho_a \cdot \gamma_{RL}}{IL(dB)FBW}$$

a	5	2	1.7	1.6	1.5
ρ_a	1	1.8	2.3	2.9	4.4

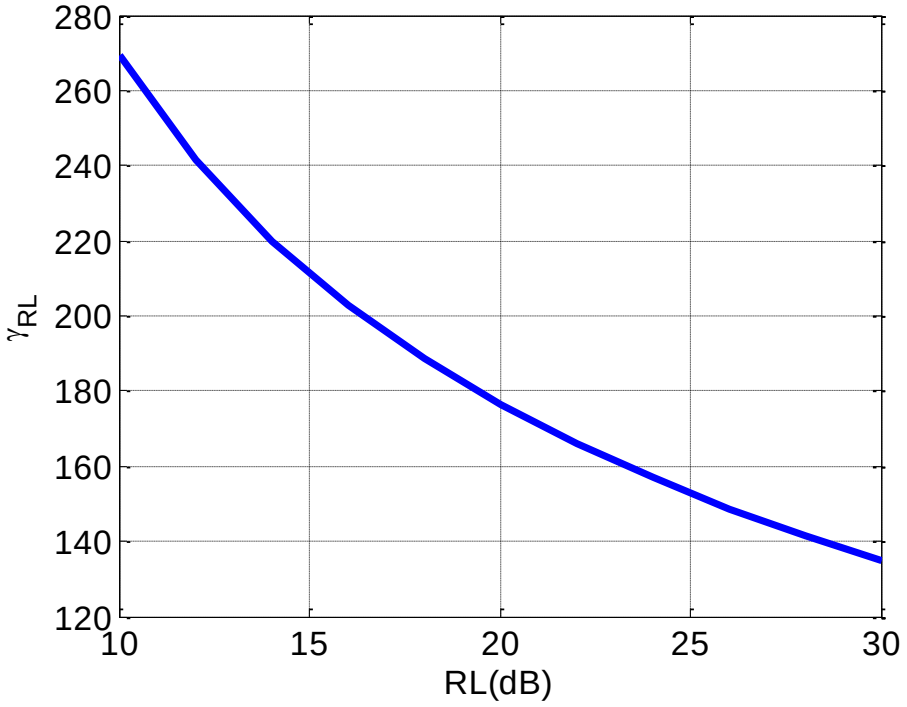

Fig. 38 - Dependence of the variable γ_{RL} as a function of the return losses.

Note that in the sixth order case the required Q is higher for a given insertion loss. Note that this is consistent with the fact that the total amount of losses are higher because of the larger number of resonators and therefore the Q to satisfy a given losses needs to be higher. Also note that this is consistent with what occurs in conventional filter where the insertion losses are proportional to the number of resonators [5][2].

Although one might expect the required Q in the sixth order filter (Table 16) results from scaling the required Q in the case of fourth order filters (Table15); this is scaling the values of Table 15 by a factor of 6/4=1.5. The required Q in the case of 6^{th} order filter is much higher. This is because the required Q, in addition of setting the total insertion losses they also set the filter selectivity which is higher in an order sixth.

As for the 4th order filter here it is also evaluated the dependence on the position of the transmission zero in the required Q. This results are set by the term ρ_a and its dependency is depicted in Fig. 39 for different several values of insertion losses (RL=15, 20 25 dB). Note that the tendency is like the one shown in Fig. 36, however in this case the scaling term ρ_a increases smoother than in the case of a fourth order filter. This is because in a sixth order filter the selectivity is higher than in order fourth and the increase in selectivity introduced by the transmission zero is closer than the initial selectivity so a smaller increment on the Q is required.

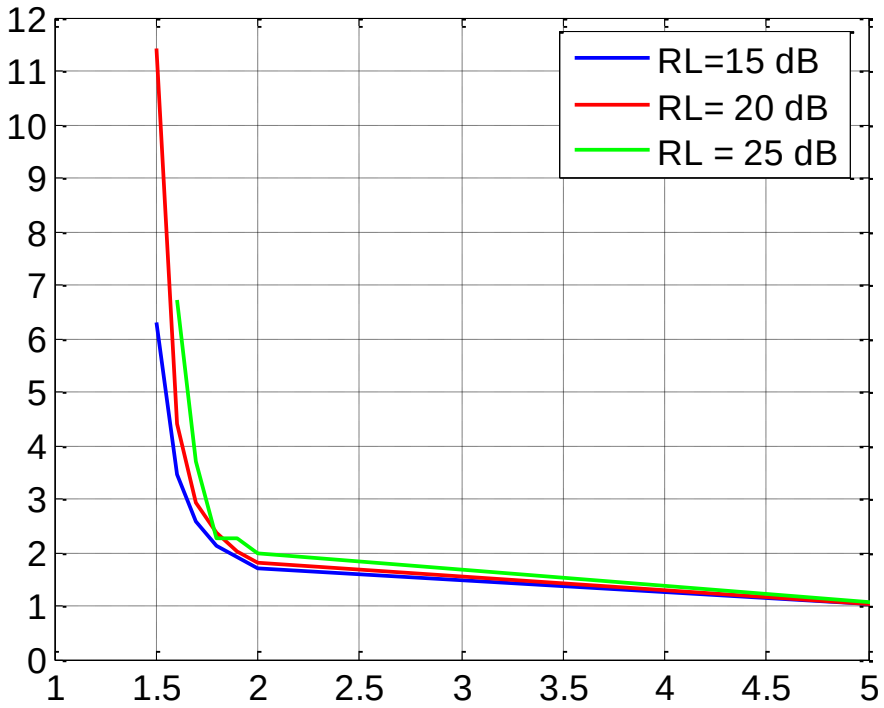

Fig. 39 - Dependence of the variable ρ_a as function of the position of the transmission zero, normalized frequency, for *RL*=25 dB (green), 20 dB (red) and 15 dB (blue).

Note that what is reported above for the 4th and 6th order filter does not yet consider the effect of a prescribed flatness, so always assume a ideal type of filter response, with an insertion loss offset. However this can easily be extended to consider the case where a certain flatness, so an effective Q (Q_{eff}) it is accepted. This is *Case C* above.

By using this procedure one can define a very useful general expression for a network with identical resonator Q_0 that relates Q_0 to a given insertion loss, the fractional bandwidth (FBW), return losses and position of the transmission zeros, through the terms γ_{RL} and ρ_a, respectively, and the value of the effective Q_{eff} corresponding to a finite Q_{eff} response. The values of γ_{RL} and ρ_a, for order 4th and 6th are given in the set of figures above, Figs. 35 and 36, and Figs. 38 and 39, respectively.

The expression is given by

$$Q_0^{-1} \approx \left(\frac{\gamma_{RL} \cdot \rho_a}{IL(dB) FBW \sqrt{M_{01}}} \right)^{-1} + Q_{eff}^{-1} \tag{65}$$

where the prescribed insertion losses are defined by k ($IL(dB)=20 \cdot log_{10}(k)$).

Equations (59) and (65) allow filter designers to systematically account for the effects of a limited Q in the filter synthesis process and therefore avoid to using resonators with uneven Q. Note that a uniform distribution in the resonators may be very convenient from a practical point of view, since all resonators can be implemented with the same technology, shape and dimensions, and therefore they would be subject to the same manufacturing tolerances and thermal effects.

- **Numerical Example**

Following we use the procedure above to distribute losses in the examples outlined in section 2.2.1 and section 2.2.3, corresponding to the responses in Figs. 26 and 31.

In the case of emulating a prescribed infinite Q_{eff} (Fig. 26) we obtain the folded network, in Fig. 34d, with a uniform required resonator Q of 2780, whose coupling matrix is:

0	3.3	0	0	0	0	0	0
3.3	-0.16j	-3.4	0.16j	0	0	0	0
0	-3.4	-0.69j	9.0	0.33j	0	0	0
0	0.16j	9.0	-0.84j	7.0	0.33j	0	0
0	0	0.33j	7.0	-0.84j	9.0	0.16j	0
0	0	0	0.33j	9.0	-0.69j	-3.4	0
0	0	0	0	0.16j	-3.4	-0.16j	3.3
0	0	0	0	0	0	3.3	0

Table 17: FCM with uniform *Q* distribution of the response of Fig.26. Note that all terms are normalized by 0.1

On the other hand if we want to emulate a response with transmission rounding is equivalent to a Q_{eff} of 2000, we obtain a folded network which requires a uniform *Q* of 1160, whose coupling matrix is:

0	3.3	0	0	0	0	0	0
3.3	-0.16j	-3.4	0.16j	0	0	0	0
0	-3.4	-1.19j	9.0	0.33j	0	0	0
0	0.16j	9.0	-1.34j	7.0	0.33j	0	0
0	0	0.33j	7.0	-1.34j	9.0	0.16j	0
0	0	0	0.33j	9.0	-1.19j	-3.4	0
0	0	0	0	0.16j	-3.4	-0.16j	3.3
0	0	0	0	0	0	3.3	0

Table 18: FCM with uniform *Q* distribution of the response of Fig.31. Note that all terms are normalized by 0.1

The coupling matrices above only differ in the losses in the resonators (diagonal terms). Note that this is consistent with the fact that their initial transversal coupling matrix only differs in the losses in the various resonators, and the rotation angle that ensures a uniform distribution does not depend on Q_{eff}.

Table 19 and Fig. 40 summarize the comparisons of the responses of the two examples above versus those achievable with standard (lossless) synthesis. To achieve an insertion loss flatness equivalent to that of a lossless filter, we require resonator *Qs* of 2780 using lossy filter synthesis (Table 19). With that resonator *Q*, a classical design would have a lower insertion loss, but a worse

insertion loss flatness (0.4 dBpp). The second example (Table 19) shows how the required *Q* (2780 in the first example) can be further reduced to 1160 by accepting a degradation in the insertion loss flatness equivalent to a Q_{eff} of 2000. Again, the classical design with resonator *Qs* of 1160 has a smaller insertion loss, but worse insertion loss flatness.

Synthesis	**IL (dB)**	**ΔIL (dBpp)**	**Q_{eff}**	**Q_0**
Lossy	2.5	0.01	Inf	2780
Lossy	3.5	0.52	2000	1160
Lossless [1][2]	0.73	0.4	2780	2780
Lossless [1] [2]	1.73	0.85	1160	1160

Table 19: Comparison of various synthesis alternatives in terms of insertion loss (*IL*), insertion loss flatness (ΔIL) and its associated effective *Q* (Q_{eff}), and the required resonator *Q* (Q_0).

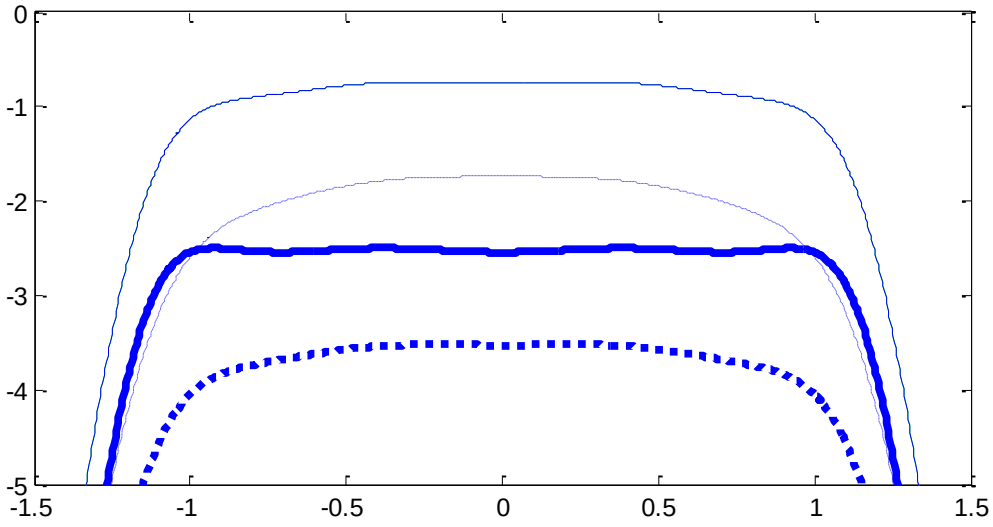

Fig. 40 - Transmission response of various synthesis alternatives: (thick-solid line) lossy synthesis equivalent to a infinite *Q* response requiring resonator *Qs* of 2780; (thin-solid line) lossless synthesis evaluated with *Qs* of 2780; (thick-dotted line) lossy synthesis equivalent to a finite *Q* response of 2000 requiring resonator *Qs* of 1160; (thin slashed line) lossless synthesis evaluated with *Qs* of 1160. Note the differences in insertion loss flatness and absolute insertion loss among the various design alternatives.

2.3.3 Loss Distribution in case B

The folded coupled topology (FCT) for case B of Fig. 33b, unlike the topology for case A of Fig. 33a, does not have resistors to ground at the load and source nodes. Thus, when trying to transfer losses from resonator 1 to 2 and 6 to 5 by using hyperbolic rotations, additional resistive cross couplings would appear from resonator 2 to the source and from resonator 5 to the load.

Additionally, losses would be transferred from the source and load to the resistive cross-couplings. Since neither the source nor the load nodes have any spare loss to be transferred, the hyperbolic rotation would result in a shunt negative resistance appearing at both these nodes. Thus, hyperbolic rotation in folded coupling topologies is not suitable for loss distribution in case B with folded coupling topologies like those in Fig. 33b.

On the other hand, the folded coupled topology for case B of Fig. 33c already has losses distributed throughout the network, thanks to the inserted pole/zero in the transmission response (48). However, as stated in previous section [15] the resulting loss distribution is not always convenient for the practical implementation, because of the uneven values of the resulting *Q*s or because some of the resonators would require negative *Q*. Moreover, this initial loss distribution resulting from the TCM to FCM transformation depends on the type of response, i.e., order of the filter, position of the transmission zeros and also on the position of the inserted pole/zero. Because of that, it is not straightforward to find a systematic way of performing the hyperbolic rotations for a more convenient distribution of losses. Following we present systematic procedure that we been used for the synthesis of 6^{th} order lossy filters and shows to be useful for most cases we tried. Nevertheless, further research for defining convenient topologies for lossy filter implementation is necessary.

The procedure starts from the folded coupling matrix of Fig. 33c. From the goal of performing a most uniform distribution of *Q* we use four different angles to perform hyperbolic rotation between the inner resonators. This is resonators 2, 3, 4 and 5, in Fig. 33c. Figure 41 indicates in arrows the way we perform the hyperbolic rotation, this is from resonator 5 to 2, from 2 to 3, from 3 to 4 and from 4 to 5. Note that this does not involve the first and last resonator in the hyperbolic rotation to avoid negative resistances at the load and source nodes, similarly to what has been explained above for Fig. 33b.

Having therefore four variables (the rotation angles) and six unknowns (the *Q* of the resonators),it is not always possible to obtain a fully uniform *Q* distribution throughout the network. However, it is possible to obtain a uniform *Q* distribution in the inner resonators, as shown in Fig. 14b, and equal *Q* in the first and last resonator. Usually the *Q* values at the outer resonators are lower than the *Q* values of the inner resonators.

The resulting network, detailed in Fig. 14 b, has several resistive cross-coupling. In practice some of those, in particular the ones from 1 to 3 and from 6 to 4 are very small and can be neglected for the final implementation. After neglecting some of those resistive couplings further adjustment can be performed on the terms of the remaining coupling matrix for optimization of the final response.

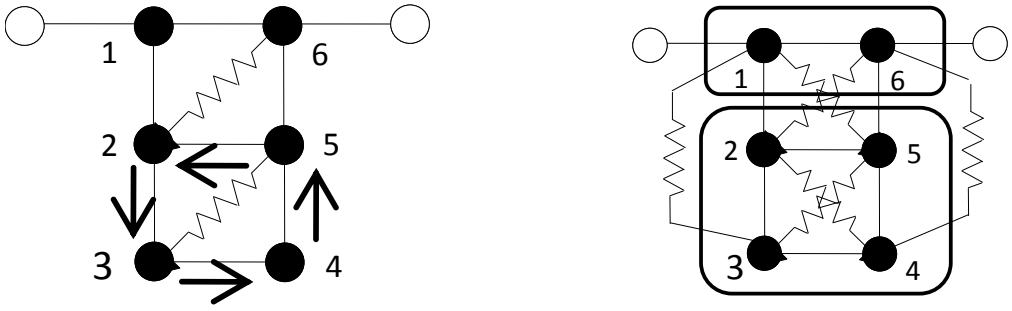

Fig. 41 - a) Folded coupling network (Case B (48)) before applying any hyperbolic rotation. b) Folded coupling network after applying hyperbolic rotation

- **Numerical Example**

We use the procedure above to synthesize a folded topology as the one in Fig. 41b. For this example we choose a six order Chebyshev with a single pair of symmetrical transmission zeros (at +/-3.3 normalized frequency), where the transfer function is defined by (48), being k=0.7 and δ=18.

The resulting coupling matrix is detailed in Table 20, and its corresponding frequency response is outlined in Fig. 42. Note from Table 20 that in this case the resistive coupling from the first and last resonator to the third and fourth resonators, respectively, can be neglected.

0	10.3	0	0	0	0	0	0
10.3	-1.17j	9.15	0	0	0.062j	0	0
0	9.15	-0.58j	6.65	0.179j	-0.285	0.089j	0
0	0	6.65	-0.64j	6,46	0.328j	0	0
0	0	0.179j	6.46	-0.49j	6.6	0	0
0	0.062j	-0.285	0.328j	6.6	-0.70j	-9.15	0
0	0	0.089j	0	0	-9.15	1.2j	10.3
0	0	0	0	0	0	10.3	0

Table 20: FCM of the response of Fig.42. Note that all terms are normalized by 0.1

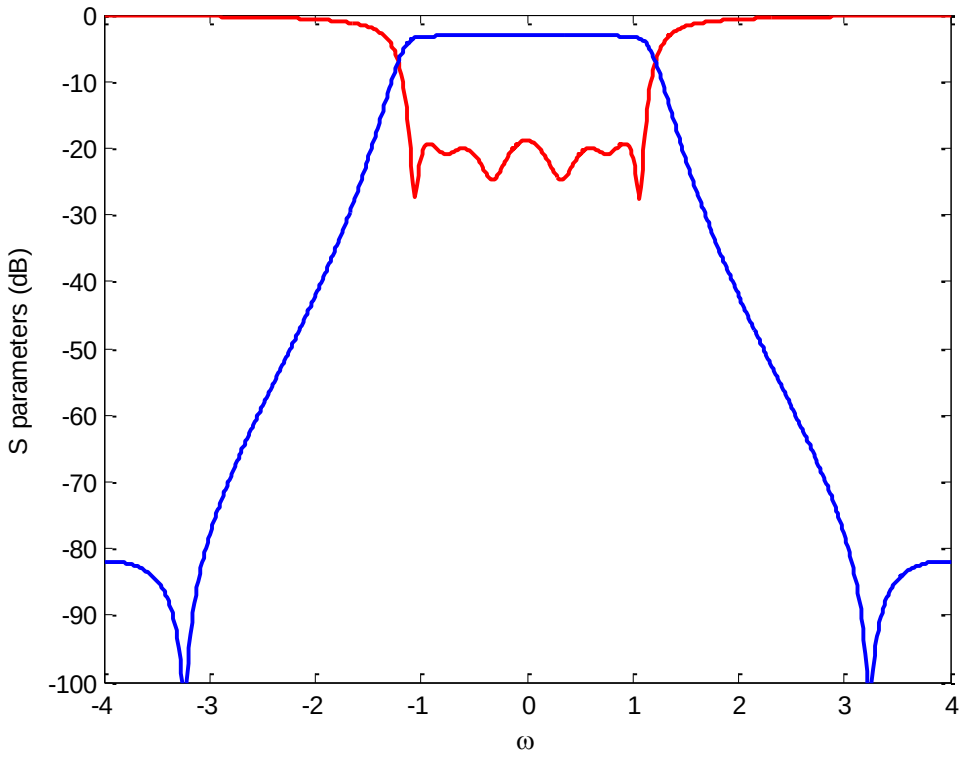

Fig. 42 - Response of a lossy filter design, k=0.7 (48), δ=18, Blue trace: $|S_{21}|$, red trace: $|S_{11}|$, $|S_{22}|$.

For a frequency response centered at 4 GHz with a 36 MHz channel bandwidth and with insertion loss flatness equivalent to that of a lossless filter, this would result in a Q factor of 1000 for the first and last resonator and a uniform Q factor of 3500 for the inner quadruplet.

2.3.4 Parallel Connected Coupling Matrix

The parallel connected networks approach [1] (see section 1.5.3) has already been successfully used to distribute losses in topologies corresponding to Case A [15]. Here we apply such approach in a frequency response type like the ones defined by Case B.

The approach consists in splitting the initial Transversal Coupling Matrix into sub-matrices. Independent circuit transformations are then applied to the sub-networks corresponding to each sub-matrix. The small size of the resulting sub-networks has the advantage of not giving rise to a very complicated set of resistive couplings when hyperbolic rotation is applied to them.

As an example, this approach is applied to a 6^{th} order transversal network corresponding to a case B response (Fig. 43a). We split the TCM into two sub-matrices with 2 and 4 resonators. Note that the selection of the initial two-sub-matrices may affect the loss distribution therefore the final network topology.

Then both sub-networks are transformed to folded sub-networks. The resulting sub-networks are represented in Figs. 43b and 43c, where now hyperbolic rotation and node scaling transformations can be separately performed. The final network is shown in Fig. 43d (the additional resonant node is not represented). Note that the concept of node scaling is briefly outlined in Appendix 5.

Further transformation can be performed on the resulting network in Fig. 43d to obtain a network where the source and load are coupled to a single resonator. We start by annihilating the coupling between the source and resonator 1 on one hand, and the load and resonator 4 on the other. As pivots we use the rotations (5, 1) and (6, 4) respectively. The resulting network is shown in Fig. 43e (very small resistive coupling elements are omitted in the figure).

Although the following transformation is not general, in some synthesized responses we may annihilate (or reduce until made negligible) the coupling between resonators 1 and 4 and the coupling between resonators 3 and 2 in Fig. 43e. After neglecting the smallest couplings, this results in network topologies such as the ones shown in Figs. 43f and 43g. Again adjustment of the remaining coupling elements can be done for obtaining an optimized response.

- **Numerical Example**

For this example we synthesize the transversal coupling matrix of a sixth order Chebyshev filter with a single pair of symmetrical transmission zeros at +/-1.3 normalized frequency, the prescribed insertion loss is 0.75 and δ=11 (48). Its frequency response it is outlined in Fig. 44.

The following tables (Table 21- Table 24) detail the coupling matrices corresponding to the topologies outlined in Figs 43b to 43e, respectively, for the frequency response of Fig. 44. The rotation angle to distribute losses in the topology of Fig. 43d was 0.0318 radians between resonator 2 and 3. Further optimization to obtain the topologies in Fig. 43f and 43g is not performed in this example.

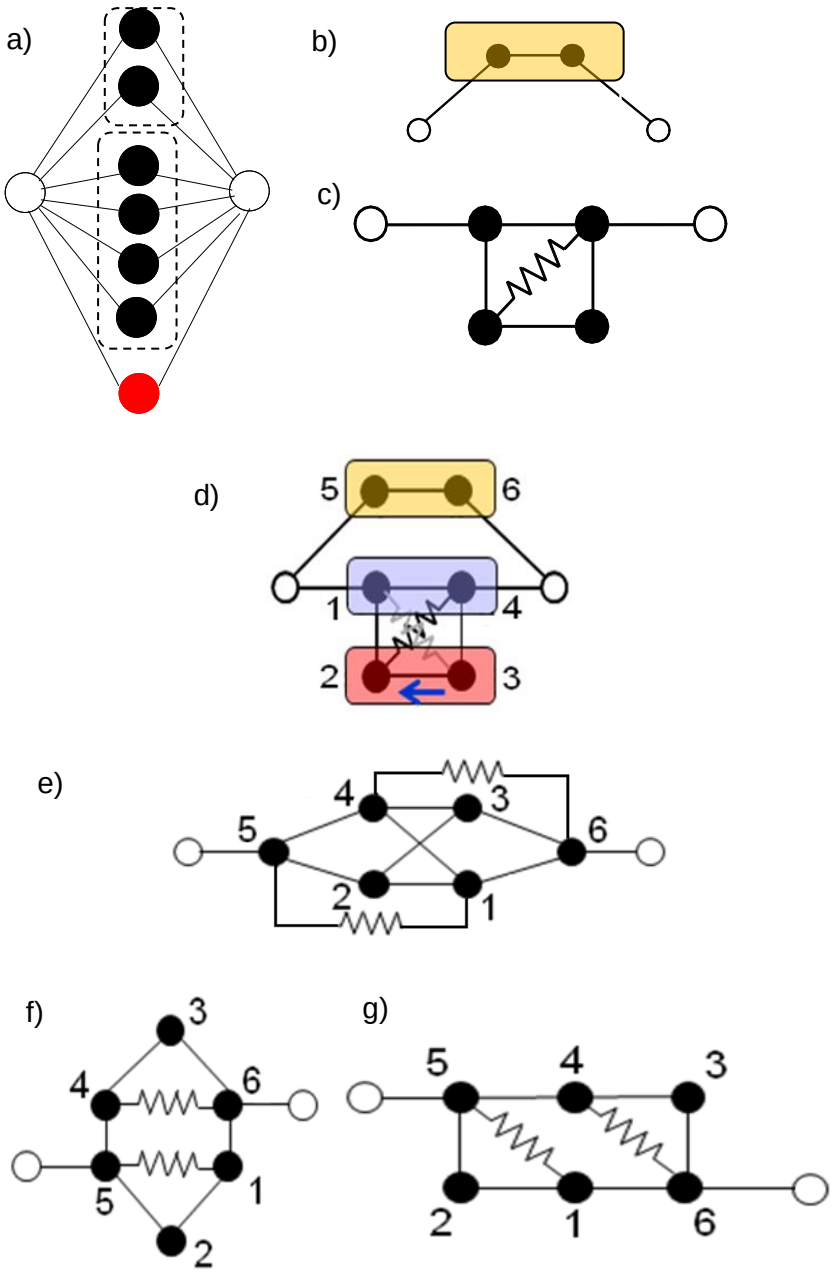

Fig. 43 - a) Transversal for the synthesis case B (8) b) Folded networks of a two resonators subnetwork c) Folded networks of a 4 resonator subnetwork after hyperbolic rotation. d) Parallel connected resulting sixth order network. a) Box section topology for a sixth order filter b), c) and d) Box section topology after annihilation of couplings 4-1 and 2-3.

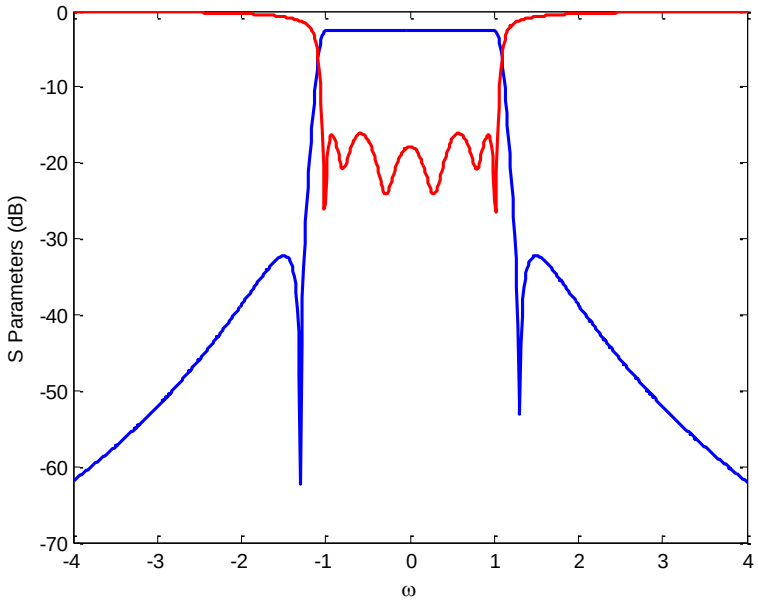

Fig. 44 - a- Response of a lossy filter design, k=0.75 (8), δ=11, Blue trace: $|S_{21}|$, red trace: $|S_{11}|$, $|S_{22}|$.

From the data in Tables 23 and 24, we can deduce the Qs required in each of the two topologies. As in the prior example, for a frequency response centered at 4 GHz with a 36 MHz channel bandwith and insertion loss flatness equivalent to a lossless filter, the topology in Fig. 43d would require the following Qs in resonators 1 through 6 respectively: 1500, 20000, 20000, 1500, 2000 and 2000. On the other hand, the topology in Fig. 43e would require Qs of 2100, 5800, 5800, 2100, 1800 and 1800. Although the later topology has a more even Q distribution, none of the two configurations has been optimized for uniformity in Q.

0	0.54	0	0
0.54	-0.056j	-0.996	0
0	-9.996	-0.056j	0.54
0	0	0.54	0

Table 21: FCM of the topology of Figure 43b

0	0.73	0	0	0	0
0.73	-0.083j	0.29	0	0.55	0
0	0.29	0.048j	0.98	0.019j	0
0	0	0.98	-0.077j	0.29	0
0	0.55	0.019j	0.29	-0.083j	0.73
0	0	0	0	0.73	0

Table 22: FCM of the topology of Figure 43c (see example in main text).

0	7.3	0	0	0	-5.4	0	0
7.3	-0.83j	2.98	0	0.09j	5.54	0	0
0	2.98	-0.15j	9.79	0.1j	0	0	0
0	0.09j	9.79	-0.15j	2.98	0	0	0
0	5.54	0.1j	2.98	-0.83j	0	0	-7.3
-5.4	0	0	0	0	-0.56j	-9.96	0
0	0	0	0	0	-9.96	-0.56j	5.4
0	0	0	0	-7.3	0	5.4	0

Table 23: Coupling M of the topology of Figure 43d and response of Figure 44. Note that all terms are normalized by 0.1

0	0	0	0	0	-9.1	0	0
0	-0.66j	1.7	0	-4.4	0.13j	-7.4	0
0	1.7	-0.19j	9.7	0	-2.3	0	0
0	0	9.7	-0.19j	1.7	0	-2.3	0
0	-4.4	0	1.7	-0.66j	-7.4	0.13j	0
-9.1	0.13j	-2.3	0	-7.4	-0.73j	0	0
0	-7.4	0	-2.3	0.13j	0	-0.73j	9.1
0	0	0	0	0	0	9.1	0

Table 24: Coupling Matrix of the topology of Fig. 43e. Some resistive couplings have been neglected. There are no noticeable differences with respect to the frequency response in Fig. 44, except for a slight degradation in insertion loss flatness of 0.1 dB. Note that all terms are normalized by 0.1

2.4 Optimization approach

From previous sections one observe that the number of resistive couplings may increase when the order of the filter increases and when we try to keep stringent specifications. Although there exist circuit transformation strategies to reduce the number of resistive couplings or even remove those that have negligible effect, there are cases when the extracted topology is not optimum in terms of designing steps, this is number of resistive couplings or location of the resistive couplings, neither the filter performance, which may improve properly optimizing the conventional and/or the resistive couplings.

To this end the optimization technique consists on proposing a suitable topology, which includes conventional and resistive coupling distribution, also a uniform value of the Q of the resonators and a goal filter performance. The goal response could be based on a filter specification mask or on characteristic polynomials with additional rounding and insertion losses.

This technique has been proven to be very useful on the synthesis and design of higher order lossy filters. Next chapter also applies this approach for the final designed of two of the filters presented.

The optimization approach has then been extended and improve to be included in the lossyfilters software (www.tsc.upc.edu/lossyfilters).

The optimization used in the thesis consists on optimizing the predefined values of the coupling matrix under certain constrains, this is negative or positive value and also real, imaginary or complex

values. Then the coupling matrix is evaluated and compared with the goal performance from which a error function is created. The new values of the coupling matrix are recalculated by use of a *Gradient* approach directly implemented in Matlab.

The efficiency of the process also stands on:

- **Frequency points**. This is the frequency points where the coupling matrix is evaluated and in turn the error function generated. It is convenient to select more frequency points where the gradient is larger, this is in the transition band, and also close to the reflection zeros.
    - Note that this last statement might be different for predistorted filters where the reflective zeros are not purely imaginary anymore.
- **Initial guessing**. Obviously the initial values that we choose as a couplings have a significant impact on the efficiency of the optimization procedure. Although several cases may exist, we have usually decided between two different cases:
    - When the goal response does not significantly differs, usually in terms of insertion loss and flatness, from the conventional one, a good option is to use the conventional coupling values resulting from an standard synthesis. Note that we need to additionally locate the resistive couplings (not existing in an standard synthesis), with a low value of coupling, usually an order of magnitude lower than the conventional couplings.
    - When the goal response is considerably different from the one resulting in a conventional synthesis, we perform an initial approach with the lossy techniques above and later applied optimization on the resulting network, in order to improve the performance and reduce the complexity on the network, i.e., number of resistive couplings.

Although the optimization approach has been applied in the following chapter, here we outlined a very illustrative example where the optimization approach has been applied.

- **Example: Folded lossy topology of a 10-4-4 filter**

This example uses the technique above to obtain a synthesized response with a lossy topology. The optimization approach has been used to reduce the number of resistive couplings and to force a uniform Q distribution along the network.

In order to demonstrate the advantages of the optimization approach we evaluate the effects in a 10 order filter *symmetric* with 4 transmission zeros and 4 equalization zeros, which would result in a folded conventional topology with 4 additional cross couplings. See Fig. 45 below. Note therefore

that by applying any of the above strategies for losses distribution would result in a tremendous complicated topology.

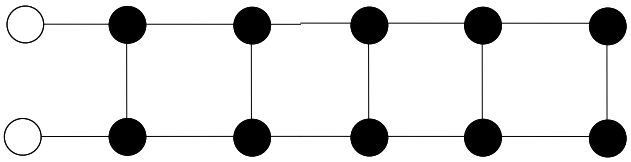

Fig. 45 - Folded topology of a 10-4-4 filter with completely symmetric response.

So that, as state above, the optimization technique consists on proposing a lossy topology, as the one in Fig. 46a for instance, and optimizing the conventional couplings and newly added resistive couplings to get a complaint filter response. The initial values on the optimization procedures are directly selected from those resulting in a standard lossless synthesis on section 1.5.

As initial topology we propose the one in Fig. 46a, after some iterative steps on the optimization process we observed that the resistors on the outer Cascaded Quadruplet section barely affect the in-band response and generally can be neglected. Then resulting in a filter topology with only resistive couplings on the inner Cascaded Quadruplet sections, as shown in Fig. 46b. This topology has the great advantage of requiring less resistive couplings and therefore considerably reduce the designing time.

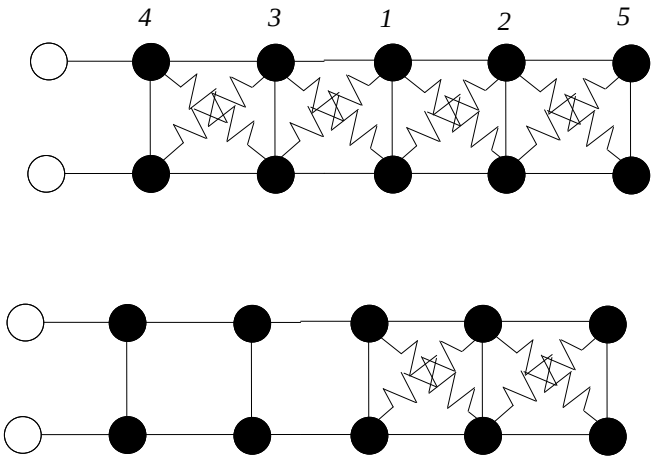

Fig. 46 : a) Folded topology with resistive couplings in all Cascaded Quadruplets. b) Folded topology with resistive couplings only on the inner Cascaded Quadruplets.

On the other hand this topology (Fig. 46b) it is not adequate to fulfill the out-of-band selectivity and losses the transmission zeros. To overcome this issue we propose a new topology which requires two additional resistive couplings. As observed in Fig. 41b another suitable topology can be

proposed by including resistive coupling between resonator 3 and 5 and resonators 6 and 8 as shown in Fig. 47.

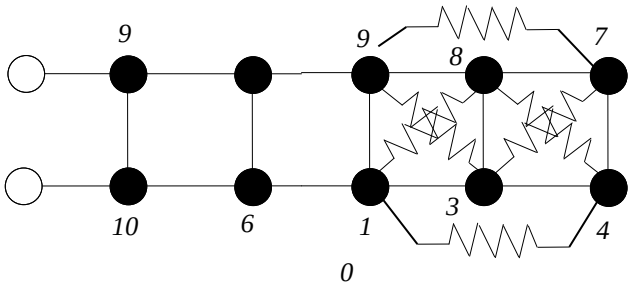

Fig. 47 - Folded topology with resistive couplings on the inner Cascaded Quadruplets and additional resistive couplings between resonators 3-5 and 8-6.

The topology outlined in Fig. 47 above is now used to synthesize the best network possible for a given values of uniform Q. This process has been done for Qs of 7000, 5000, 4000 and 2000. Figure 48 below, shows the synthesized responses in blue in comparison with the goal response, in red, which corresponds to the synthesized conventional filter with Qs of 13000. Note that the reduction of Q it is always at expenses of additional insertion losses. Thus in order to compare the synthesized responses with the pretended response, they are shown normalized. Also note that for each synthesized responses on the right side of the figure give further details on the in-band response. The coupling matrices corresponding to all frequency responses below are detailed in Appendix 8.

As expected when the Q value is reduced the insertion losses increase. Details on that can be seen in Table 25. Note also that other parts of the filter performance might be also affected, as the ripple in the passband, or the position of the transmission zeros. It is also worth to mention that since these are responses obtained from an optimization procedure, different results may be obtained by adjusting the optimization criteria, i.e., increase the weight of the return losses, selectivity or flatness.

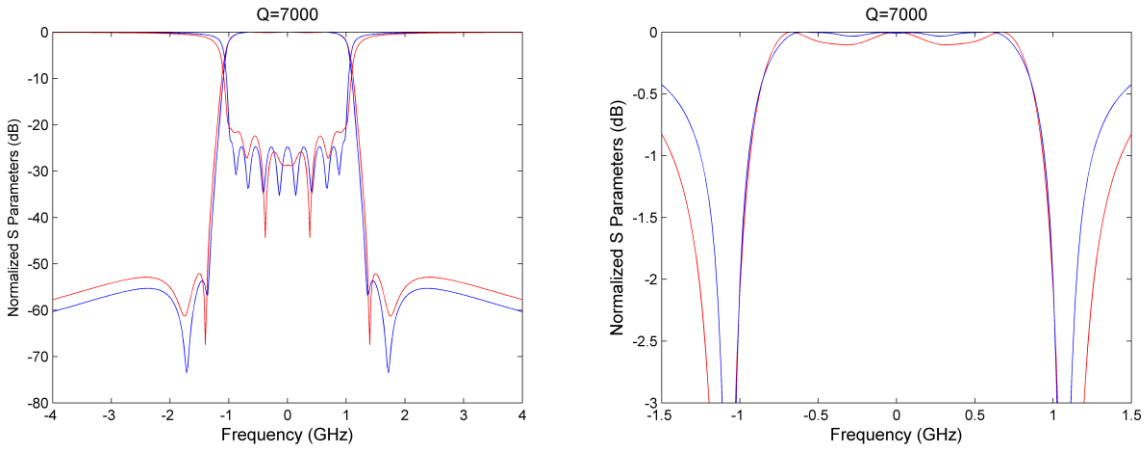

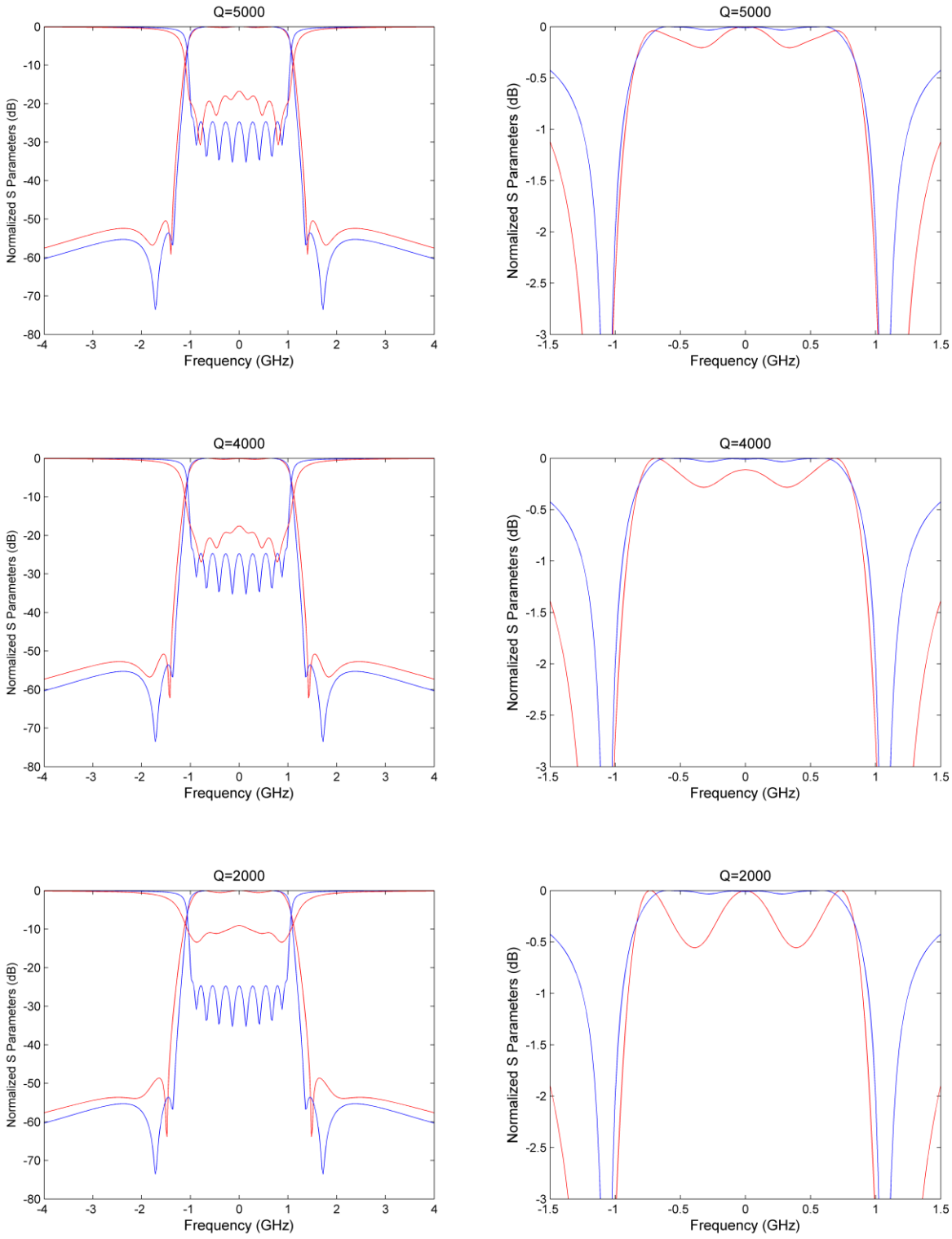

Fig. 48 - Synthesized lossy responses in red, in comparison with a conventional response with Qs of 13000.

To complete this study, Fig 49 shows the transmission response of several synthesizes lossy responses for several values of Q, ranging from 12000 to 2000. Comparison of the group delay it is also shown in the right side figure of Fig. 49.

Note that the degradation of the group delay it is not very significant, although the group delay performance has not been considered on the optimization procedure.

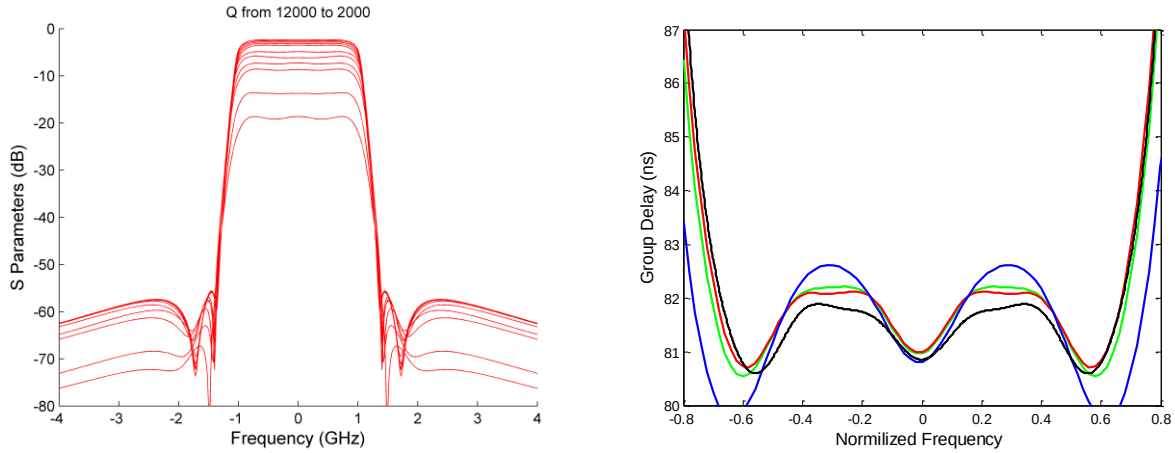

Fig. 49. Transmission filter response for synthesizes response with Q ranging from 12000-2000. Group delay of synthesized responses: conventional synthesis (in black), lossy synthesis Q_0=2000 (blue), Q_0=5000 (green) y Q_0=7000 (red).

The table below summarizes the insertion loss values as a function of the Q. These results confirm the linear dependence between Q and insertion loss, as occurs in the direct synthesis formulation of equation (65).

Q_0=7000	IL=-4.5 dB
Q_0=6000	IL=-6 dB
Q_0=5000	IL=-7.5 dB
Q_0=4000	IL=-9 dB
Q_0=3000	IL=-13 dB
Q_0=2000	IL=-19 dB

Tabla 25: Q vs IL for the optimized responses.

2.5 Sensitivity considerations in lossy filters: Case study of a 4th order Chebyshev filter

This section complements the information above on the synthesis and solution space of lossy filters, with a study on their sensitivity to manufacturing tolerances.

Two types of deviations over the nominal values are considered:

- A random and uncorrelated variation on the filter parameters (resonant frequencies, couplings and Qs).
- A uniform variation in the Qs and in the resistive couplings of the lossy filter.

For example, in the fabrication of a cavity filter, machining tolerances would give rise to the first type of deviations, whereas the effect of a surface coating or a metal conductivity different from the one assumed in the design would tend to provoke a uniform deviation of the Qs from their nominal value.

The goals of the study are:

- To establish how sensitive is the lossy filter design to tolerances in the resistive coupling elements as compared to the sensitivity of conventional (lossless) couplings;
- To study how uniform deviations in Qs and resistive couplings affect the filter, provided that loss is taken into account from the onset of the process of lossy filter synthesis.

The sensitivity analysis has been performed on a fourth order Chebyshev lossy filter using the procedure outlined in section above. The synthesized response corresponds to a symmetric network where the transmission (S_{21}) and reflection coefficients (S_{11}) are given by $S_{21}=k\cdot S_{21\_lossless}$ and $S_{11}=k\cdot S_{11\_lossless}$, being k<1. Note that *k* sets the passband insertion loss.

Figure 50 depicts the topology of the resulting network for a fourth order Chebyshev response. The black circles correspond to the lossy resonators, grey circles represent additional non-resonant nodes that improve the loss distribution and the white circles correspond to the input and output nodes. The solid lines connecting the different nodes represent the reactive (conventional) coupling between resonators and the resistors are the resistive couplings between resonators.

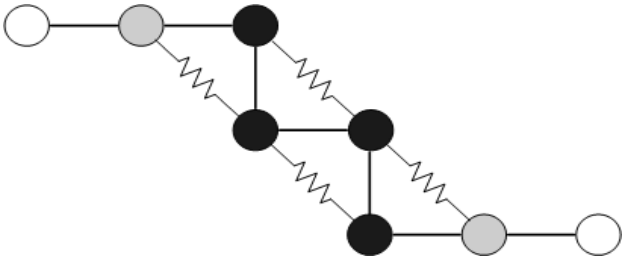

Fig. 50 - Network topology of an 4th order inline lossy filter with non-resonant nodes and uniform losses distribution

For the design of a fourth order Chebyshev lossy filter with 15 dB return loss and centered at 1 GHz, with 50 MHz bandwidth and using microstrip technology (with quality factor of 290) and a flat in-band response (Q_{eff}=*Inf*), we need to set the *k* to 0.5 (IL=6dB). The γ_{RL} for 15 dB return losses is 88 (see Fig. 35 and equation (66)). The frequency response is depicted in Fig. 51.

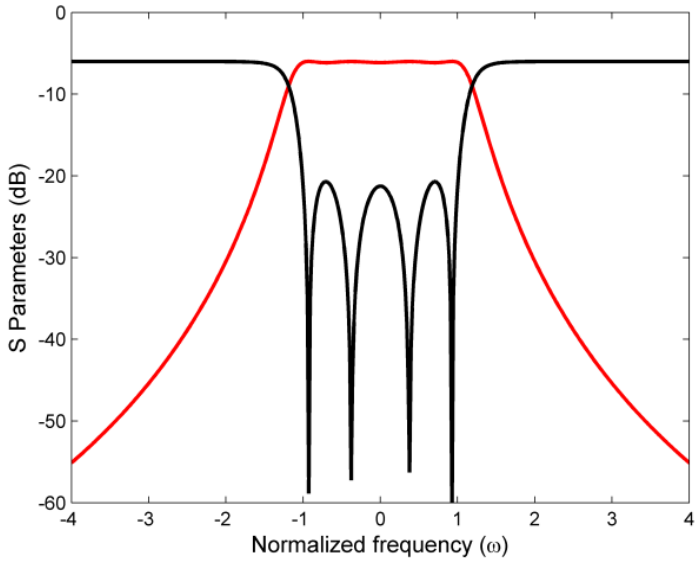

Fig. 51- Frequency response of the synthesized lossy filter.

This results in the coupling matrix detailed below (Table 26), which is consistent with the topology of Fig. 50. The non-diagonal real and imaginary elements of the coupling matrix correspond to the reactive (conventional) and resistive couplings between resonators, respectively. The imaginary elements of the diagonal gather all resistive elements connected to the corresponding resonator, this is the resistive coupling elements and the losses due to the finite Q factor of the resonators.

0	0.243	0	0	0	0	0	0
0.243	-j0.019	-0.211	j0.019	0	0	0	0
0	-0.211	-j0.129	0.79	j0.06	0	0	0
0	j0.019	0.79	-j0.148	0.648	j0.06	0	0
0	0	j0.06	0.648	-j0.148	0.79	j0.019	0
0	0	0	j0.06	0.79	-j0.129	-0.211	0
0	0	0	0	j0.019	-0.211	-j0.019	0.243
0	0	0	0	0	0	0.243	0

Tabla 26: Coupling matrix of the case under study in this section

Now the coupling matrix above it is used to perform the sensitive analysis. The study consists in assessing the deviation in the frequency response of the filter when its parameters change as a result of changes in the elements of the coupling matrix. Only changes in couplings, resonant frequencies and quality factors will be taken into account. Although this study only considers a single topology, some of the conclusions that we will derive from this analysis are also qualitatively correct for the other topologies resulting from the synthesis of lossy filters.

In the sensibility analysis, we will consider random and uncorrelated variations due to component, manufacturing and assembly tolerances in:

- Reactive (conventional) couplings between resonators and the external couplings from the source and load to the network.
- Self-coupling or resonant frequencies.
- Resistive couplings between resonators and from the non-resonant nodes to the inner resonators.
- Quality factors.

The percentage of deviation to be considered in the parameters above depends on the technology to be used, the type of couplings, materials, fabrication process and so on. In order to consider all possible scenarios we will use large deviation values [3]:

- +/- 20 % on conventional couplings, resistive couplings and on the Qs of the resonators.
- +/-0.2 % on self-couplings (resonant frequencies)

Following, we separately evaluate the deviation on the conventional (reactive) couplings and detuning of the resonant frequency and the effects due to the variation of the resistive elements and quality factors of the resonators.

2.5.1 Deviation in the conventional couplings and resonant frequencies of the resonators

The deviation in the coupling coefficients can be directly evaluated from the coupling matrix. This can be demonstrated from the frequency and circuit transformation from the low pass to the band pass prototype. Thus, sensitivity to the coupling matrix elements does not depend on the fractional bandwidth of the filter to be implemented.

To account for the variation of the resonant frequencies in the coupling matrix we need to turn the ratio between nominal (ω_0) and actual (ω_{0i}) frequency into a susceptance *B* that can be included in the diagonal terms of the coupling matrix. This can be done with the low-pass to band-pass transformation relations, according to which:

$$B = \frac{2}{FBW}\frac{1-\left(\frac{\omega_{0i}}{\omega_0}\right)^2}{1+\left(\frac{\omega_{0i}}{\omega_0}\right)^2} \tag{66}$$

From Fig. 52 we can see that the deviation of conventional coupling affects the ripple in the passband and the filter bandwidth, as occurs in lossless filters [3]. This ripple is mainly due to the deviation on the external couplings [3].

The +/-0.2% deviation of the resonant frequency of the resonators produces small variation in the ripple (see Fig. 53). Note however that this effect might be significant in higher order filters [3].

2.5.2 Random deviation in the resistive couplings and Q

Figure 54 shows the effects of introducing a random variation on the resistive couplings on the frequency response. Note these changes are small in comparison to those occurring when the conventional couplings deviate from their nominal values. Thus, the implementation of these couplings might not be critical. This lack of sensitivity to variations in resistive couplings is highly desirable and may prove useful in the future deployment of lossy filters. Additionally, the study also revealed that the external resistive couplings (from the non-resonant node to the inner resonators) are more sensitive that the ones between resonators. Note however that in this study we have not reported the effects due to the existence of a phase term on the implementation of the resistive couplings.

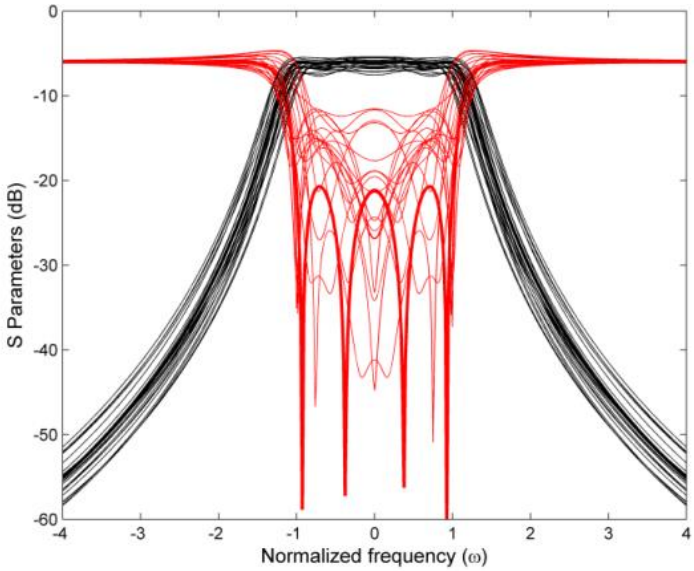

Fig. 52- Transmission and reflection coefficient deviation when the conventional couplings are randomly changed within a +/-20%, for 15 trials.

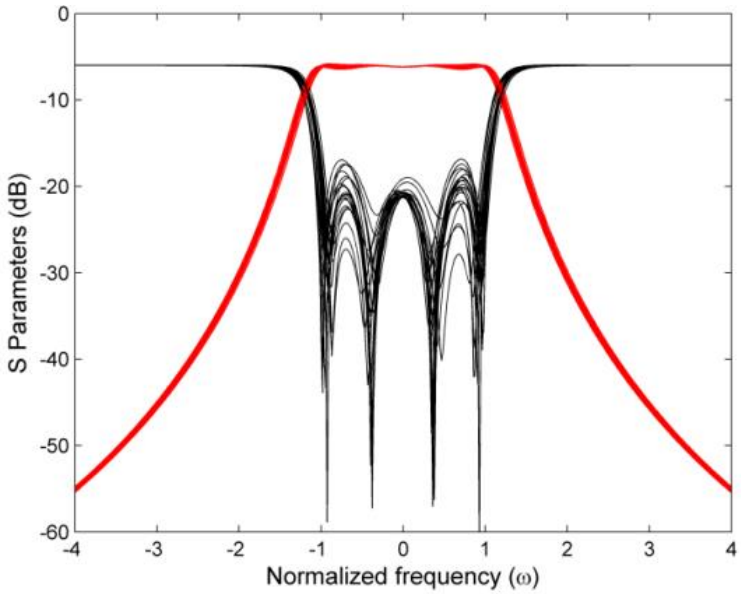

Fig. 53- Transmission and reflection coefficient deviation when resonant frequency of the resonators are randomly changes within a +/-0.2%, for 20 trials.

Figure 55 outlines the effects of randomly changing the Q of the resonators. For Q values lower than the nominal one, the frequency response rounds at the band edges and the reflection and transmission zeros become less distinct, whereas for higher Q values, the frequency response exhibits an “ear cat” shaping at the filter bandedges.

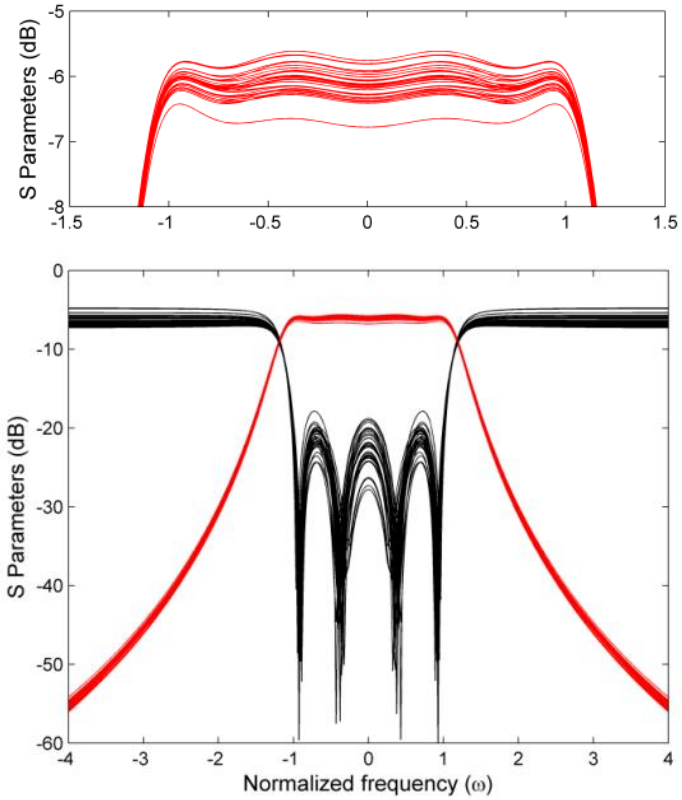

Fig. 54- Transmission and reflection coefficient deviation when the resistive couplings are randomly changed within a +/-20%, for 30 trials. Inset: Zoom of the in-band transmission performance.

2.5.3 Uniform deviation in the resistive couplings and Q

This section evaluates the effects of a uniform deviation in the resistive couplings and the quality factors on the frequency response. Figure 56 shows the frequency response of the filter when the Q factor is uniformly changed from 500 to 100 in all the filter resonators. Note that in this case the resistive couplings are considered to be the synthesized ones. When the Q is set to a value higher than the designing value 290 the expected “ear cat” effects are observed and the IL reduces. Whereas, when the Q is reduced below 290 the IL increases and rounding effects appear in the in-band response. In this case (65) relates the actual Q and the IL with the effective Q (Q_{eff}) that describes the rounding in the response.

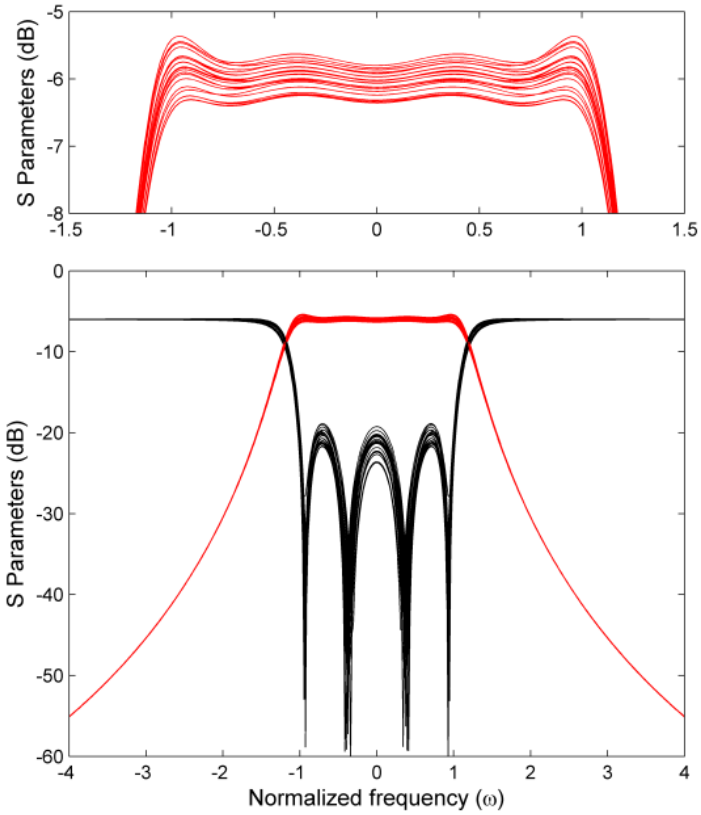

Fig. 55- Transmission and reflection coefficient deviation when the Q are randomly scaled, for 20 trials.

Figure 57 outlines the effects on the frequency response of jointly increasing the values of all coupling resistors in the filter from the synthesized value up to infinity (this is, removing the resistive coupling) without changing the Q factor (290). In this case the frequency response shifts up and the rounding increases. Note that in the case of removing the resistive couplings the frequency responses is close to the one obtained in a losses synthesis with a uniform Q of 290. As in Figure 56 we could have obtained Q_{eff} from the IL and Q_0 using (65).

Figure 58 shows the frequency response when both the resistive couplings and the Q factors are changed uniformly. In this case the shape of the frequency response barely changes and the in-band flat response is maintained, with only a shift of the filter insertion losses. From the practical point of view this is very beneficial since if one designs for a given Q and then the actual Q deviates, one can recover the flatness and selectivity of the frequency response by just modifying the resistive couplings by the same (relative) amount and still have a good filter response.

From this study we conclude that sensibility of the reactive (conventional) couplings and resonant frequency of the resonators in a lossy network (Figure 50) are qualitatively the same than in a lossless network. The sensitivity of reactive couplings to tolerances is higher than that of the resistive couplings. This work also shows that a degradation of the in-band flatness due to a uniform reduction of the Q factor can be compensated by modifying the resistive couplings.

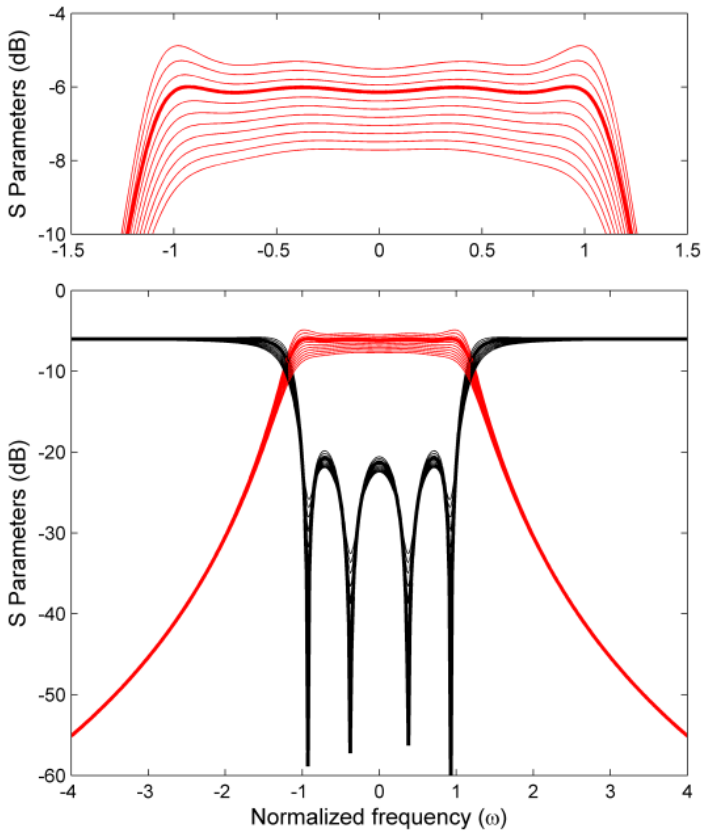

Fig. 56 - Transmission coefficient deviation when the Q are uniformly scaled within 500 to 100.

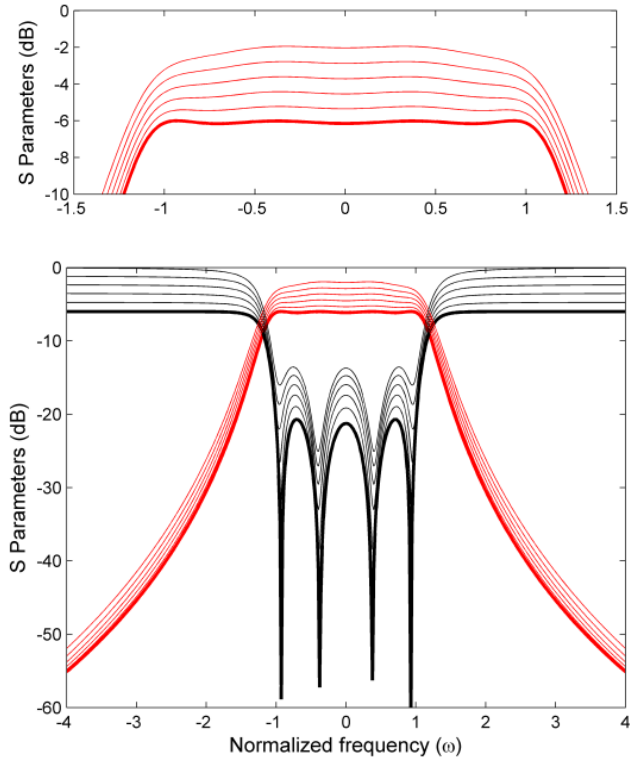

Fig. 57- Details of the transmission and reflection coefficients deviation when the resistive couplings are uniformly changed.

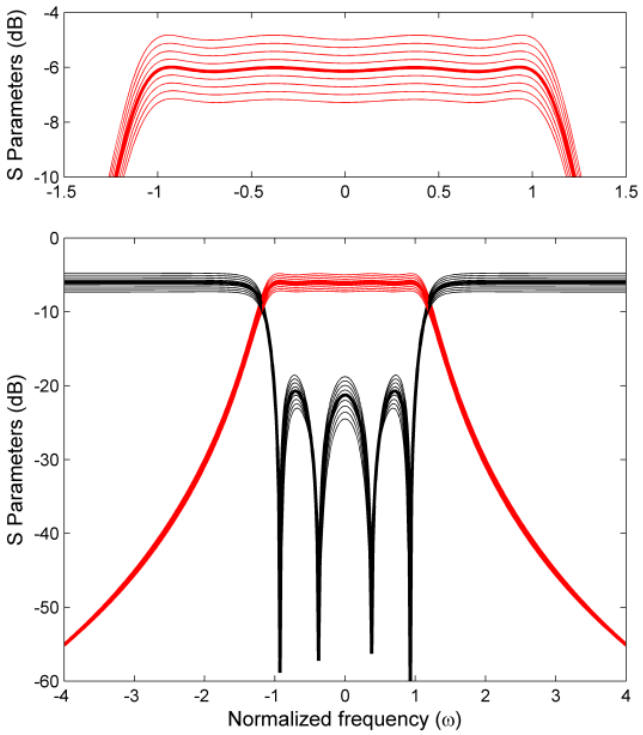

Fig. 58 - The transmission and reflection coefficients when both Q and resistive coupling are uniformly scaled.

2.6 Conclusions

This chapter exposed all the mathematical details for the synthesis of lossy filters. Note as well that part of the mathematical details and other aspects regarding the outlined examples are extended in the Appendices.

From this development we may conclude that for any lossy synthesis, this is for the different cases described in sections 2.2.1, 2.2.2 and 2.2.3, respectively, there is a transversal coupling network that synthesizes such responses. Note that this conclusion is equivalent to the one in standard lossless synthesis.

As occurs in conventional synthesis techniques a transversal topology is not very suitable for real implementation and transformation to more convenient topologies it is required. The most natural step is to transformed into a folded network, which in the case of lossy filters follows the same recipe than in conventional ones, and it is fully detailed along section 1.5.2. The resulting topologies from this transformation are folded network with a non-uniform Q distribution, which in most cases becomes impractical for real implementation. Additional transformations for a proper loss distribution along the network -usually a desired uniform Q distribution- are required. Such transformations are based on matrix rotation following a hyperbolic rotation.

Although in cases with low order filter, hyperbolic rotation results in a direct synthesis approach. This is a fully defined network. Most case required the definition of special transformation strategies. This study concludes that in some cases there exist resistive couplings with small influence in the final filter performance and would be removed in a real implementation.

Following the conclusions above an optimization technique has been proposed and used for the synthesis of lossy. The optimization technique consists on defining an *a priori* the network topology which already includes resistive couplings and then optimizes the values of the network to obtained the best performance possible. This approach proved to be useful in the synthesis of a complex lossy network of 10-4-4 topology normally used in channeling filters.

The last part of this chapter presents a sensitivity study of a lossy network corresponding to a 4th order filter with uniform Q distribution. This study concludes on the resistive couplings are not very sensitive and do not spoil the filter performance. The behavior of conventional couplings and resonant frequency is the same that it might be observed in conventional filters. Besides these conclusions the most interesting results are the one shown in Figs. 57 and 58. These figures reveal that the resistive couplings might be used to tune the prescribed flatness of the filter or to recover the full flatness when a misestimating of the Q is produced.

The following chapter uses the synthesis procedure described here for the synthesis design and implementation of three prototypes of lossy filters.

3 CHAPTER 3: IMPLEMENTATION OF DISSIPATIVE FILTERS

This chapter presents the implementation of three lossy filters, these are filters which include an additional resistive network in order to provide a frequency selective absorption of power, and then offer an improved in-band flat response.

All the implementations presented here are based on the synthesis approaches outlined in chapter 2. With these real implemented filters this work demonstrates the viability of the synthesis techniques above. The three different filters synthesized and fabricated here follow a different synthesis approach.

Although further details are given along the chapter, the three prototypes are:

- 4th order planar filter. This filter has been implemented following a direct synthesis approach. This is the procedure detailed in section 2.3.2.
- 6th order planar filter. For the synthesis of this filter we used an optimization approach. This result in a filter with a reduced number of resistive couplings. This procedure is described in section 2.4.
- 6th order Combline filter with a single pair of transmission zeros. The synthesized topology made used of transformation strategies to obtain the final configuration.

The following table summarizes the main features of the reported filters:

Filter	Filter order	Central frequency Bandwidth	Lossy Synthesis	Technology
Filter 1	4	1 GHz, 36 MHz	CASE A Direct synthesis (section 2.3.2)	Planar
Filter 2	6	1.65 GHz, 80 MHz	CASE B Optimization (section 2.4)	Planar
Filter 3	6-2 (Transmission zeros)	3 GHz, 36 MHz	CASE B Sections 2.4 and 2.3.3	Combline (additional planar resistive network)

Tabla 27: Summary of the filters implemented in the Chapter 3.

For all the filters above this chapter details on the initial filter specifications, the synthesis procedure and on the equivalent circuit implementation. To do that we made used of the software development inside the framework of the ESA Project [25], which implements the synthesis techniques of Chapter 2, and to which the author of the thesis has contributed as one of the main co-authors.

Details on the electromagnetic design are also presented with special emphasis on those which differs from a conventional design (this is without resistive couplings). Special emphasis will be made on the combline filter due to complexity on the design.

Fabrication and measurement are also reported for each filter, including tuning requirements when necessary. Measurements include also the temperature behavior over temperature as required in the Statement of Work of the ESA Project [25].

3.1 4th order Chebyshev planar lossy filter. Direct Synthesis

This section presents the synthesis and design of a 4th order planar filter. The initial polynomials $S_{ij\_lossless}$ correspond to a Chebyshev filter [1], in which the return loss is set to 20 dB. The filter is centered at 1 GHz with 36 MHz bandwidth. The filter specifications are outlined in Table 28 below.

Parameter	Value	UNIT
Center frequency (f_0)	1000	MHz
Channel Bandwidth	36	MHz
Insertion loss over Bandwidth	<10	dB
Input and Output Match	20	dB
Insertion loss variation over frequency		
f_0+/- 18 MHz	0.2	dBpp
Out of Band rejection		
f_0+/-40 MHz	22	dB

Table 28. Specification of the filter 1.

Since the synthesis of lossy filters requires knowing the losses from the very beginning, the first step is to determine the Q of the resonators to be used on the filter implementation.

The material used to implement the filter has the following properties:

ROGERS	
Dielectric Thickness	1.27 mm
Permittivity	10.2
Loss tangent	0.002
Conductor	Copper
Conductivity	5.8e7
Metallic Thickness	35μm

Table 29. Properties of the material used for implementing filter 1.

The basic resonator consists of a halfwave transmission line hairpin resonator – 60.7 mm length – of 50 Ω impedance – 1.17 mm width –, which results in an unloaded Q factor of nearly 200. Details on the basic resonator appear in Fig. 59.

The Q value is then used to determine the insertion losses IL=10 dB from (65), which in turn gives the *k* value in (42), necessary to define the initial polynomials.

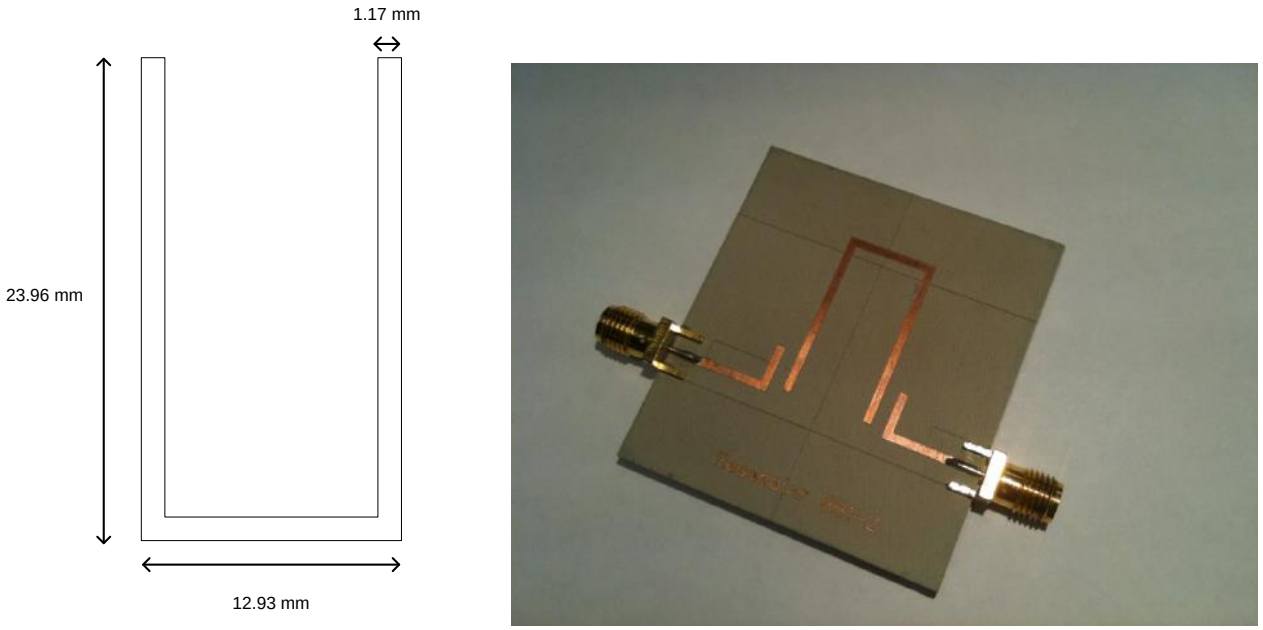

Fig. 59- Outline and picture of the basic resonator for Filter 1.

3.1.1 Synthesis and coupling matrix

The resulting N+4 coupling matrix with a uniform Q distribution is shown in Fig. 60 below, which corresponds to a screen shot of the software *lossyfilters* (www.tsc.upc.edu/lossyfilters). Note that in this case all resonators require the same quality factor of 206. Note also that this corresponds to the low pass prototype coupling matrix and scaling factors have to be applied for the filter design [1][2][3].

Once the coupling matrix is obtained and the basic resonant structure is defined, the next step in the design procedure is determining the conventional couplings, usually set by the spacing between the resonators, and the resistive coupling.

The filter topology of the synthesized network it is outlined in Fig. 61, where conventional couplings, resistive couplings and non-resonant nodes are accordingly indicated.

The filter transfer function from the evaluation of the above coupling matrix and therefore our target design is shown in the following figure (Fig. 62).

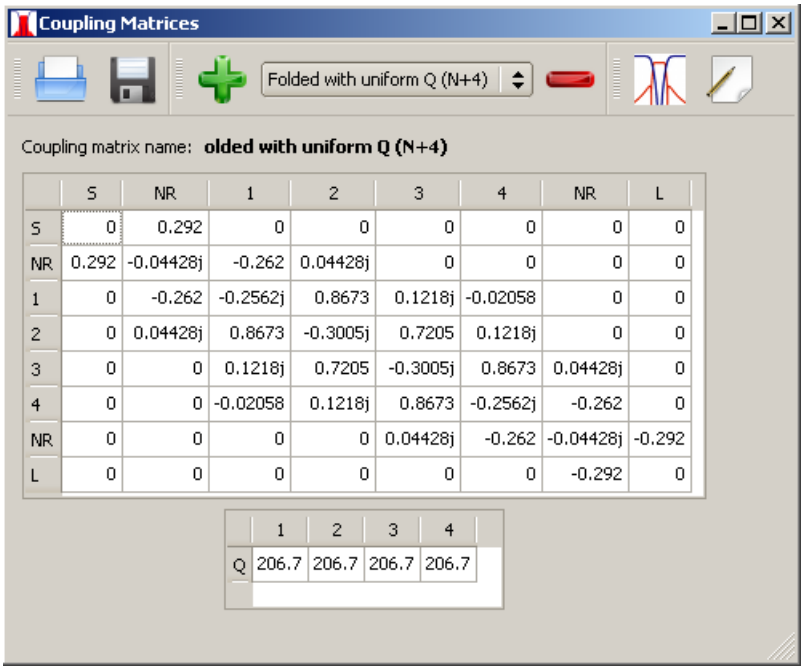

	S	NR	1	2	3	4	NR	L
S	0	0.292	0	0	0	0	0	0
NR	0.292	-0.04428j	-0.262	0.04428j	0	0	0	0
1	0	-0.262	-0.2562j	0.8673	0.1218j	-0.02058	0	0
2	0	0.04428j	0.8673	-0.3005j	0.7205	0.1218j	0	0
3	0	0	0.1218j	0.7205	-0.3005j	0.8673	0.04428j	0
4	0	0	-0.02058	0.1218j	0.8673	-0.2562j	-0.262	0
NR	0	0	0	0	0.04428j	-0.262	-0.04428j	-0.292
L	0	0	0	0	0	0	-0.292	0

	1	2	3	4
Q	206.7	206.7	206.7	206.7

Fig. 60. FCM with uniform *Q* distribution of the filter to design.

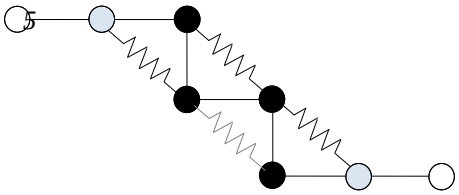

Fig. 61. Network topology of the filter.

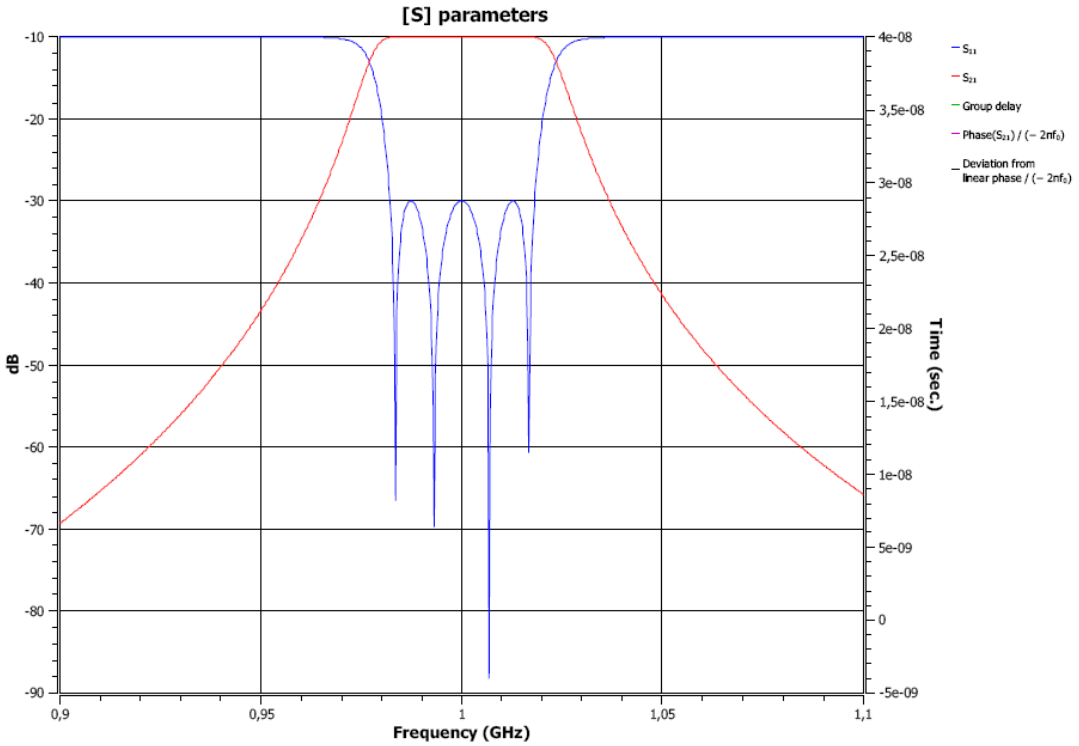

Fig. 62. Frequency response of the filter to be developed. Corresponds to a screen shot from the software *lossyfilter.*

3.1.2 Filter design

Although the existence of an additional resistive network somehow affects the design of the conventional couplings and the nominal frequency of each resonator, typically the design of a lossy filter could be performed into two different steps. First we design the conventional couplings and the resistive couplings are included afterwards. Note however that additional resizing and trimming steps it is required at the end to account for the effects of the whole structure. This phenomena it is more prominent on the design of filter 3 where it is commented in more details.

3.1.3 Electromagnetic design of conventional couplings

The design of the conventional coupling elements essentially consists on determining the spacing between the resonators to meet the magnitude and phase of the values set in the coupling matrices. To do that we use the well-known procedure described elsewhere [3] where the coupling between two resonators can be related with the resonant frequency of the two resonant modes, f_1 and f_2, existing when the two resonators are coupled, as $m = \pm\frac{f_2^2 - f_1^2}{f_2^2 + f_1^2}$. The m values are obtained from the coupling matrix as $k = M \cdot FBW$, being M the values of the coupling matrix. Additionally one also needs to design the external coupling elements, this is the coupling between the source/load with the first/last resonator. Details on how to define this coupling can also be found in [3] .

Therefore following the standard procedure described in [3] and using as the basic resonator structure of Fig. 59 we found the filter configuration as depicted in Fig. 63. Since this filter does not perform any transmission zeros an inline configuration with only adjacent couplings is required. We arrange the resonators as illustrated in Fig. 63, alternating their up and down position. This type of arrangement shows to be very convenient for the placement of the resistive coupling elements [26].

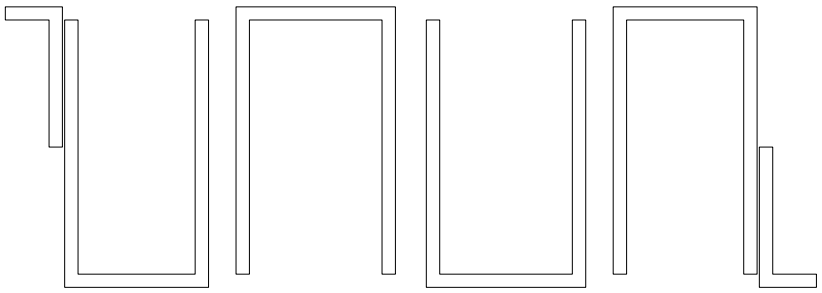

Fig. 63 Filter configuration of Filter 1 without resistive couplings.

To evaluate the proper design of the conventional couplings the filter response of the design topology of Fig. 63, simulated with a full-wave simulator (Momentum from ADS / Agilent), has been compared with the synthesized response without resistive couplings. The results of this comparison are outlined in Figure 64, showing very good agreement in both the transmission coefficient S_{21} and

the reflection coefficient S_{11}. The dotted lines correspond to the ideal response (evaluated from the coupling matrix) and the solid lines correspond to the full-wave simulated response.

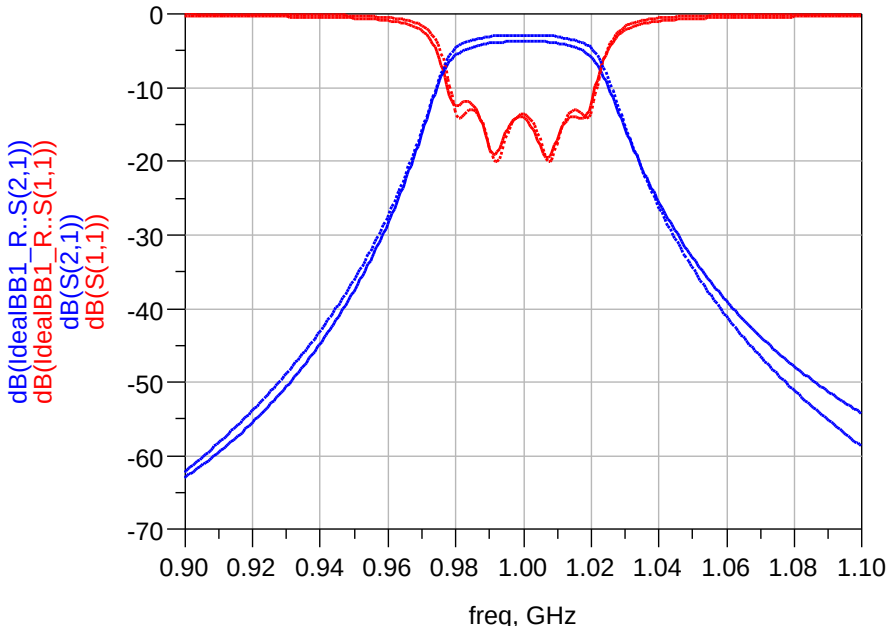

Fig. 64. Frequency response of the synthesized and designed filter without resistive couplings.

3.1.4 Electromagnetic design of resistive couplings

According to the network topologies of Fig. 61 lumped resistors have to be used to perform the resistive couplings between resonators. Since from the practical point of view this is not straightforward, we perform lumped resistors by means of distributed elements that allows connecting them between resonators [12][21].

Figure 65 shows how to model a single lumped resistor by using admittance inverters and transmission lines. The second figure in Fig. 65 outlines a circuit corresponding to two cascaded inverters connected at each side of a lumped resistor. Note that the ABCD matrix of this two port network is expressed by (67), where the condition $\frac{J_2}{J_1}\frac{J_{1p}}{J_{2p}}=1$ should be met. Note that this happens when $J_1=J_{1p}$ and $J_2=J_{2p}$. In this case the resulting resistor of the circuit is $R_p\left(\frac{J_2}{J_1}\right)^2$. Note therefore that the lumped resistor R_p can be adjusted according to the inverters J_1 and J_2.

$$\begin{bmatrix} \frac{J_2}{J_1}\frac{J_{1p}}{J_{2p}} & R\frac{J_2}{J_1}\frac{J_{2p}}{J_{1p}} \\ 0 & \frac{J_1}{J_2}\frac{J_{2p}}{J_{1p}} \end{bmatrix} = \begin{bmatrix} 1 & R_p\left(\frac{J_2}{J_1}\right)^2 \\ 0 & 1 \end{bmatrix} \tag{67}$$

Additionally one can also implement an admittance inverter by means of multiple of quarter wave lengths transmission lines, where the value of the inverter is set by the transmission line inverter [5]. This approach is outlined in third figure of Fig. 65, and is actually the one used in the designs presented here. In this case the value of the lumped resistor can be also adjusted by the transmission line impedance (ZZ). Again we can also formulate the analytical expression by using conventional network analysis [5] as:

$$\begin{bmatrix} 0 & {}^{j}/_{J} \\ jJ & 0 \end{bmatrix}\begin{bmatrix} cos\beta l & jZZsin\beta l \\ j\frac{1}{ZZ}sin\beta l & cos\beta l \end{bmatrix}\begin{bmatrix} 1 & R_p \\ 0 & 1 \end{bmatrix}\begin{bmatrix} cos\beta l & jZZsin\beta l \\ j\frac{1}{ZZ}sin\beta l & cos\beta l \end{bmatrix}\begin{bmatrix} 0 & {}^{j}/_{J} \\ jJ & 0 \end{bmatrix} =$$

$$= \begin{bmatrix} 0 & {}^{j}/_{J} \\ jJ & 0 \end{bmatrix}\begin{bmatrix} 0 & jZZ \\ j\frac{1}{ZZ} & 0 \end{bmatrix}\begin{bmatrix} 1 & R_p \\ 0 & 1 \end{bmatrix}\begin{bmatrix} 0 & jZZ \\ j\frac{1}{ZZ} & 0 \end{bmatrix}\begin{bmatrix} 0 & {}^{j}/_{J} \\ jJ & 0 \end{bmatrix} = \begin{bmatrix} 1 & \frac{R_p}{J^2ZZ^2} \\ 0 & 1 \end{bmatrix} \quad (68)$$

Equating this expression with the one corresponding for a lumped resistor $\begin{bmatrix} 1 & R \\ 0 & 1 \end{bmatrix} = \begin{bmatrix} 1 & \frac{R_p}{J^2ZZ^2} \\ 0 & 1 \end{bmatrix}$, we get that the relation between the resistor to be used in the design R_p and the resistor obtained from the synthesis is : $R = \frac{R_p}{J^2ZZ^2}$.

The fourth figure of Fig. 65 shows how to design a resistive coupling between resonator 1st and 3rd. From Fig. 65 we conclude that to implement the resistive coupling first we need to implement an admittance inverter, which in this case has been performed by coupling a transmission line at one extreme of the 1st resonator, then this coupling is cascaded into a quarter wave-length transmission line, which would be connected at the lumped resistor. A symmetric configuration has also been used to connect the lumped resistor to the 3rd resonator.

Note however that this approach is narrowband for due to: 1) the coupling from the resonator to the transmission line and 2) the length of the transmission line. The bandwidth in which the approach of Fig. 65 can be increased by:

- Making the couplings from the resonator to the transmission line as weak as possible. This can be achieved by reducing the confronted area of coupling. Besides, this is also beneficial from the design point of view since the effects on the resonant frequency of the resonator itself is very small and can be tuned by simply adjusting the length of the resonators without affecting the conventional couplings.
- Using high impedance transmission lines as a multiple quarter wavelength inverters.

We use the approach described above for the design of the resistive coupling between resonators.

Note as well that at this point we also need to consider the resistive coupling between the non-resonant node and the inner resonators. To do that, we used an analogous approach resulting with an equivalent circuit model and layout as outlined in Fig. 66.

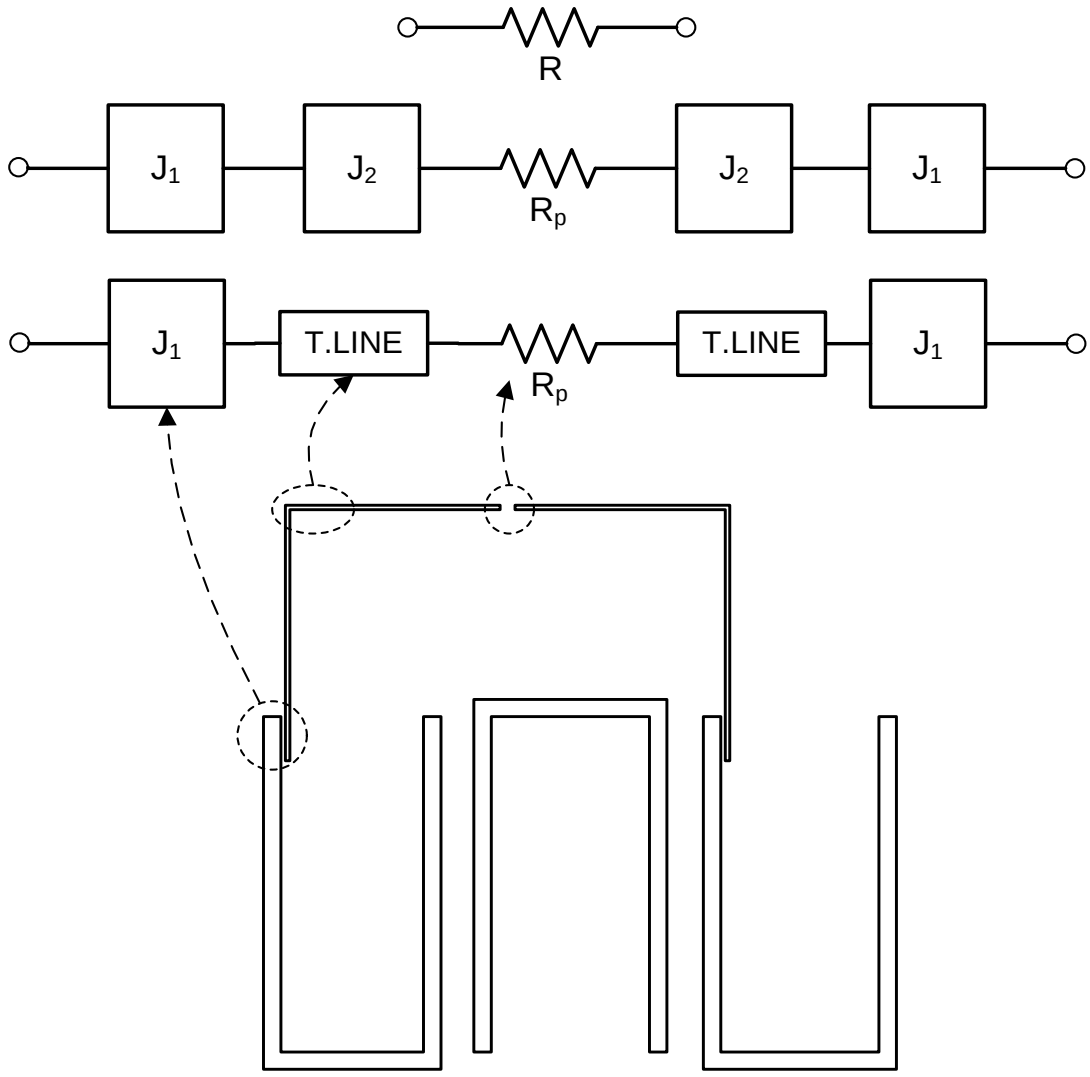

Fig. 65. (First) Lumped resistor, (Second) lumped resistor with two cascaded inverters at the input and output, (third) lumped resistor with a inverter cascaded to a transmission line at the input and output, (fourth) outlined layout.

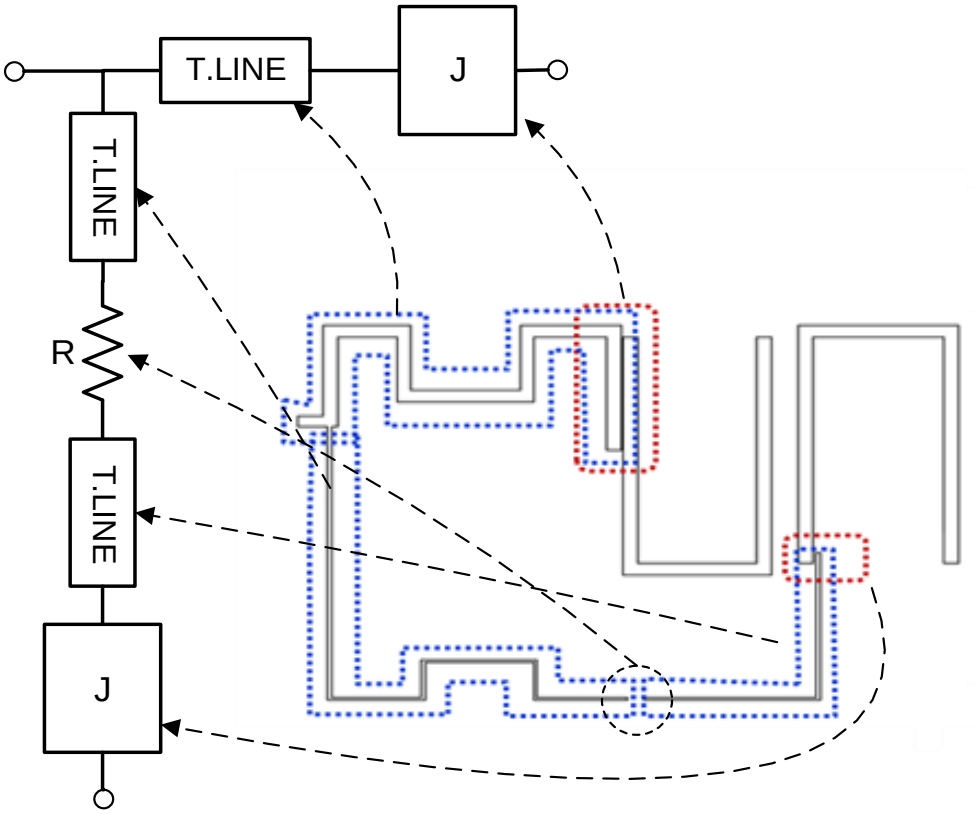

Fig. 66. Non-resonant node and resistive coupling, a) Circuit model b) layout

The non-resonant node is implemented by means of a half wavelength transmission line which is coupled to the first resonator and directly connected to the input (or output) port. The resistive coupling to resonator is implemented by a high impedance half wavelength transmission line connected from the non-resonant node to the lumped resistor, and then the lumped resistor is connected to the resonators as in the equivalent circuit of Fig. 65, this is a quarter wavelength and a coupling. To illustrate this Fig. 66 also shows the correspondence of the circuit elements to the filter layout.

3.1.5 Final design: Conventional couplings and resistive couplings

For the final filter design, including both the conventional and resistive couplings, we take the topology of Fig. 63, whose dimensions are adjusted to match the frequency response given by the coupling matrix without resistive couplings.

Then, the overall circuit, including resistive couplings, is split in two main parts (Fig. 67) and optimized with co-simulation: a six port network (input, output and the four ports to insert the resistive couplings) is simulated with an electromagnetic simulator and the rest is simulated using circuital techniques. In the co-simulation, the length of the transmission lines (~λ/4), its impedance and the value of the lumped resistors are adjusted to obtain the desired filter response. The

resulting impedance of the transmission lines in the resistive couplings is 83Ω, and the lumped resistors are 151 Ω for the couplings between the non-resonant node and second resonator (or third resonator) and 51 Ω for the coupling between the first and third resonator (or fourth and second resonator).

Figure 68 shows the comparison between the simulated response with the synthesized response. Note that the simulated response corresponds to the full-wave simulation of both conventional couplings and resistive couplings.

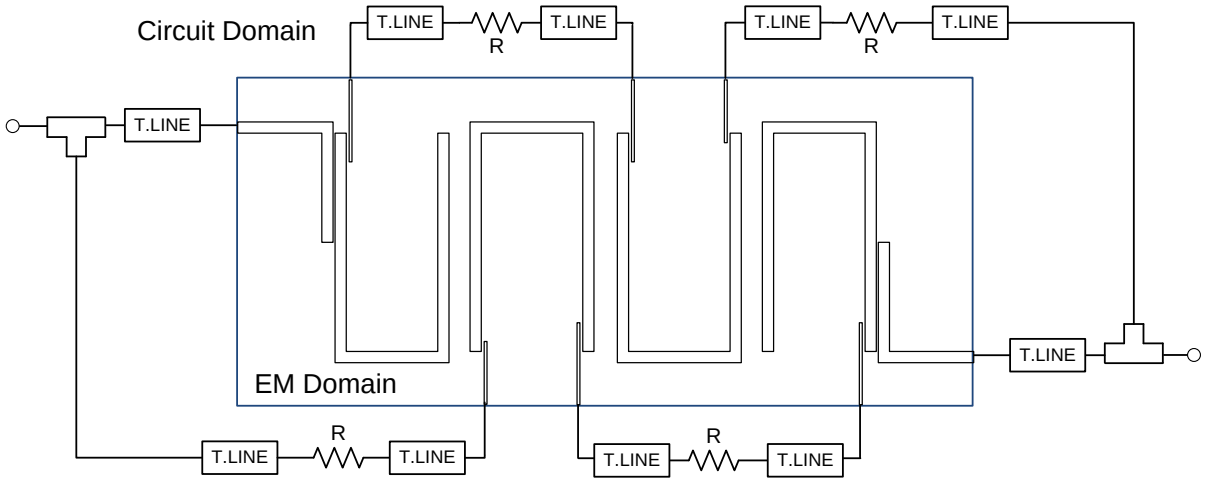

Fig. 67. Outline of the filter topology with an electromagnetic domain and the circuit domain

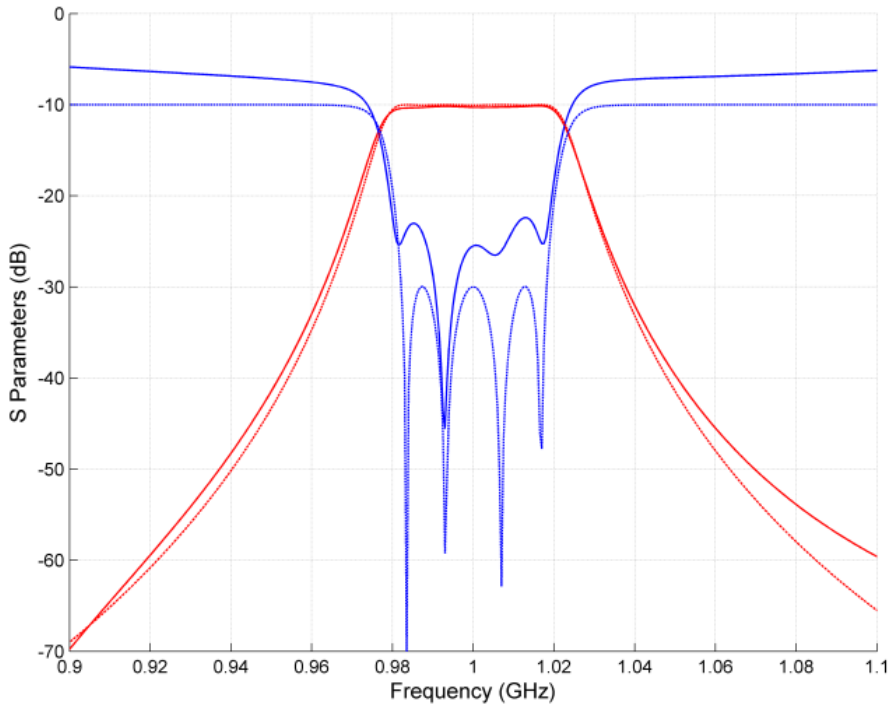

Fig. 68 Full-wave simulated (dotted line) response and synthesized response (solid line) of the filter defined by Fig. 60.

3.1.6 Fabrication, measurements, temperature stability and validation of the mathematical formulation

Figure 69 shows the transmission and reflection coefficient of the measured filter response (solid line). The transmission coefficient exhibits an in-band flat response with the expected 10 dB of insertion loss. Comparison with the simulated response is also shown in Fig. 69 in dashed line. The implemented filter is outlined in Fig. 70.

The upper part of Fig. 69 shows the normalized in-band response for the measured (solid), simulated (dashed) and synthesis response using a conventional synthesis technique [1] which considers the effects of the losses (Q=200) afterward (dotted). The comparison clearly illustrates the advantage of using the novel synthesis technique described in this work.

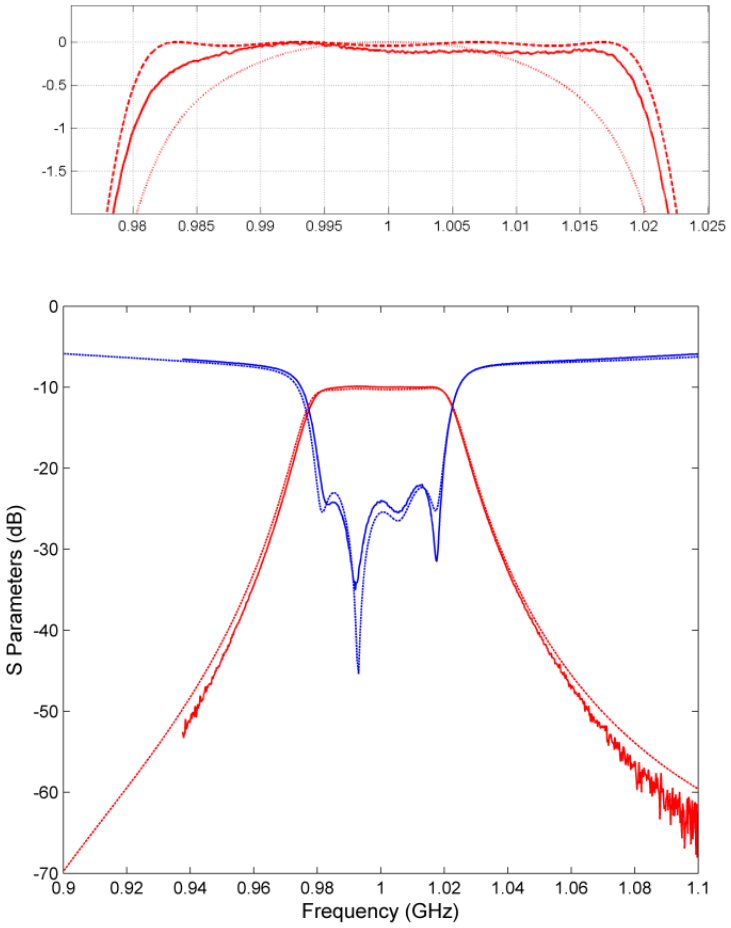

Fig. 69. Frequency response of the measured filter (solid-line), electromagnetic simulated response (dashed-line) and synthesized conventional response (dotted-line). Upper part: Details of the normalized to 0 dB in-band transmission responses. Inset: outlined of the implemented filter. Note that the measured frequency response has been shift up in frequency by 40 MHz, in order to be centered at 1 GHz.

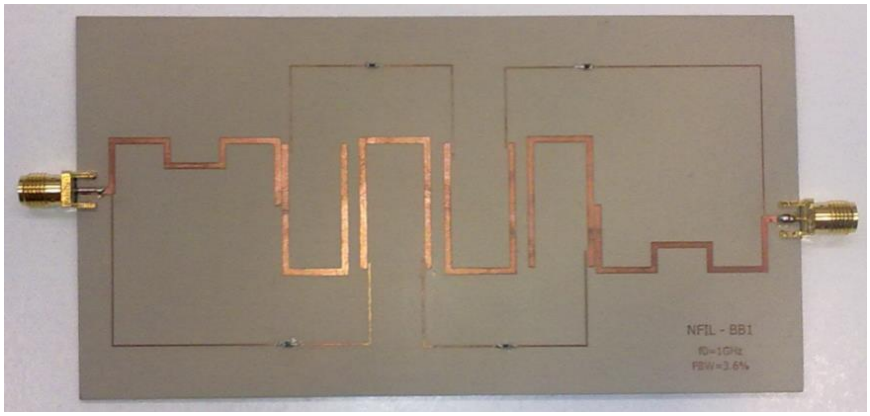

Fig. 70. Picture of the fabricated filter

Additionally, in order to demonstrate the theory presented, we have performed measurements using different sets of resistors in the coupling network (Table 30). As shown in Fig. 71, the results reproduce the simulations on the sensitivity analysis of section 2.5 and Fig. 56 and 57. The solid black line in Fig. 71 shows the nominal unperturbed response also shown in Fig. 69. Note that the expected rounding and “ear-cat” effects appear in the frequency responses of Fig. 71, and a flat response is only achieved when the values of the resistors are in correspondence to the resonator Qs.

Note that this also confirms therefore that we can recover the flatness of the frequency response in case the Q is degraded just by changing the resistors, see also section 2.5.

	R_{13} (R_{24})	R_{NR2} (R_{NR3})
C1	No resistors	No resistors
C2	62	200
C3	100	270
C4	33	120
C5	24	75

Table 30: Summary of the lumped resistors used in the topology of Fig. 70, whose measurements are outlined in Fig. 70.

3.1.7 Broadband frequency response of Filter 1

The following figure, in dashed lines, shows the simulated broadband frequency response from 100 MHz to 10 GHz. In order to assess the effect of the transmission lines used for the realization of the coupling resistor, the same layout has also been simulated without the resistive network, i.e., the frequency response of the

layout in Fig. 70, and shown in solid lines. As can be seen both topology exhibit almost the same broadband spurious behavior.

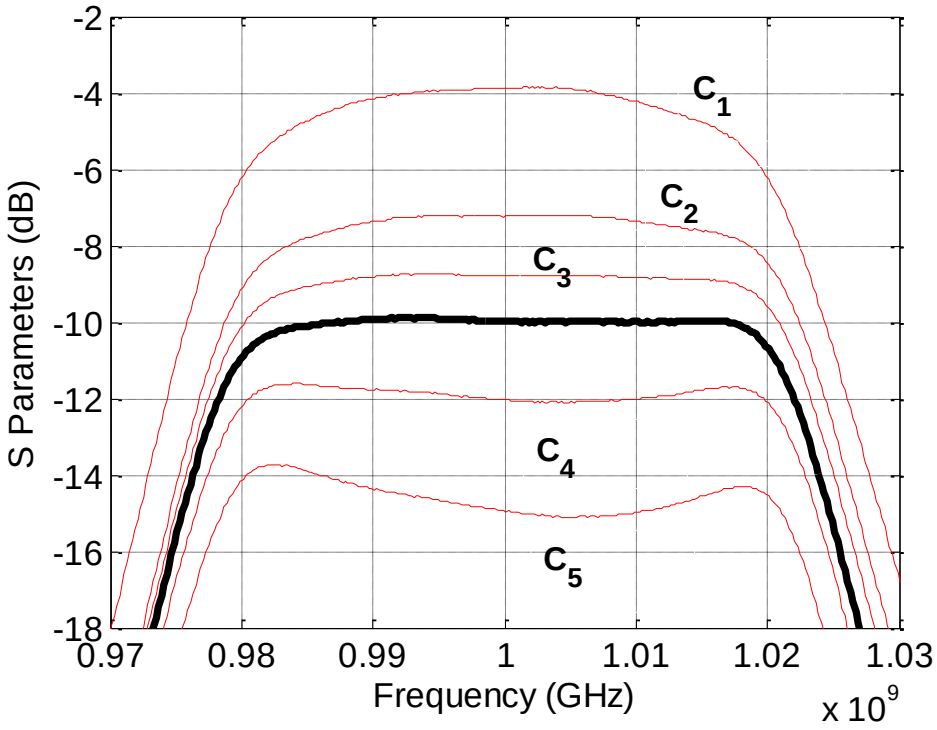

Fig. 71. Measured frequency response of the implemented filter, when the initial resistors are changed according to Table 30

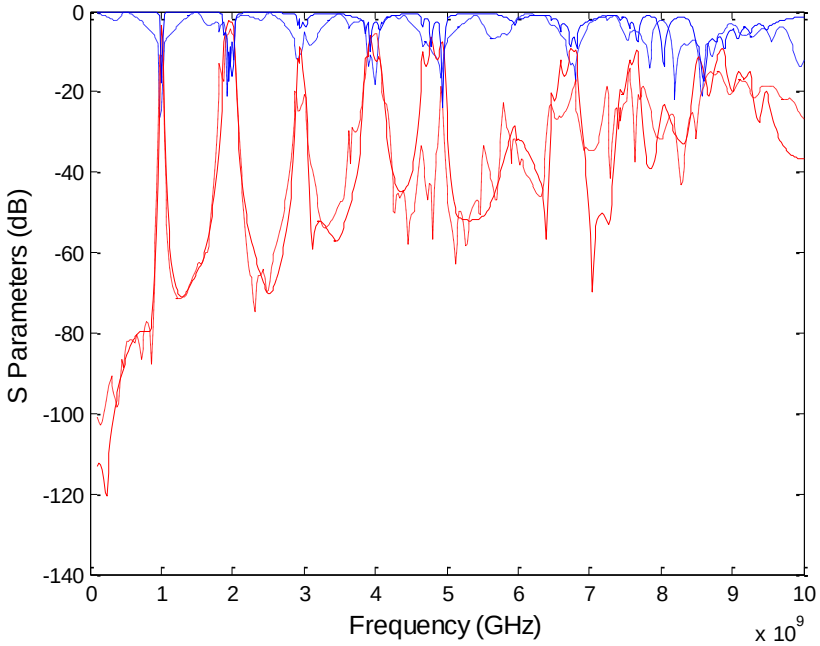

Fig. 72 - Broadband frequency response of the transmission (in red) and reflection (in blue) coefficients. Dashed line corresponds to the simulated response of filter topology with resistive couplings, and solid line corresponds to the simulated response without the resistive couplings.

3.1.8 Temperature performance

The temperature performance it is evaluated in this section by comparison of the frequency response at several temperatures ranging from -10 ºC to 85 ºC. Also worth to mention here that those measurements where performed at ESA facilities in ESTEC. From these results we can summarize the temperature effects as:

a) Shift in frequency: The central frequency of the filter increases when the temperature increases
b) Increase the insertion losses: The insertion losses increase when the temperature increases
c) Band edges: The rounding increases when the temperature increases and some “ear-cat” effect can also be seen for low temperatures.

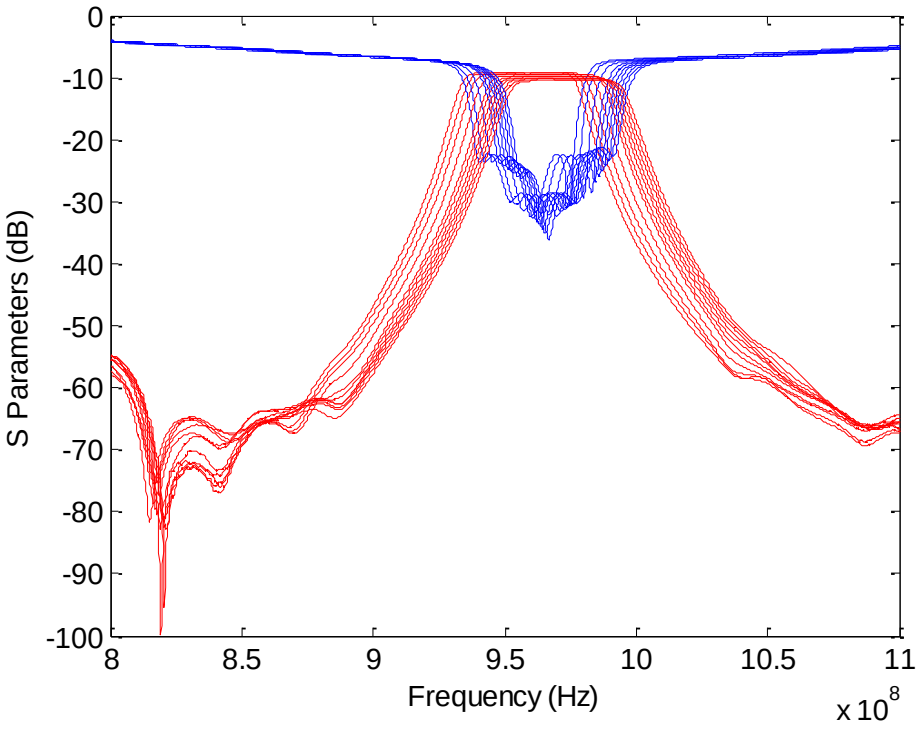

Fig. 73: Measured response as a function of temperature

The frequency shift (point a) in list above) is due to the variation of the dielectric permittivity as a function of temperature. This variation produces a frequency shift of the resonant frequency of each individual resonator. Note however that this variation on the permittivity does not significantly affect the filter bandwidth neither the input nor the output matching, being therefore negligible the effects of permittivity variation on the filter conventional couplings. More details of the filter bandwidth and input matching are shown in Figs. 74 and 75 below.

The frequency shift of the resonant frequency has been measured in an individual resonator and the results are reported in the subsection below. These results show a 2% variation of the resonant frequency for all the temperature range.

By using simulations, we conclude that the 2% variation in resonant frequency is due to a 2% variation in effective permittivity which, in turn, is caused by a 2.1% change in the substrate permittivity.

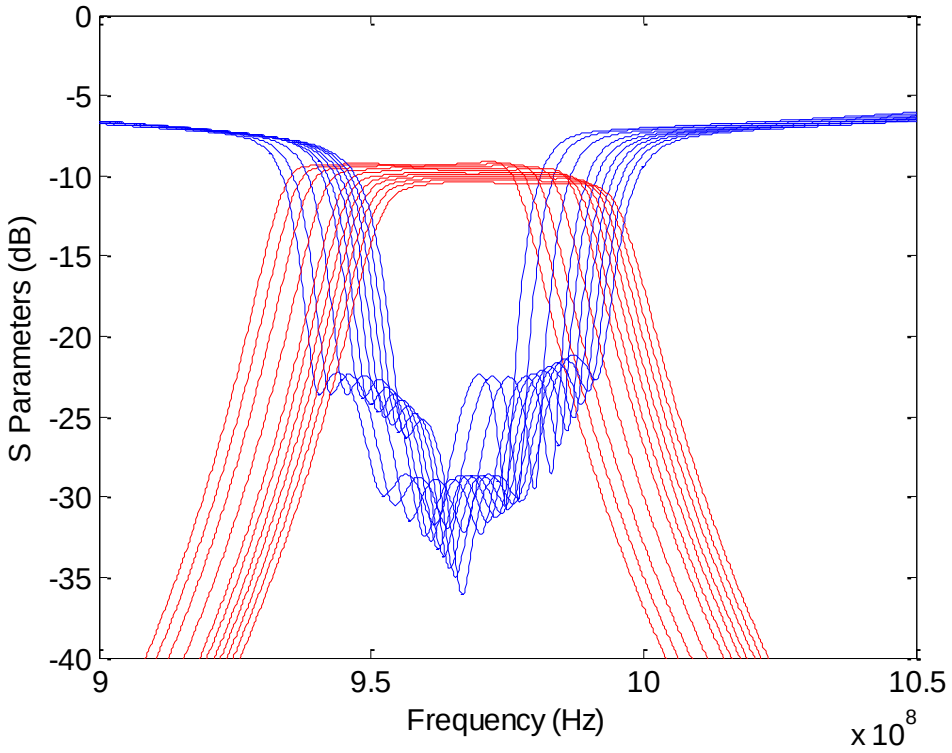

Fig. 74: Detail of the temperature dependence of transmission and reflection responses in the passband

Figure 75, illustrates the temperature dependence of the passband insertion loss and the insertion loss flatness (points b) and c) in the list above). The black line corresponds to the filter response at room temperature. These results show that when the temperature is below room temperature, the insertion losses decrease and a very small ear-cat effect can be observed, whereas when the temperature rises above room temperature the insertion loss increase and a rounding effect appears at the band edges.

According to the formulation in Chapter 2, the effects outlined above appear when the values implemented in the resistive couplings do not correspond with the actual Qs of the resonators.

In order to explore the origin of these effects, measurements of the Q factor of an isolated single resonator as a function of temperature has been performed, as well as measurements of the variation of the resistive values of the lumped resistors used in the resistive couplings.

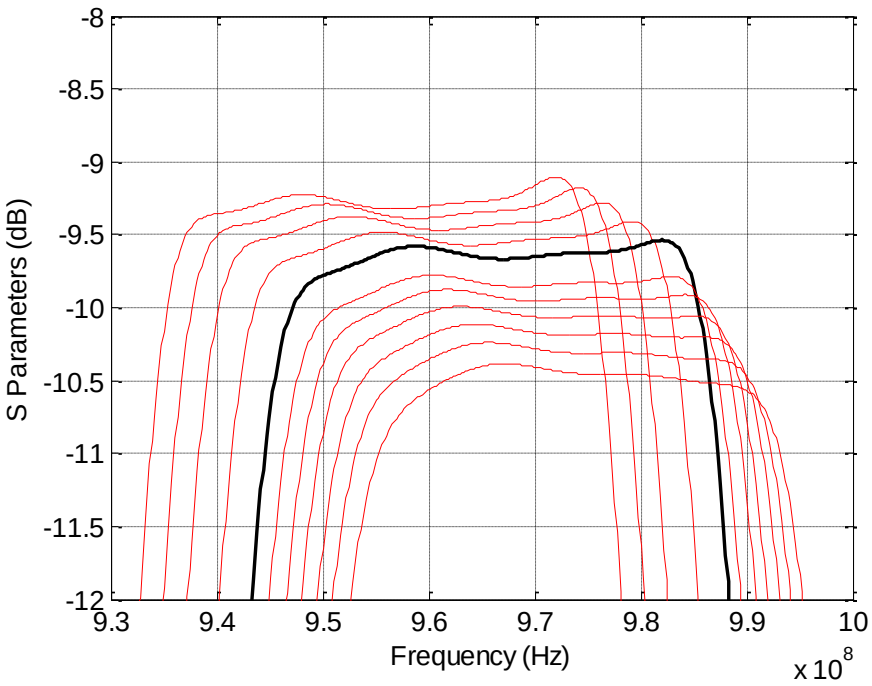

Fig.75: Detail of the In band filter response, showing the details of the insertion losses and rounding at the band-edges

3.1.8.1 Temperature performance of a single resonator

Figure 76 shows the measurements performed on a single resonator as a function of temperature. These responses have then been used to extract the resonant frequency and unloaded Q factor of the resonator. Note that the transmission coefficient of the resonator frequency response is always below -28 dB, which essentially indicates that the resonator is very lightly coupled and the bandwidth of its frequency response is not affected by the input and output ports. In these conditions, the Q factor can be obtained directly by the 3dB resonant bandwidth. Figure 76b shows the variation of the Q factor as a function of temperature, which reduces from 208 to 157 when the temperature goes from -10 ºC to 90 ºC. This corresponds to a reduction of 25%. On the other hand Fig. 77 shows the variation of the lumped resistors used in Filter 1 (100 Ohms and 51 Ohms). These results show that the resistive values barely change over temperature with a variation range of only 0.5%.

Note that according to section 2.5.3, if both the Q values and resistive coupling deviates by the same amount, the frequency filter response would maintain its flatness and only the absolute insertion loss would be affected. Since this is not the case, and the resistive values barely change, the effects observed in the in-band transmission response are only due to the degradation of Q, which is responsible for the passband rounding and ear-cat effects shown in Fig. 75.

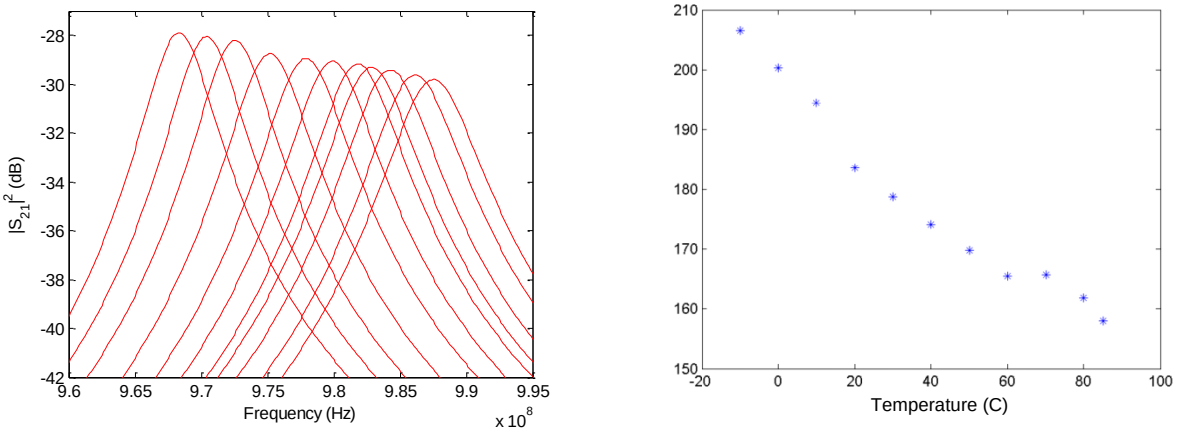

Fig. 76: a) frequency response of a single resonator as a function of temperature. b) Dependence of the Q factor as a function of temperature

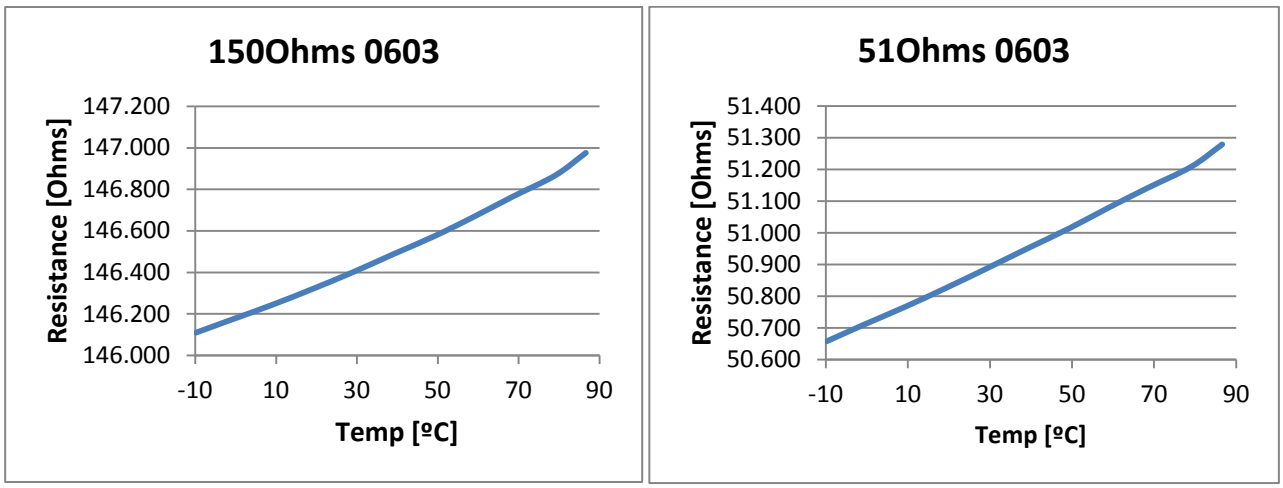

Fig. 77: Variation of the resistive value as a function of temperature

To verify these conclusions, Fig. 78 compares the insertion loss variation and flatness of the measured responses (Fig. 75) versus the simulated response when the Q degrades (Fig. 76b). We can see how the degradation of Q explains both insertion loss variation and the increment in the flatness.

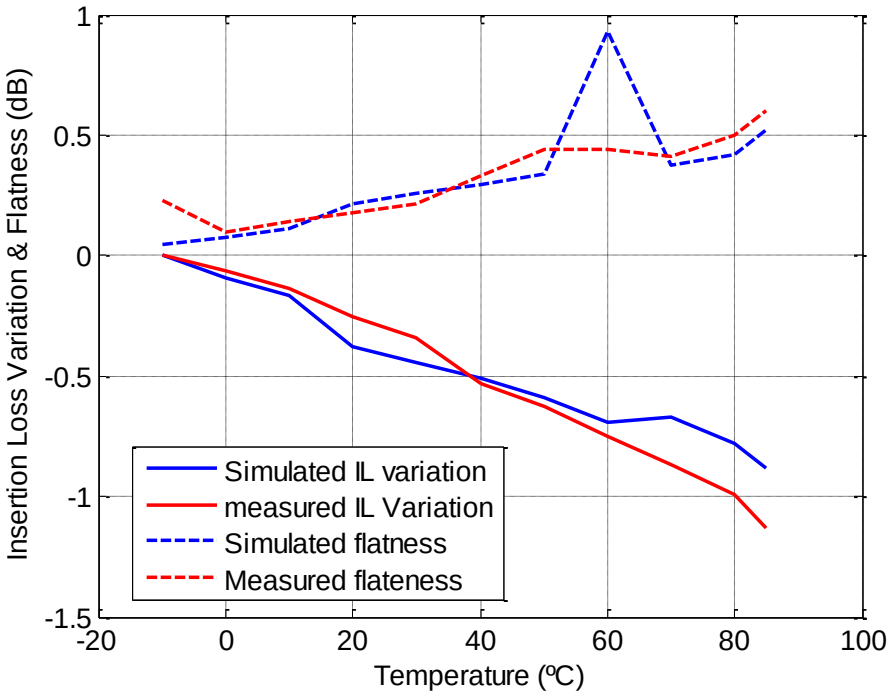

Fig. 78- Measured and simulated insertion loss variation and flatness for Filter 1

Note that Fig. 78 also shows that almost perfect insertion loss flatness is possible if the resonator quality factor used in the synthesis is achieved in the real implementation of the filter. As can be seen in measurements above the prototype at room temperature was not fully compliant in terms of insertion loss flatness (0.5 dB measured, vs. 0.2 dB specified, see Table 28) because the predicted resonator Q was 200 and the implemented one had Q≈180 at 20ºC (Fig. 76b). However, Fig. 76b and Fig. 78 show that at 0ºC Q is about 200 and the passband flatness is close to ideal (0.1 dB).

3.2 6th order Chebyshev planar lossy filter. Optimization approach

The optimization procedure presented in section 2.4 is used below for the synthesis of a 6th order Chebyshev filter. The filter will be implemented in planar technology using a microstrip configuration on alumina substrate with metalized gold. The filter has been synthesized to be compliant with the specifications listed in Table 31. Note also from the table that the dimension it is also a parameter which has to be fulfilled.

Centre frequency	MHz	1650,75
Channel bandwidth	MHz	**80.5**
Insertion losses over bandwidth	dB	-
Insertion losses at Centre frequency	dB	<10
Input and output match	dB	> 15
Insertion losses variation over frequency		
In-band	dB	**< 0.5**
Out-of-band rejection		
F0 +/- (132.75MHz +/-15 MHz) to F0 +/- (91.75MHz -/+15 MHz)	dB	30
Size	58x31	

Table31. Specification of the Filter 2.

As indicated in previous chapter, and in particular in section 2.4, in a lossy filter synthesis the losses need to be known in advanced since they will essentially set the lossy network to be synthesized. Equally as in previous design a satisfactory way to quantify the losses states on the determination of the Q factor of the basic resonant structure to be used. To do that one could simply go through simulation results, nevertheless this section also outlines the measured Q factor in a single resonator. Although generally speaking a lossy filter could consist on resonators with unequal Q, the foreseen design also aims for a filter with uniform Q distribution.

In this case the material used to implement the filter has Alumina as a dielectric, since it is certified for space applications, whose permittivity is 9.6, with a thickness of 1.27 mm and an specified loss tangent of 0.0001. Metallization on top is of 5 μm gold. Properties of the material are summarized in Table 32.

Alumina	
Dielectric Thickness	1.27 mm
Permittivity	9.6
Loss tangent	0.0001
Conductor	Au
Conductivity	4.1e7
Metallic Thickness	5 μm

Table 32. Properties of the material used in Filter 2

The basic resonator consists of a halfwave transmission line hairpin resonator – 37.7 mm length – of 50 Ω impedance – 1.23 mm width –, which results in an unloaded Q factor of nearly 300. Details on the basic resonator and its coupling to the input and output port appear in Fig. 79.

The Q value is then used to determine the insertion losses IL=10 dB from (65), which in turns gives the *k* value in (42), necessary to define the initial polynomials.

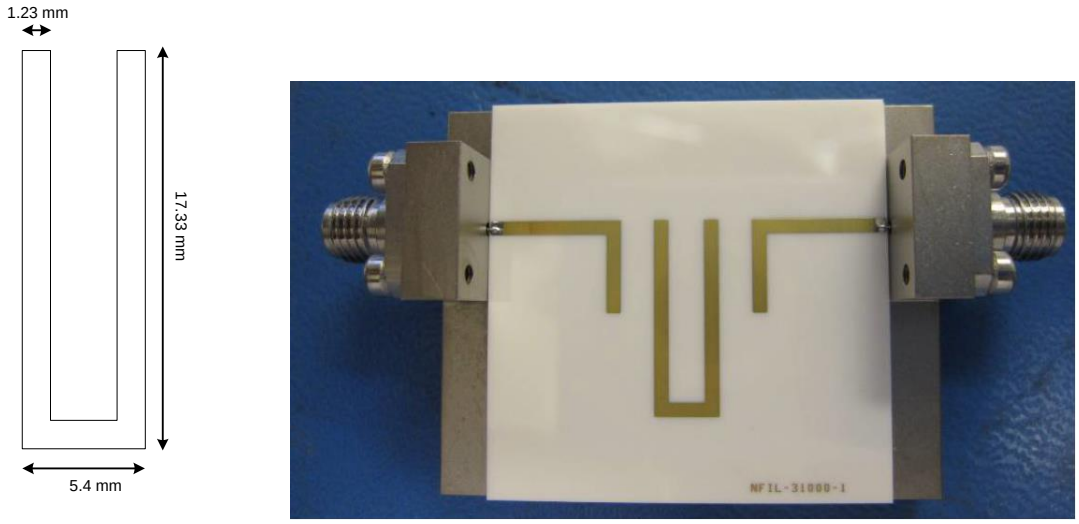

Fig. 79- Outline and picture of the basic resonator for Filter 2.

3.2.1 Synthesis and coupling matrix

As mentioned above the Q value will be then used into the synthesis procedure. In contrast with previous case where a direct synthesis approach was used to obtain the coupling matrix and therefore state the value of the insertion losses from the Q value of the resonator, the following approach is based on optimization. This is that the insertion loss of the filter, flatness and selectivity are achieved by optimizing the values of an initial coupling matrix. Recall here that the optimization procedure allows to change the nominal values of the conventional couplings and the values of the resistive couplings. Also note that the Q value of the resonators is not optimized in this approach, and the Q are kept to the 300 initially estimated/measured value.

The initial coupling matrix has been selected from a conventional 6th order Chebyshev filter. Due to the losses of the resonators such implementation would result in non-complaint specification in terms of flatness in the passband. In order to avoid this an additional resistive network will be attached. Note that this is consistent with the aim of lossy filters approach, which propose achieving flatness in the passband by means of a selective dissipation along the passband and a distribution of the losses through the network. In order to obtain a non very complex structure only two resistive couplings have been proposed, resulting on the network topology of Fig. 80.

The optimization procedure to obtain the final coupling matrix has used the software tool developed during the thesis (www.tsc.upc.edu/lossyfilters). The resulting coupling matrix is detailed in Fig. 81.

As can be seen in the network topology of Fig. 80 and Fig. 81 this results in a inline filter for the conventional couplings, so no transmission zeros on the filter response, and two resistive couplings, one between resonator 2 and 4 and the other between resonator 3 and 5.

The coupling matrix defines the coupling between resonators and their required quality factors, which in this case all resonators require the same Quality factor of 293. Note moreover that the two resistive couplings (see coupling matrix values) are equal, which also facilitates the designing process.

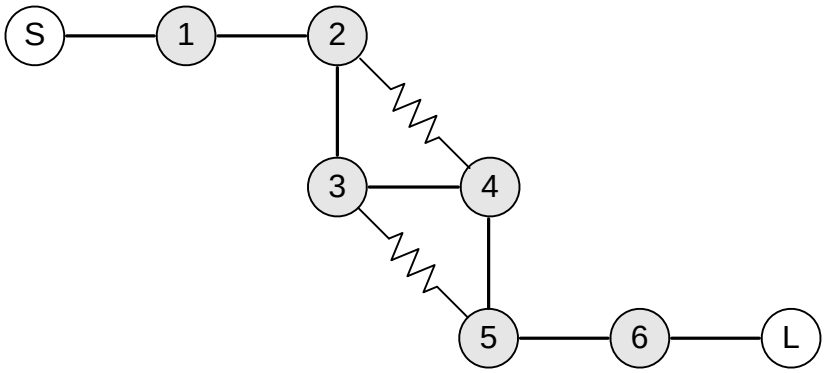

Fig. 80- Outline of the filter network topology for the Filter 2.

	S	1	2	3	4	5	6	L
S	0	1	0	0	0	0	0	0
1	1	-0.07j	0.85	0	0	0	0	0
2	0	0.85	-0.125j	0.64	0.055j	0	0	0
3	0	0	0.64	-0.125j	0.6	0.055j	0	0
4	0	0	0.055j	0.6	-0.125j	0.64	0	0
5	0	0	0	0.055j	0.64	-0.125j	0.85	0
6	0	0	0	0	0	0.85	-0.07j	1
L	0	0	0	0	0	0	1	0

	1	2	3	4	5	6
Q	293.2	292.9	292.9	292.9	292.9	292.9

Fig. 81- Details on the coupling matrix corresponding to the synthesis filter of Fig. 80. The Q factors of the resonators are also indicated.

Finally the filter transfer function from the evaluation of the above coupling matrix and therefore our targeted design is depicted in the following figure (Fig. 82).

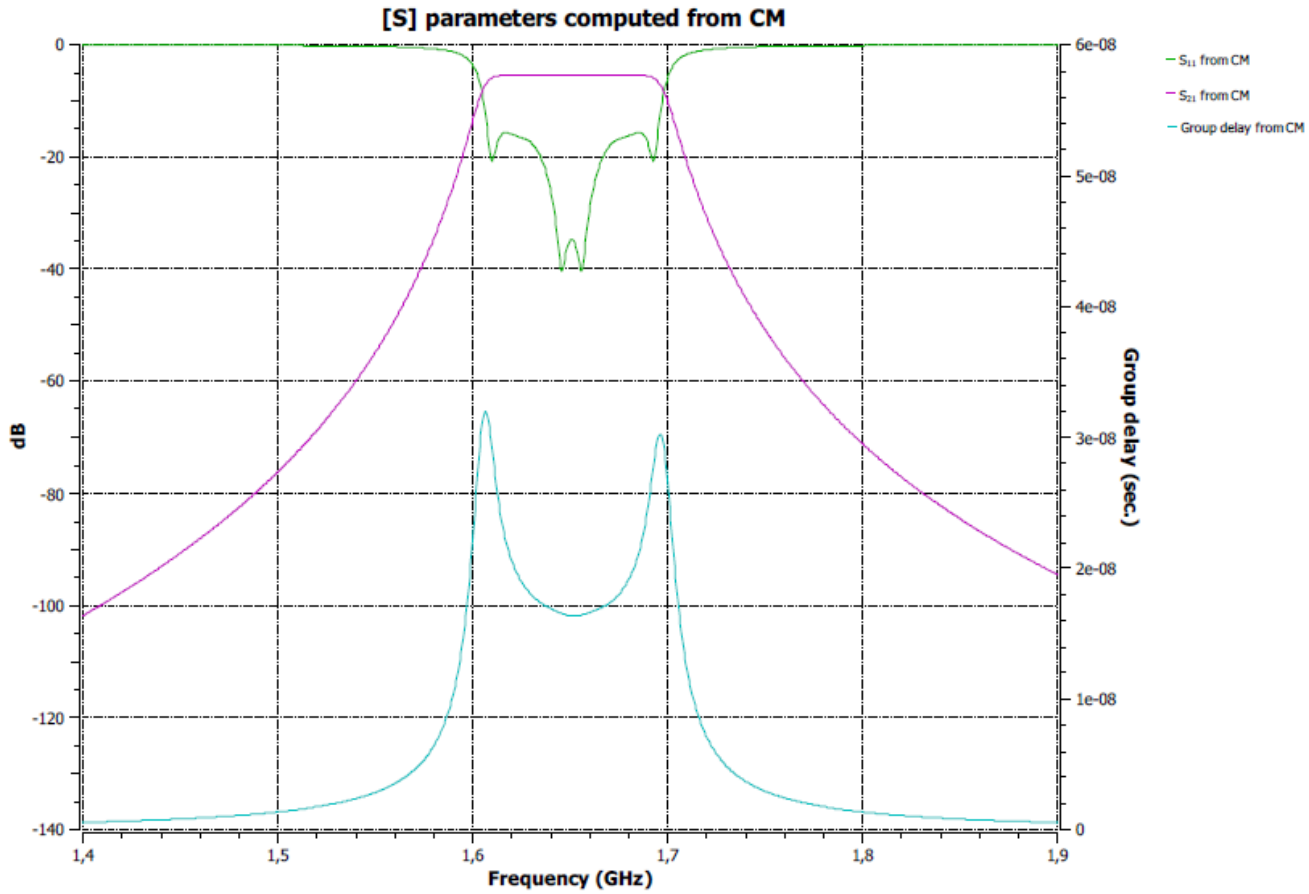

Fig. 82- Frequency response of the filter to be developed.

3.2.2 Filter design

As in previous filter the design process consists in two steps: first we design the conventional couplings and the resistive couplings are included afterwards. Note however that additional resizing and trimming steps it is required at the end to account for the effects of the whole structures.

3.2.3 Electromagnetic design of conventional couplings

In this case we use the basic resonator structure of Fig. 79 to obtain the filter configuration as depicted in Fig. 83 . As done for the previous design we use an in-line configuration where the coupling between resonators is performed by alternating them up and down as outlined in Fig. 83.

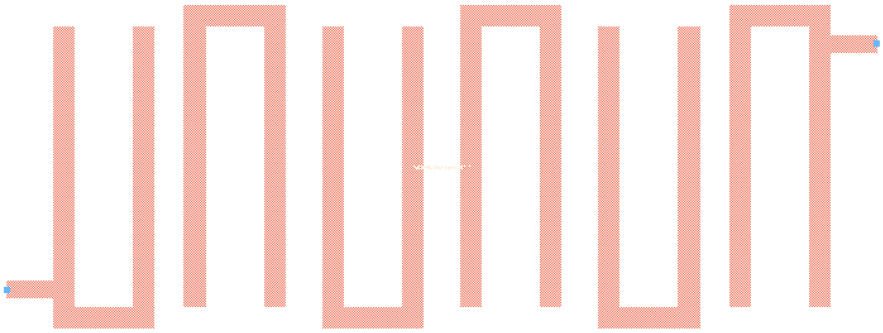

Fig. 83- Filter configuration of BB-2 without resistive couplings.

To evaluate the proper design of the conventional couplings, the filter response of the design topology of Fig. 83 has been simulated with a full-wave simulator (Momentum from ADS / Agilent), and has been compared with the synthesized response without resistive couplings. The results of this comparison are outlined in Fig. 84, showing very good agreement in both the transmission coefficient S_{21} and the reflection coefficient S_{11}. The green and orange lines correspond to the ideal response (evaluated from the coupling matrix) for the transmission coefficient S_{21} and the reflection coefficient S_{11}, respectively, and the blue and red lines correspond to the full-wave simulated response, transmission coefficient S_{21} and the reflection coefficient S_{11}, respectively.

3.2.4 Electromagnetic design of resistive couplings and co-simulation

For the design of the resistive coupling network, in this case two identical resistive couplings, we follow the procedure detailed in section 3.1.4. This results in the filter configuration detailed in Fig. 85.

The simulation of the complete designed, this is the filter including the resistive network, is depicted in Fig. 86. The red line and blue line respectively correspond to the S_{11} and S_{21} designed parameters, whereas the synthesized response of Fig. 82 is depicted in orange and green for S_{11} and S_{21} respectively.

As shown in Fig. 86, both the designed and synthesized responses are in good agreement, being therefore the design compliant with the filter specifications of Table 31.

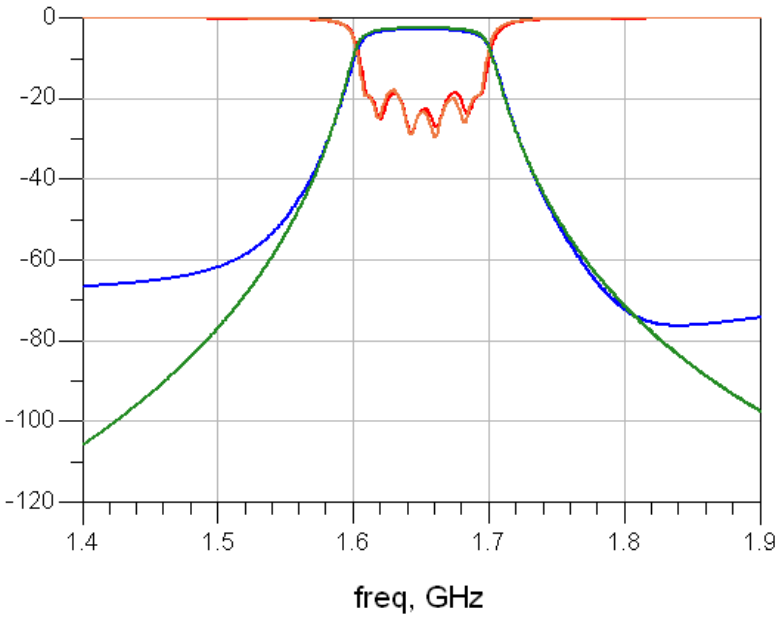

Fig. 84- . Frequency response of the synthesized and designed filter without resistive couplings.

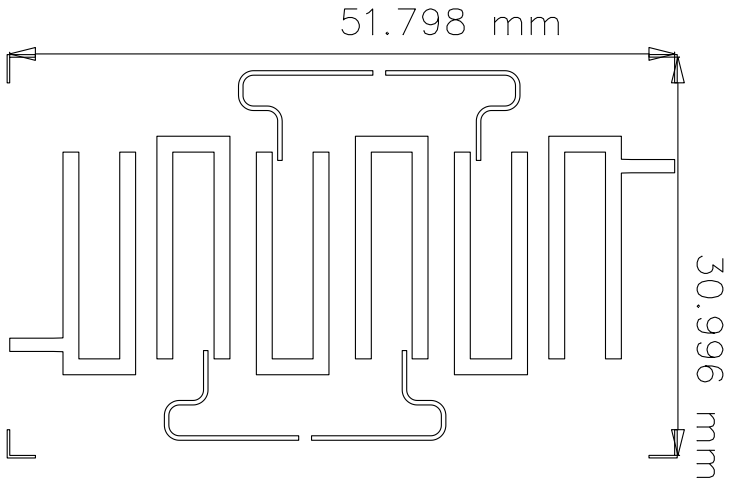

Fig. 85- Layout of the Filter 2.

Note as well from the layout in Fig. 85 that the filter designed is also complaint from the dimensions point of view. This essentially has been achieved by bending the quarter-wavelength transmission lines required on the resistive coupling implementation.

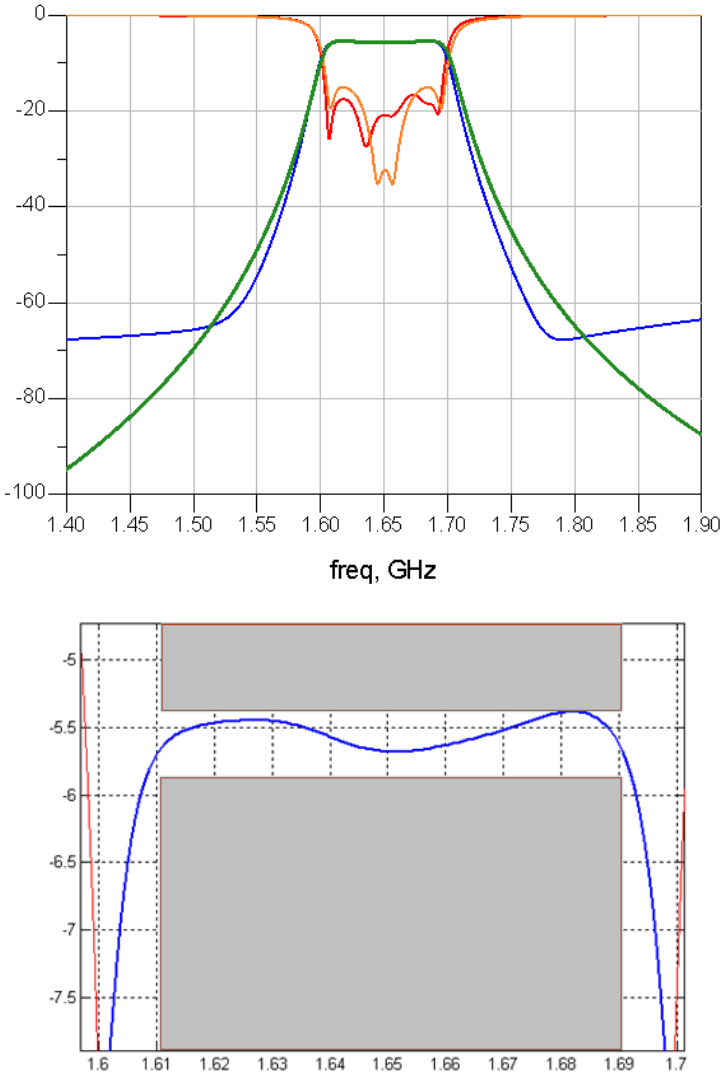

Fig. 86 - Comparison between circuital simulations of the lossy filter and simulation ADS-Moementum of the planar filter of Fig. 85

3.2.5 Fabrication and measurement

Then the filter has been fabricated and tested. Measurements and stability versus temperature will also be shown along this section. The picture of the fabricated filter is shown in Fig. 87.

Measurements at room temperature are compared with the full-wave simulated response. Figure 88 compares the measured (red line) and simulated response (blue line) of both the reflection and transmission coefficients of the planar filter of Fig. 87.

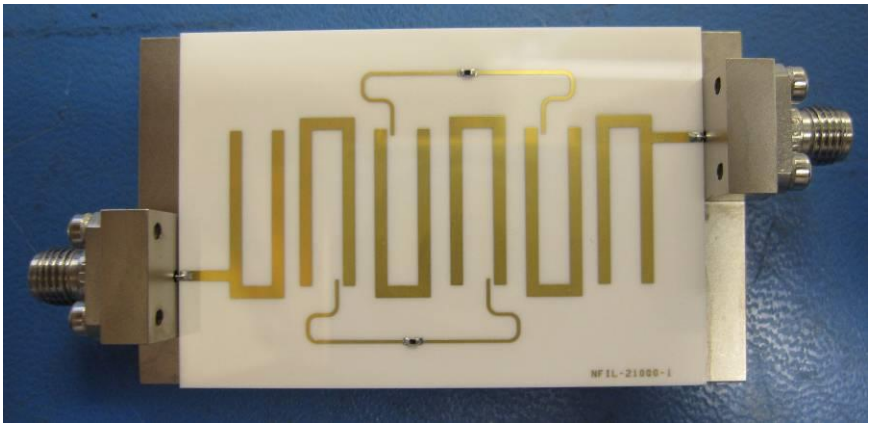

Fig. 87- Picture of the fabricated filter

Mention here however that the central frequency of the measured response is 27 MHz below the design frequency (1650.75 MHz), which corresponds to a 1.6% deviation. This disagreement is essentially due to the tolerance in dielectric permittivity. In the following figure the measured response has been centred at 1650.75 MHz for a better comparison with the simulated response.

Besides the frequency shift, the measured and simulated responses are in very good agreement in both transmission and reflection.

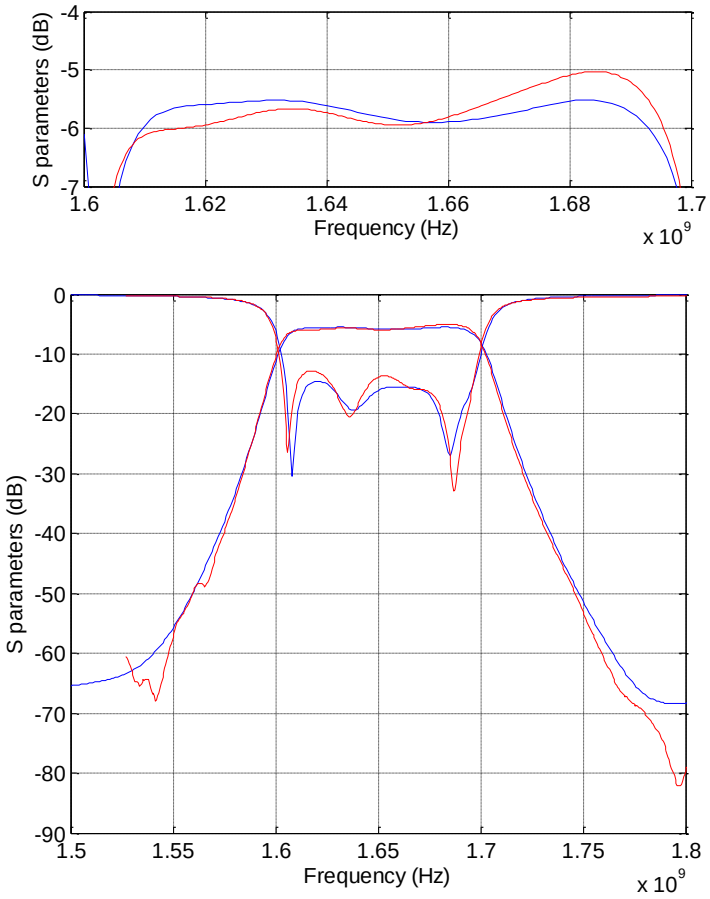

Fig. 88: Measured response (in red) shifted 27 MHz to higher frequencies, and simulated response (in blue).

The overall dimensions of the filter and its mass, including connectors it is listed in Table 33 below.

Parameter	Value	Units	Comments
Size	64x37.1	mm^2	
Mass	10.2	gr	Alumina substrate
Mass	130.4	gr	Alumina substrate + test jig

Table 33: Resulting dimensions and weight of the fabricated Filter 2.

3.2.6 Broadband frequency response of Filter 2

The following figure (Fig. 89), in dashed lines, shows the simulated broadband frequency response from 100 MHz to 10 GHz. In order to assess the effect of the transmission lines used for the realization of the coupling resistor, the same layout has also been simulated without the resistive network, i.e., the frequency response of the layout in Fig. 85, and shown in solid lines. As can be seen both topology exhibit almost the same broadband spurious behavior.

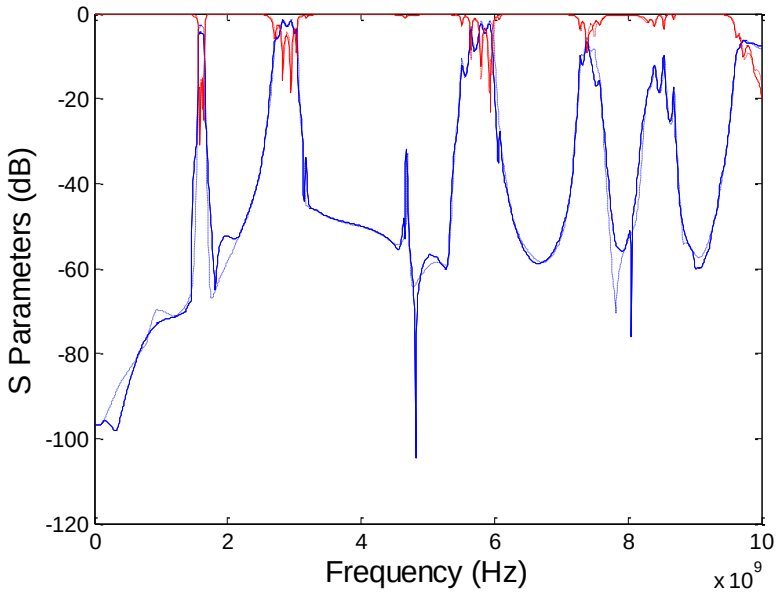

Fig. 89: broadband frequency response of the transmission (in red) and reflection (in blue) coefficients. Dashed line corresponds to the simulated response of the filter topology with resistive couplings, and solid line corresponds to the simulated response without the resistive couplings.

3.2.7 Temperature performance

This section analyses the effects of varying the temperature on the filter performance. We follow the same procedures that in the previous analysis for Filter 1 (section 3.1.8).Figures 90 and 91 show the transmission and reflection filter responses when the temperature changes from -10 ºC to 85 ºC.

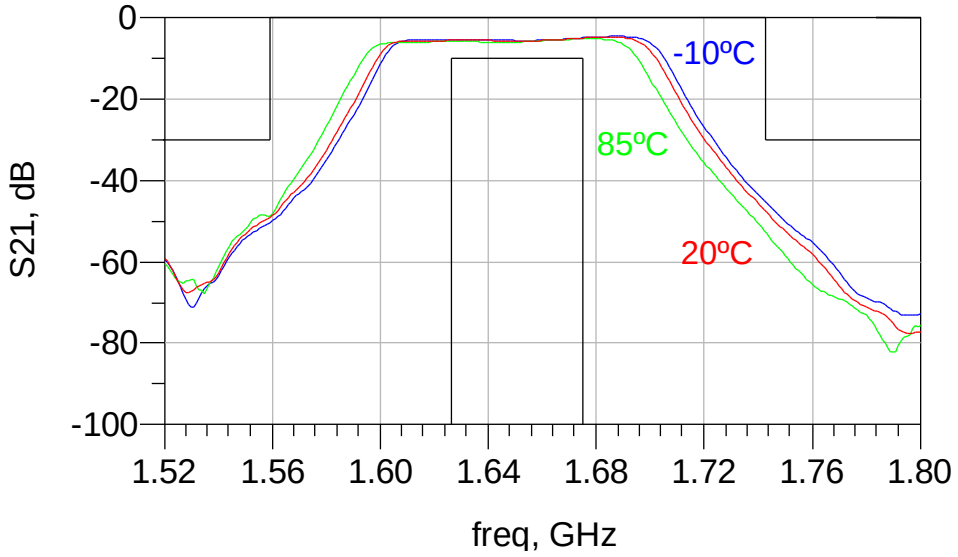

Fig. 90 - Measured response of the filter as a function of temperature

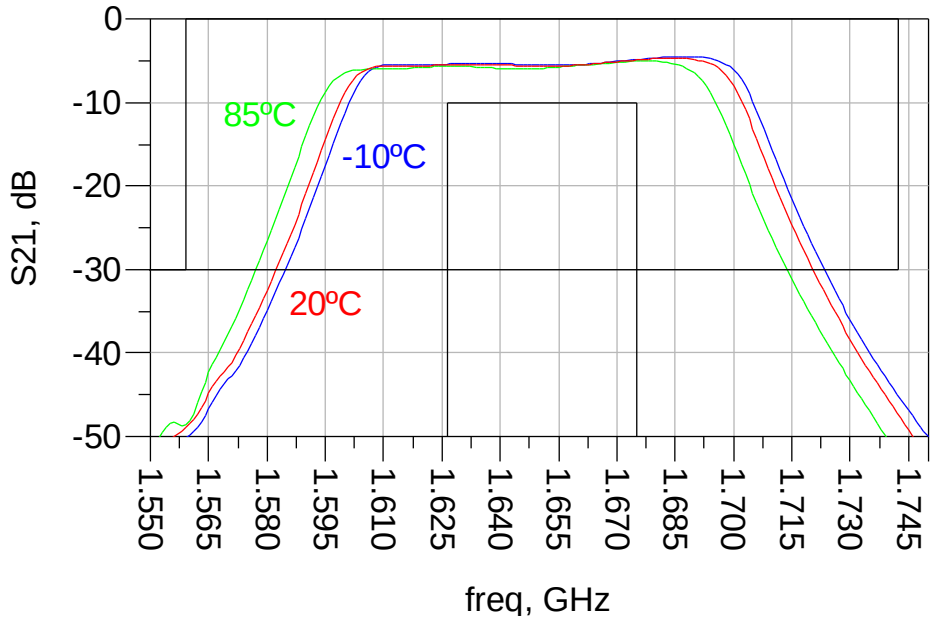

Fig. 91 - In-band detailed of the measured response of the filter as a function of temperature

Although the effects are the same than those outlined for Filter 1 in section 3.1.8, these are much less pronounced due to the weaker temperature dependence of the resonant frequency and Q of the filter resonators (discussed below):

a) Shift in frequency: The central frequency of the filter increases when the temperature increases

b) Increase the insertion losses: The insertion losses increase when the temperature increases

c) Band edges: The rounding increases when the temperature increases and some “ear-cat” effect can also be seen for low temperatures.

3.2.7.1 Temperature performance of a single resonator

Figure 92 shows the measurements performed on a single resonator as a function of temperature. These responses have then been used to extract the resonant frequency and unloaded Q factor of the resonator. Note that the transmission coefficient of the resonator stays always below -28 dB, which essentially indicates that the resonator is very lightly coupled and the bandwidth of its frequency response is not affected by the input and output ports. In these conditions, the Q factor can be obtained directly by the 3dB resonant bandwidth.

Figure 92 b shows the variation of the Q factor as a function of temperature, which reduces from 335 to 285 when the temperature goes from -10 ºC to 80 ºC. This corresponds to a reduction of 15%.

On the other hand Fig. 93 shows the variation of the lumped resistor used in the filter (whose nominal value at room temperature is 10 Ohms). These results show that the resistive values barely change over temperature with a variation range of only 0.4%, as in previous case, the resistive value barely changes thus the effects observed in the in-band transmission response are predominantly due to the variation in Q.

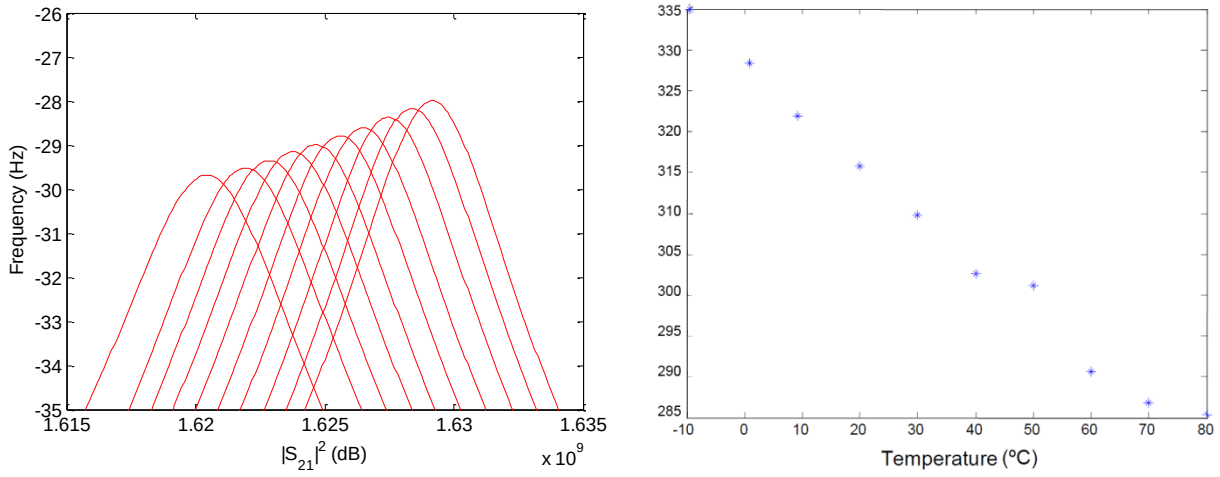

Fig. 92: a) frequency response of a single resonator as a function of temperature. b) Dependence of the Q factor as a function of temperature.

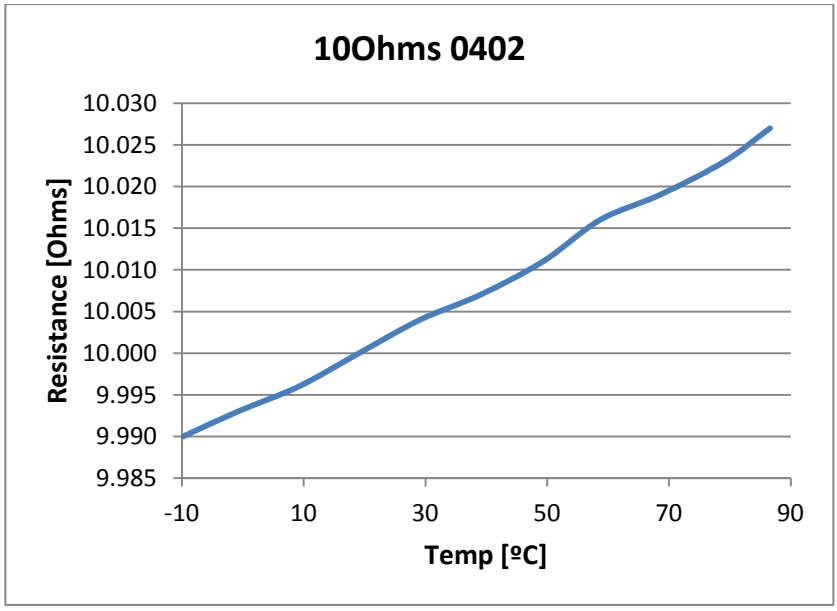

Fig. 93: Variation of the resistive value as a function of temperature.

To verify these conclusions, the figure below compares the insertion loss variation and flatness of the measured responses (Fig. 91) versus the simulated response when the Q degrades (Fig. 92). We can see how the degradation of Q explains both insertion loss variation and the increment in flatness.

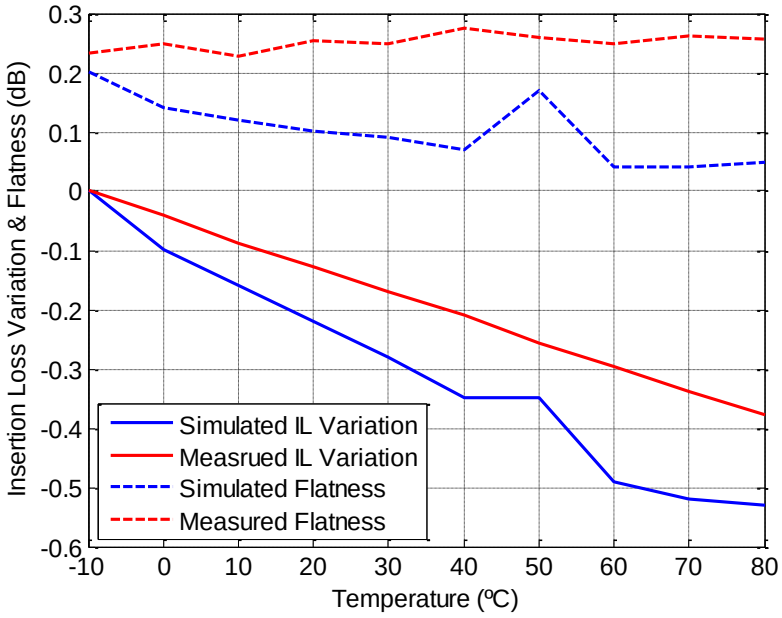

Fig. 94: Measured and simulated insertion loss variation and flatness for the filter response

3.3 Combline Channelizing lossy filter at C-Band

This section presents the design of a combline channelizing lossy filter breadboard at C band. Table 34 shows the in-band specifications used for this study. They are set to produce a simple breadboard that demonstrates the desired features of IMUX channelizer filters before facing the difficulties that a more realistic set of specifications would bring (among other issues, group delay specifications are omitted). Table 35 shows the rejection specifications and a summary of the extensive comparison study made in [27] to evaluate various synthesis alternatives. That study uses a sixth order Chebyshev frequency response centered at 4 GHz with 36 MHz bandwidth and a single pair of symmetric transmission zeros at 3.97 GHz and 4.03 GHz. The study shows that, for this particular case, if return loss specifications could be omitted, predistortion synthesis would be the choice requiring lowest Q, otherwise, lossy filter synthesis would be the best choice.

Parameter	**Value**	**UNIT**
Center frequency (f_0)	4000	MHz
Channel Bandwidth	36	MHz
Insertion loss over bandwidth	<6.6	dB
Insertion loss at center frequency	<6	dB
Input and Output Match	<18	dB
In-band Insertion loss variation		
F0+/- 13 MHz	0.2	dBpp
F0+/- 16 MHz	0.3	dBpp
F0+/- 18 MHz	0.6	dBpp

Table 34: In-band filter specifications. See Table 35 for selectivity requirements.

As we did in the two previous cases and as it is mandatory on the synthesis of lossy filters the losses of the basic resonant structures is need it during the selection of the lossy characteristic polynomials. To this end, and although simply full-wave simulations would work, we following present the measured Q value of several combline resonators. Table 36 summarizes the dimensions, Quality factor and resonant frequencies.

Filter	IL (dB)	RTL (dB)	ΔIL(dB)	Sel ± 23 MHz (dB)	Sel ± 30-500 MHz (dB)	Q
SPECS	6	18	0.6	10.5	40	
FPD2	6.3	4	0.01	10.3	41.9	1600 Min. Q IL=6dB
LF	3	18	0.01	10.6	42.1	6700 800 (In/output)
LF_QR	2.67	18	0.46	10.3	42	3500 2800 (In/output) (Q_{eff}=8000)
CONV2	1.2	18	1.1	14.7	49.7	3500

Table 35: Summary of the comparison several synthesis alternatives made in [27] indicating the filter specifications (SPECS), a full pre-distortion synthesis (FPD2), a conventional synthesis (CONV2) and variations of a lossy filter synthesis (LF, LF_QR). Highlighted cells indicate that the specifications are not met.

Fig. 95: Combline cavities fabricated for Q tests.

Cavity dimensions		Measurements	
Cavity side (mm)	**Inner radius (mm)**	**Q**	**fo (GHz)**
20.4	2.92	2210	4.0410
20.4	6.35	1600	4.0223
25.4	2.92	2580	4.0896
25.4	6.35	2130	4.0528
30.4	2.92	3210	4.1145
30.4	6.35	2770	4.0572

Table 36: Measurements in various combline cavities tested. Quality factors agree within 10% with HFSS simulations.

3.3.1 Single resonator

From the results above we proceed to the design of the single cavity which would be later used as a basic structure of the resonator. Also as in both previous cases a uniform Q topology will be foreseen leading to the design of a unique resonant structure.

The basic resonator consists in a conventional combline cavity where its dimensions and material properties are selected to meet the desired resonant frequency and required quality factor.

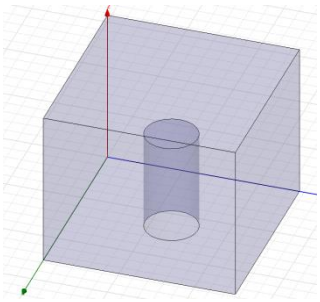

Fig. 96: Outline of the basic combline resonator

Material	Aluminium
Conductivity (Ω-1 m-1)	2.38e7

Table 37: Properties of the material used for the fabrication of the cavity

Radius Post	3 mm
Cavity dimensions	22 mm x 22 mm x 21 mm
Length Post	4.416 mm

Table 38: Nominal dimensions of the cavity to be used as a basic resonator.

The dimensions of the cavity have been selected to obtain the maximum Q. Simulations of the Q as a function of the ratio of the cavity and the aluminum rod are depicted in Fig.97.

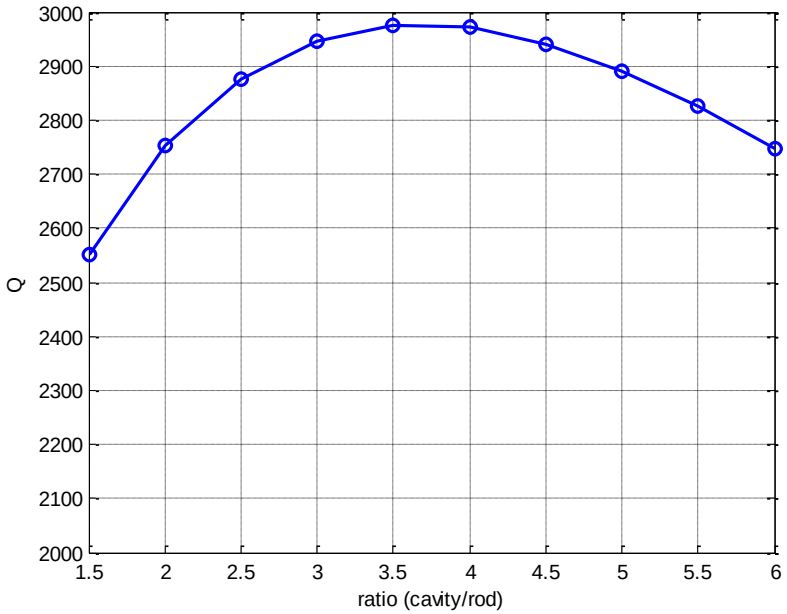

Fig. 97. Q of the combline resonator as a function of the ratio between the cavity and the aluminium rod.

The electromagnetic behavior of the cavity has been evaluated by using EigenMode analysis. This would allow us to obtain its resonant frequency and quality factor. The final dimensions of the cavity are summarized in Table 38.

Once the cavity dimensions are selected we further modify the cavity structure in order to consider the rounded corners due to the mechanical fabrication process, see Fig. 98. The results show that the Qualtiy factor of the cavity barely changes and the slight increment on the resonant frequency can be recovered by means of tuning screws or by adjusting the length of the resonators. So for the design of the filter we will use as a basic resonator the structure outlined in Fig. 96.

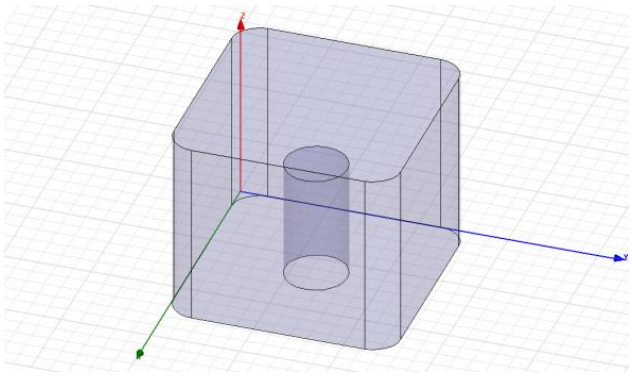

Fig. 98. Outlined of the basic combline resonator with rounded corners.

3.3.2 Synthesis and extraction of the lossy network

While for the design of the first planar filter we used a direct synthesis approach, this is obtaining directly the lossy network of the filter to be implemented and in the second planar design we use an optimization approach, this is proposing a lossy network to optimize their values to comply with the specifications, the following design uses a different approach.

In the following case we apply the synthesis procedure described in section 2.2.2. The synthesis results in a transversal coupling network as outlined in Fig. 29. Then strategies of loss distribution described in section 2.3.3 are used in order to obtain a realizable network. Although part of the general process is already outlined in section 2.3.3, for sake of clarity is recalled below.

1- First trigonometric rotations are applied to get a folded topology, detailed in the figure below, Fig. 99 (note that it is the same figure detailed in Fig. 41) .

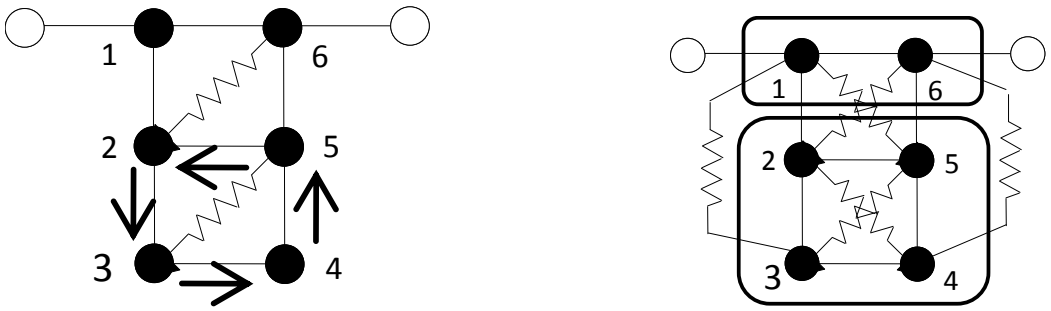

Fig. 99 - a) Folded coupling network indicating the hyperbolic rotations performed. b) Resulting network after applying the rotations.

2- The next step is to even out the resonator *Q*s needed by using hyperbolic rotations. The hyperbolic rotations involve resonators 2, 3, 4 and 5 in Fig. 99a and are performed according to what is indicated by the arrows in the same figure, this is from resonator 5 to 2, from 2 to 3, from 3 to 4 and from 4 to 5. Figure 99b indicates the topology resulting after these rotations.

3- With the steps performed up to here, we would obtain the synthesis of a filter whose passband flatness is that of an ideal lossless filter (LF row in Table 35). This requires *Qs* of 800 in resonators 1 and 6 and 6700 in all other resonators.

4- The insertion loss flatness provided by this solution is much more stringent than the requirements. This can be used to relax the required *Qs* in the resonators. By manual optimization on the coupling matrix, we find another solution (labeled LF_QR in Table 35) requiring Qs of 2800 in resonators 1 and 6 and 3500 in the rest. Note however that we would still require an uneven Q situation which is not desired.

5- Finally and using the solution in previous step 4) as starting point, we then run a computer optimization procedure on the resulting equivalent circuit to find a solution which is simple to manufacture by imposing the following conditions:

- Set all resonator Qs to 3000 (achievable with combline technology)
- Eliminate the resistive couplings 1-3 and 6-4 (R_{13} and R_{64})
- Set $R_{15}=R_{26}$ and $R_{24}=R_{35}$
- Eliminate coupling 1-6
- Set return loss to 18 dB to have some margin over the specs in Table 34..

The resulting coupling matrix and thus is corresponding network topology are outlined below, in Fig.100 and Fig.101, respectively.

0	1.091	0	0	0	0	0	0
1.091	j1.042	0.934	0	0	-j1.006	0	0
0	0.934	j1.0941	0.598	-j0.051	-0.107	-j1.006	0
0	0	0.598	j0.0881	0.686	-j0.051	0	0
0	0	-j0.051	0.686	j0.0881	0.598	0	0
0	-j1.006	-0.107	-j0.051	0.598	j1.0941	0.934	0
0	0	-j1.006	0	0	0.934	j1.042	1.091
0	0	0	0	0	0	1.091	0

Fig. 100 - Coupling matrix of the filter cavity to be designed

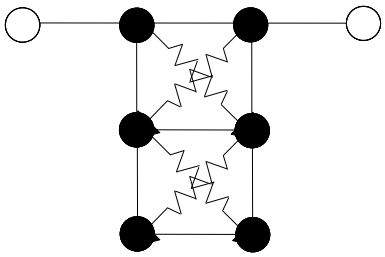

Fig. 101 - Network topology of the filter cavity to be designed

Note that from the coupling matrix of Fig. 100 the coupling between resonators are defined, this is the conventional couplings and resistive couplings and the required quality.

The resulting frequency response of this solution (referred as LF_OPT in Table 35) is shown in Fig. 102 and 103.

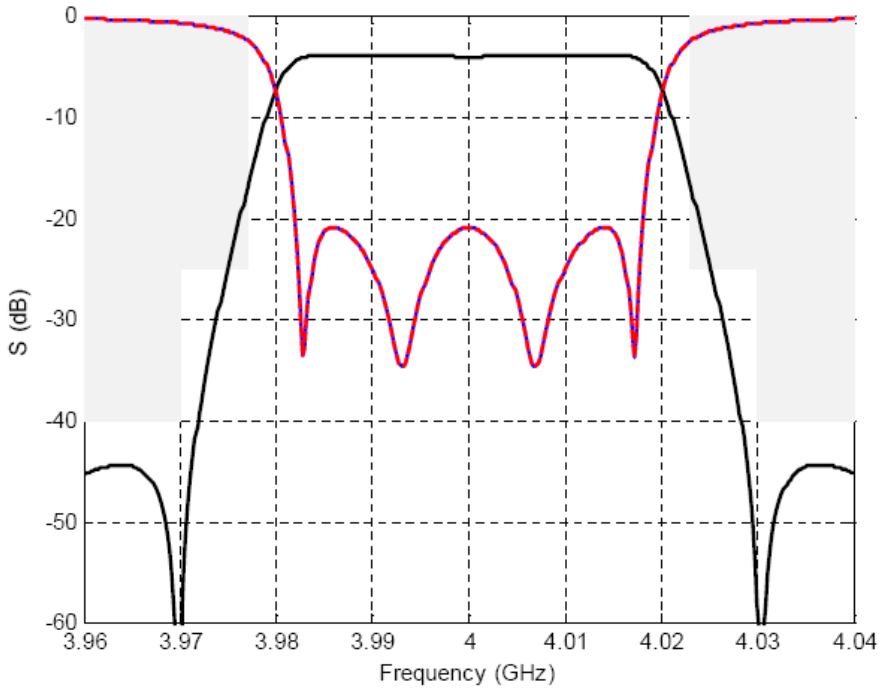

Fig. 102. Transfer and return responses of the synthesis alternative LF_OPT

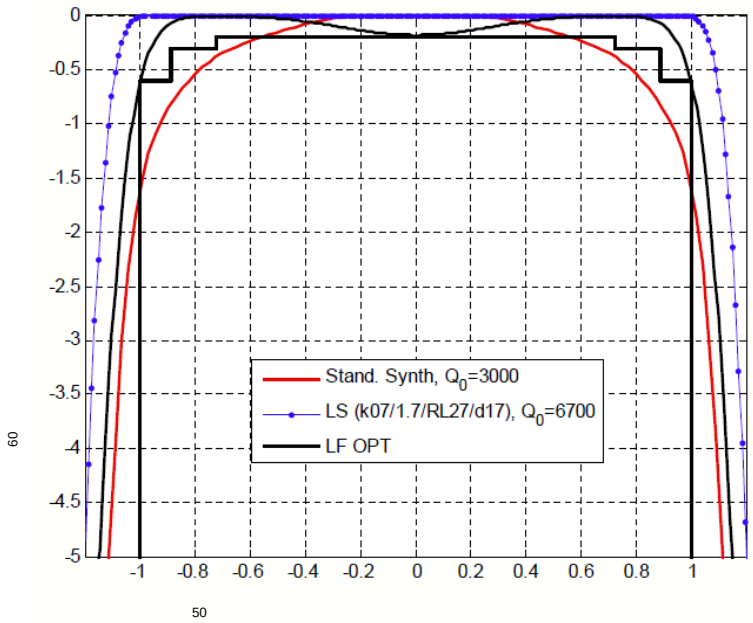

Fig. 103. In-band normalized transmission response of LF_OPT (black trace), a lossless design with Q=3000 and 21dB return loss (red traces) and that of the original design using lossy filter synthesis LF (blue traces)). The straight black lines show the specs template for the transmission response.

3.3.3 Electromagnetic simulation of couplings

Figure 100 contains all the information about the coupling between resonators; this is conventional couplings (either magnetic and electric coupling and input/output external coupling) and resistive coupling. As is has previously been done with the two planar lossy filters reported above, design of the conventional and resistive coupling can be done separately. However, a final resizing optimization approach will be necessary.

Although the design of conventional coupling is a well-known procedure, here we outline the procedure and emphasize some of the practical considerations in the case of lossy filters.

3.3.3.1 Conventional Magnetic Couplings

The pure imaginary terms of the coupling matrix above indicates that all the non-resistive couplings between resonators. Note that all couplings have the same phase but the coupling between resonators 2nd and 5th. We will use electric coupling for the cross-coupling (2nd and 5th) and magnetic couplings for the rest. The magnetic couplings can be performed by means of apertures between resonators and the electric coupling can be performed through a probe between resonators [1]. Therefore the outlined filter structure may be depicted as show in Figs. 104 and 105. Figure 104 corresponds to the top view, whereas Fig. 105 corresponds to a 3D view.

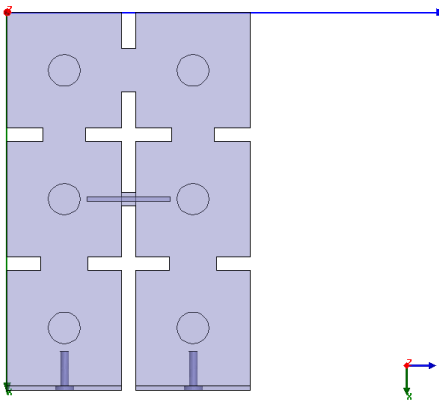

Fig. 104 : Top view of the filter structure

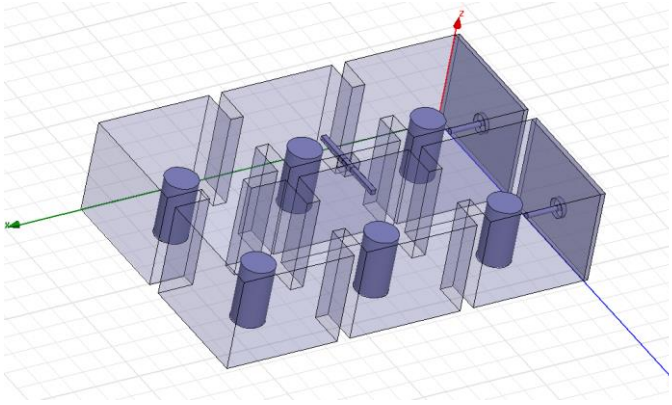

Fig. 105: 3D outlined of the filter structure.

This section describes how to obtain the dimensions of the apertures between resonators in order to obtain the desired coupling. To do that we use the procedure described in [1][2] where the coupling between two resonators can be related with their resonant frequencies as $k = \pm\frac{f_2^2 - f_1^2}{f_2^2 + f_1^2}$.

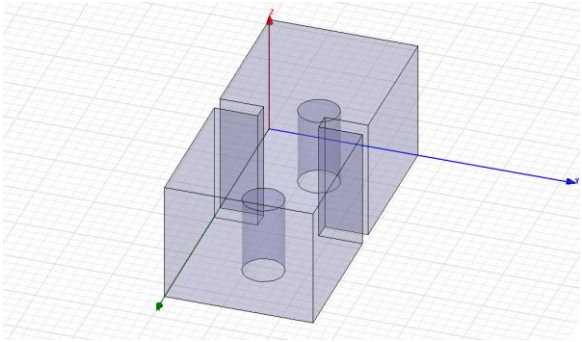

Fig. 106. Outline of two coupled cavities

In our case, since we are only interested in the resonant frequencies of the two resonant modes we performed an eigenMode analysis (in HFSS we do that by selecting Number of Modes=2) of the structure of Fig. 106 as a function of the aperture. The result of doing so is the dependence outlined in Fig. 107. As expected, as the aperture increases the coupling between resonators also increases.

At this point we also evaluate how the central resonant frequency of the two mode structure deviates from the nominal frequency of 4 GHz due to the aperture. Note that the resonant frequency of each resonator is a critical parameter in such narrow band type of filters.

Figure 108 shows the deviation of the resonant frequency as a function of the aperture. This figure is used to recalculate the length of the resonator considering the apertures found in this section in order to have all cavities resonating at the same frequency. Discussion of the frequency adjustment will be reported later in this chapter.

3.3.3.2 Conventional Electric Couplings

As mentioned previously, the electric coupling will consist on a probe that couples resonators 2nd and 5th as detailed in Fig. 109. The position of the probe is adjusted to fit the desired coupling. As occurring with the magnetic coupling, the existence of the probe close to the rods of the cavity affects the resonant frequency of the cavity and some additional adjustment of the length of the resonators are performed.

3.3.3.3 External Coupling

The external coupling will be designed as detailed in [1][27], where the strength of the external couplings is assessed through the external quality factor. The structure used for the evaluation of the external couplings is outlined in Fig. 110. It consists of a combline cavity coupled to a non-resonant cavity at the output. This arrangement reproduces the geometry of the walls in the first and last filter resonators, so their resonant frequency and unloaded Q can be realistically assessed through simulation. Furthermore, due to the weak output coupling, the external quality factor of the combline resonator can be evaluated from the transfer response of the overall structure.

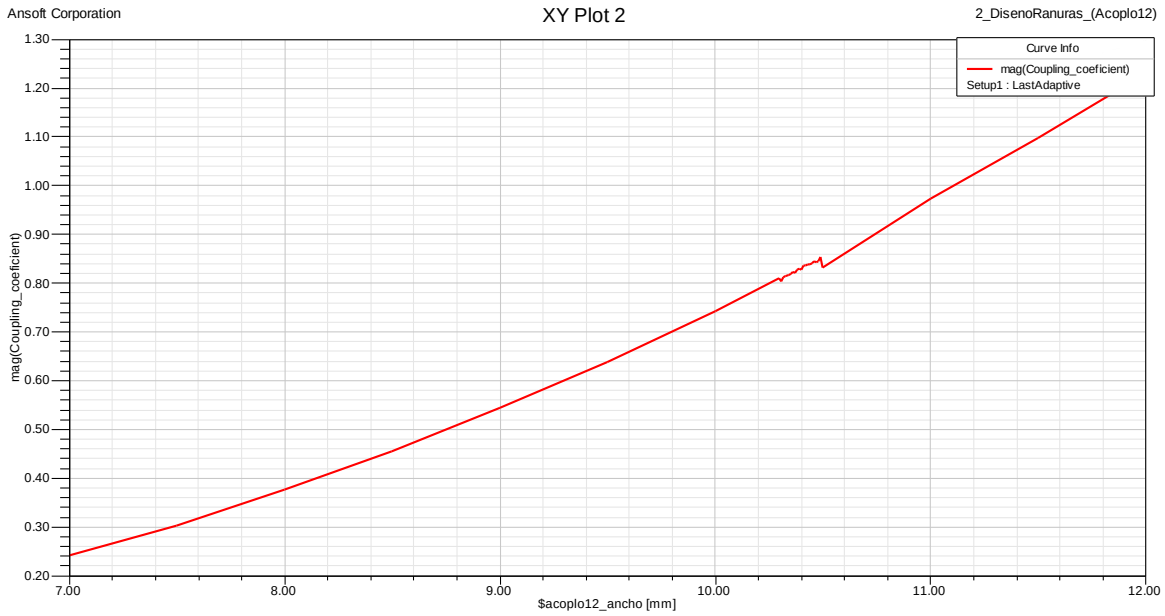

Fig. 107: Magnetic coupling between two resonators as a function of the aperture between the cavities.

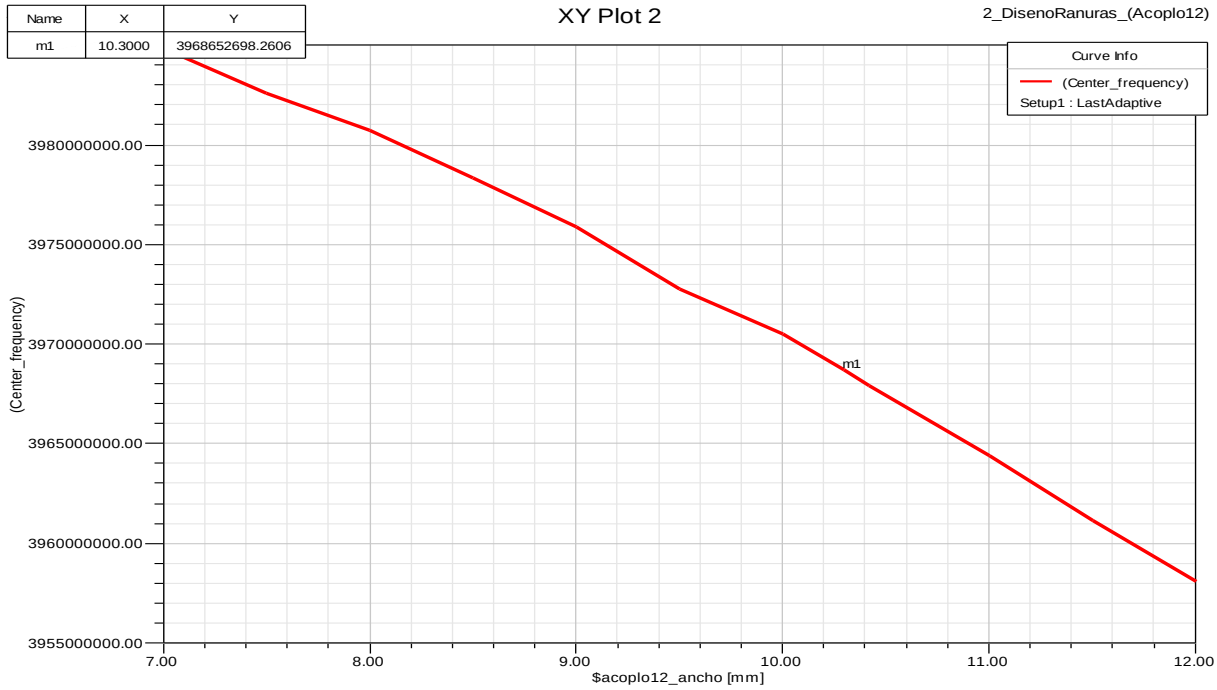

Fig. 108: Deviation of the resonant frequency as a function of the aperture.

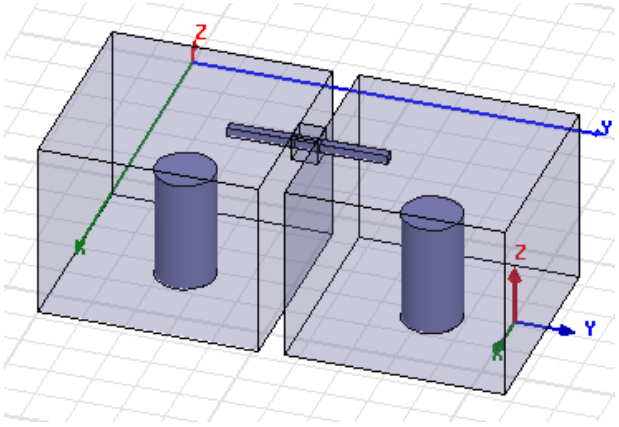

Fig. 109: Deviation of the resonant frequency as a function of the aperture.

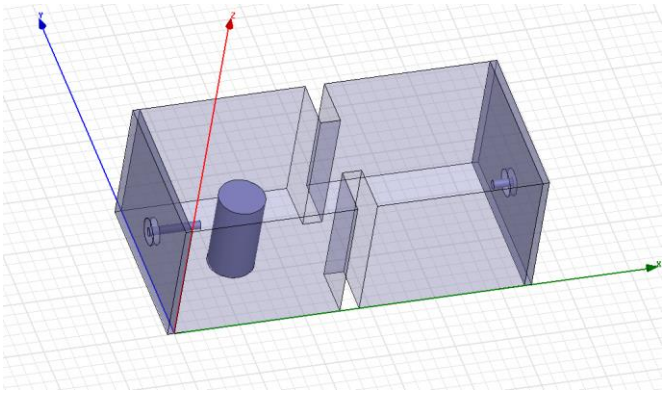

Fig. 110: Structure used to design the external coupling.

The structure of Fig. 110 is then evaluated to obtain the frequency response, depicted in Fig. 111. Note that the maximum of the transfer frequency response is very low because of the very weak external output coupling.

In order to guarantee that the resonant frequency of the first and last resonator is equal to 4 GHz even after those are loaded by the input and output coupling respectively, we adjust the length of the resonator to fit the 4 GHz frequency. Then this changes the external coupling which has to be readjusted, being therefore an iterative procedure.

From the procedure described so far we obtain the dimension of the structure outlined in Fig. 110. The following steps describe how to introduce resistive coupling to the mentioned structure and how these may affect the initial cavity dimensions.

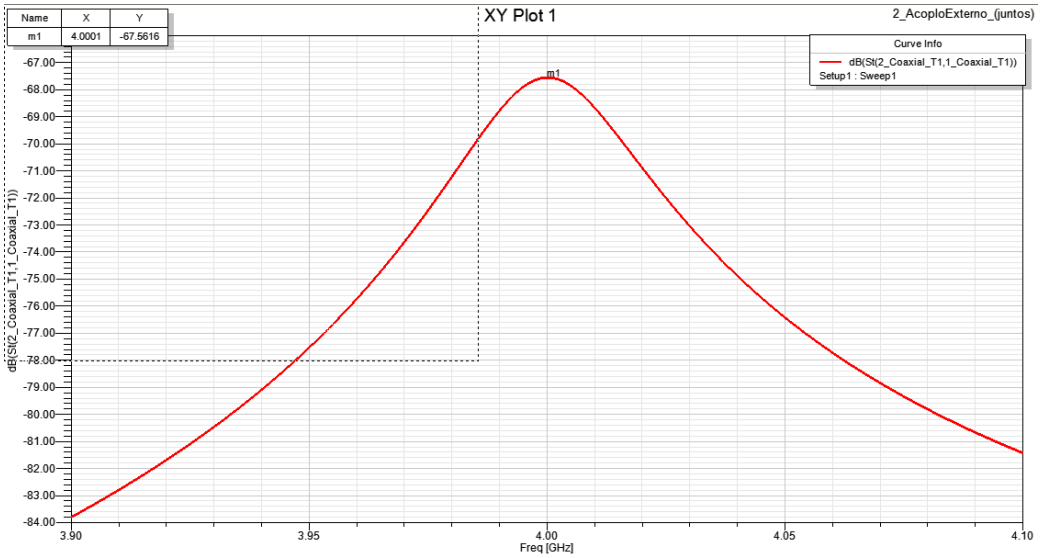

Fig. 111: Frequency response of the first (last) resonator coupled to the source.

3.3.4 Resistive Couplings

To introduce the resistive coupling network, the resistors is coupled into the resonant cavity as outlined in Fig.112, by means of a coaxial cable whose centre conductor penetrates into the cavity. The coaxial cable will be then connected to a microstrip transmission line with an inserted lumped resistor.

The filter configuration with all coaxial cables inserted is detailed in Fig. 113. Note that the cable center conductor penetrates into the cable for electric field coupling. This slightly perturbs the field distribution within the cavity and affects its resonant frequency. Thus, a readjustment of the length of the resonators is performed to obtain the nominal resonant frequency.

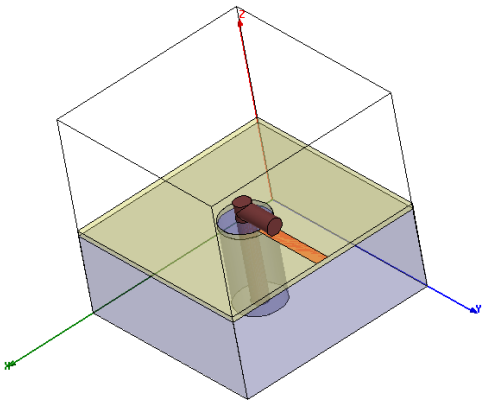

Fig.112: Coaxial cable connected to a microstrip transmission line.

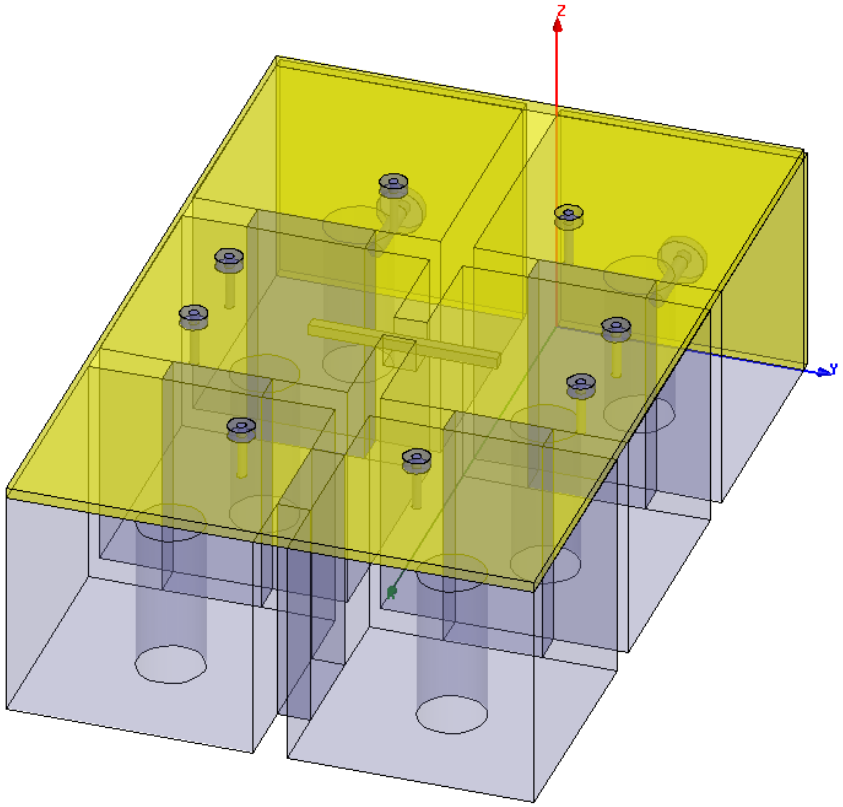

Fig. 113: Cavity with the coaxial cable to introduce the resistive coupling.

3.3.5 Adjustment of Resonant frequencies

The recalculated lengths of the resonators are then cross-checked by obtaining the resonant frequency of the six modes of the filter structure. We do that by performing eigenMode analysis in the structure of Fig. 113, the frequencies of these modes are then compared with the ones obtained from the coupling matrix of Fig. 100 (or eventually by evaluating the circuit network with ADS).

Figure 114 shows the ideal frequency response of the filter after decoupling the source and load (this corresponds to the ADS circuit network of the synthesized coupling matrix), so we can observe the resonant frequency of each mode, whereas Fig. 115 summarizes the resonant frequency of the modes of the structure of Fig. 114. Both are in good agreement indicating that the resonant frequency of each resonator is adjusted spite the apertures, and coaxial pins introduced into the cavity.

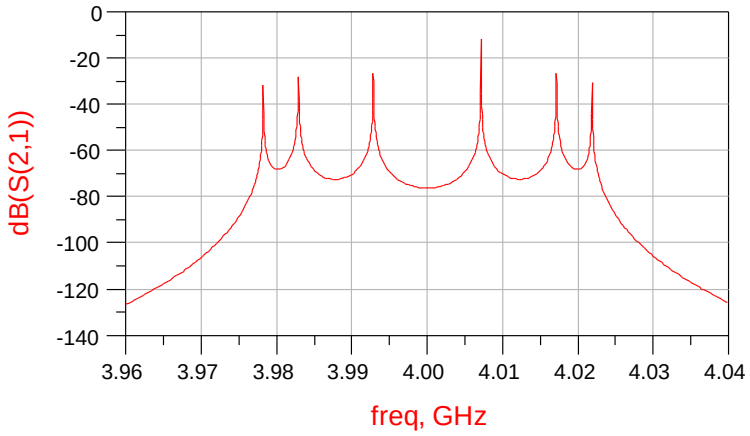

Fig. 114- Frequency response of the ideal filter after decoupling the input and output ports

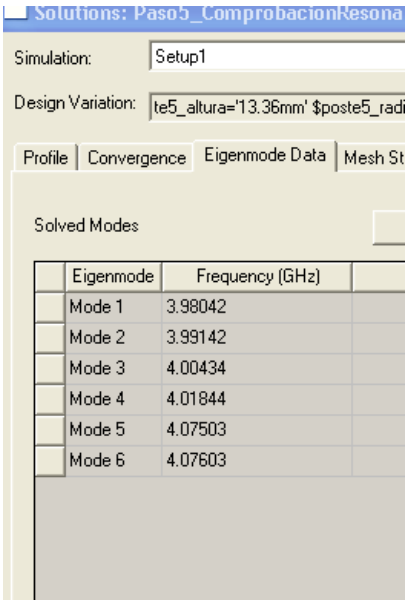

Fig. 115- Resonant frequencies of the modes of the structure of Fig. 114.

3.3.6 HFFS Simulation

This section compares the frequency response of the designed filter without resistive couplings, this is the response of the structure of Fig. 113, with the ideal response of the filter without resistive couplings, this is evaluating the coupling matrix of Fig. 100 by removing the resistive couplings. Figure 116 outlines the frequency response from 3.94 GHz to 4.06 GHz, whereas Fig. 117 outlines the in-band response from 3.975 GHz to 4.03 GHz. The blue and cyan lines correspond to the simulated response with HFFS and the red lines correspond to the ideal response (evaluating the coupling matrix). Note that there is very good agreement between the synthesized and the designed responses.

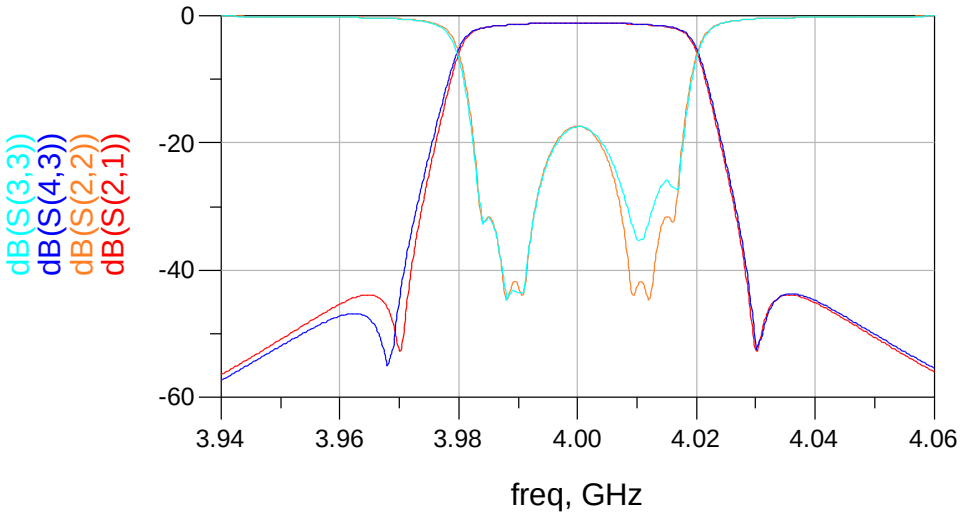

Fig. 116- Frequency response of the designed and synthesized filter without resistive coupling. The red and orange lines indicate the circuit evaluated response (synthesized response), whereas the blue and cyan lines indicate the full-wave designed response.

Fig. 117- In-band frequency response of the designed and synthesized filter without resistive coupling. The red and orange lines indicate the circuit evaluated response (synthesized response), whereas the blue and cyan lines indicate the full-wave designed response.

3.3.7 Co-Simulation HFFS-ADS

Co-simulation between HFSS and ADS consists on using the results of the design described above and introduce them into ADS in order to design the resistive network. Since this resistive network has to be connected into the HFFS design we first need to have the frequency response of the design for each port in which we have to connect the resistive network. This makes a total of ten ports, two for the input and output and eight corresponding the network resistors.

The ten port response is then saved into a file to be used in ADS as indicated in Fig. 118. Figure 118 also shows how the ten port network is connected to the resistors, indicated as X31, X32, X33 and X34.

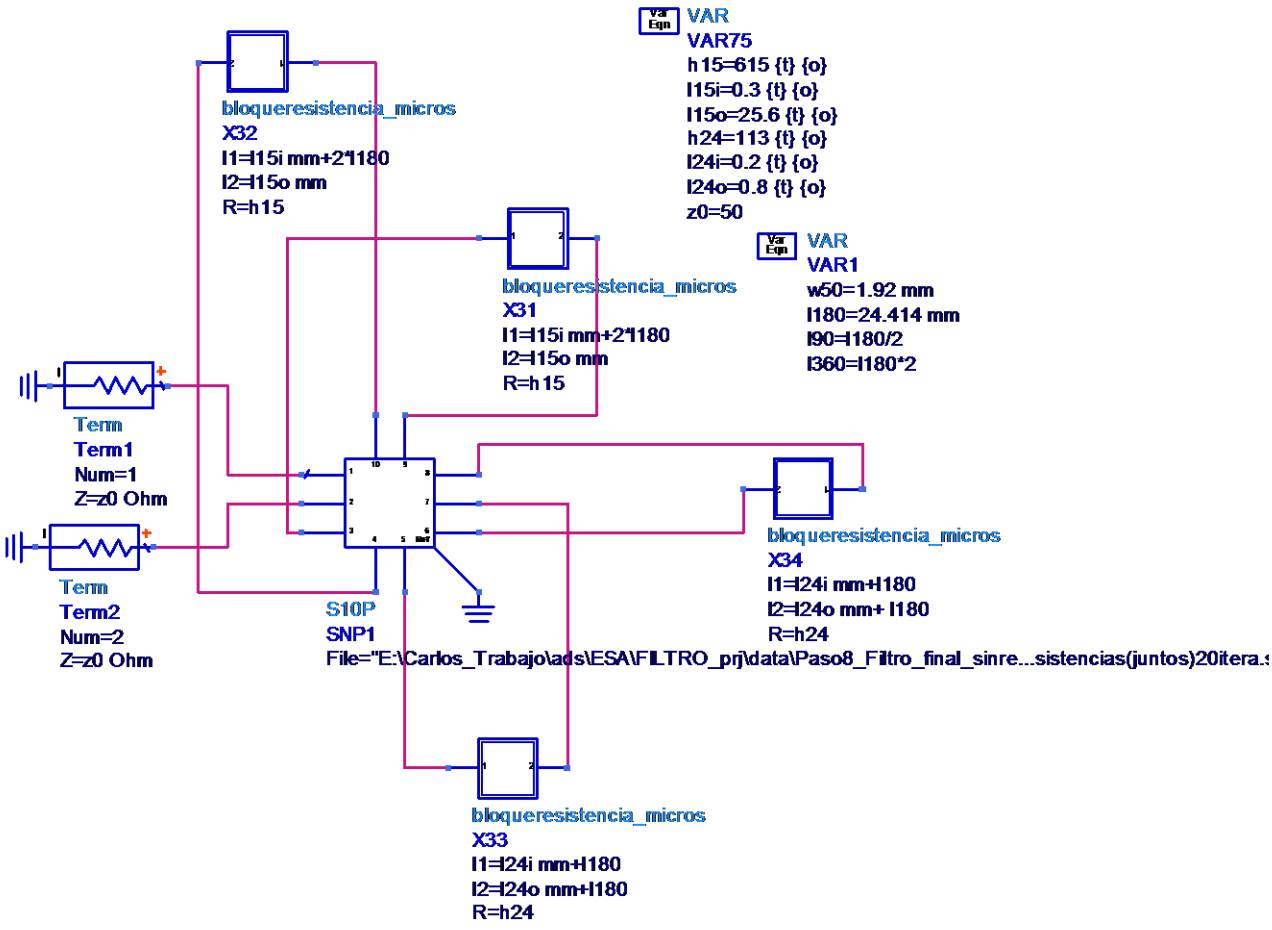

Fig. 118- 10-Ports HFSS- S matrix for the whole cavity simulation

To properly model the resistor, we first need to have an accurate model of the transition from the coaxial pin coupled to the cavity to the microstrip transmission line. To do that, we use HFSS to simulate the structure of Fig. 112, above. The frequency response of this transition over the 3.5 GHz

– 4.5 GHz frequency range is very good, is detailed in Fig. 119 showing a transmission coefficient of -0.0259 dB at 4 GHz and reflection coefficients below -30 dB.

The transitions go through an aluminium cover of 4 mm, the coaxial cable is a Semi-rigid EZ-118 from Suhner with a copper pin of 0.81 mm and a PTFE of 2.41 mm, and for the planar layer we use a RO6002 substrate 0.01” thick and the resulting 50 Ohm transmission lines is 0.63 mm width. The length of the microstrip model in Fig. 112 is 5 mm.

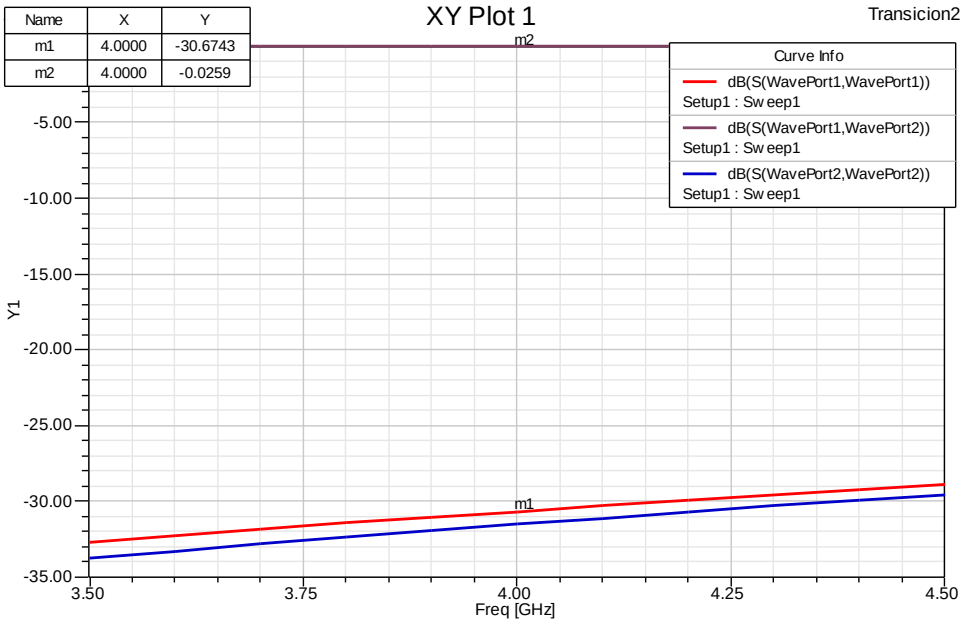

Fig. 119. Response of the coaxial to microstrip transition. Blue and red lines correspond to the reflexion coefficients to each port, and the purple line corresponds to the transmission coefficient.

The transmission modelled above is then used for the final design of the resistive network. The ADS outline of each resistive coupling is detailed in Fig. 120 and consists of two transitions, one at each side of the coupling, two lines transmission line segments of L1 and L2 length, respectively, and a lumped resistor, R, in the middle. Note that the configuration of the resistive coupling is somehow equivalent to the one presented in previous planar breadboards.

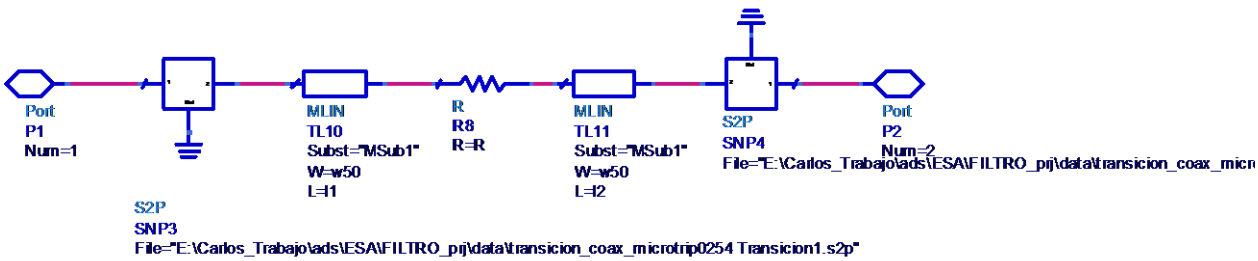

Fig. 120. Resistive path including the HFSS simulations of the transitions. The length of the transmission lines and the values of the resistances are optimized to fit the theoretical response.

Then ADS is used to simulate the circuit in Fig.118 and adjust parameters of the resistive coupling (Fig. 120), this is L1, L2 and R.

The complete simulation of the circuit in Fig. 118 is shown in the following figure, Fig. 121. The synthesized response is indicated in red for the transmission coefficient and in blue and pink for the input and output reflection coefficients. The designed response is detailed in cyan and purple for the transmission and reflection coefficient, respectively. Results in Fig. 121 show very good agreement between both, synthesized and designed responses.

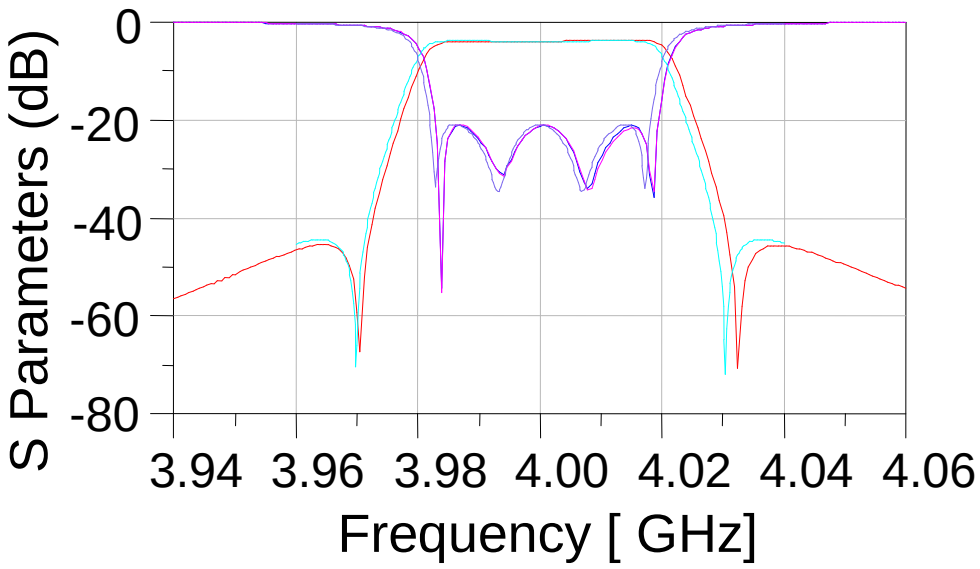

Fig. 121. Synthesized and designed response of the filter prototype.

The resulting layout of the resistive network it is also detailed in Fig. 22.

3.3.8 Implementation, Test and Tuning

The designed filter has then been fabricated and measured. The set of figures below show pictures of the implemented filter. Figure 123 contains the picture of the whole filter, with the resistive network on top and tuning screws for the resonant frequency of the resonator. In Fig. 124 further details of the implemented filter can be seen by removing the top lid (which include the resistive network). The bottom view of the top lid it is shown in Fig. 125, where it can be observed the pins which help to coupling the resistive network into the resonator. Further details on the resistive network connection (feedthroughs) are then depicted in Fig. 126.

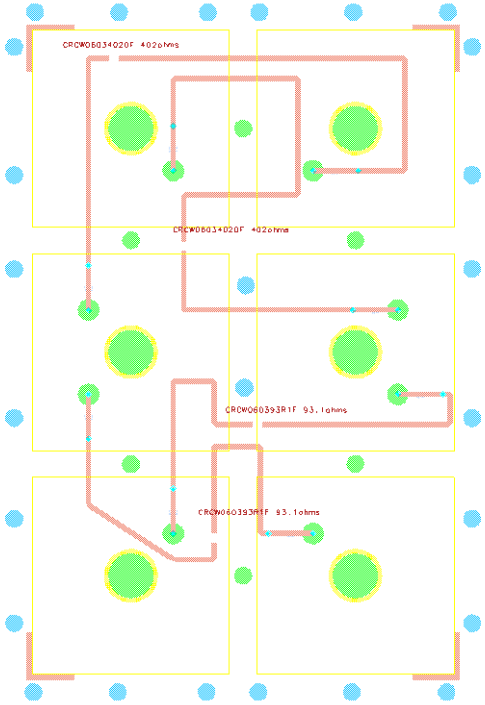

Fig. 122: layout of the filter top showing the microstrip lines (pink) coupling probes (green), coupling screws (green), grounding screws (blue) and the outline of the combline cavities (yellow).

The first measurements consist of the cavity filter without the resistive network connected (see Fig. 27), in order to check the conventional couplings. The measured response it is also compared with the simulated responses without the resistive coupling. Measurements and results should quite fairly good agreement but the return losses. Note however that the comparison has been performed without any tuning.

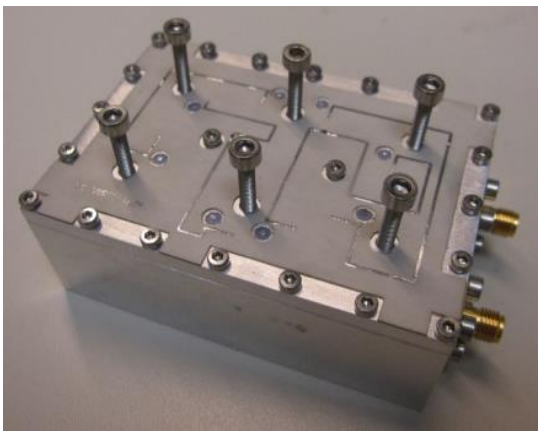

Fig. 123: Manufactured Combline Lossy Filter.

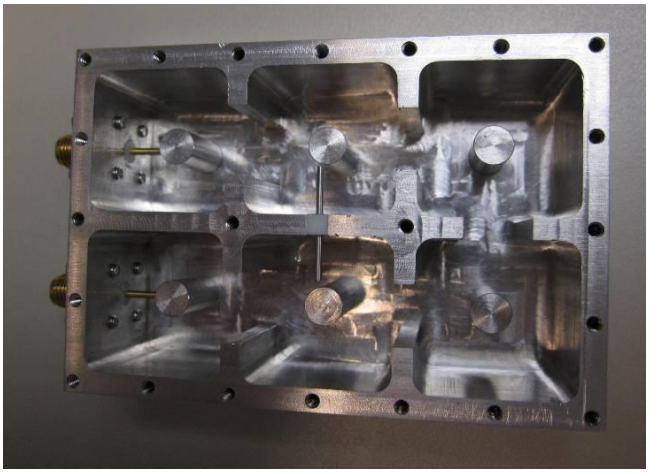

Fig. 124: Cavity Filter (internal cavities)

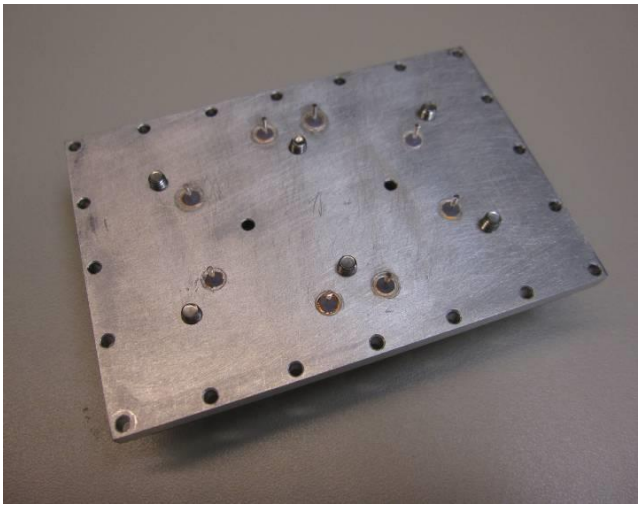

Fig. 125: – Cavity filter lid (bottom view)

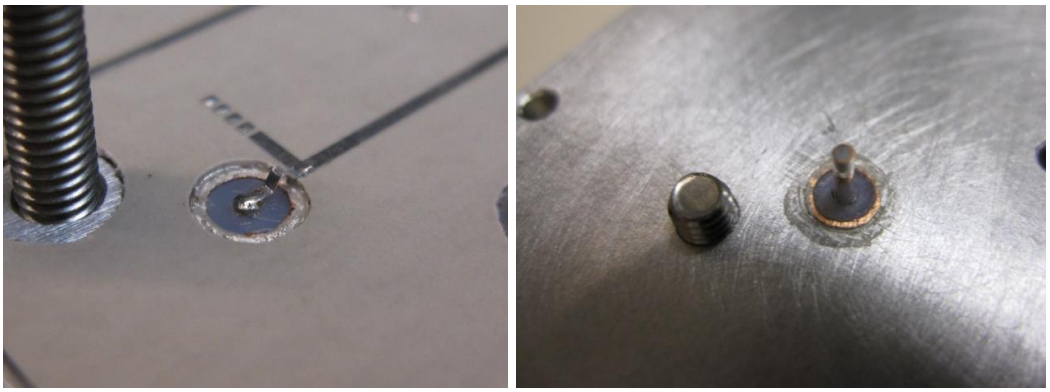

Fig. 126: – Custom RF feedthroughs (top and bottom views)

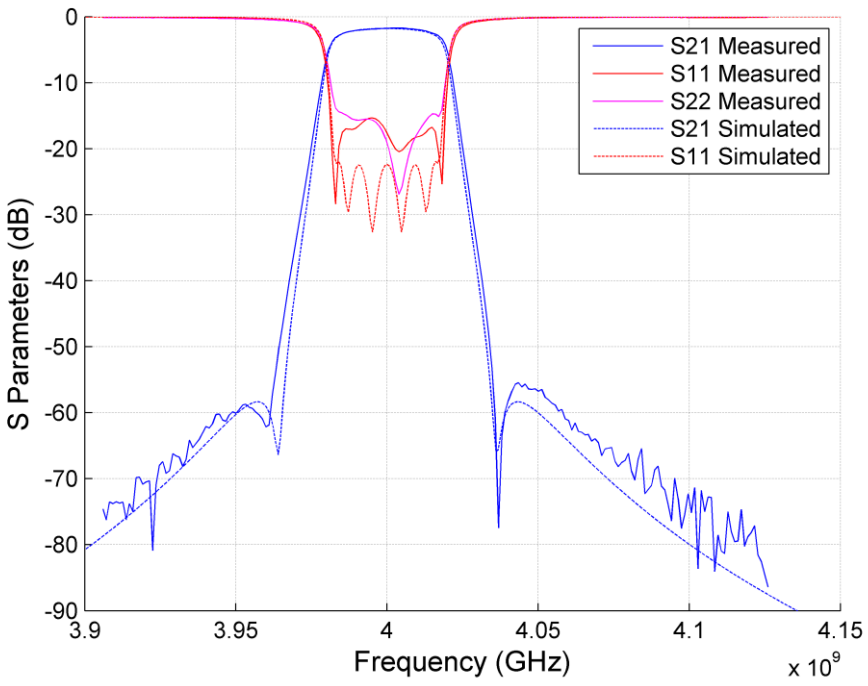

Fig. 127: Measured and Simulated Filter Response without Resistive Coupling.

The results in Fig.128 compare the measured (solid line) and simulated (dotted line) response of the prototype cavity filter when the lid with the resistive network it is included. As can be seen very good agreement can be observed between simulation and measurements, for both the transmission and reflection coefficients. Note that in this cases tuning of the central frequencies have been applied. Additional details of the in-band filter response are depicted in Fig. 129. This reveals also an additional increment of the insertion losses.

Tuning of the filter response also required of a readjustment of and increment of the electrical coupling between cavities 2 and 5. This has been achieved by introducing a larger probe between the two cavities. Additionally, the SMD resistances in the PCB has been decreased by about 25% to recover the passband flatness (see details in the following Table 39) which is lost due to the degradation in Q caused by the extra penetration of tuning screws necessary to bring the center frequency down to 4 GHz.

Cavities coupled	Initial Value (expected from design)	Value 2nd iteration	Units
1-5 and 2-6	523	390	Ohm
2-4 and 3-5	105	82	Ohm

Table 39 – BB3 filter: values of the SMD resistances

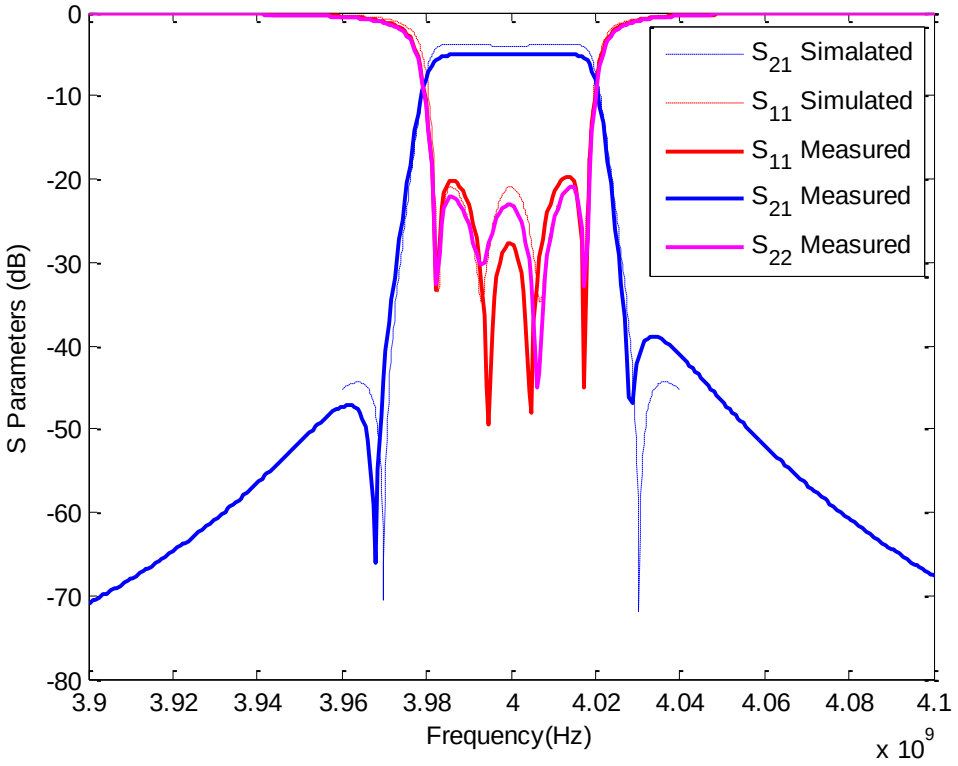

Fig. 128: Measured (tuned response) and Simulated Filter Response with Resistive Coupling.

Note that this outlines a very important conclusion, which actually it is common to all the implemented filters in this chapter. This is: the in-band flatness synthesized by the given Q values results in a certain resistive coupling network, but the in-band response can be recovered by a simply readjustment of the resistive coupling values (usually defined by an SMD lumped external resistor).

3.3.9 Temperature Performance

Measurement as a function of temperature of the prototype filter presented above has been performed on the framework of the ESA contract [25].

The ESA contract [25] indicates that the thermal test must be performed with the equipment inside a climatic chamber which must enable to vary the base plate temperature within the acceptance ranges, which in this case goes from -10 ºC to 85 º. In addition the thermal facility must be accompanied with a test set-up enabling to monitor and measure the required functional parameters.

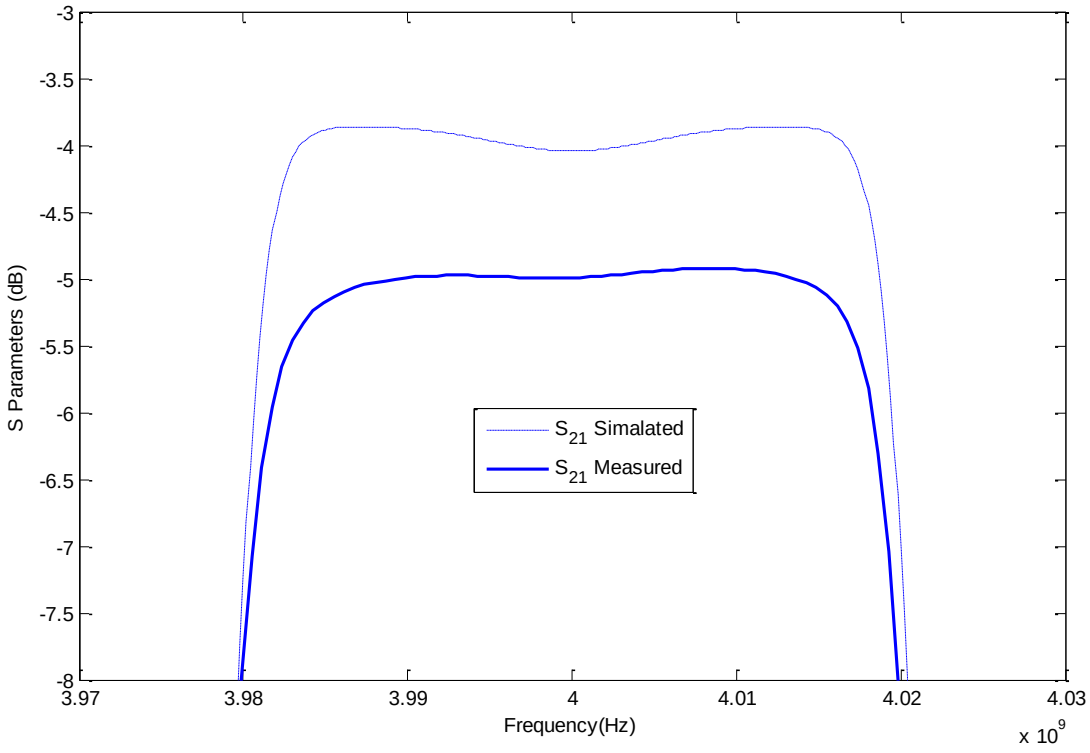

Fig. 129: Insertion loss details of the measured (tuned response) vs simulated response of the filter with resistive coupling.

The equipment undergoes a thermal cycle during which several temperature stabilization periods are settled. Temperature stabilization is achieved when the equipment temperatures have been maintained within tolerance.

S-parameter measurements will be taken at specific points of the thermal cycle. In all these tests, the same test set-up will be preserved.

The thermal test has been performed at ESTEC facilities (by the author of the Thesis).

- **Test Equipment**

The test equipment and facilities use for the following measurements are outlined in the following figure, Fig. 130.

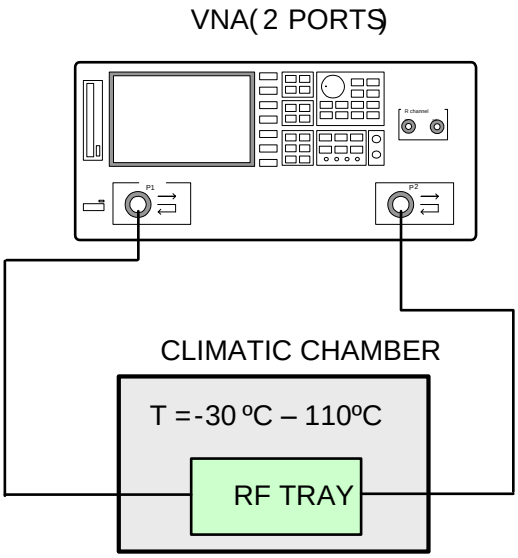

Fig. 130: Test Bench for the Thermal Tests

S-parameters measurements will be taken at specific temperature points within the operating temperature range (-10ºC to +85ºC) at 10ºC intervals and including the maximum (+85ºC) and minimum (-10ºC) operating temperatures.

The following figures, Figs. 131, 132 and 133, show the measured response for each temperature under evaluation. Responses at room temperature are indicated in thick lines, blue for the transmission and red for the reflection. Measurements have been taken by increasing the temperature, indicated in thin lines blue and red - for the transmission and reflection coefficients, respectively. Equivalent measurements have been taken when the temperature is decreased. Results are indicated in thin lines cyan and magenta, for the transmission and reflection coefficients, respectively.

Results indicate the filter responses, this is reflection coefficient and transmission response including transmission zeros, are preserved at different temperatures and the unique difference is the expected shift in frequency. The central frequency shifts up when the temperature goes up.

Regarding the in-band responses, details in Fig. 133, reveal that the difference of bandwidth (at 0.5dB level) from the coldest measure (-10ºC) to the hottest (+60ºC) is 1MHz (2.7% bandwidth change). The insertion loss value deviates only from 5.1 dB at the hottest temperature to 4.9 dB at the coolest temperature, following the same flatness. Figures 132 and 133 also reveal overlayed responses from the comparison between increasing and decreasing the temperature.

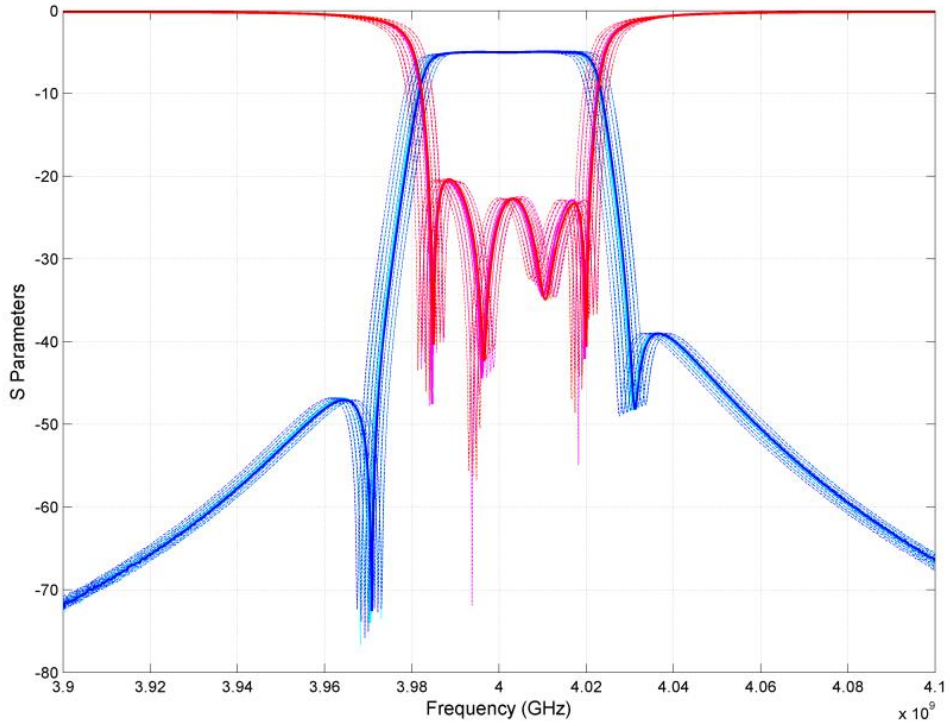

Fig. 131: Measured filter response at different temperatures. From -10 ºC to 85 ºC, with intervals of 10 ºC.

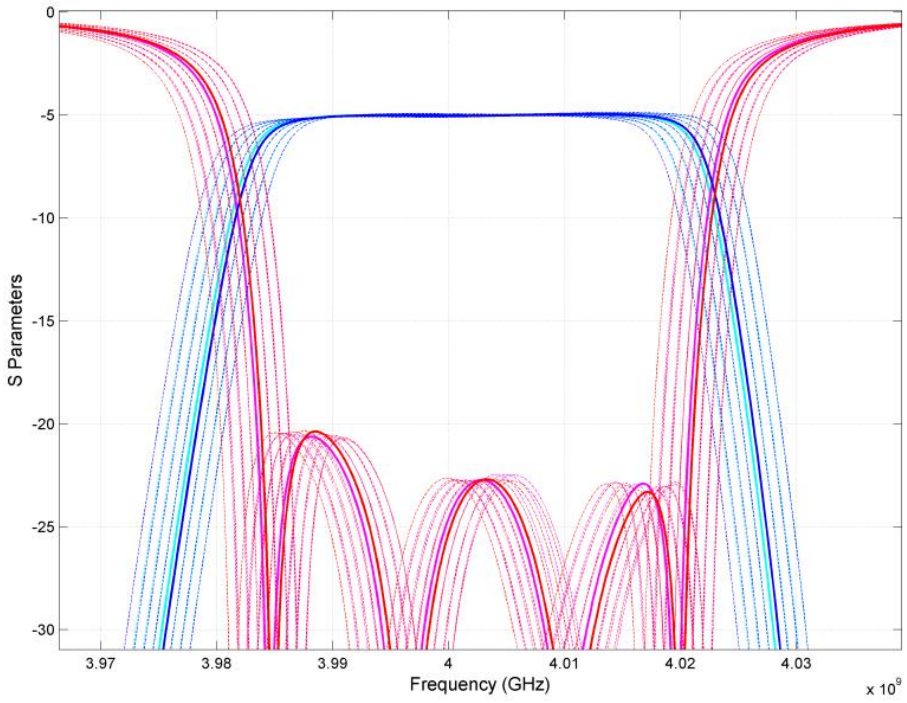

Fig. 132: Measured filter response at different temperatures. From -10 ºC to 85 ºC, with intervals of 10 ºC. Details on the reflection coefficient.

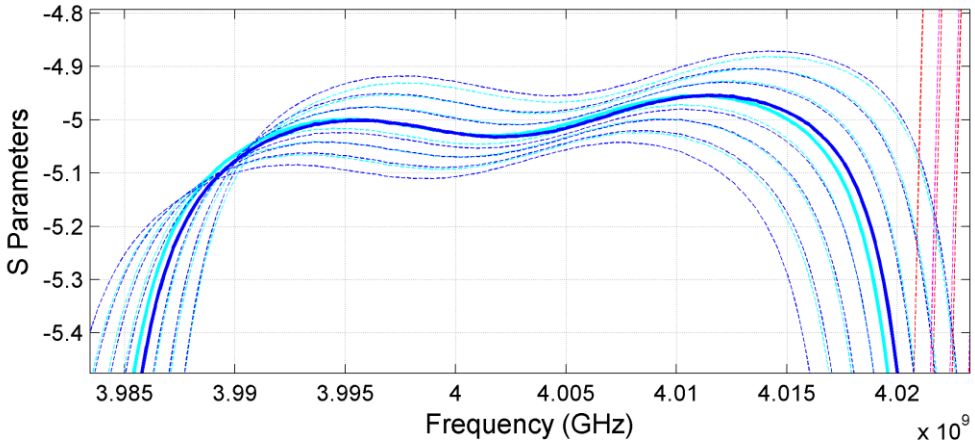

Fig. 133: Measured filter response at different temperatures. From -10 ºC to 85 ºC, with intervals of 10 ºC. Details on the insertion loss.

3.4 Conclusion

This chapter presented the design, fabrication and test of three different lossy filter prototypes. The major conclusion of this chapter is that the realization of lossy filters is very feasible and can be reached by following different approaches, such as direct synthesis, section 3.1, by obtaining the lossy network by following an optimization procedure, section 3.2, and by a combination of circuit transformation strategies and optimization, section 3.3.

Also the type of synthesized response are different, proving the use of such technique and design in out-of-band absorptive filters as in section 3.1, or fully reflective in the stop band as in sections 3.2 and 3.3.

Moreover these techniques have been proven on two very different technologies as it is planar technology and cavity technology.

So we may definitely conclude that lossy filter synthesis is a promising approach to filter design and is capable of producing filters with very good specifications in passband flatness at the expense of some insertion loss in the passband. Significant advantages in terms of matching and insertion loss flatness with respect to conventional and pre-distorted filters have been experimentally proven.

Although no major limitations in the design of lossy filters are foreseen some improvements may still be beneficial for a further expansion of this approach, and can be therefore considered as a future research lines or research lines which need more investigation.

Practical consideration of the results in sections 3.1 and 3.2, for planar circuits indicate that the realization of lossy filters in planar circuits can be improved with technologies different from those used above (microstrip). In sections 3.1 and 3.2, long transmission lines had to be used to implement

the resistive coupling network. These lines introduce an unwanted frequency dependence which is evident in the out of band reflection coefficients (contrary to the design specs, the magnitude of the reflection coefficient is not constant with frequency in the stopband) and make the prototype sensitive to fabrication tolerances. Alternative technologies (such as multilayer LTCC) capable of placing the resonators to be resistively coupled close to each other might provide interesting options for the design of these types of filters. An additional desired feature would be the possibility to implement resistors integrated in the substrate having trimming capabilities to account for a tolerance in the resonator Qs.

The realization of lossy filters in combline cavity resonators, section 3.3, might also be improved with respect to the breadboard developed in several aspects:

- The arrangement of the tuning screws should be such that it does not perturb the fields in the coupling structures (electrical probes in our case) of the resistive coupling network. This is not the case in section 3.3, and we suspect that the effect of the resistive network depends on the degree of penetration of the screws used for frequency tuning in the combline resonators. There are several possibilities for this, including the realization of the resistive coupling network with a PCB circuit at the bottom of the cavity (at the opposite side of the tunning screws), or the use of frequency tuning screws that penetrate inside the centre cylinder of the combline and thus, they produce little perturbations of the fields outside of the cylinder.
- Use screws for tuning frequencies and couplings that do not perturb the Q of the cavities (as opposed to the stainless steel screws used in our prototype for frequency tuning).

4 CHAPTER 4: CONCLUSION AND FUTURE RESEARCH WORK

The main objective of this work was to demonstrate the viability of lossy filters. We can certainly conclude the results of the thesis demonstrate the promising and reality on the implementation of lossy filters.

To reach such objective research activities have been performed on mainly three research lines, elaborated on the three core chapters of the thesis. These are:

- Mathematical description of the characteristic polynomials defining the lossy response (Chapter 1 and Chapter 2).
- Network topologies and strategies for the loss distribution along the filter configuration (Chapter 2)
- Design and practical consideration of lossy filters (Chapter 3).

Although each of the research lines above could be subject of further research and topics for a PhD dissertation, the achievement of the main objective of the thesis, requires to leave some pending issues on each of the research lines above. The future research or pending issues will be listed below. At the same time important conclusions and practical considerations can be extracted from the work reported in this work.

The goal of proving the viability of lossy filters frames into the projects that the research work has been done. This is essentially the ESA contract [25] (TRP-Design and Synthesis of a New Class of Receiver Filters), the contract with THALES Alenia Space (Study of lossy and predistorted techniques on Ku Band filters) and the project into the ARTES 5.1 program, AO6575 Compact Ku-band channel filters for input multiplexer.

The involvement of industrial partners to the results of the thesis gives definitely an added value to the presented work, nevertheless forces the undisclosement of some practical aspects. In spite of that several publications have result from this work. List of such publication are detailed in the following section PUBLICATIONS.

Also mention, as it was outlined in the introduction, results of this work are the basis for the development of the commercial software ***lossyfilters*** (www.tsc.upc.edu/lossyfilters/). The software is currently used by ESA, MIER Comunicaciones and THALES Alenia Space Spain.

4.1 Conclusion

As a general conclusion it can be certainly state that there are no major limitations in the design of lossy filters provided that the synthesis procedure developed in this work is available. This enables the designer to obtain the (lossy) coupling matrix of the filter to be developed. From that point onwards, all the other design steps can be performed using commercial software such as, usually combining circuit analysis software, and full-wave 2D or 3D simulators.

Synthesis of lossy filter configurations demonstrate to produce filters with very good specifications in passband flatness at the expense of some insertion loss in the passband. As expected enhanced performance in terms of matching and insertion loss flatness with respect to conventional and pre-distorted filters have been experimentally proven with the development of three prototypes that perform better than their counterparts designed using classical (lossless) synthesis.

This prompts therefore lossy/dissipative filter as a real alternative to be chose when the effects of the finite resonator Q on the passband flatness have to be minimized and, at the same time, the filter has to have good return loss properties. Otherwise, if return loss is of no concern, pre-distortion synthesis might be a better choice (lower requirements in Q for a given bandpass flatness).

As specific conclusion regarding the three research lines listed above:

- Mathematical description of the characteristic polynomials defining the lossy response

The mathematical description allow the synthesis of several types of filter responses, demonstrating to be a very flexible approach, allowing to select the more convenient response for the particular application. Note however that each of the potential response may require an specific circuit transformation for obtaining an implementable filter network. The responses and example show along the mathematical description offer:

- Asymmetric response between the reflections coefficients between the input and output port. This type of response allows to concentrate the losses either at the input or at the output of the filter or in any case unevenly along the network.
- Symmetric responses, which in fact it is a particular case of the previous one and set the basics for obtaining filter configurations with uniform distribution of the losses, resulting in topologies with equal Q along all resonators of the filter.
- Purely reflective response at the stop band. In contrast with the two previous ones, this formulation offers a filter response without absorption on the reflection coefficients. These types of responses have a direct application into the design of IMUX.

Additionally the mathematical description of lossy filter also show its flexibility on the prescription of the flatness of the in-band response. This is defining the emulated Q of the desired response. This concept has shown to be very powerful to find filter responses complaining with a non-ideal filter response with the minimum suitable Q, and therefore with a certain degree of miniaturization.

As occurs with conventional filter responses, the mathematical description of lossy filters founds its transversal decomposition which results in a transversal network. Transversal networks need then to be transformed to more suitable topologies. Due to the specific characteristics of lossy networks special care should be taken on the network transformation, which opens other research lines of the thesis.

- Network topologies and strategies for the loss distribution along the filter configuration

The filters designed using lossy synthesis techniques need a resistive coupling network in order to distribute losses along the network. The way these losses are distributed defines the resistive network and essentially it is the main difference in comparison with conventional filter topologies. Several techniques have been proposed to distribute such losses, whose success essentially depends on the initial mathematical description. This is in some cases a resistive network that provides a uniform distribution which moreover could be obtained analytically, this is following a set of specific steps and rotation angles. This analytical solution, although may give rise to complex network resistors, have been very useful to set the limits of the lossy filter response, this is selectivity, flatness, insertion loss and position of transmission zeros, with the minimum required Q - which will be eventually related with the dimensions of the resonator.

In other cases, several strategies have been proposed and proved to obtain suitable topologies. Additionally we have also demonstrated the use of optimization routines for the definition of a certain network resistance. This later approach shows to be very convenient on practical implementation, since one can reduce complexity on the final network resistance.

The ultimate advantage of using a lossy approach is performing a high-Q filter response with low Q resonators, which may simply imply a size reduction for a given technology or even the option the change technology, for instance used planar technology instead of cavity technology.

Whichever the approach used to obtain the lossy network the results of this thesis also prove that the resistor of the network provides an opportunity to trim for a good passband flatness, i.e., if the flatness is out of specs because the Qs in the filter are different from the ones assumed in the design, this can be compensated be trimming/replacing the resistances in the resistive coupling network.

- Design and practical consideration of lossy filters

The conclusions below obviously focus on the technologies employed on the three prototypes presented in this work, this is planar microstrip technology and cavity combline technology.

In both technologies combination of transmission lines coupled to the resonators and connected to a lumped resistor are used to emulate the resistive coupling. Note that this results in a distributed component though from a circuit point of view a lumped component would be required. This approximation show to work fine for the filter responses above and certainly can be considered as a standard procedure. Nevertheless deviations of the expected responses at frequencies far from the central frequency have already been pointed out along the thesis and certainly it could be subject of further research.

Important conclusion is the fact that although the resistive network may affect the conventional couplings, the design procedure could be performed in separately steps for the design of conventional couplings and for the resistive couplings. This makes the procedure very similar to the one used in conventional filter. So that from the coupling matrix values one may design the filter topology to performed the conventional coupling between resonators. Fine tuning of such configuration, without resistive couplings, could be done by fitting the design response to the circuit (or coupling matrix) response without resistive couplings. Then the resistive coupling network could be designed based on the transmission line approach mentioned above. The effects of the resistive coupling into the overall filter configuration require a trim procedure afterward.

4.2 Future Research Work

As in the previous conclusion section we may list some pending issues of future research work activities on the three research lines above. However we do also identify more general topics of research:

- The focus of the research presented in this thesis for the synthesis and design of lossy filters has been its application into filters for space applications in order to obtain filter with high performance with a reduced size. Nevertheless the use of such technique in already miniaturized technologies, such nanotechnologies, to obtain very small devices with higher performance it is still pending. From the mathematical description point of view of the desired response, one would not expect any deviation from the research presented in this work, but from the resulting topologies and practical design considerations many issues would need to be addressed.

- Agile filters could be also take advantage of the lossy technique and conclusions on this work. Many reconfigurable filter technologies are essentially based on novel materials where their properties are affected by electric or magnetic field or both. These material properties are certainly beneficial to make an agile component externally control. Nevertheless it is also usual that while the filter response is tuned in frequency or in bandwidth the overall losses are also affected and therefore resulting in a degraded response when is tuned. Integration of lossy networks into such agile materials may result in tunable filter with non-degraded performance.

- The concept presented above it is based on selective dissipation of the energy along the filter bandwidth. Analysis of the dissipated power at each resonator and couplings would be necessary for a better understanding on how this type of filters works. Although part of this study have already been done on this thesis further research on this line would be required. Following this line, assessment of heating effects into the resistive couplings it is also a pending activity to complete the understanding of this novel approach.

Minor research activities resulting from some pending outcomes or conclusions of this work are:

- Mathematical description of the characteristic polynomials defining the lossy response

One of the most promising characteristic polynomials proposed are the ones outlined in section 2.2.2, which introduces and additional pole/zero ($kS_{21}(s)\frac{s-p}{s+p}$). These polynomials offer a type of response suitable on the design of filters for IMUXes. The main advantage is that the additional introduced pole/zero (*p value*) allows for a better distribution of the losses along the filter topology. Further understanding of the consequences of the value of the pole/zero *p* would help to select this value in advance and eventually to find more suitable topologies for the final implementation.

- Network topologies and strategies for the loss distribution along the filter configuration

A crucial aspect into the definition of the network topology is to know the effects of the different resistive couplings into the final response. This may eventually result in topologies with a reduce number of resistor. Further research on this would help also to a full understanding of the suitable networks.

- Design and practical consideration of lossy filters

On the realization of lossy filters in planar circuits long transmission lines had to be used to implement the resistive coupling network. These lines introduce an unwanted frequency dependence which is evident in the out of band reflection coefficients (contrary to the design specifications, the magnitude of the reflection coefficient is not constant with frequency in the stopband) and make the prototype sensitive to fabrication tolerances. Alternative technologies (such as multilayer LTCC) capable of placing the resonators to be resistively coupled close to each other might provide interesting options for the design of these types of filters. An additional desired feature would be the possibility to implement resistors integrated in the substrate having trimming capabilities to account for a tolerance in the resonator Qs.

The realization of lossy filters in combline cavity resonators might also be improved with respect to the breadboard developed in several aspects:

- The arrangement of the tuning screws should be such that it does not perturb the fields in the coupling structures (electrical probes in our case) of the resistive coupling network. This is not the case in the prototype developed in this work, and we suspect that the effect of the resistive network depends on the degree of penetration of the screws used for frequency tuning in the combline resonators. There are several possibilities for this, including the

realization of the resistive coupling network with a PCB circuit at the bottom of the cavity (at the opposite side of the tunning screws), or the use of frequency tuning screws that penetrate inside the center cylinder of the combline and thus, they produce little perturbations of the fields outside of the cylinder.

- Use screws for tuning frequencies and couplings that do not perturb the Q of the cavities (as opposed to the stainless steel screws used in our prototype for frequency tuning).

Further research therefore on the implementation of the resistive network would be needed for a specific technology.

PUBLICATIONS AND OUTCOMES

Contribution to journals

1) Rocas, E. ; Padilla, A. ; Mateu, J. ; Orloff, N. ; O'Callaghan, J. M. ; Collado, C. ; Booth, J. C., "Superconducting Multiplexer Filter Bank for a Frequency-Selective Power Limiter", IEEE Transaction on Applied Superconductivity, November 2010.
2) Rocas , E., Collado, C., Orloff, N.D., Mateu, J., Padilla, A., O'Callaghan, J.M., Booth, J.C., "Passive Intermodulation Due to Self-Heating in Printed Transmission Lines", IEEE Transactions on Microwave Theory and Techniques, Volume:59 , Issue: 2, February 2011.
3) Collado, C., Rocas, E., Padilla, A., Mateu, J., O'Callaghan, J.M., Orloff, N.D., Booth, J.C., Iborra, E., Aigner, R., "First-Order Elastic Nonlinearities of Bulk Acoustic Wave Resonators", IEEE Transactions on Microwave Theory and Techniques, Volume 59 , Issue 4, May 2010.
4) Rocas, E., Collado, C., Padilla, A., Booth, J.C., "On the Relation Between the Nonlinear Surface Impedance and the Superfluid Current Density in High-Temperature Superconductors", IEEE Transactions on Applied Superconductivity, Volume 21 , Issue 3, November 2010.
5) Collado, C., Rocas, E., Mateu, J., Padilla, A., O'Callaghan, J.M., "Nonlinear Distributed Model for Bulk Acoustic Wave Resonators", IEEE Transactions on Microwave Theory and Techniques, Volume 57 , Issue 12, November 2009.
6) Mateu, J., Collado, C., Orloff, N., Booth, J.C., Rocas, E., Padilla, A., O'Callaghan, J.M., "Third-Order Intermodulation Distortion and Harmonic Generation in Mismatched Weakly Nonlinear Transmission Lines", IEEE Transactions on Microwave Theory and Techniques, Volume 57, Issue 1, January 2009.

Contribution to conferences

1) J. Mateu, A . Padilla, C. Collado, M. Martinez-Mendoza, E. Rocas, J. M. O'Callaghan, C. Ernst, Direct *Synthesis of Lossy Filters: Use for 4th order filter with uniform Q distribution*, International Workshop of Microwave Filters, Toulouse, November 2009, *Invited*
2) A. Padilla, J. Mateu, C. Collado, E. Rocas, O. Cuñado, J. M. O'Callaghan, C. Ernst, *Bandwidth Trade-off Considerations in the Design of a Planar Filter using lossy filter synthesis Techniques*, International Workshop of Microwave Filters, Toulouse, November 2009
3) J. Mateu, A. Padilla, C. Collado, M. Martinez-Mendoza, E.Rocas, C. Ernst, J. M. O'Callaghan, *"Synthesis of 4th order lossy filters with uniform Q",* International Microwave Symposium 2010.

4) A. Padilla J. Mateu, C. Collado, C. Ernst, J.M. Tamayo, J.M. Rius, J. M. O'Callaghan, *"Comparison of lossy filters and predistorted filters using novel software".* International Microwave Symposium 2010.
5) Padilla, A.; Collado, C.; Mateu, J.; Rocas, E.; Ernst, C.; Rius, J.M.; Tamayo, J.M. ; O'Callaghan, J.M.; *"Application of Lossy Filter Synthesis to a C-band Cavity Filter and its Prospect for use in IMUX",* Microwave Technology and Techniques Workshop 2010, Noordwijk (The Netherlands), May 2010.
6) Padilla, A.; Collado, C.; Mateu, J.; Rocas, E.; Ernst, C.; Rius, J.M.; Tamayo, J.M. ; O'Callaghan, J.M.; *"Lossy Filter Synthesis of L-Band Planar Filters using novel software.",* Microwave Technology and Techniques Workshop 2010, Noordwijk (The Netherlands), May 2010.

Software:

LossyFilters software (http://www.tsc.upc.edu/lossyfilters)

Authors: J. M. Rius, J. Mateu, J. M. Tamayo, C .Collado, A. Padilla and J. O'Callaghan. Dpt. Signal Theory and Communications, Universitat Politècnica de Catalunya (UPC),

Description: The LossyFilters software package has been written to synthesize filters following various forms of classical (no-loss considered in the synthesis), pre-distortion and prescribed insertion loss synthesis. This software obtains the coupling matrix of several network topologies for a given response and allows performing rotations on them to find the desired topology. Additionally, the software allows to evaluate the effect of loss in the networks resulting from the synthesis, even in those cases where the synthesis results in an ideal lossless network (i.e., classical and pre-distortion synthesis).

Secondments:

- European Space Agency (ESA). June 2010-November 2010.
- National Institute of Standards and Technology (NIST). Oct 2011- December 2013

APPENDIX 1: Matrix Rotation. From TCM to FCM

This appendix describes in some detail the rotation matrix procedure applied to circuit network transformation. The matrix rotation procedure can be applied to transform a given circuit network, and therefore a given filter topology into a more convenient topology, maintaining the same filter frequency response. Most of the material from this appendix can be found in many basic references on filter synthesis [1].

The basic concepts outlined in this appendix will be also used in circuit transformation of lossy filters.

For a given matrix M_r it is possible defined is rotated matrix M'_r as:

$$[M'_r] = [R_r] \cdot [M_r] \cdot [R_r]^{-1} \qquad \text{(A.1.1)}$$

Where R_r] is the rotation matrix and R_r^{-1} is the inverse of the rotation matrix. For a 7x7 matrix the rotation matrix with [3,5] pivot can be defined as:

	1	2	3	4	5	6	7
1	1						
2		1					
3			c_r		$-s_r$		
4				1			
5			s_r		c_r		
6						1	
7							1

Fig. A.1.1: Example of a rotation matrix [R_r] of orden 7 with a [3,5] pivot.

Note that all elements of the diagonal of R_r are 1 except those corresponding with the pivot locations *i* and *j*, R_{ii} and R_{jj}, which values are $R_{ii} = R_{jj} = c_r$, being c_r related with the rotation angle. On the other hand the values out of the diagonal are zero except $R_{ji} = -R_{ij} = s_r$, where s_r is also related with the rotation angle.

The values of c_r and s_r are related with the rotation angle θ_r as:

1. Trigonometric Rotation:

$$\begin{aligned} c_r &= \cos\theta_r \\ s_r &= \sin\theta_r \end{aligned} \qquad \text{(A.1.2)}$$

2. Hiperbolic Rotation:

$$\begin{aligned} c_r &= \cosh\theta_r \\ s_r &= j\cdot\sinh\theta_r \end{aligned} \qquad \text{(A.1.3)}$$

By simply evaluating ec. I.28 and using the rotation matrix of Fig. y, we obtain the values of the rotated matrix as:

$$\begin{aligned} M'_{ik} &= c_r M_{ik} - s_r M_{jk} \\ M'_{jk} &= s_r M_{ik} + c_r M_{jk} \\ M'_{ki} &= c_r M_{ki} - s_r M_{kj} \\ M'_{kj} &= s_r M_{ki} + c_r M_{kj} \end{aligned} \qquad \text{(A.1.4)}$$

The elements of the diagonal result as:

$$\begin{aligned} M'_{ii} &= c_r^2 M_{ii} - 2 s_r c_r M_{ij} + s_r^2 M_{jj} \\ M'_{jj} &= s_r^2 M_{ii} + 2 s_r c_r M_{ij} + c_r^2 M_{jj} \\ M'_{ij} &= M_{ij}\left(c_r^2 - s_r^2\right) + s_r c_r \left(M_{ii} - M_{jj}\right) \end{aligned} \qquad \text{(A.1.5)}$$

From the two sets of equations above, I.31 and I.32, it can be concluded that:

1. For a given pivot [i,j], only the elements of the rows and columns i and j are affected by the rotation, whereas all of the other elements of the matrix remain unchanged.
2. The elements of the M_r matrix located at [*k*,*i*] and [*k*,*j*] or at [*i*,*k*] and [*j*,*k*] that are zero will also be zero in the rotated matrix M'_r.

Now the sets of equations II.31 and II.32 can be used to define the values of the rotated matrix. In case we want eliminate certain couplings of the matrix with need to set to zero the corresponding element of the coupling matrix. So that using the first equation of I.31, we can turn to zero the [*i,k*] element as:

$$0 = c_r M_{mn} - s_r M_{jn} \qquad \text{(A.1.6)}$$

Substituting I.29 or I.30 on I.33 the rotation angle is obtained as:

$$\frac{s_r}{c_r} = \frac{M_{mn}}{M_{jn}} \quad \Rightarrow \begin{cases} \tan\theta_{rt} = \dfrac{M_{mn}}{M_{jn}} \\ j \cdot \tanh\theta_{rh} = \dfrac{M_{mn}}{M_{jn}} \end{cases} \tag{A.1.7}$$

Applying the same procedure to obtain I.34 we can use the whole set of equations I.31 and I.32 to define the required angle to eliminate the coupling from the resonator *m* to *n*, using the [*i, j*] pivot. The following table summarizes the resulting angles:

Element to eliminate	***i***	***j***	***k***	***tan(θ$_{rt}$) = j·tanh(θ$_{rh}$) =***
M_{mn}	*m*	≠ *n*, *m*	*n*	$\frac{M_{ik}}{M_{jk}}$
M_{mn}	≠ *n*, *m*	*m*	*n*	$-\frac{M_{jk}}{M_{ik}}$
M_{mn}	*n*	≠ *n*, *m*	*m*	$\frac{M_{ki}}{M_{kj}}$
M_{mn}	≠ *n*, *m*	*n*	*m*	$-\frac{M_{kj}}{M_{ki}}$
M_{mm}	*m*	≠ *m*	-	$\frac{-M_{ij} \pm \sqrt{M_{ij}^2 - M_{ii}M_{jj}}}{M_{jj}}$
M_{mm}	≠ *m*	*m*	-	$\frac{M_{ij} \pm \sqrt{M_{ij}^2 - M_{ii}M_{jj}}}{M_{ii}}$
M_{mn}	*m*	*n*	-	$\frac{2M_{ij}}{(M_{jj} - M_{ii})}$
M_{mn}	*n*	*m*	-	$\frac{2M_{ij}}{(M_{jj} - M_{ii})}$

Table A.1.1 Resulting angles to eleminate the element of M_{mn} of the matrix

The rotation matrix will be used also to swift couplings between resonators and transfer coupling strength from one resonator to another.

APPENDIX 2: Output Scattering Reflection Parameter in Case A

To obtain the output scattering reflection parameter S_{22} we start by considering a particular case where k_{11}=1 and k_{22}=1, and k_{21}<1, being therefore S_{21}=k_{21}·$S_{21\_lossless}$ and S_{11}= $S_{11\_lossless}$. To introduce the insertion loss offset k_{21} and keep S_{11} as in a lossless case we can introduce a series resistor (R) at the output of the network as detailed in Fig. A.2.1, which value must fulfill

$$k_{21}^2 = \frac{Z_0}{R + Z_0} \tag{A.2.1}$$

Additionally in order to achieve the desired S_{11} (=$S_{11\_lossless}$) we need to introduce an impedance inverter (*K*) between the resistor and the lossless network to guarantee that the impedance seen from the lossless network is Z_0. The value of the impedance inverter *K* should satisfy

$$K = \frac{Z_0}{k_{21}} \tag{A.2.2}$$

Now from the resulting network of Fig. A.2.1 and (A.2.1) and (A.2.2) is straight forward to extract the output reflection parameter by using conventional network analysis [5]

$$S'_{22}(s) = 1 - {k_{21}}^2 + k_{21}^2 S_{11\_lossless}(s) \tag{A.2.3}$$

Additional losses at the input and/or output reflection ports, k_{11}<1 and k_{22}<1, respectively, can be introduced by simply adding attenuators at the input and output of the network of Fig.18 [12]. And the corresponding output reflection parameter, equation (43), is again obtained by applying conventional network analysis [5].

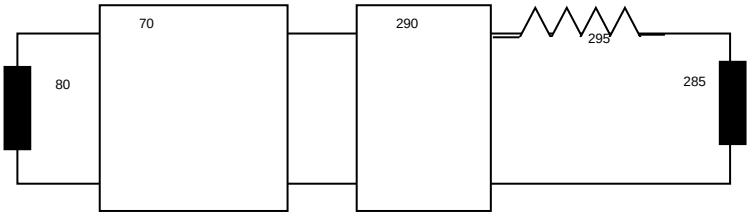

Fig. A.2.1 Equivalent network

APPENDIX 3: Scattering Reflection Parameter in a Symmetric Network

To obtain S_{11} we first write the S parameters as a function of the even S_e and odd S_o reflection coefficient (and they corresponding numerator and denominator polynomials):

$$S_e(s) = S_{11}(s) + S_{12}(s) = \frac{S_{en}(s)}{S_{ed}(s)}$$
$$S_o(s) = S_{11}(s) - S_{12}(s) = \frac{S_{on}(s)}{S_{od}(s)} \quad \text{(A.3.1)}$$

Using the relation between the characteristic polynomials and S parameters we obtain

$$E(s) = S_{ed}(s)S_{od}(s) \quad \text{(A.3.2)}$$

Where *E(s)* is a polynomial of order *N*, and $S_{ed}(s)$ and $S_{od}(s)$ are polynomials of order *N*/2 (or *N*/2-1 or *N*/2+1) that can be obtained from the roots of *E(s)*. Note that there are $\binom{N}{2}$ options to distribute the *N* roots of *E(s)* among the polynomials $S_{ed}(s)$ and $S_{od}(s)$, however not all of them yield a realizable $S_{11}(s)$ (a realizable network).

Using again the relation between the characteristic polynomials and S parameters we obtain

$$2\frac{P(s)}{\varepsilon} = S_{en}(s)S_{od}(s) - S_{on}(s)S_{ed}(s) \quad \text{(A.3.3)}$$

$$2F(s) = S_{en}(s)S_{od}(s) + S_{on}(s)S_{ed}(s) \quad \text{(A.3.4)}$$

Evaluating (A.3.3) and (A.3.4) at the roots of $S_{ed}(s)$ and $S_{od}(s)$, respectively, we directly obtain the polynomials $S_{en}(s)$ and $S_{on}(s)$. Now from $S_{ed}(s)$, $S_{od}(s)$, $S_{en}(s)$ and $S_{on}(s)$ we find the reflection coefficient $S_{11}(s)$. Now directly from the above S parameters (A.3.1), we may write down the Y_{ij} parameters of the two port admittance matrix as

$$Y_{12}(s) = Y_{21}(s) = \frac{S_{on}S_{ed} - S_{en}S_{od}}{(S_{od} + S_{on})(S_{ed} + S_{en})} \quad \text{(A.3.5)}$$

$$Y_{11}(s) = Y_{22}(s) = \frac{S_{od}S_{ed} - S_{en}S_{on}}{(S_{od} + S_{on})(S_{ed} + S_{en})}$$

From the equation above we can straightforward extract the numerator Y_{12n}, Y_{11n} and denominator Y_d of the *Y* parameters.

APPENDIX 4: Hyperbolic Rotation

Hyperbolic rotation allows moving losses from one resonator to another as long as exists coupling between them. Note that is this would not possible with conventional trigonometric rotation (see Appendix 1). Another effect of applying hyperbolic rotation between two resonators is that additional resistive couplings appear.

We start applying hyperbolic rotation to the FCM corresponding to Case A. Recall that this case in contrast to Case B has a resistor connected the input and output port (or analogously to the introduced non-resonant nodes). Let us consider the circuit topology of a fourth order filter of Fig.A.4.1a, where only resonator 1 and 4 are lossy, and perform a hyperbolic rotation from 1 to 2 and from 4 to 3. The angle of rotation depends on the losses distribution we want to achieve and the couplings between resonators. Note that in a symmetric network the initial losses at 1 and 4 are identical and the couplings to 2 and 3 respectively too, so in this case is convenient to keep such a symmetry by using the same angle to move losses from 1 to 2 than from 4 to 3. In this case a uniform losses distribution, this is all resonators with the same Q may be achieve.

Since it exists coupling between resonator 1 and the non-resonant node at the source an additional resistive coupling would appear between the non-resonant node and the second resonator, and analogously a resistive coupling between 2 and 4 and 1 and 3. Note that similar results could occur when hyperbolic rotation is applied between the 4th and 3th resonator. The resulting topology for a quasi-elliptic filter and a Chebyshev fourth order filter is outlined in Fig. A.4.1.b and A.4.1.c, respectively.

At this point it is very important to mention that when a resistive coupling between one of the non-resonant nodes and a resonator appears, losses from the shunt resistance at the non-resonant are then transferred to the resistive coupling, being therefore mandatory to have initial losses to the non-resonant nodes. Note that the angle of hyperbolic rotation could be applied for a full transfer of the losses of the non-resonant node, this is removing completely the shunt resistor at the non-resonant node.

Applying a hyperbolic rotation to the folded topology of a sixth order filter (equivalent to Fig. A.4.1a, but for order six), first from resonators 1 to 2 and 6 to 5 and then from 2 to 3 and 5 to 4, the resulting folded topology is as detailed in Fig. A.4.1.d. Note that this topology only shows the more significant couplings and does not include very small resistive couplings resulting from the matrix rotation.

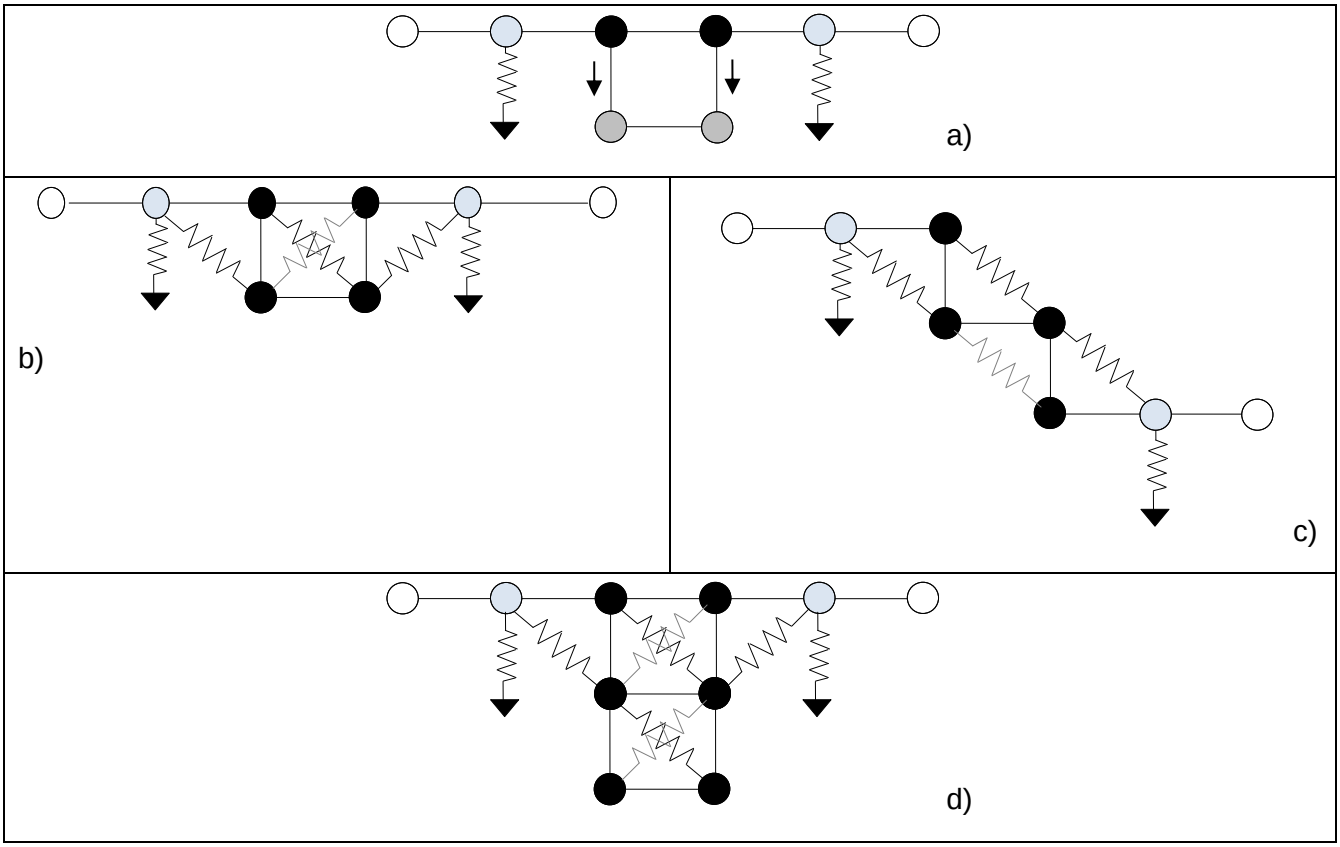

Fig. A.4.1. a) FCT before hyperbolic rotation b) FCT after hyperbolic rotation in a Quasi-Elliptic response c) FCT after hyperbolic rotation in a Chebyshev response. d) FCT after hyperbolic rotation in a Quasi-Elliptic response for a 6^{th} order filter.

Although the technique outlined in this section show to be very powerful for losses distribution does not always offers enough flexibility. Additional flexibility may be introduced by scaling nodes, briefly outlined below.

APPENDIX 5: Node Scaling

We will scale nodes of the network topology to transform for a better control of the losses distribution. Scaling nodes could be applied at both non-resonant nodes and resonant nodes, and essentially consists of multiplying the row and column corresponding of the coupling matrix to the node to scale by a given value k. Note that by doing so the losses in the node are scaled by k^2 and the conventional and resistive couplings to that node are scaled by k. This essentially changes the losses in the node and the way they may be transfer to other resonators.

Applying a scaling factor to a resonant node of the coupling requires also apply such scaling to the frequency dependence terms of the admittance matrix, which in practice results in change of the characteristic impedance of the resonator. Therefore the scaling factors to apply are usually limited by the technology used in the filter implementation.

APPENDIX 6: Sixth order folded lossy coupling matrix

In this appendix we will describe in some detail of the matrix rotation procedure to perform circuit network.

Coupling matrix after matrix rotation of α and α_1.

	S	*NS*	*1*	*2*	*3*
S	*0*	*1*	*0*	*0*	*0*
NS	*1*	*-jG*	crM_{01}	$-js_rc_{r1}M_{01}$	$-s_rM_{01}s_{r1}$
1	*0*	crM_{01}	$-jc_r(c_rG_1-2s_rM_{12})$	$c_{r1}M_{12}(c_r^2+s_r^2)-G_1c_{r1}c_rs_r$ $-M_{23}s_{r1}s_r$	$-jM_{12}s_{r1}(c_r^2+s_r^2)+jG_1s_{r1}c_rs_r$ $+jc_{r1}M_{23}s_r$
2	*0*	$-js_rc_{r1}M_{01}$	$c_{r1}M_{12}(c_r^2+s_r^2)-G_1c_{r1}c_rs_r$ $-M_{23}s_{r1}s_r$	$jc_{r1}(G_1c_{r1}s_r^2-2c_rc_{r1}M_{12}s_r$ $+2c_rM_{23}s_{r1})$	$G_1s_r^2c_{r1}s_{r1}-2c_rM_{12}s_rc_{r1}s_{r1}$ $+c_rM_{23}(c_{r1}^2+s_{r1}^2)$
3	*0*	$-s_rM_{01}s_{r1}$	$-jM_{12}s_{r1}(c_r^2+s_r^2)+jG_1s_{r1}c_rs_r$ $+jc_{r1}M_{23}s_r$	$G_1s_r^2c_{r1}s_{r1}-$ $2c_rM_{12}s_rc_{r1}s_{r1}+c_rM_{23}(c_{r1}^2+s_{r1}^2)$	$-js_{r1}(G_1s_{r1}s_r^2-2c_rM_{12}s_{r1}s_r$ $+2c_rc_{r1}M_{23})$
4	*0*	*0*	*0*	$jc_{r1}M_{34}s_{r1}$	$c_{r1}^2M_{34}$
5	*0*	*0*	*0*	$-M_{34}s_{r1}^2$	$jc_{r1}M_{34}s_{r1}$
6	*0*	*0*	*0*	*0*	*0*
NL	*0*	*0*	*0*	*0*	*0*
L	*0*	*0*	*0*	*0*	*0*

Coupling matrix after node scaling **h**.

S	*0*	***h***	*0*	*0*	*0*
NS	***h***	$-j\mathbf{h}^2G$	$\mathbf{h}c_rM_{01}$	$-j\mathbf{h}s_rc_{r1}M_{01}$	$-\mathbf{h}s_rM_{01}s_{r1}$
1	*0*	$\mathbf{h}c_rM_{01}$	$-jc_r(c_rG_1-2s_rM_{12})$	$c_{r1}M_{12}(c_r^2+s_r^2)-G_1c_{r1}c_rs_r-M_{23}s_{r1}s_r$	$-jM_{12}s_{r1}(c_r^2+s_r^2)+jG_1s_{r1}c_rs_r+jc_{r1}M_{23}s_r$
2	*0*	$-\mathbf{h}s_rc_{r1}M_{01}$	$c_{r1}M_{12}\ (c_r^2+s_r^2)-G_1c_{r1}c_rs_r-M_{23}s_{r1}s_r$	$jc_{r1}(G_1c_{r1}s_r^2-2c_rc_{r1}M_{12}s_r+2c_rM_{23}s_{r1})$	$G_1s_r^2c_{r1}s_{r1}-2c_rM_{12}s_rc_{r1}s_{r1}+c_rM_{23}(c_{r1}^2+s_{r1}^2)$
3	*0*	$-\mathbf{h}s_rM_{01}s_{r1}$	$-jM_{12}s_{r1}(c_r^2+s_r^2)+jG_1s_{r1}c_rs_r+jc_{r1}M_{23}s_r$	$G_1s_r^2c_{r1}s_{r1}-2c_rM_{12}s_rc_{r1}s_{r1}+c_rM_{23}(c_{r1}^2+s_{r1}^2)$	$-js_{r1}(G_1s_{r1}s_r^2-2c_rM_{12}s_{r1}s_r+2c_rc_{r1}M_{23})$
4	*0*	*0*	*0*	$jc_{r1}M_{34}s_{r1}$	$c_{r1}^2M_{34}$
5	*0*	*0*	*0*	$-M_{34}s_{r1}^2$	$jc_{r1}M_{34}s_{r1}$
6	*0*	*0*	*0*	*0*	*0*
NL	*0*	*0*	*0*	*0*	*0*
L	*0*	*0*	*0*	*0*	*0*

APPENDIX 7: Details on the transfer function obtained in Case B

Further details on how to obtain the transfer function for Case B synthesized responses is detailed below.

As described in Chapter 1 the roots of E(s) are used to defined the denominator of the even and odd scattering parameters, S_{ed} and S_{od}, respectively. In the specific case illustrated here the roots of E(s) are:

-0.3138 + j·1.1948
-0.3138 – j·1.1948
-0.7577 + j·0.4949
-0.7577 – j·0.4949

Table A.7.1:Roots of the characteristic polynomial *E(s)* of a 4th order Chebyshev filter with L_r=20dB

Which correspond to a 4th order Chebyshev filter with 20 dB return losses. Note that those roots satisfy the Hurwitz condition.

The possible combinations of the roots of E(s) listed above are summarized in the following table.

k	Roots (S_{ed})	Roots(S_{od})
1	-0.3138 + j·1.1948 -0.3138 - j·1.1948	-0.7577 + j·0.4949 -0.7577 - j·0.4949
2	-0.3138 + j·1.1948 -0.7577 + j·0.4949	-0.3138 - j·1.1948 -0.7577 - j·0.4949
3	-0.3138 - j·1.1948 -0.7577 + j·0.4949	-0.3138 + j·1.1948 -0.7577 - j·0.4949
4	-0.3138 + j·1.1948 -0.7577 - j·0.4949	-0.3138 - j·1.1948 -0.7577 + j·0.4949
5	-0.3138 - j·1.1948 -0.7577 - j·0.4949	-0.3138 + j·1.1948 -0.7577 + j·0.4949
6	-0.7577 + j·0.4949 -0.7577 - j·0.4949	-0.3138 + j·1.1948 -0.3138 - j·1.1948

TableA.7.2: Selected roots for the polynomials S_{ed} and S_{od}, respectively

Each of the polynomials S_{ed} and S_{od} defined in the table are then used to find the resulting F(s) characteristic polynomial.

1	1.000	2.143 – j·0.737	3.296 -j·2.167	2.827 -j·2.195	1.250-j·1.731
2	1.000	2.958	4.532	5.253	2.583
3	1.000	3.643	4.904	4.806	2.038
4	1.000	0.643	1.689	0.848	0.463
5	1.000	1.328	2.061	0.400	-0.083
6	1.000	2.143+j·0.737	3.296+j·2.167	2.827+j·2.195	1.250+j·1.731

Table A.7.3: Coefficients of the resulting F(s) polynomials

The figure below shows the roots for the F(s) polynomials listed in previous table

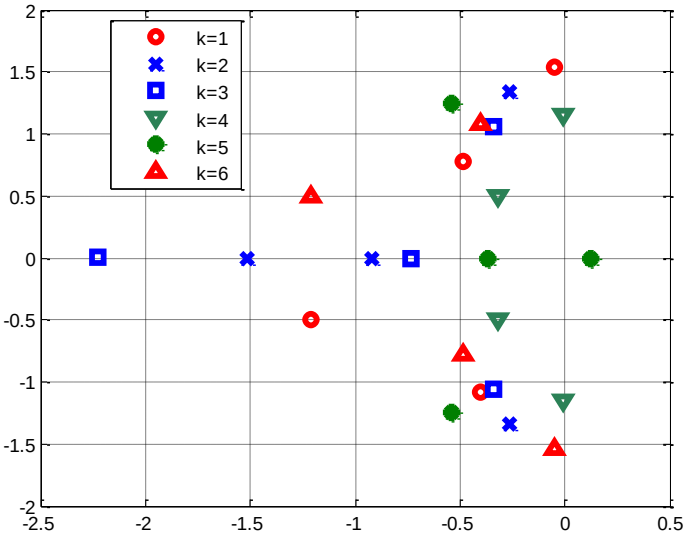

Fig. A.7.1- Roots of the F(s) extracted polynomials.

Using the F(s) polynomials above we obtain the resulting reflection function of the synthesized response. The outlined of such reflection functions are detailed in the figure below.

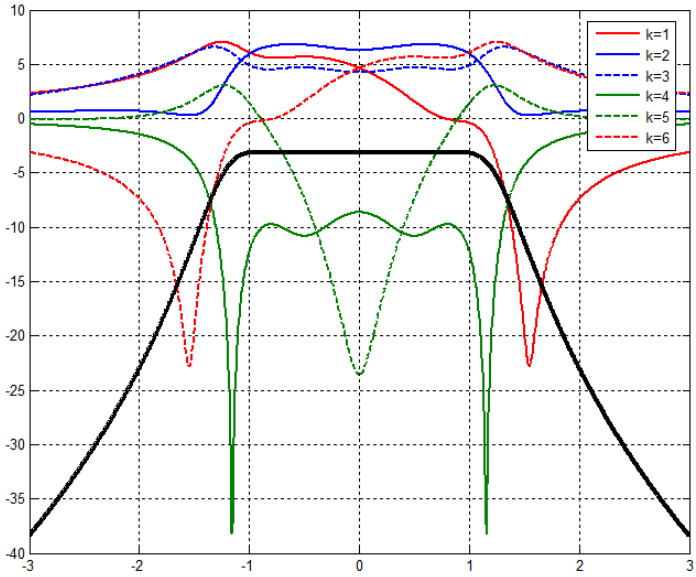

Fig. A.7.2- Reflection response for each F(s) of Table A.7.3.

These results show that only one of the possible solutions satisfies passive network condition, the case corresponding to k=4. Note that the case of k=4 is the only one that the F(s) polynomial has roots in conjugate pairs.

APPENDIX 8: Matrices: Lossy filters on section 2.4

Coupling matrices corresponding to the 10-4-4 Ku Band filter presented in section 2.4. The corresponding Q is labeling each Matrix.

Q=7000

	S	1	2	3	4	5	6	7	8	9	10	L
S	0	1.037	0	0	0	0	0	0	0	0	0	0
1	1.037	0-0.05i	0.861	0	0	0	0	0	0	0	0.006	0
2	0	0.861	0-0.05i	0.618	0	0	0	0	0	-0.02	0	0
3	0	0	0.618	-0.066i	0.563	0.01i	0	0.006i	-0.021	0	0	0
4	0	0	0	0.563	-0.058i	0.54	0.002i	0.157	0.006i	0	0	0
5	0	0	0	0.01i	0.54	-0.062i	0.431	0.002i	0	0	0	0
6	0	0	0	0	0.002i	0.431	-0.062i	0.54	0.01i	0	0	0
7	0	0	0	0.006i	0.157	0.002i	0.54	-0.058i	0.563	0	0	0
8	0	0	0	-0.021	0.006i	0	0.01i	0.563	-0.066i	0.618	0	0
9	0	0	-0.02	0	0	0	0	0	0.618	-0.05i	0.861	0
10	0	0.006	0	0	0	0	0	0	0	0.861	-0.05i	1.038
L	0	0	0	0	0	0	0	0	0	0	1.038	0

Q=5000

	S	1	2	3	4	5	6	7	8	9	10	L
S	0	0.955	0	0	0	0	0	0	0	0	0	0
1	0.955	-0.07i	0.85	0	0	0	0	0	0	0	0.006	0
2	0	0.85	-0.07i	0.606	0	0	0	0	0	-0.019	0	0
3	0	0	0.606	-0.096i	0.561	0.015i	0	0.011i	-0.019	0	0	0
4	0	0	0	0.561	-0.088i	0.547	0.007i	0.148	0.011i	0	0	0
5	0	0	0	0.015i	0.547	-0.092i	0.449	0.007i	0	0	0	0
6	0	0	0	0	0.007i	0.449	-0.092i	0.547	0.015i	0	0	0
7	0	0	0	0.011i	0.148	0.007i	0.547	-0.088i	0.561	0	0	0
8	0	0	0	-0.019	0.011i	0	0.015i	0.561	-0.096i	0.606	0	0
9	0	0	-0.019	0	0	0	0	0	0.606	-0.07i	0.85	0
10	0	0.006	0	0	0	0	0	0	0	0.85	-0.07i	0.955
L	0	0	0	0	0	0	0	0	0	0	0.955	0

Q=4000

	S	1	2	3	4	5	6	7	8	9	10	L
S	0	0.964	0	0	0	0	0	0	0	0	0	0
1	0.964	-0.088i	0.848	0	0	0	0	0	0	0	0.005	0
2	0	0.848	-0.088i	0.608	0	0	0	0	0	-0.018	0	0
3	0	0	0.608	-0.112i	0.567	0.015i	0	0.01i	-0.017	0	0	0
4	0	0	0	0.567	-0.105i	0.548	0.008i	0.156	0.01i	0	0	0
5	0	0	0	0.015i	0.548	-0.11i	0.443	0.008i	0	0	0	0
6	0	0	0	0	0.008i	0.443	-0.11i	0.548	0.015i	0	0	0
7	0	0	0	0.01i	0.156	0.008i	0.548	-0.105i	0.567	0	0	0
8	0	0	0	-0.017	0.01i	0	0.015i	0.567	-0.112i	0.608	0	0
9	0	0	-0.018	0	0	0	0	0	0.608	-0.088i	0.848	0
10	0	0.005	0	0	0	0	0	0	0	0.848	-0.088i	0.964
L	0	0	0	0	0	0	0	0	0	0	0.964	0

Q=2000

	S	1	2	3	4	5	6	7	8	9	10	L
S	0	0.753	0	0	0	0	0	0	0	0	0	0
1	0.753	-0.175i	0.795	0	0	0	0	0	0	0	0.003	0
2	0	0.795	-0.175i	0.587	0	0	0	0	0	-0.013	0	0
3	0	0	0.587	-0.226i	0.551	0.032i	0	0.019i	-0.008	0	0	0
4	0	0	0	0.551	-0.214i	0.548	0.019i	0.157	0.019i	0	0	0
5	0	0	0	0.032i	0.548	-0.226i	0.488	0.019i	0	0	0	0
6	0	0	0	0	0.019i	0.488	-0.226i	0.548	0.032i	0	0	0
7	0	0	0	0.019i	0.157	0.019i	0.548	-0.214i	0.551	0	0	0
8	0	0	0	-0.008	0.019i	0	0.032i	0.551	-0.226i	0.586	0	0
9	0	0	-0.013	0	0	0	0	0	0.586	-0.175i	0.795	0
10	0	0.003	0	0	0	0	0	0	0	0.795	-0.175i	0.753
L	0	0	0	0	0	0	0	0	0	0	0.753	0

REFERENCES

[1] R. Cameron, C. M. Kudsia, R. R. Mansour, “Microwave filters for communication systems” John Wiley, 2007.

[2] G. Matthaei, L. Young, and E. M. T, Microwave Filters, Impedance Matching Networks and coupling structures, Artech House, Norwood, MA, 1980

[3] J-S Hong and M. J. Lancaster, Microstrip filters for RF/Microwave Applications, John Wiley & Sons

[4] R. Levy , Filters with single transmission zeros at real or imaginary frequencies, MTT-24 (4), 1976, pp.172-181.

[5] D. Pozar, *Microwave Engineering*, John Wiley & Sons, Inc., 1998

[6] R.J. Cameron , General coupling matrix synthesis methods for Chebyshev filtering functions, IEEE MTT-47(4), pp. 433-442, April 1999.

[7] R.J. Cameron, “ Advanced Coupling Matrix synthesis Tehcniques for Microwave Filters” *Microwave Theory and Techniques, IEEE Transactions on* , vol.51, no.1, pp.1-10, January. 2003

[8] Rao, K. R.; Ahmed, N. (1968). "Recursive techniques for obtaining the partial fraction expansion of a rational function". *IEEE Trans. Educ.* **11** (2). pp. 152–154

[9] M. Yu, W-C Tang, A. Malarky, V. Dokas, R. Cameron, Y. Wang, “Predistortion Technique for Cross-Coupled Filters and its application to satellite communication systems”, IEEE Trans. On Microwave Theory and Techniques, vol. 51, No.12, Dec. 2003.

[10] A. E. Williams, W. G. Bush, and R. R. Bonetti, Predistortion Tecnique for multicoupled resonator filters methods for Chebyshev filtering functions, IEEE Trans. Microwave Theory and Techniques, MTT-33, 402-407, May 1985.

[11] M. Yu et al., “Predistortion Technique for Cross-Coupled Filters and its application to satellite communication systems”, IEEE MTT-51, pp. 2505-2515, Nov. 2003

[12] M. Yu, V. Miraftab, “Shrinking Microwave Filters” IEEE Microwave Magazine, October 2008, pp. 40-54.

[13] I. Hunter, A. Guyette, R. D. Pollard, “Passive Microwave Receive Filter Networks Using Low-Q Resonators”, IEEE Microwave Magazine, Sept. 2005

[14] Miraftab, V.; Ming Yu, "Generalized Lossy Microwave Filter Coupling Matrix Synthesis and Design Using Mixed Technologies," Microwave Theory and Techniques, IEEE Transactions on, vol.56, no.12, pp.3016-3027, Dec. 2008.

[15] Miraftab, V.; Ming Yu, "Advanced Coupling Matrix and Admittance Function Synthesis Techniques for Dissipative Microwave Filters," Microwave Theory and Techniques, IEEE Transactions on , vol.57, no.10, pp.2429-2438, Oct. 2009

[16] M. Dishal, Design of dissipative filters producing desired exact amplitude frequency characteristics, IER Proc. Vol. 37, pp. 1050-1069, 1949.

[17] J.D. Rhodes, I.C. Hunter, “Synthesis of Reflection-mode prototype networks with dissipative circuit elements” IEE Proc.- Microwave Antennas Propagation, Vol. 144, No.6 December 1997.

[18] W. M. Fathelbab, I.C. Hunter, J.D. Rhodes, “Synthesis of predistorted reflection-mode hybrid prototype networks with symmetrical and asymmetrical characteristics”, International Journal of Circuit Theory and Applications, 2001, 29, 251-266.

[19] W. M. Fathelbab, I.C. Hunter, J.D. Rhodes, “Synthesis of predistorted reflection-mode hybrid prototype networks with symmetrical and asymmetrical characteristics”, International Journal of Circuit Theory and Applications, 2001, 29, 251-266.

[20] B. S. Senior, I.D. Hunter, and J.D. Rhodes, “Synthesis of lossy filters” in 32nd Eur. Microwave Conference, Milan, Italy, 2002, pp. 401-404.

[21] A.C. Guyette, I. C. Hunter, R. Pollard, “The design of microwave bandpass filters using resonators with nonuniform Q”, IEEE MTT-54 (11), November 2006, pp.3914-3922.

[22] A.C. Guyette, I. C. Hunter, R. Pollard, “Exact synthesis of Microwave Filters with nonuniform dissipation”, IEEE MTT-S Digest 2007.

[23] Z.Zakaria, I. C. Hunter, A. C. Guyette, “Design of a Coaxial Resonator Filter with nonuniform Dissipation”. International Microwave Symposium 2008

[24] F-J. Görtz, Executive Summary. “New Generation Input Demultiplexer NGIMUX”. ESA program AO 4184 Multimedia Satellite Equipment.

[25] European Space Agency. TRP - Statement of Work. *Design and Synthesis of a New Class of Receiver Filers.* Appendix 1 to Invitation to ESA Invitation to Tender AO/1-5477/07/NL/GLC (ESA contract 21398/08/GLC).

[26] J. Mateu, A. Padilla, C. Collado, M. Martinez-Mendoza, C. Ernst, E.Rocas, J. M. O’Callaghan, “Synthesis of 4th order Lossy Filters with uniform Q distribution”, IEEE MTT-S Digest 2010.

[27] A. Padilla, J. Mateu, C. Collado, C. Ernst, J. M. Rius, J. M. Tamayo, J. M. O'Callaghan, Comparison of lossy filters and predistorted filters using novel software. 2010 International Microwave Symposium Digest.